Relativistic Effects on Electronic Structure and Nuclear Magnetic Resonance Shifts in Heavy Metal Systems

vorgelegt von
M. Sc.
Anja Helene Greif
geb. in Berlin

Von der Fakultät II – Mathematik und Naturwissenschaften
der Technischen Universität Berlin
zur Erlangung des akademischen Grades
Doktor der Naturwissenschaften

– Dr. rer. nat. –

genehmigte Dissertation

Promotionsausschuss:

Vorsitzender:	Prof. Dr. rer. nat. Arne Thomas
Gutachter:	Prof. Dr. rer. nat. Martin Kaupp
Gutachter:	Prof. Dr. rer. nat. Stephan P. A. Sauer

Tag der wissenschaftlichen Aussprache: 14. September 2017

Berlin 2017

"Der Forscher fühlt sich dann dem noch nicht Erkannten gegenüber wie ein Kind, das der Erwachsenen überlegenes Walten zu begreifen sucht."

Albert Einstein

Zusammenfassung

Untersucht wird der Einfluss relativistischer Effekte auf die Elektronenstruktur und die chemische Verschiebung von NMR Kernen in diamagnetischen 5d Übergangsmetall- und Uran-Hydriden wie auch metallorganischen Uran-Komplexen. Neue Trends und Bereiche im NMR Spektrum dieser Verbindungen werden aufgezeigt basierend auf voll- und quasi-relativistischen Dichtefunktionalrechnungen, die an experimentell bekannten NMR Daten für Pt(II) und U(VI) Komplexen evaluiert wurden.

Es zeigt sich, dass für die akkurate relativistische Berechnung der Abschirmungskonstante die Verwendung des Austausch-Korrelations-Kernels sowie PBE0-Hybridfunktionals notwendig ist. Die NMR Signale in den untersuchten Komplexen werden durch beträchtliche relativistische Beiträge dominiert, welche durch Spin-Bahn (SB) Kopplung am schweren Atom bedingt werden und sowohl entschirmend als auch abschirmend sein können. Die wiederholt beobachteten qualitativen Unterschiede zwischen d^6/d^8 und d^{10} Komplexen hinsichtlich der Größe und des Vorzeichens von SB-induzierter NMR Abschirmung an einem benachbarten ^1H Atom können auf einen auffallend allgemeingültigen *trans*-Liganden Einfluss zurück geführt werden, der die Metallorbitalbeteiligung in relevanten Molekülorbitalen sowie deren Energie moduliert. Die daraus resultierenden Unterschiede für die σ-/π-Spinor-Vermischung durch die SB Kopplung führen zu unterschiedlich effizienten magnetischen Kopplungen der metallbasierten Orbitale. Stark abschirmende Beiträge von vorrangig π-artigen Spinoren für schwache *trans*-Liganden sind für starke *trans*-Liganden vermindert oder sogar verschwunden infolge einer Destabilisierung von besetzen σ-Orbitalen, was schließlich zur Vorzeichenänderung für die SB-induzierten NMR Verschiebungen führt. Ähnliche Effekte können auch für andere NMR Kerne festgestellt werden. Im Gegensatz zu früheren Annahmen lässt sich die Veränderung der ^1H NMR Verschiebung nicht durch die Änderung der M-^1H Bindungslänge in einem gegebenen Komplex begründen.

Für die ^{1}H und ^{13}C NMR Signale für Ligandenatome an einem U(VI) Zentrum werden sehr hohe Resonanzfrequenzen vorhergesagt, die bis zu +170 ppm für ^{1}H und über +550 ppm für ^{13}C betragen können und damit außerhalb der normalen Messbereiche für die jeweiligen Kerne liegen. Der Ursprung der enormen SB-Beiträge zur NMR Verschiebung steht in Verbindung mit der Position des Liganden im Komplex sowie der allgemeinen Elektronenstruktur.

Abstract

The role of relativistic effects on the electronic structure and ligand NMR chemical shifts in diamagnetic 5d transition-metal and uranium hydrides as well as organometallic uranium complexes is investigated. New NMR trends and spectral regions for these compounds are suggested based on fully and quasi-relativistic density functional theory calculations carefully calibrated on the experimentally known NMR data for Pt(II) and U(VI) complexes.

For accurate relativistic shielding computations, the exchange-correlation kernel on NMR chemical shifts and the use of the PBE0 hybrid functional is found to be mandatory. The NMR signals in the investigated complexes are dictated by sizable relativistic contributions due to spin−orbit (SO) coupling at the heavy atom and can be highly shielding and deshielding, as well. The frequently observed qualitative differences between d^6/d^8 and d^{10} complexes in the magnitude and the sign of SO-induced nuclear magnetic shielding at a vicinal ^{1}H atom are found to be dominated by surprisingly general *trans* ligand effects modulating the metal orbital participations in relevant MOs as well as their energy. The resulting changes in σ-/π-spinor mixing by SO coupling modify the efficiency of metal-based orbital magnetic couplings. Large shielding contributions from predominantly π-type spinors for weak *trans* ligands are diminished or even removed for strong *trans* ligands due to a destabilization of occupied σ levels, causing a sign change from shielding to deshielding of the dominant SO-induced shifts. Similar effects are operative also for other NMR nuclei. In contrast to previous assumptions, the change of the M−H distances for given complexes does not allow correlations with the hydride shifts.

The ^{1}H and ^{13}C NMR signals of ligand atoms directly bonded to U(VI) centers are predicted to resonate at very high frequencies, up to +170 ppm for ^{1}H and above +550 ppm for ^{13}C, outside the usual measurement area for the given type of nuclei. The origin of the vast SO contributions to the NMR shift is traced to the ligand position in the complex, and on the overall electronic structure.

Danksagung

Große Dankbarkeit gilt meinem Doktorvater Prof. Dr. Martin Kaupp, der mir die Möglichkeit gegeben hat, mich an verschiedenen Projekten auszuprobieren, Anregungen und Hilfestellungen gab und mir immer unterstützend zur Seite stand.

Bei allen Mitgliedern der Arbeitsgruppe Kaupp bedanke ich mich ebenfalls. Besonders hervorheben möchte ich meine Bürokollegen Dr. Matthias Parthey, Dr. Toni Maier und Sascha Klawohn. Außerdem danke ich unserer stets hilfreichen IT-Managerin Heidi Grauel sowie unserer Sekretärin Nadine Rechenberg, ohne die wohl kaum etwas im Alltag funktionieren würde.

Dr. Peter Hrobárik und Prof. Dr. Jochen Autschbach gilt mein Dank für die Zusammenarbeit an verschiedenen Projekten. Vielen Dank auch an Dr. Michal Repisky, der meinen Forschungsaufenthalt jenseits des Polarkreises betreute.

Herzlichen Dank möchte ich meinen lieben Freunden aussprechen, allen voran Marcel Schmidt, der nicht nur während des Studiums sondern auch auf dem Weg zur Promotion mein treuer Mitstreiter war und mir den Alltag stets versüßte.

Für ihre Liebe und Unterstützung danke ich meiner Familie, insbesondere meinen Eltern.

Zu guter Letzt möchte ich mich bei meinem Mann Ludwig bedanken. Es ist mir kaum möglich, den Beistand, das Verständnis und die Geduld, welche er mir entgegenbrachte auch nur annähernd in Worte zu fassen.

List of Publications

Publications included in the thesis

Paper I: A relativistic quantum-chemical analysis of the *trans* influence on ^{1}H NMR shifts in square-planar Pt(II) complexes

A. H. Greif, P. Hrobárik, V. Hrobáriková, A. V. Arbuznikov, J. Autschbach and M. Kaupp, *Inorg. Chem.*, 2015, **54**, 7199–7208.

DOI: 10.1021/acs.inorgchem.5b00446

Paper II: Insights into *trans*-Ligand and Spin-Orbit Effects on electronic Structure and Ligand NMR Shifts in Transition-Metal Complexes

A. H. Greif, P. Hrobárik and M. Kaupp**,** *Chem. Eur. J.*, 2017, **23**, 9790.

DOI: 10.1002/chem.201700844

Paper III: Giant Spin-Orbit Effects on ^{1}H and ^{13}C NMR Shifts for Uranium(VI) Complexes Revisited: Role of the Exchange-Correlation Response Kernel, Bonding Analyses, and New Predictions

A. H. Greif, P. Hrobárik, J. Autschbach and M. Kaupp, *Phys. Chem. Chem. Phys.*, 2016, **18**, 30462-30474.

DOI: 10.1039/C6CP06129J

Non-contributing Publication

Giant Spin-Orbit Effects on NMR Shifts in Diamagnetic Actinide Complexes: Guiding the Search of Uranium(VI) Hydride Complexes in the Correct Spectral Range

P. Hrobárik, V. Hrobáriková, A. H. Greif, M. Kaupp, *Angew. Chem. Int. Ed.* **2012**, *51*, 10884–10888.

DOI: 10.1002/anie.201204634

Contents

List of Abbreviations

1c	one-component
2c	two-component
4c	four-component
ADF	Amsterdam Density Functional
DE	Dirac Equation
DFT	Density Functional Theory
DKH	Douglas-Kroll-Hess
ECP	Effective Core Potential
ESR	Electron Spin Resonance
EXX	Exact-Exchange
FC	Fermi-Contact
GGA	Generalized Gradient Approximation
GIAO	Gauge Invariant Atomic Orbitals
GTO	Gaussian Type Orbital
HAHA	Heavy-Atom Effect on the Heavy Atom
HALA	Heavy-Atom Effect on the Light Atom
HF	Hartree-Fock
HK	Hohenberg-Kohn
HOMO	Highest Occupied Molecular Orbital
KS	Kohn-Sham
LCAO	Linear Combinations of Atomic Orbitals
LDA	Local Density Approximation
LMO	Localized Molecular Orbital
LUMO	Lowest Unoccupied Molecular Orbital
mDKS	Matrix-Dirac-Kohn-Sham
MO	Molecular Orbital
NBO	Natural Bond Orbital
NHD	Normal Halogen Dependence
NLMO	Natural Localized Molecular Orbital
NMR	Nuclear Magnetic Resonance

ppm	parts per million
RMB	Restricted Magnetic Balanced (Orbitals)
SCF	Self-Consistent Field
SE	Schrödinger Equation
SO	Spin-Orbit
SOS	Sum-Over States
SR	Scalar relativistic
STO	Slater Type Orbitals
TM	Transition Metal
TMS	tetramethyl silane
XC	Exchange-Correlation
ZORA	Zeroth-Order Regular Approximation

1 General Introduction

A good scientist does not only discover new information but make sense of it. One such person was Dmitri Mendeleev, who often is considered to be the *father of the Periodic Table*. The world's first view of Mendeleev's tabular arrangement of chemical elements in the Periodic Table is shown in Figure 1 extracted from *Zeitschrift für Chemie*, 1869,[1] and compared to the modern Periodic Table. As opposed to the popular layout of the Periodic Table Mendeleev's early arrangement presents the periods vertically, and the groups horizontally. Although Mendeleev could not know the concepts of atomic numbers or electron configurations, explaining each period (row) in the modern Periodic Table, he drew almost perfect consequences for the ordering and could even predict several elements yet to be discovered. Instead of atomic numbers Mendeleev used mainly the atomic weight to organize the elements but also kept their chemical properties in mind. Thus, he placed tellurium before iodine despite its larger weight as iodine's properties are so similar to those of fluorine, chlorine and bromine, whereas tellurium is more similar to oxygen, sulfur and selenium.

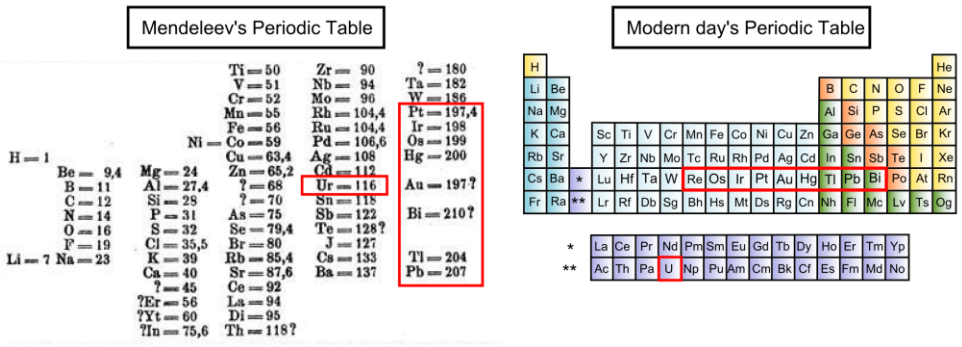

Figure 1. Comparison of the periodic Table of Mendeleev as published in 1869[1] and the modern one. The deviating locations for heavy elements are highlighted with red boxes.

In fact, incorrect locations concern exclusively the lanthanides, which now are known to represent a separate series, and the heavy elements as of tungsten, particularly uranium (today's symbol U instead of Ur). What Mendeleev could

not know is that *special relativity* changes several chemical and physical properties and, thus, periodic trends.

A long time has passed since the formulation of relativistic quantum mechanics by Paul Dirac in 1928, and meanwhile it is textbook knowledge that chemical systems containing heavy atoms exhibit *relativistic effects*. Relativistic effects denote the deviation of results obtained in a non-relativistic theoretical framework from one which is in accordance with Albert Einstein's theory of special relativity. In leading order those effects rise roughly as $(Z/c)^2$ relative to the non-relativistic quantity, where c is the speed of light (c = 137.036 a. u.) and Z the atomic number. Hence, they often can be neglected for elements in the upper part of the Periodic Table. In contrast, for elements like platinum, gold and mercury this factor is already about one third, causing the many unique properties of those elements in comparison to their lighter congeners. The formidable catalytic effectiveness of platinum, the yellow color of gold and the unusually low boiling point of mercury are just a few examples of how relativity manifests itself in the observable world.[2]

Based on this it is comprehensible that Mendeleev had some problems with the correct ordering of those elements. The misplacement of uranium, in contrast, was primarily caused by an incorrect atomic weight, which is actually more than double the value given in Figure 1. The correct element indium was placed between cadmium and tin in Mendeleev's next version of 1872.[3] The proper place for uranium, however, was not found until the 1940s, when Glenn T. Seaborg redrew the Periodic Table into its current configuration by adding the actinide series below the lanthanide series during the Manhattan Project. The outstanding fame of Einstein's equation $E = mc^2$ is strongly associated with the result of this project using the nuclear fission of uranium-235 that led to the death of thousands of Japanese citizens in Hiroshima and Nagasaki. While special relativity actually did not have an immense impact on the development and construction of nuclear bombs, uranium, as one of the heaviest naturally existing elements and with a $(Z/c)^2$ factor of 0.45, can be expected to show extraordinary relativistic effects.

One impressive example, inspired from the results of my bachelor thesis, was published in 2012 where we predicted ^{1}H NMR shifts for diamagnetic ura-

nium complexes to be at unprecedentedly high frequencies.[4] Nuclear magnetic resonance (NMR) spectroscopy is a very sensitive experimental probe for the electronic (and geometrical) structure of a compound and emerged as a technique of seemingly endless fruitfulness by physicists, chemists, biologists and physicians as well. Based on relativistic quantum-chemical calculations we could show that the predicted unusual extension of the spectral area for diamagnetic complexes (up to +150 ppm in ^{1}H NMR shifts) is the result of unexpectedly large spin-orbit (SO) effects at the uranium(VI) central atom that are transferred to the hydrogen nucleus through the bond. SO coupling is one of the consequences of special relativity apparent in the splitting of atomic or molecular orbitals, whereupon the energy and symmetry of the orbitals changes. Already in 1969, Nomura *et al*.[5] found SO contributions to be responsible for the changing ^{1}H shifts of the hydrogen halides, making this transfer of relativistic effects on the heavy atom (HA) to the light atom (LA) one of the oldest examples for a discussion of the consequences of special relativity in chemistry. That those HALA effects are decisive also for transition metal hydride complexes, particularly with 5d metals, was further shown by Hrobárik *et al.*[6] who could substantially improve the correlation of computed and experimental ^{1}H NMR shifts by inclusion of SO contributions. It is not a coincidence that ^{1}H NMR shifts are the most prominent examples for HALA effects, as they are mainly transmitted by a Fermi-contact-type mechanism and thus atoms featuring a high s-orbital character are most susceptible to SO-induced effects.

This work focuses on the impact of SO coupling on ^{1}H but also ^{13}C NMR shifts. Based on quantitative relativistic methodology it is tried to unravel the relations between electronic structure and NMR shifts in diamagnetic 5d transition-metal and uranium hydride complexes as well as in organometallic uranium complexes. The fruitful insights gained by computational chemistry aim towards an improved prediction of NMR shifts and towards the rationalization of relevant trends.

1.1 Contributing Publications

As could already be estimated from the discrepancies of Mendeleev's Periodic Table (Figure 1), platinum is known to be significantly affected by relativ-

ity. Due to this and the general importance, particularly in catalysis, and the numerous (theoretical and experimental) previous studies, the work in Paper I focuses on square-planar Pt(II) d^8 hydride complexes, for which especially the influence of the ligand in *trans* position to the hydride is analyzed.

In Paper II, this work is extended by having a more detailed look at those *trans* ligand influences manifesting in the electronic structure and the ^{1}H NMR shifts, especially the SO contributions. The investigated linear Au(I) hydrides exhibit a notably smaller experimental database than the Pt(II) hydrides but facilitate a considerably improved interpretation due to their simple structure. Moreover, the dictum of the *gold maximum of relativistic effects*[7] may promise an even more pronounced impact of relativistic contributions. Notably, the very general results of these analyses pertain far beyond hydride shifts and to other nuclei.

Nevertheless, the already large SO effects for the Pt(II) and Au(I) complexes are outperformed by the giant SO effects analyzed for several uranium(VI) complexes. The results of Paper III are strongly related to the aforementioned work from 2012,[4] which is not directly contributing in this thesis. The method evaluation for those sparsely studied organometallic uranium(VI) complexes is followed by the prediction of unknown NMR signals, a deeper analysis of observed trends related to the geometrical position of the nucleus under consideration, and a careful study of various methodological aspects.

1.2 Personal Contribution to the Publications

For all contributing publications, I carried out basically all optimizations and NMR calculations as well as all kinds of molecular orbital (MO) analyses. The prediction of NMR shifts, the determination of correlations, trends and significant patterns in the electronic structures and relevant MO resulted mainly from my considerations.

For Paper I, P. Hrobárik did notice that the optimized structures at B3LYP/TZVP level which I initially used, tend to overestimate the experimentally known bond lengths. The final numerical values in the published tables (with PBE0/TZVP optimized structures) were produced by P. Hrobárik and V. Hrobáriková. However, this replacement did only changed the actual numbers

somewhat but not my previous analyses and conclusions. Besides, the addition of the BH_2 and the SiH_3 ligand in Paper I was encouraged by P. Hrobárik. He also plotted the hydride shielding tensors and calculated the QTAIM delocalization indices; the latter also for Paper III. For Paper III, P. Hrobárik helped finding out the differences in the NBO modules of ADF where one version provided incorrect results for actinide complexes. Overall, P. Hrobárik supported me with the interpretation, particularly for Paper I but also for Paper III.

A. V. Arbuznikov modified the MAG module of the ReSpect program for Paper I allowing me to calculate not only the 1c MO-MO analysis (in Supporting Information of Paper I) but also to trace back which operators are responsible for the calculated values.

J. Autschbach's contribution to Paper I and Paper III was providing us with a modified version of the ADF program which allowed the inclusion of the exchange-correlation (XC) kernel. He moreover gave me helpful notes on the different analysis opportunities in the ADF program and on the understanding of the corresponding outputs.

M. Kaupp gave clues for further investigations to all three publications and helped a lot with the interpretation. He had a huge impact on the final structure of Paper I, II and III and also of the verbalization of the results.

1.3 Outline

Following this introductory part, chapter 2 provides the necessary theoretical formalism embedded in the historical context. The subsequent chapter 3 summarizes and discusses the original research of this thesis. Chapter 4 gives a general conclusion encompassing all contributing papers, whereas chapter 5 describes some implications for continuing research. In the last chapter the original publications Paper I, Paper II and Paper III are attached as supplements together with their respective Supporting Information.

2 Theoretical Background

The results of this work were obtained by different computational methods. The theoretical background is briefly presented in the subsequent sections and reflects approximately the historical chronology; starting with the first ideas of quantization (section 2.1) and special relativity (section 2.2) made by Planck and Einstein, respectively, in the beginning of the 20th century, followed by the combination of Schrödinger's wave mechanics and Einstein's theory by Dirac in 1928 (section 2.3). Afterwards, the theory of special relativity awaited until the late 1970s for recognition of its fundamental significance for chemical systems and trends, which will be referred to in section 2.4. As the main topic of this work is related to NMR spectroscopy, in the following (section 2.5) the focus will be on methods for calculating NMR shielding. Unless stated otherwise, dimensionless atomic units are used in most equations, such that $m_e = 1$, $\hbar = 1$, $e = 1$, $4\pi\varepsilon_0 = 1$ and $c = 137.036$.

The real power of the computational chemistry applied in this work, based on relativistic quantum-chemical methods, is the ability to produce data from which one may be able to rationalize certain trends or a specific behavior. While the treatment regarding the theoretical formalism will not be extensive, it should help to understand the underlying calculations leading to the results in chapter 3. Additional computational details can be found in the enclosed manuscripts at the end of the thesis.

2.1 Molecular Quantum Mechanics

In Newtonian mechanics, all measured physical quantities like energy and momentum can obtain each value in a continuum. In atomic and subatomic systems, in contrast, those quantities are restricted to discrete values dependent on the system. This is called quantization and determines the name of the fundamental theory of nature at small scales, the *quantum mechanics*.

The quantum hypothesis was postulated by Planck in 1900 as a result of deriving *Planck's Law* which describes the black body radiation.[8,9] In 1905, the idea was extended by Einstein, who offered a quantum-based theory to explain

the photoelectric effect.[10] In the following years, this theoretical basis began to be applied not only by physicists but also by chemists and resulted in a new subfield of theoretical chemistry. The main focus of this so-called *molecular quantum mechanics* or *quantum chemistry* is to solve chemically related problems with computational quantum mechanics.

In contrast to macroscopic particles in Newtonian mechanics, electrons and protons do not exhibit deterministic behavior leading to the *wave-particle duality* and *Heisenberg's uncertainty principle*.[11] Hence, it is only possible to compute the probability of finding an electron in a certain region around the nucleus at a particular time. All physical information about a (non-relativistic) quantum chemical system is fully described by the solutions of the time-independent *Schrödinger equation* (SE)

$$H\psi = E\psi. \tag{1}$$

The quantum mechanical state, ψ, which is called *wave function* mainly for historical reasons, has no direct physical interpretation, but its absolute square can be interpreted as a probability density distribution (*Born interpretation*).[12] The many-electron Hamiltonian, H, corresponds to the total energy E of the system containing the kinetic energy of electrons and nuclei as well as the attractive and repulsive interactions of those particles. Within the adiabatic *Born-Oppenheimer approximation*[13] one can separate the movement of electrons and nuclei. The resulting electronic Hamiltonian is then given by the kinetic energy of the electrons and the potential-energy terms describing the electron-electron repulsion and the electron-nucleus attraction. In principle, determining the electronic structure of a molecule with this equation enables one to make deductions of its chemical properties. But, as Dirac once wrote, "[t]he underlying physical laws necessary for […] chemistry are thus completely known, and the difficulty is only that the exact application of these laws leads to equations much too complicated to be soluble."[14]

An exact solution for the SE can only be obtained for one-electron systems, whereupon the time-independent *electronic* SE for an electron for a given set of nuclear coordinates in a potential V in the absence of other electromagnetic fields is given by

$$h_{el}\psi_{el} = \left(V + \frac{1}{2m_e}\boldsymbol{p}\cdot\boldsymbol{p}\right)\psi_{el} = E\psi_{el}\,. \tag{2}$$

Here, h_{el} marks the one-electron Hamiltonian, including kinetic energy and nuclear attraction, and $\boldsymbol{p}$ is the momentum operator for the electron. Subscripts "el", denoting that only electronic states and energies are described, will be dropped as we will not discuss others in the following.

2.1.1 Hartree-Fock Theory

An approximate solution of the SE for the electronic Hamiltonian can be obtained with the *Hartree-Fock (HF) method* by reformulating the problem of the unknown N-electron wavefunction as one composed out of N one-electron functions ψ_i. Following the *variational principle*, which states that the exact ground state energy is always the lower limit to the energy obtained from calculations with an approximate wave function, the electronic energy can be obtained by searching the lowest energy.

The electronic energy of the N-electron system is then described by

$$E = \sum_i \langle\psi_i|h|\psi_i\rangle + \frac{1}{2}\sum_{i,j}\langle\psi_i|J_j - K_j|\psi_i\rangle \tag{3}$$

where J is the Coulomb operator and K is the exchange operator, which arises from the *fermionic* character of ψ_i. The antisymmetric exchange relation of Fermions led Pauli to the new physical quantity known as *spin*.[15] The spin is a fundamental quantum mechanical property which is not found in macroscopic objects. Pauli stated that no two electrons are allowed to be in the same quantum state, but in non-relativistic quantum mechanics, spin is phenomenological and cannot be explained. To account for the antisymmetry of wave functions with respect to electron permutations the electron spin is introduced in an *ad-hoc* manner by describing the one-electron wave-functions ψ_i by the product of a spatial and a spin part.

The unknown one-electron wave-functions ψ_i, also called molecular spin orbitals, can be approximated as *linear combinations of atomic orbitals* (LCAO), i. e. known basis functions, which are centered on the nuclei. The corresponding expansion coefficients are then determined after a series of op-

timization steps using the *Roothaan-Hall equations*,[16,17] a matrix representation of the HF equation:

$$\boldsymbol{FC} = \boldsymbol{SC\epsilon} \tag{4}$$

wherein $\boldsymbol{F}$ is the Fock matrix corresponding to the electronic Hamiltonian of the system, $\boldsymbol{C}$ is the coefficient matrix, $\boldsymbol{S}$ the overlap matrix between atomic orbitals and $\boldsymbol{\epsilon}$ is a diagonal matrix containing the MO energies. One starts with an initial guess of $\boldsymbol{C}$, which is used to construct the $\boldsymbol{F}$ matrix. By diagonalizing $\boldsymbol{F}$, new coefficients $\boldsymbol{C}$ are obtained. Those steps are repeated until self-consistency is reached (*self-consistent field*, SCF).

In the HF method, the movement of an electron is considered in the average field of other electrons. Hence, this model does not describe the instantaneous interactions of the electrons.

2.1.2 Density Functional Theory

By turning the many-body problem into many one-body problems interacting with the average field of the other nuclei and electrons, HF theory neglects electron correlation and, thus, a part of the real ground state energy, which is called the *correlation energy*. One way of including this Coulomb correlation is *density functional theory* (DFT), which is based on the electron density $\rho = \rho(\boldsymbol{r})$. According to the variational principle, the electron density that minimizes the energy is the best approximation for the ground state of the system, which allows again a self-consistent solution similar to the SCF method used in the wave-function formalism.

In 1964 Hohenberg and Kohn[18] formulated that the electronic ground-state energy E can be written with the help of an universal functional $F_{HK}[\rho]$ which is independent of the external potential V(**r**):

$$E[\rho] = F_{HK}[\rho] + V_{ne}[\rho] \tag{5}$$

where $V_{ne}[\rho]$ corresponds to the nucleus-electron interaction. Within the *Kohn-Sham (KS) approximation*[19] the unknown $F_{HK}[\rho]$ is divided into three parts, the Coulomb repulsion between the orbital densities, the kinetic energy of a so called KS reference system (non-interacting system of electrons) and the *exchange-correlation potential* $E_{XC}[\rho]$. The XC potential contains all unknown parts of the system such as the electron interactions not caused by the Coulomb

repulsion of the averaged charge density and the kinetic-energy difference between the real and the reference system. E_{XC} can be approximated within a *local density approximation* (LDA)[20], where the electron density is assumed to vary slowly, and the energy depends only on the local electron density $E_{XC} = E_{XC}[\rho(\boldsymbol{r})]$. However, this does not work well for molecular systems where the electron density can have steep changes. To account for non-uniform densities one can make use of the *generalized gradient approximation* (GGA), where the energy depends on the density and its gradient $E_{XC} = E_{XC}[\rho(\boldsymbol{r}), \nabla\rho(\boldsymbol{r})]$. If a fraction of the exchange part of the XC functional is replaced by the HF "exact exchange", this provides a *hybrid functional*.

The consideration of electron correlation, the favorable scaling with the number of electrons as well as compatibility with relativistic treatment makes DFT attractive for large many-electron systems.

2.1.3 Localized Molecular Orbitals

Upon diagonalization of the Fock or KS matrix, standard HF or DFT methods lead to delocalized orbitals, often called canonical orbitals, which tend to extend over the entire molecular system and transform as irreducible representations of the molecular symmetry point group. Other valid (non-canonical) representations of the solutions of the HF- or DFT type SCF equations can be obtained by *localized molecular orbitals* (LMOs). The LMOs provide a valence bond-type description of the wavefunction ψ and are closely linked to classical *Lewis structure* concepts. Thus, the LMOs are concentrated in a specific spatial region of a molecule resembling molecular bonds or lone pairs on a certain atom.

A frequently used localized orbital set are *natural bond orbitals* (NBOs).[21] The NBOs provide a complete and orthonormal set of localized maximum-occupancy orbitals whose leading *N*/2 members give the best possible Lewis-like description of the total *N*-electron density matrix. They are determined by searching all possible ways of localizing the bonds and lone pairs for the variationally optimal bonding, placing the maximum occupancy in the leading *N*/2 Lewis-type orbitals. Next to the Lewis-type NBOs, additional non-Lewis-type NBOs complete the span of the basis and describe the remaining delocali-

zation effects. Those delocalizations, needed to describe the density of a full electron pair, are already captured by the *natural localized molecular orbitals* (NLMOs) that can be considered to result from a transformation of the NBO basis set.[21,22]

2.2 Special Relativity

In 1905, the *annus mirabilis* also called the *Wunderjahr* in German, where Einstein's theories for the photoelectric effect[10] extended the quantum theory (cf. section 2.1), he published three additional papers that, in the end, should dramatically change the views on space and time as well as mass and energy and contribute substantially to the foundation of modern physics. His work "Zur Elektrodynamik bewegter Körper"[23] later became known as Einstein's theory of *special relativity.* The special relativity harmonizes Maxwell's equations for electricity and magnetism with the laws of mechanics and became a generally accepted and experimentally well-confirmed physical theory. The term *special* notes that it only applies in the special case where the force of gravity is omitted.

The theory of special relativity is based on two postulates, namely

1. *The Principle of Relativity*:

Physical laws (of electrodynamics, optics as well as mechanics) are the same in all inertial reference frames.

2. *The Principle of Invariant Light Speed*:

Light in a vacuum is propagated with a constant velocity, regardless of the motion of the emitting body or the observer.

As a consequence, all time and space coordinates in all reference frames are equivalent and time and space are combined into a single continuum known as space time. Thus, different events that occur at the same time for one observer can occur at different times for another. To be in accordance with the special theory of relativity, equations describing physics must be invariant to a so-called *Lorentz transformation* that illustrates how varying measurements of space and time can be turned into each other’s frame of reference.

Based on the postulates of special relativity, Einstein[24] predicted the equivalence of mass m and energy E, as expressed in the most famous equation in the field of physics:

$$E = mc^2 \tag{6}$$

where c is the speed of light in a vacuum.

Special relativity implies a wide range of consequences not only in physics but also in chemistry, which will be referred to in section 2.4. Unfortunately, the theory of special relativity is not in accordance with Schrödinger quantum mechanics as introduced in the previous section, which is therefore called a non-relativistic theory. On the one hand this is related to the fact that the electron spin does not appear in the SE and needs to be added *ad hoc*. On the other hand, the SE is not invariant with respect to the Lorentz transformations, i. e. it does not have the same form in every inertial reference frame and is thus in contradiction with the *Principle of Relativity*. However, the following section will display that special relativity can be combined with quantum mechanics to form relativistic quantum mechanics.

2.3 Relativistic Quantum Mechanics

The first relativistic corrections to the SE were published in the 1920s and are known as the Klein-Gordon equation.[25,26] This equation is Lorentz invariant and describes spin-zero particles correctly in a relativistic regime. However, it is not suitable for fermions like electrons.[27]

In 1928, the British physicist Dirac derived a quantum mechanical equation capable of matching with the requirement of relativistic covariance and considering spin. In his honor this equation is known as the Dirac equation (DE). It represents the foundation of *relativistic quantum mechanics* as it is consistent with both, the principles of quantum theory and the theory of special relativity.

2.3.1 Four-Component Dirac Equation

The DE represents a relativistic description of one electron which may be written as

$$h^D\psi^D = \begin{bmatrix} V & c\boldsymbol{\sigma}\cdot\boldsymbol{p} \\ c\boldsymbol{\sigma}\cdot\boldsymbol{p} & V-2c^2 \end{bmatrix}\psi^D = E^{rel}\psi^D. \quad (7)$$

Here, V is the electrostatic potential energy, c is the speed of light, $\boldsymbol{\sigma}$ a three-vector of the 2 x 2 Pauli spin matrices, $\boldsymbol{p}$ is the three-component momentum operator and E^{rel} is the energy, whereupon the superscript 'rel' for the relativistic energy is dropped from here on. Next to the known electronic states, the DE provides a continuum of negative energy solutions dominated by positronic states. Dirac introduced the notion that those negative-energy states, the so-called *Dirac sea*, are occupied, so that electrons of positive energy do not spontaneously fall into negative-energy states with the release of energy. Those transitions are forbidden by the *Pauli exclusion principle*.

The wave function ψ in the SE in section 2.1 is a scalar function, whereas the introduction of spin and the 4 x 4 matrix structure of the Dirac Hamiltonian h^D renders it necessary to turn to four-component (4c) objects as solution of the DE called *four-spinors*

$$\psi^D = \begin{bmatrix} \psi^U \\ \psi^L \end{bmatrix}. \quad (8)$$

ψ^U and ψ^L are called the *upper* and *lower* components, respectively, or more often the *large* and the *small* components, as for bound electronic states in atoms or molecules the lower components are much smaller than the upper components outside of the atomic cores. Both ψ^U and ψ^L are two-component (2c) spinors

$$\psi^U = \begin{pmatrix} \psi_1 \\ \psi_2 \end{pmatrix} \text{ and } \psi^L = \begin{pmatrix} \psi_3 \\ \psi_4 \end{pmatrix}, \quad (9)$$

which means that the components have certain transformation properties under rotations in spatial and spin coordinates that differ from those of vectors of the same dimension.

The components of the Dirac four-spinor are coupled and do not vary independently, which can be obtained directly from equation (7) resulting in

$$V\psi^U + c\boldsymbol{\sigma}\cdot\boldsymbol{p}\psi^L = \psi^U E \quad (10)$$

and

$$c\boldsymbol{\sigma}\cdot\boldsymbol{p}\psi^U + (V-2c^2)\psi^L = \psi^L E. \quad (11)$$

Thus, the coupling can be described as

$$\psi^L = X\psi^U \quad (12)$$

where

$$X = \frac{1}{2c}\left(1 + \frac{E-V}{2c^2}\right)^{-1} \boldsymbol{\sigma} \cdot \boldsymbol{p}. \tag{13}$$

If the components of the four-spinor are allowed to vary independently, self-consistent field-type equations in a basis set suffer from variational collapse. To avoid this one can use a basis set $\{\chi\}$ for the large and a basis for the small components that includes or only uses the function set $\{\boldsymbol{\sigma}\cdot\mathbf{p}\chi\}$ which is referred to as *kinetic balance* or *restricted kinetic balance*, respectively.[28]

2.3.2 Two-Component Approximation

As the large and the small component are related by equation (12), the small component can be formally eliminated to give the following eigenequation for the large component

$$(V + c\boldsymbol{\sigma} \cdot \boldsymbol{p}X)\psi^U = E\psi^U \tag{14}$$

which is a two-component (2c) relativistic framework without any new approximations. Approximations to the 2c operators lead to so-called *quasi-relativistic* methods. In many practically relevant scenarios, the quasi-relativistic operators are accurate enough in order to treat relativistic effects, especially, considering that computational results are affected by many other factors such as basis set limitations, approximations in the electronic structure model, and other approximations like neglecting solvents, temperature and so on.

One famous example which is frequently used in this work is the *zeroth order regular approximation* (ZORA[29,30]). The variationally stable ZORA operator can be obtained by rewriting equation (13), obtaining

$$X = \left(\frac{c}{2c^2 - V}\right)\left(1 + \frac{E}{2c^2 - V}\right)^{-1} \boldsymbol{\sigma} \cdot \boldsymbol{p}. \tag{15}$$

When assuming that $E \ll (2c^2 - V)$, the expansion in $\frac{E}{2c^2-V}$ is valid and the expansion to the zeroth order gives the ZORA[29] operator

$$h^{ZORA} = \boldsymbol{\sigma} \cdot \boldsymbol{p}\frac{K}{2}\boldsymbol{\sigma} \cdot \boldsymbol{p} + V \tag{16}$$

where $K = \left[1 - \frac{V}{2c^2}\right]^{-1}$.

In this case the assumption that $E \ll (2c^2 - V)$ in the core region remains valid as well as does the expansion which leads to the ZORA Hamiltonian. As a result, the ZORA Hamiltonian does not suffer from variational instabilities and can be used in all-electron calculations. The ZORA operator is gauge dependent, i.e. it depends on a change in the origin of the energy scale such that $V + \Delta$ does not translate into an eigenvalue $E + \Delta$. Hence, for core orbitals with large E the error of ZORA is substantial. However, ZORA is justified for valence orbitals in heavy atoms and thus quite accurate for valence-shell properties, which includes NMR chemical shifts, but not absolute shieldings (cf. section 2.5.4.2).[31,32]

2.3.3 Relativistic Effective Core Potentials

Elements from the lower part of the Periodic Table have a large number of core electrons. In order to reduce this number as well as the size of the basis set, an *effective core potential* (ECP) may be used. The ECP is an effective operator modeling the core electrons and therefore replaces the atomic all-electron potential such that only valence electrons are treated explicitly. An *relativistic* ECP[33], parameterized based on all-electron relativistic calculations of heavy atoms, can already be used to include a part of relativistic effects without performing a fully relativistic calculation using a non-relativistic valence Hamiltonian. This is especially interesting for the optimization of molecular structures, as calculations with ECPs do not need core basis functions and thus are faster and less memory demanding than all-electron relativistic calculations. Additionally, such structures are comparable with those obtained with all-electron relativistic ones, and far better than the non-relativistic ones. Since ECPs do not allow an accurate modeling of the electron density in the core region, they are not useful for the computation of NMR parameters of heavy nuclei. However, perturbational calculations, using SO-ECPs, were successfully applied for light nuclei in systems containing heavy atoms.[34]

2.4 Consequences of Special Relativity in Chemistry

In Figure 2 the tabular arrangement of chemical elements in the Periodic Table is indicated together with the overall trends of some physical and chemical properties, namely the atomic radii, the ionization energy and the electron affinity. The latter describes the energy released when an electron is added to an atom to form an anion, whereas the ionization energy is the energy needed to remove one electron from the atom. Generally, across a period, the atomic size decreases, ionization energy and electron affinity increases. Furthermore, going down a (main) group leads to increasing atomic radii, but decreasing ionization energy and electron affinity. To a first approximation those points are connected as an electron in a larger orbital should be less attracted to the nucleus and thus, is easier to remove or release less energy if it is added.

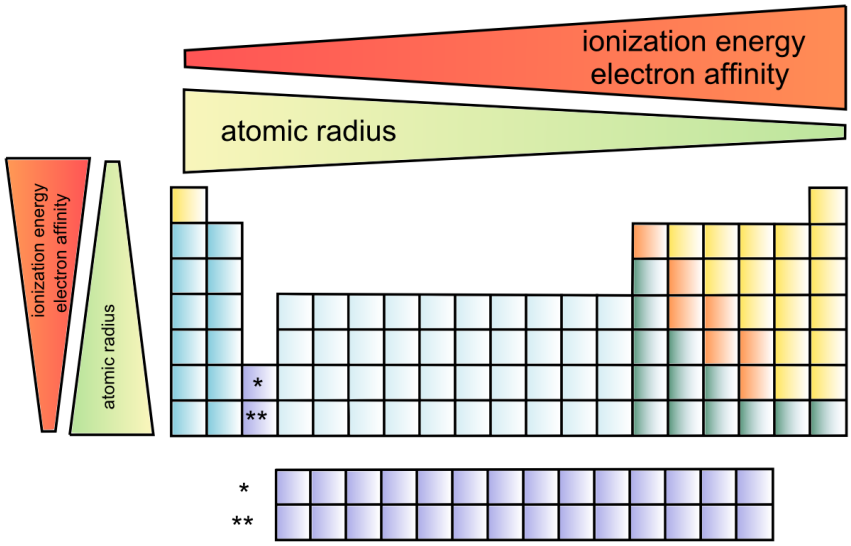

Figure 2. Trends of atomic radii, ionization energies and electron affinities in the Periodic Table.

Interestingly, there are some anomalies for those periodic trends which can be connected to different aspects. For lighter elements leading factors are the absence of radial nodes, which concerns the elements with 1s (H, He), 2p (Li-Ne), 3d (Sc-Zn) and 4f valence shell (Ce-Lu, Lanthanides), as well as the incomplete shielding of the nuclear charge caused by the scandide contraction.[35] For heavier elements, the lanthanide and actinide contraction has some impact, but deviations are mainly connected to *relativistic effects* (which already cause

a part of the lanthanide and actinide contraction).[36] Prototypical elements for which significant relativistic effects have been observed are 5d transition metals (TM) like Au, Hg, Pt and heavy 6p main group elements like Tl, Pb, Bi as well as the lanthanides and actinides.[2] The consequences of special relativity and, thus, the term *relativistic effects* can be expressed as a difference between the relativistic and the non-relativistic description of a quantum-chemical system. While the latter is related to the Schrödinger quantum mechanics (cf. section 2.1), relativistic methods can range from fully-relativistic (4c Dirac) to quasi-relativistic (2c) Hamiltonians, but can also use ECPs (cf. section 2.3).[37,38] Many applications in relativistic quantum chemistry are performed using DFT as it is applicable to large systems and provides an expedient treatment of many-electron correlation at relativistic level.

When Dirac himself published his famous relativistic wave equation in 1929, he did not expect an importance of his theory "in the consideration of atomic and molecular structure and ordinary chemical reactions"[14] as it was believed that valence electrons (important for chemical reactions) move rather slowly compared to the velocity of light. In the 1970s,[7,39–41], however, the relevance of relativity for chemistry became apparent, and it will be shown in the following that the effects caused by special relativity are unavoidable for explaining many anomalous behaviors in the general trends and unexpected properties of systems, particularly those containing heavy metal elements.

2.4.1 Dirac Quantum Numbers

To specify the state of a Dirac (hydrogen–like) atom, one can use *quantum numbers*, which are discrete sets of integers or half-integers referring to the quantization of observable quantities. In case of the Dirac atom those quantum numbers are:

1) The *principal quantum number*, $n = 1, 2, 3, \ldots$, that describes the electron shell of an electron.
2) The *azimuthal quantum number*, $l = 0, 1, 2, \ldots , (n - 1)$, that is usually denoted by the alphabetical symbols s, p, d, f, ... and describes the electron subshell of an electron, i. e. the orbital type.

3) The *total angular quantum number*, $j = |l \pm 1/2|$, that is typically written as a subscript of the alphabetical symbol of the azimuthal quantum number l, i. e. $p_{1/2}$, $p_{3/2}$, $d_{3/2}$, $d_{5/2}$ etc.
4) The *projection of the total angular momentum* along a specified axis, $m_j = -j, -j + 1, -j + 2, \ldots, j - 2, j - 1, j$.

In contrast to the Schrödinger description of the atom, the l number does not determine the orbital shape. The j and m_j numbers are the crucial factors dictating the orbital shape in the Dirac picture. Orbitals with the same value of j and m_j have the same angular distribution. Hence, the $p_{1/2}$ orbital has a spherical symmetry like $s_{1/2}$, $d_{3/2}$ has the same angular distribution as $p_{3/2}$ for the same m_j and so on.

2.4.2 Relativistic Effects across the Periodic Table

Probably the first broad overview on relativistic effects on the Periodic Table was given by Pyykkö in 1978.[41] It was a milestone on a long way towards the recognition of relativistic effects in understanding general trends of molecular properties. The three most frequently occurring relativistic effects are indicated in Figure 3 and are the *relativistic contraction* and stabilization of s (and to a lesser extent also p) orbitals, the *relativistic expansion* and destabilization of d and f orbitals, and the *spin–orbit (SO) splitting* for $l > 0$, i.e. of p, d and f orbitals. The first is due to the fast-moving electrons near the nucleus with velocity v, which – caused by relativity – exhibit an increased mass

$$m = m_0 \left(\sqrt{1 - \frac{v^2}{c^2}} \right)^{-1} \tag{17}$$

compared to their rest mass m_0. The increased mass in turn results in a smaller Bohr radius

$$a_o = \frac{\hbar^2}{me^2} \tag{18}$$

where $\hbar$ is the Planck constant and e is the elementary charge. The contraction and stabilization of all s and most p orbitals of many-electron systems is a *direct* consequence of special relativity. In contrast, the relativistic expansion and destabilization of d and f shells is called an *indirect effect*, as it is mainly caused by the better screening of the nuclear attraction by the relativistically

contracted s and p shells. Both effects are called *scalar* or spin-free relativistic (SR) effects. The SO splitting, in contrast, needs to be distinguished from the scalar relativistic effects. It is a direct consequence of the relativistic property of the electron spin that is able to couple to other angular momenta like the orbital angular momentum. This results in the total angular momentum $j = |l \pm 1/2|$. Thus, orbitals with $l > 0$ are split due to relativity, and the symmetry and shape of the p, d and f orbitals changes (cf. section 2.4.1).[2]

Especially the relativistic stabilization of the 6s orbital and the destabilization of the 5d orbitals are connected to a series of consequences for periodic trends and chemical systems containing gold and other heavy elements. Contrarily to the general trend indicated in Figure 2, some 6th-row elements like Au and Hg exhibit smaller radii compared with their 5th-row counterparts.[42] In addition, the 5d expansion facilitates ionization out of the d-shell whereas ionization out of the valence s-shell is hindered by the 6s contraction. For instance, this leads to a higher electron affinity for Au in comparison with Ag as well as to an ionization energy for Hg that is larger compared to Cd.[43]

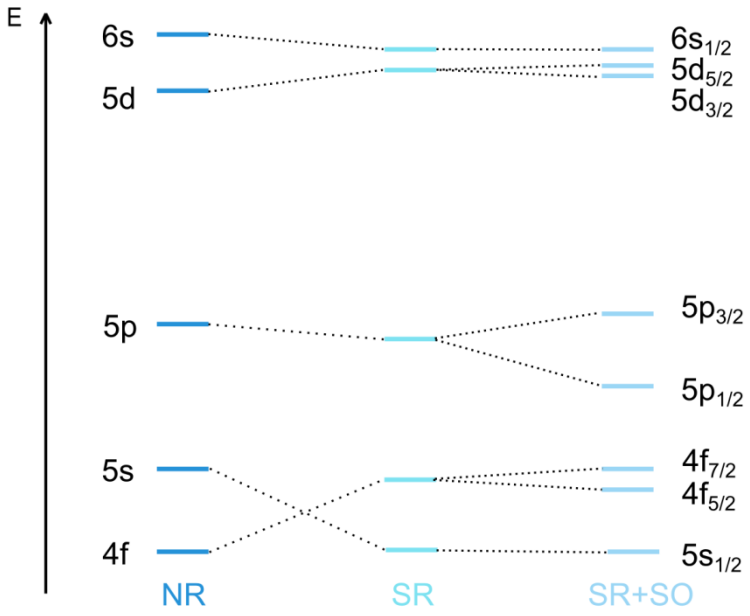

Figure 3. Qualitative energies for non-relativistic (NR), scalar relativistic (SR) and fully relativistic (SR+SO) valence orbitals/spinors of a 5d atom.

In addition to the scalar relativistic effects, SO effects can also modify periodic trends. For the light p elements the ionization energy and the electron

affinity are connected to the stability of the s^2, s^2p^3 und s^2p^6 configurations. For the 6p elements, in contrast, the p orbitals are not degenerate any longer, due to SO coupling, and thus the $s^2p_{1/2}{}^2$ configuration becomes decisive rather than s^2p^3.[35]

In light elements relativistic effects already cause fine structure effects but their magnitude significantly increases with increasing nuclear charge expressed by parameter Z. For valence shells – which are decisive for chemical properties – down a given group relativistic effects grow roughly as Z^2. Note, that it is the full nuclear charge that matters also for valence-shell orbitals even though they are kept away from the heavy nucleus by the inner ones.[44] This is due to nuclear 'tails' of the orbitals with $l \neq 0$, which reach inside the lowest shell all the way to the nucleus and cause a cascade of relativistic effects.[32] Nevertheless, the actual Z-dependence of relativistic effects of a given property depends on the property itself. The interplay between direct and indirect contributions consequently does not lead to a monotonous behavior.

2.4.3 Gold Maximum of Relativistic Effects

Pyykkö and Desclaux[7] found that the relativistic contraction of the 6s orbital had local minima in the 6th period for groups 1 (Cs) and 18 (Rn) but a pronounced maximum at the gold atom in group 11. This led to the so-called *gold maximum of relativistic effects*. The underlying reasons were analyzed later by Autschbach *et al.*[45] and can be traced back to the two possible valence configurations $d^{g-2}s^2$ and $d^{g-1}s^1$ (g = 4 for Hf and g = 12 for Hg). The s^1 configuration for the gold atom exhibits a stronger relative property change (e.g. for 6s binding energy, relativistic increase, orbital energies) than the s^2 configuration. Based on this it is not surprising that many properties of gold are affected greatly by relativistic effects, in particular compared to its lighter homologue silver. The probably most prominent example is the yellowish color of gold. With explicit calculations of the dielectric constants for gold, Romaniello and de Boeji[46,47] could show that the onset of the optical absorption is in middle of the visible (near 2 eV) in relativistic calculations, whereas it is shifted in the UV (approximately 3.6 eV) in a non-relativistic treatment. Thus, the stabilization of the 6s and destabilization of the 5d orbitals due to special relativity re-

duces the excitation energy from the top of the 5d band to the half-filled 6s band.[2]

Other properties of gold that are connected to relativistic effects are for instance the aurophilicity, i.e. a closed-shell interaction between two or more $5d^{10}$ Au(I) metal ions, and the shape of small gold clusters. The latter were found to be two-dimensional up to 11 Au atoms which could be explained qualitatively by strong 5d-6s hybridization enhanced by scalar relativistic effects.[48] Additionally, it was recognized that non-relativistic CsAu would be a metal, whereas it actually is a (relativistic) semiconductor.[36]

2.4.4 Relativistic Effects for Molecular Properties and Chemistry

Enumeration of all relativistic effects for molecular properties and chemistry would go beyond the scope of this work. However, a short overview of some consequences of special relativity should provide an overall impression to rate their importance for systems containing heavy elements.

Next to the already mentioned color of gold (cf. Section 2.4.3), also other colors could be traced back to relativistic effects. Those are, for instance, the yellow color of hexachloroplumbate(IV) ($PbCl_6^{2-}$) and the violet color of pentaphenylbismuth ($BiPh_5$). Both can be described as *relativistic colors* as they are attributed to the relativistic stabilization of the LUMO owing to its heavy-metal 6s character.[49] The corresponding Sn and Sb compounds, in contrast, are colorless.[2]

Another prominent bulk property is the liquid state of mercury at room temperature. Although an explicit proof was missing for a long time, the liquidity was early connected to relativistic effects causing a more stable $6s^2$ shell.[41] In 2013, Calvo *et al.*[50] used Monte Carlo simulations derived from accurate ground- and excited-state relativistic calculations for Hg_2 and could verify that the melting temperature for bulk mercury is lowered (by 105 K) due to relativistic effects. Besides, the strikingly high oxidation state of Hg(IV) in HgF_4 is caused by the destabilization of the 5d shell and the stabilized 6s shell.[51] This leads to higher possible oxidation states or rather a higher stability of those higher oxidation states for all 5d metals in comparison with their 4d analogs.[52]

Scalar relativistic effects often affect molecular structures by influencing angles and bond lengths. The latter become mostly contracted due to relativity. As found by Ziegler *et al*.,[53] this does not necessarily reflect the contraction of atomic orbitals but seems to be connected to a decreased repulsion between inner shells and the valence shell. Another explanation is given by Schwarz[54] attributing relativistic bond length contractions to relativistic effects on the molecular density.

Also SO effects can influence molecular structures.[36] One example is the octahedral structure of the $[Tl_6]^{6-}$ polyanion in Cs_2Tl_2O. Following the Wade's rules one would expect a Jahn-Teller distorted octahedral structure for a system with 24 valence electrons. However, relativistic SO-including DFT calculations revealed a gap at the Fermi-level which prevents the Jahn-Teller distortion. The closed-shell configuration was only observed if SO coupling is considered.[55]

Bond energies in general can become either weaker or stronger with consideration of relativistic effects. The expansion of 5d and 5f orbitals is typically connected with a less effective *Pauli repulsion* of the semi-core shells.[36] The resulting strengthening of bonds of many TM and actinides with ligands has a large influence on chemistry. An important field benefitting from relativity is catalysis, where large binding energies of side-products may be driving factors. For the catalytic methane activation by platinum

$$CH_4 + Pt^+ \rightarrow Pt(CH_2)^+ + H_2$$

the Pt-CH_2 binding energy of the metal carbene is 112 kcal/mol. Other catalytic reactions driven by relativity include, for instance, C-C couplings, alkene oxidations and alkadiene oligomerizations.[56]

A famous example for the consequences of the 6s stabilization is the lead-acid battery, used especially in automobile starter motors, whose voltage is mainly due to relativity. Recent calculations by Ahuja *et al*.[57] showed that the experimental electromotoric force is only well reproduced by the average relativistic value of about 2.1 V, whereas the average non-relativistic value was only 0.4 V.

Finally, SO coupling is connected with photochemical reactions of organic systems where a change of the spin state takes place, i.e. *phosphorescence* or *intersystem crossing*, and with spectroscopic methods like *electron spin reso-*

nance (ESR) and *nuclear magnetic resonance* (NMR) spectroscopy.[35] The ESR is restricted to systems with unpaired electrons which are not discussed in this work, but the basic concepts are related to those of NMR that will be explained in the subsequent chapter. Relativistic effects on NMR parameters can be significant and examples will be referred to after the introduction of NMR and the (relativistic) quantum chemical calculation of the NMR shielding.

2.5 Nuclear Magnetic Resonance

The spin was already introduced (cf. section 2.1) as a fundamental property of nature, like the electrical charge or mass. Just like electrons, discussed so far, nucleons have a spin and if they couple the nucleons can produce a nucleus N with an overall non-zero spin $\boldsymbol{I}_N$ resulting in a nuclear magnetic moment

$$\boldsymbol{\mu}_N = \gamma_N \boldsymbol{I}_N \tag{19}$$

where γ_N is the gyromagnetic ratio, a proportionality constant unique to each nucleus. A spin-½ nucleus, such as the ^{1}H and ^{13}C nuclei, possesses two spin states associated with the magnetic spin quantum number $m_I = \pm ½$. In an external magnetic field those states are separated due to Zeeman splitting (cf. Figure 4), and the transition between these magnetic energy levels due to absorbing and re-emitting of electromagnetic radiation of a specific frequency is called nuclear magnetic resonance, NMR.

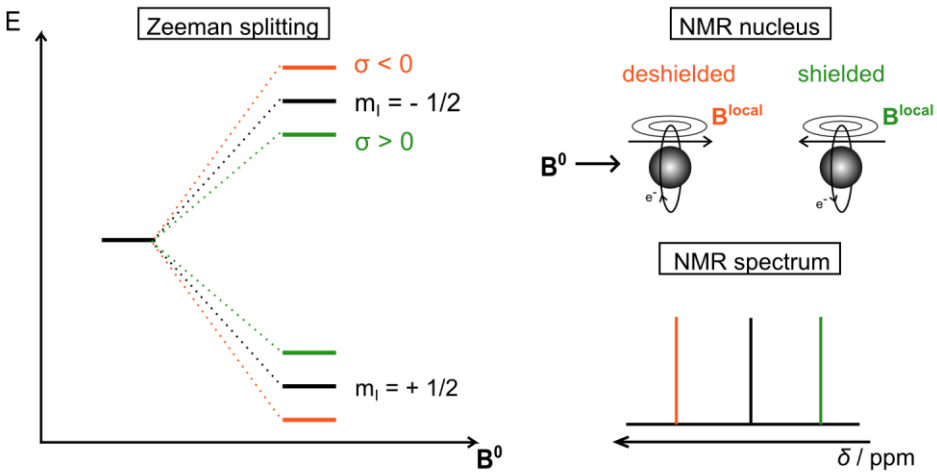

Figure 4. Separation of nuclear spin states due to Zeeman splitting for a bare nucleus (black) in comparison with a deshielded (orange) and shielded nucleus (green); the resulting NMR shifts are also indicated.

Experimentally, an electromagnetic pulse sequence in the field of radiofrequency (50-500 MHz) induces transitions of the nuclear spin. The NMR response is obtained by the free induction decay and converted into a frequency spectrum after Fourier transformation.

Resonance is observed if the resonance condition

$$\Delta E = \hbar\gamma_N \left| \boldsymbol{B}^{\boldsymbol{eff}} \right| \tag{20}$$

is satisfied. Only a bare nucleus would experience the applied magnetic field $\mathbf{B^0}$ whereas for atoms and molecules the nucleus experiences an effective field

$$\boldsymbol{B}^{\boldsymbol{eff}} = \mathbf{B^0} - \mathbf{B^{local}} = \mathbf{B^0}(1 - \boldsymbol{\sigma}). \tag{21}$$

This is due to an additional field $\mathbf{B^{local}}$ arising from the circulations of electrons induced by $\mathbf{B^0}$. In a free atom the nuclear magnetic shielding $\boldsymbol{\sigma}$ is always positive as the circulation of electrons generates a field which opposes the applied one (cf. shielded nucleus in Figure 4). In contrast, in molecules the lower symmetry hinders this textbook behavior. In dependence of the electronic distribution one can observe positive and negative $\boldsymbol{\sigma}$, thus, shielding and deshielding. Hence, the absolute shielding is characteristic for different nuclei with different chemical surroundings making the NMR spectroscopy such a powerful tool for chemical structure elucidation.

The nuclear magnetic shielding $\boldsymbol{\sigma}$ is a tensor quantity, since the environment in which the nucleus finds itself is generally not spherically symmetric. In liquid- or gas-phase measurements the motion of a molecule, rapid rotations and random collisions, lead to equal probability for all possible orientations and this isotropic average of the tensor is equal to one third of the trace

$$\sigma = \frac{1}{3}\left(\sigma_{xx} + \sigma_{yy} + \sigma_{zz}\right). \tag{22}$$

The isotropic shielding constant σ is given relative to the bare nucleus, which is not a practical reference. Therefore, *chemical shifts* are commonly measured relative to a standard substance, such as tetramethyl silane (TMS), used for ^{1}H and ^{13}C NMR. The chemical shift is defined as

$$\delta = \frac{\sigma_{ref} - \sigma}{1 - \sigma_{ref}} \approx \sigma_{ref} - \sigma \tag{23}$$

where the subscript *ref* refers to the reference.

2.5.1 NMR Shielding Contributions

In 1941, Lamb[58] proposed a classical model for an atom in an external magnetic field which induces a diamagnetic current density in the electron distribution, producing an induced field at the nucleus which is proportional to the applied field but opposite in sign. Ramsey[59,60] added a paramagnetic contribution for the nuclear magnetic shielding, such that

$$\sigma_{uv} = \sigma_{uv}^{d} + \sigma_{uv}^{p}; u, v = x, y, z \tag{24}$$

which so far neglects SO coupling and any other relativistic correction. Physically, the diamagnetic contribution σ^d is caused by the circulation of charges in the ground-state electron distribution. The diamagnetic contribution is always shielding, whereas the paramagnetic contribution σ^p is often deshielding but can be shielding as well. The paramagnetic contribution arises from mixing of certain excited states with the electronic ground state in the presence of the magnetic field. Providing a simple picture, one can imagine a tensor component along a given axis is produced by the circulation of electrons in the plane that is perpendicular to the axis and contains the nucleus (analogue to NMR nucleus in Figure 4). Thus, the symmetry of the electronic distribution around the nucleus determines the paramagnetic contribution. Destroying symmetry elements of the electronic distribution by substitution can lead to marked changes in σ^p.[61] Accordingly, symmetry restrictions can be applied to the approximate determination of the shielding as has be done by Griffith and Orgel[62] for the shielding of the center of an octahedral TM complex or by Buckingham and Stephens for the shielding of a hydride in octahedral and square-planar TM complexes (cf. section 2.5.3).[63,64]

2.5.2 Non-Relativistic Computation of NMR Shielding

The nuclear magnetic shieldings are so-called *response properties*, thus, derivative properties that represent the response of the electronic structure of a molecule to the presence of external or internal electromagnetic fields or other perturbations like nuclear displacements.[32] The calculations usually start with a field-free, i.e. unperturbed, electronic ground state which has been obtained by a single-point quantum chemical calculation with a given basis set and an electronic structure model such as DFT. The desired derivative property is then

calculated in the next step: for NMR shifts, a second-order property (double perturbed), a set of linear-response equations needs to be solved.

Based on perturbation theory, one can expand the electronic energy in terms of perturbation parameters (κ, λ), characterizing perturbations by external and internal fields

$$E(\kappa,\lambda) = E_0 + \kappa E_{10} + \lambda E_{01} + \kappa^2 E_{20} + \lambda^2 E_{02} + \lambda^2 E_2 + \kappa\lambda E_{11} + \cdots \tag{25}$$

with

$$E_{10} = \left(\frac{\partial E}{\partial \kappa}\right), E_{01} = \left(\frac{\partial E}{\partial \lambda}\right) \text{und } E_{11} = \left(\frac{\partial^2 E}{\partial \kappa \partial \lambda}\right). \tag{26}$$

If κ, λ are the component of the external magnetic field and the nuclear spin magnetic moment, respectively, E_{11} represents a component of the NMR shielding tensor

$$\sigma_{uv} = \left(\frac{\partial^2 E}{\partial \mu_u \partial B_v}\right); u, v = x, y, z. \tag{27}$$

The use of perturbation theory is justified as the external and internal magnetic fields give rise to energetically small effects, as compared to the dominating energetic of the nucleus-electron attraction and the electron-electron repulsion.[65] Assuming knowledge of the unperturbed wave functions of the ground (0) and excited states (n) with the energies E_0 and E_n, this energy derivative in second order reads

$$\sigma_{uv} = \langle\psi_0|H_{11}|\psi_0\rangle + 2\sum_{\mathrm{n}\neq 0} \mathrm{Re}\frac{\langle\psi_0|H_{10}|\psi_n\rangle\langle\psi_n|H_{01}|\psi_0\rangle}{E_0 - E_n} \tag{28}$$

with

$$H_{01} = \left(\frac{\partial H}{\partial \mu_u}\right) \text{ and } H_{10} = \left(\frac{\partial H}{\partial B_v}\right). \tag{29}$$

In analogy to equation (24), the first part of equation (28) represents the diamagnetic shielding contribution defined as the ground state expectation value

$$\sigma_{uv}^{d} = \frac{1}{2c^2}\left\langle\psi_0\left|\sum_i \frac{(\boldsymbol{r_{i0}}\boldsymbol{r_{iN}})\delta_{uv} - r_{i0,v}r_{iN,u}}{r_{iN}^3}\right|\psi_0\right\rangle. \tag{30}$$

whereas the *sum-over states (SOS)* expression indicates the paramagnetic part

$$\sigma_{uv}^{p} = \frac{1}{2c^2}\sum_{n\neq 0}\frac{\langle\psi_n|L_{0,v}|\psi_0\rangle\cdot\langle\psi_0|L_{N,u}r_{kN}^{-3}|\psi_n\rangle}{E_0 - E_n} + c.c. \tag{31}$$

where $\boldsymbol{r_{i0}}$ is the position vector for electron i and $L_{0,v}$ the angular momentum operator with respect to the chosen origin (gauge origin), whereas $\boldsymbol{r_{iN}}$ and $L_{N,u}$ are defined with respect to the observed nucleus N. The SOS expression is largely symbolic. As in DFT, response equations are solved to obtain the perturbations without explicit calculations of excited-state densities as those are typically not available in DFT.[32] The first matrix element in equation (31) represents the interaction of the external magnetic field with orbital angular momentum and is called the Orbital-Zeeman term (OZ), the second one describes the interaction with the nuclear magnetic moment and is called the paramagnetic spin-orbit term (PSO).[66] For the paramagnetic term, the action of the angular momentum operator couples an occupied with a virtual orbital which can be visualized as a 90° rotation about one of the axes of an occupied MO lying in a plane perpendicular to this axis. An overlap of the rotated orbital with a vacant orbital results in a non-zero matrix element and, thus, in a local induced field.

2.5.3 The Buckingham-Stephens Effect

In the 1960s Buckingham and Stephens[63,64] delivered the first studies explaining the low-frequency ^{1}H NMR shifts of d^6 or d^8 TM hydride complexes. They found paramagnetic shielding effects being responsible for those characteristic, strongly shielded, hydride signals for complexes with incomplete d shells.

The shielding Buckingham-Stephens σ^p contributions were analyzed in more detail in 1996 by Ruiz-Morales *et al.*[67] based on quantitative DFT calculations. The paramagnetic contribution was further separated into a parallel and two perpendicular terms regarding the direction of the applied magnetic field $\mathbf{B^0}$ and connected to the paramagnetic ring current $\boldsymbol{J_p}$ which is due to $\mathbf{B^0}$. They show that the shielding Buckingham-Stephens σ^p contributions can be traced back to the perpendicular components causing an off-center diatropic current loop around the hydride position, which is qualitatively illustrated in Figure 5 and often referred to as *Buckingham-Stephens effect*.

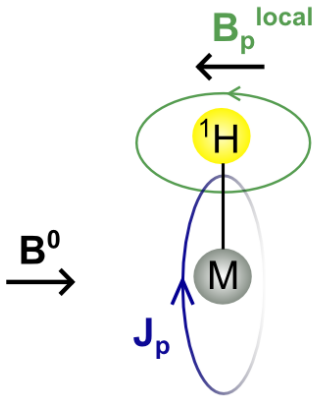

Figure 5. Schematic representation of the Buckingham-Stephens effect. A magnetic field perpendicular to the M-H bond produces a paramagnetic ring current inducing a shielding local magnetic field at the off-center position of the hydride.

2.5.4 Relativistic Computation of NMR Shieldings

For heavy-element systems, relativistic effects need to be included in a response calculation. Relativistic effects on NMR parameter can be automatically included either *fully relativistically* based on a 4c Dirac Hamiltonian for the kinetic and potential energy or *quasi-relativistically* based on (approximate) variationally stable 2c Hamiltonians (cf. section 2.3.2). The magnetic field-perturbed operators are obtained by introducing the magnetic vector potential $\boldsymbol{A}$ including the external static magnetic field and the field from the spin-magnetic moment. It is important to note, that once the magnetic potential is introduced into a (2c or 4c) Hamiltonian, it is necessary to deal with problems of an unphysical gauge invariance, which result when incomplete basis sets are used. As

$$\boldsymbol{B} = \boldsymbol{\nabla} \times \boldsymbol{A} \tag{32}$$

each $\boldsymbol{A} + \boldsymbol{\nabla} f(r)$ with an arbitrary scalar function f(r) results in the same magnetic field. The use of distributed gauge-origin methods such as the adoption of gauge-including atomic orbitals (GIAO)[68,69] basis sets solves this problem.

2.5.4.1 4c NMR calculation

The 4c magnetic field term as a consequence of the *minimal substitution* $\boldsymbol{p} \rightarrow \boldsymbol{p} + \boldsymbol{A}$ in the one-electron Dirac Hamiltonian reads

$$h_{mag}^{D} = c\boldsymbol{\alpha} \cdot \boldsymbol{A}. \tag{33}$$

For the calculation of magnetic-field-dependent properties with basis sets in the 4c framework one has to deal with the concept of *magnetic balance*[70] which is in close analogy to the already mentioned *kinetic balance* reflecting the coupling between upper and lower components of the Dirac wave function in the basis set (cf. section 2.3.1). Hence, in the presence of a magnetic field, the lower component basis set has to contain $\{\boldsymbol{\sigma}\cdot\boldsymbol{A}\chi\}$ functions in addition to the $\{\boldsymbol{\sigma}\cdot\boldsymbol{p}\chi\}$ set.[71]

Komorovsky *et al.*[72] developed the 4c-ReSpect/MAG program used in this work for the calculation of 4c NMR shielding tensors. It uses restricted magnetic balance (RMB)[72,73] and was extended for the use of GIAO basis functions.[73]

2.5.4.2 2c NMR Calculation[1]

The main part of the results in this work uses the ZORA framework and was carried out with the ADF ("Amsterdam Density Functional") package. ADF uses Slater-type orbitals (STOs) instead of the more commonly used Gaussian-type orbitals (GTOs). The ZORA part was developed by van Lenthe *et al.*,[29] the NMR shielding code by Wolff *et al.*[74] and later extended for calculations with hybrid functionals by Krykunov *et al.*[75] As already mentioned in section 2.3.2, the ZORA quasi-relativistic Hamiltonian is quite accurate for valence but not for core shells in heavy atoms. In ZORA NMR calculations, the absolute shielding can be affected by large errors from the core orbitals, as demonstrated for instance for ^{199}Hg shielding.[31] However, these errors depend on rather invariant core contributions, which cancel when the chemical shift is evaluated.

The starting point in the ZORA-DFT approach is the following eigenvalue problem

$$h^{ZORA}\Psi_{\mathrm{i}} = E_i^{ZORA}\Psi_{\mathrm{i}}\,. \tag{34}$$

For calculation of the NMR shielding tensor the magnetic field needs to be included in the ZORA Hamiltonian

$$h_{mag}^{ZORA} = \boldsymbol{\sigma}\cdot\boldsymbol{\pi}\frac{K}{2}\boldsymbol{\sigma}\cdot\boldsymbol{\pi} + V \tag{35}$$

[1] This Chapter is mainly based on the explanation given by Reference [74].

with $\boldsymbol{\pi} = \boldsymbol{p} + \left(\frac{1}{c}\right)\boldsymbol{A}$. The NMR shielding tensor is now obtained from the total energy using the response equation

$$\sigma_{uv} = \left(\frac{\partial^2 E^{ZORA}}{\partial \mu_u \partial B_v}\right) = \frac{\partial}{\partial B_v} \sum_{i}^{N_{occ}} \left\langle \Psi_{\mathrm{i}}(\mathbf{B}) \middle| \frac{\partial h_{mag}^{ZORA}}{\partial \mu_u} \middle| \Psi_{\mathrm{i}}(\mathbf{B}) \right\rangle. \tag{36}$$

The two-electron contribution to the NMR shielding response equations consists of the exchange-correlation (XC) and the exact-exchange kernels. The *normal* ADF implementation until recently neglected the response of the XC functional to the external magnetic field perturbation, but since 2013[76] the XC kernel contribution can be added and can have considerable impact when SO effects are large (cf. section 3.1.2.1).

To evaluate the expression above, the derivative with respect to μ_u is needed as well as the spinors $\Psi_{\mathrm{i}}(\mathbf{B})$ up to first order in the magnetic field. To obtain the latter, the ZORA equation (34) without magnetic field is solved (cf. equation (16)). The solution can be written in terms of atomic basis functions. Next the solutions of the ZORA equations including the external magnetic field up to first order can be calculated

$$h^{ZORA}(\boldsymbol{B})\Psi_{\mathrm{i}}(\boldsymbol{B}) = E_i^{ZORA}(\boldsymbol{B})\Psi_{\mathrm{i}}\,(\boldsymbol{B}). \tag{37}$$

Using GIAOs ensures that the calculated results do not depend on the gauge origin of the magnetic vector potential. The basis functions now depend on the external magnetic field. It is convenient to use an auxiliary basis set with the basis functions $\boldsymbol{\phi}_j$ and write the solution $\Psi_{\mathrm{i}}(\boldsymbol{B})$ in terms of these basis functions:

$$\Psi_{\mathrm{i}}(\boldsymbol{B}) = \sum_{j}^{N} u_{ij}\boldsymbol{\phi}_j\,. \tag{38}$$

Developed up to first order in the magnetic field one gets the expansion coefficients $\boldsymbol{u}_{ij}^{1}$ which build the so-called *U1 matrix* in ADF. The U1 matrix is important for finding the first-order change in the wave function, density, and current density due to a magnetic field. Using first-order perturbation theory the v-th component of the expansion coefficient are

$$u_{ii}^{1,v} = -\frac{1}{2}S_{ii}^{1,v} \; and \; u_{ji}^{1,v} = \frac{F_{ji}^{1,v} - \epsilon_i^0 S_{ji}^{1,v}}{\epsilon_i^0 - \epsilon_j^0} \; for \; i \neq j \tag{39}$$

with first-order overlap matrix $S_{ii}^{1,v}$ and zeroth-order eigenvalues ϵ_i^0.

2.5.4.3 1c NMR calculation

Next to 4c and 2c relativistic approaches, NMR calculations can be done at one-component (1c) perturbational level. In addition to the first-order σ^d (cf. equation (30)) and the second-order σ^p (cf. equation (31)) at non-relativistic level, the treatment of SO coupling as a third-order perturbation leads to the dominant SO corrections. The advantage of this formalism is that each contribution has a straightforward interpretation and is thus, highly illustrative.[65]

The most important SO contribution to the shielding of light nuclei in the vicinity of heavy atoms (*HALA, heavy-atom effect on light atom*) is given schematically as

$$\sigma_{uv}^{SO} = \frac{\partial^2}{\partial \boldsymbol{\mu}_u \partial \boldsymbol{B}_v^0}\left[\sum_{m,n\neq 0} P\left[\frac{\langle\psi_0|H^K|\psi_m\rangle\langle\psi_m|H^{SO}|\psi_n\rangle\langle\psi_n|H^{B^0}|\psi_0\rangle}{(E_0-E_m)(E_0-E_n)}\right]\right] \quad (40)$$

where P denotes a permutation operator. The hyperfine interaction between electronic and nuclear spin is represented by H^K which includes a Fermi-Contact (FC) and a spin dipolar (SD) term. H^{SO} illustrates the one- and two-electron SO operators and H^{B^0} the orbital Zeeman interaction with the external magnetic field.[66] Among these terms especially the coupling of the one-electron SO operator with the FC Hamiltonian is dominant for the HALA effect (cf. section 2.5.5 for dominant SO/FC mechanism). In contrast, for *heavy-atom effects on heavy atom* shielding (*HAHA*) also SD terms may have some larger influence and second-order contributions of σ^{SO} may be as important as the third-order SO contributions given above.[77]

In this work, 1c NMR calculations were done within the framework of the mixed 3rd order perturbation treatment by Vaara *et al.*[34] where the SO corrections are obtained from SR wave functions using quasirelativistic ECPs (cf. section 2.3.3). The FC hyperfine term is included in the KS SCF calculation as a finite perturbation, and afterwards the influence of OZ and SO operators is obtained by 2nd order perturbation theory for the perturbed (spin-polarized) MOs.

2.5.5 Relativistic Effects on NMR Shifts

As relativistic effects influence substantially the electronic structure of chemical systems, they can be recognized in spectroscopic properties reflecting this electronic structure. Already with light elements, relativistic effects are visible in the fine structure of atomic and molecular optical spectra, and they grow dramatically for systems containing heavy elements. Due to the relativistic contraction of orbitals close to the nucleus, there is a pronounced increase of electron density close to the nucleus. It is therefore not surprising that especially properties like the electron nucleus hyperfine coupling or NMR parameters are affected notably for heavy elements. Regarding the latter, influences on nuclear spin-spin coupling constants are usually due to scalar relativistic effects, as for instance shown by Zheng and Autschbach[78] for Hg-C of $[Hg(CN)_2]$ and $[CH_3HgCl]$ in solution. Benchmark data for the X-H couplings of a series of XH_4 molecules were also dominated by SR effects, whereas additional large corrections for X=Pb due to SO coupling were found.[79] Particularly pronounced SO effects were found for the spin-spin-coupling in the diatomic molecule Tl-I.[80,81]

Relativistic contributions for a heavy "relativistic" atom (HA), which is influencing its own NMR shielding (HAHA effect) can be very large for absolute shieldings, but they often largely cancel out in relative NMR shifts as shown for instance for ^{235}U NMR chemical shifts by Schreckenbach.[82] Benchmark relativistic calculations for the HX series (X=F,Cl,Br,I) showed that coupling terms, arising from the interplay between SO and field-dependent operators, are almost negligible for the isotropic shieldings of the heavy nuclei. In contrast, the ^1H shielding is affected substantially by the coupling terms.[72] While SR effects can also play a role, the relativistic effects for nuclei neighboring heavy atoms are often dominated by SO coupling.[66] The SO-origin of NMR heavy-atom shifts was first shown, already in 1969, by Nomura *et al.*[5] for hydrogen halides. NMR experiments revealed that the increasing charge of X = F, Cl, Br, and I, leads to decreasing shifts of atoms in the vicinity of X which is known as *normal halogen dependence* (NHD) and is one of the best known examples of the HALA effect (cf. section 2.5.4.3). The HALA effect was traced back to spin polarization created by the heavy-atom SO interaction that

propagates in the molecular electronic system much like in the *Fermi-contact (FC) mechanism* of indirect spin-spin coupling (cf. Figure 6).[83] The induced spin density is detected in the NMR shift through a FC interaction, which is a magnetic interaction of the induced electron spin with the atomic nucleus and only can occur for s-orbitals which have a non-zero electron density at the nucleus.

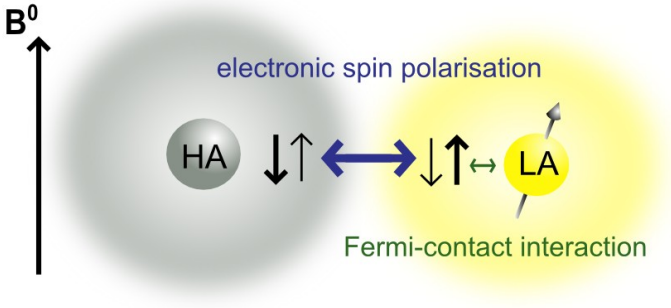

Figure 6. Schematic mechanism of the main FC-based HALA effect. The spin-orbit induced spin polarisation of the heavy atom (HA) extends throughout the system to the light atom (LA) affecting its nuclear spin states by hyperfine interactions.

In 1980, Cheremisin and Schastnev[84] used third-order perturbation theory to investigate the influence of SO effects on ^{13}C chemical shifts in methyl halides. Additional insights into the interpretation of SO effects in hydrogen halides were provided by Pyykkö *et al.*[85] using relativistically parametrized extended Hückel theory. Later, Schreckenbach and Ziegler[86,87] included effects of relativity non-perturbationally in calculations of NMR shieldings at scalar-relativistic DFT level within ADF. Wolff and Ziegler[88] extended the work to include SO coupling and also the FC interaction. Almost at the same time Malkin *et al.*[89] used DFT to calculate SO effects on NMR shielding constants. In the late 1990s Kaupp *et al.*[83] investigated ^{13}C shifts with DFT and double perturbation theory and could show that increasing charge of the heavy metal as well as the s-character of the light atom is related to decreasing ^{13}C NMR shifts. Later, they could show, that the spin-orbit coupling contribution to the shielding constant is inversely proportional to the energy gaps between occupied and virtual orbitals in a series of organomercury compounds.[90]

In more recent years, SO effects on chemical shifts of light atoms in TM complexes attracted some attention. In 2009, Hyvärinen *et al.*[91] examined

characteristic SO induced $^{1}H(CH_2)$ shifts for several Co, Rh and Ir polyamine aqua and alcohol complexes transmitted over three bonds from the d^6 center. In 2011, Hrobárik *et al.*[6] did 4c DFT calculations for hydride chemical shifts and noticed a substantially improved correlation between calculated and experimental shifts for all hydride TM complexes upon inclusion of SO contributions. Thereby, they showed that the Buckingham-Stephens effect[63,64,67] (cf. section 2.5.3) is not sufficient to explain all aspects of the origin of the low-frequency hydride signals for TM complexes with incomplete d orbital occupation. Significant SO contributions could also be observed for other nuclei in ZORA DFT calculations of ^{29}Si shielding for the Ni, Pd, Pt triad of hypervalent silicon complexes with direct Si-metal bond.[92] The same theoretical basis was used, when we predicted hydride ^{1}H NMR shifts in U(VI) hydride complexes in 2012 and found extremely large SO contributions up to +150 ppm.[4]

The currently mentioned examples display the importance of relativistic effects, particularly due to SO coupling, for the computation and especially for the interpretation of NMR shifts in systems containing heavy metal atoms. The subsequent results aim to extent those insights and consequences.

3 Results and Discussion

The actual results of this work, accompanied with the detailed description of the individual projects and the methodological details, can be found in the enclosed manuscripts at the end of the thesis. This chapter summarizes the main results of Paper I, Paper II and Paper III, outlining the connection between the projects and putting them together into an overall context.

First, the relativistic computational methods that were evaluated for the Pt hydrides in Paper I and for organometallic uranium complexes in Paper III are sketched. Subsequently, the relativistic effects in the electronic structure and their influences on ^{1}H NMR shifts (but also ^{13}C and ^{195}Pt) shifts in dependence of the *trans* ligand to the NMR nucleus for 5d TM complexes are discussed (Paper I and the even more general Paper II). Even larger relativistic effects on NMR shifts were found for diamagnetic uranium complexes, where a number of methodological aspects had to be evaluated to be sure of the quantitative predictive character of such calculations. This methodology is then used to make predictions for ^{13}C NMR shifts of experimentally known and ^{1}H shifts of so far unknown uranium complexes. Structural influences to the NMR shifts are illustrated from a localized point of view using NLMOs (Paper III).

3.1 Evaluation of Methods

For the accurate calculation of NMR chemical shifts a calibration of the DFT methodology for structure optimization as well as the NMR shift computation is required. The evaluation of the methods was performed for a series of square-planar *trans*-HPtL$(PMe_3)_2$ (L = NO_3^-, Cl^-, CH_3^-,…) (Paper I) and miscellaneous organometallic U(VI) complexes (cf. Paper III) for which experimental structures and shifts were available and could be compared to calculated ones. Afterwards, the methodology that provided the best reproduction of experimental values was applied also for the other systems in the work, where no validation with experimental parameters was possible, i. e. other TM and uranium hydrides (in Paper II and Paper III, respectively).

3.1.1 Structure Optimization

The quality of the optimized structures was assessed by comparing specific bond lengths with crystallographic data for these or closely related complexes. As hydrogen atoms near a heavy metal are difficult to locate experimentally, calculated Pt-P and Pt-L bond lengths were compared to experiment for the Pt(II) hydrides (Paper I), whereas the structures for the uranium complexes were evaluated in particular regarding the U-C bonds (Paper III).

The structure optimization has been carried out using the TURBOMOLE program package[93] with def2-TZVP basis sets[94–96] that include quasi-relativistic, energy-adjusted small-core ECP for the heavy central metals as well as iodine.[33,95] Method calibration involved variation of the functional, namely PBE[97] and its hybrid form PBE0[97,98] as well as B3LYP,[99,100] and adding dispersion-forces via Grimme's D3 model with Becke-Johnson damping,[101,102] and adding bulk solvent effects by the conductor-like screening model (COSMO).[103–105] The popular B3LYP functional tended to overestimate bond lengths but PBE0 was found to be a good choice for TM hydrides, with a standard deviation (SD) of 0.02 Å for Pt-P bonds, 0.01 Å for Pt-L bonds. For uranium complexes the results could be improved by using PBE0-D3 structures (SD of 0.02 Å for U-C bonds, 0.02 Å for U=O, 0.01 Å for U-N). Bulk solvent effects were found to be negligible.

3.1.2 NMR Shift Calculations

The PBE0(-D3)/def2-TZVP structures were used as a basis to evaluate the relativistic calculations of NMR chemical shifts. Two-component (2c) quasirelativistic ZORA[74,88] DFT calculations of nuclear shieldings have been carried out using the Amsterdam Density Functional (ADF) program[106] with all-electron Slater-type orbital basis sets of triple-ζ doubly polarized (TZ2P) quality,[107] and an integration accuracy of 5.0. The calculations used gauge-including atomic orbitals (GIAOs).[68] Four-component (4c) fully relativistic DFT calculations were performed at the matrix Dirac-Kohn-Sham (mDKS) level of theory with the ReSpect program.[108] The method combines GIAOs with restricted magnetically balanced (RMB) orbitals for the small component.[70,71] For the Pt and U atoms, Dyall's all-electron valence-double-ζ (Dyall

VDZ)[109] and valence-triple- ζ (Dyall TZ)[110] basis sets were employed, respectively. Fully uncontracted Huzinaga–Kutzelnigg-type IGLO-III basis sets[111] were used for the lighter ligand atoms. The calculated ^{1}H and ^{13}C nuclear shieldings σ were converted to chemical shifts δ = σ(TMS) - σ (in ppm) relative to the shielding of tetramethylsilane (TMS).

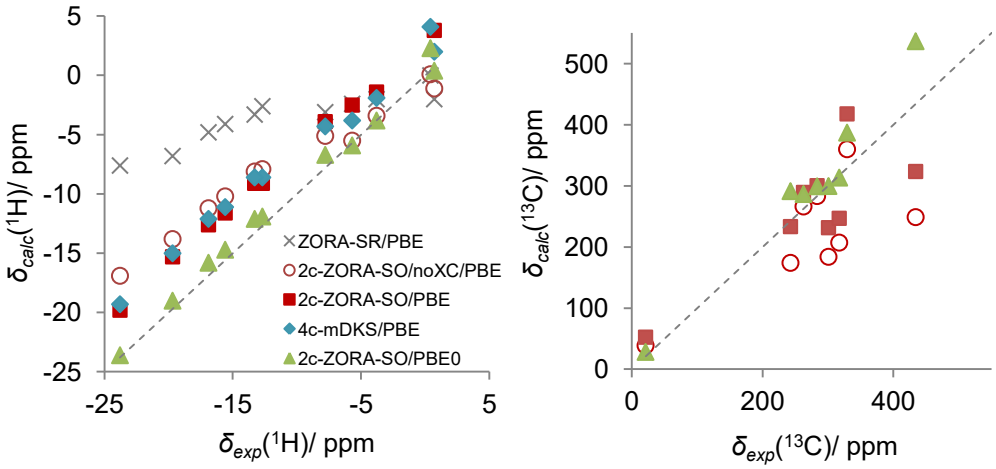

Figure 7. Computed vs. experimental NMR shifts (in ppm vs. TMS) for a series of *trans*-[HPtL(PMe_3)$_2$] complexes (left) and for various organometallic U(VI) complexes (right) (adapted from Paper I and Paper III, respectively). The dashed line represents the ideal agreement with experiment.

Figure 7 represents some of the computed shifts in comparison with the experimental ones, which will be discussed in the following. Initially, it can be noted that the scalar-relativistic ZORA results for the ^{1}H NMR hydride shifts in the platinum hydrides (gray crosses in Figure 7, left) tend to be insufficiently negative, showing without doubt importance of including SO effects to reproduce the experimental values. Inclusion of bulk solvent effects with the COSMO model did not improve computed shifts notably, and the effects tend to be overall low.

3.1.2.1 Importance of the XC Kernel for ZORA Calculations

The previous ZORA implementation of nuclear shieldings in ADF missed the linear response of the exchange-correlation (XC) potential (i.e. the shielding contribution from the response XC kernel) to the external perturbation.[76] For Paper I and Paper III, the original (red circles in Figure 7) and a modified (red squares in Figure 7) ZORA implementation were

compared for ^{1}H shifts in platinum hydride complexes and ^{13}C shifts of U(VI)-bound carbon atoms in some model complexes, respectively.

Caused by the impact of the electron spin-dependent part of the hyperfine interaction for the SO nuclear shielding effects, the influence of the kernel is connected to the magnitude of SO effects and affects almost exclusively the SO part of the nuclear shielding constants. The inclusion of the kernel is usually associated with an appreciable increase of the total value of NMR shifts (cf. Figure 7), making positive SO shifts more shielding and negative ones more deshielding. For the uranium complexes in Paper III the kernel contributions may amount up to ~30% of the total shifts, which means more than 50 ppm difference for the metal-bonded carbon shifts in some extreme cases (cf. Figure 7 right). Initially, the kernel contribution were expected to decrease when going from a GGA functional like PBE to its hybrid form PBE0, as 25 % of the PBE exchange have been replaced by exact exchange which do not enter the kernel. Instead, large increases of the kernel contributions were noticed upon going from PBE to PBE0 for complexes where the overall shift increases with EXX admixture (cf. Paper III).

The importance of the kernel terms is very similar at 4c- and 2c-levels and needs to be taken into account for accurate relativistic shielding computations. Note, that the implemented XC kernel in ADF is only available for a specific case, namly VWN5[112] for the LDA part and the GGA terms from PBE. Thus, if the XC kernel is desired in the ZORA calculations, one is limited to the PBE functional and its hybrid forms.

3.1.2.2 ZORA Calculations in Comparison with mDKS Calculations

The 4c-mDKS ReSpect version that was available for the time of this work did not allow GIAO calculations with hybrid functionals. Thus, the comparison of 2c relativistic ZORA-SO (including SO coupling) and the 4c mDKS results was only done with the PBE functional.

From Figure 7 (left) it is apparent that the ZORA-SO (red squares) and mDKS results (blue diamonds) with the PBE functional agree well with each other, and both reproduce the experimental trend in hydride shifts very well (coefficient of determination $R^2 > 0.98$) although the computed shifts are sys-

tematically too deshielded. Also in case of the corresponding ^{195}Pt shifts in the platinum complexes in Paper I as well as ^{13}C NMR shifts in the U(VI) complexes in Paper III, the 4c-mDKS results are overall close to the 2c-ZORA results. For the latter, only a few smaller model complexes were tested. Note, that the inclusion of the XC kernel in the modified ADF implementation is important for good agreement as the standard 4c-mDKS implementation includes a correct XC kernel treatment, too. The moderate differences between 2c- and 4c-results reflect technical differences between implementations, i. e. basis sets, grids, functionals and spin-orbit operators.

3.1.2.3 Calibration of Exact-Exchange Admixture

The exact-exchange (EXX) admixture of the DFT exchange-correlation functional has a pronounced importance for the NMR chemical shift calculations and was therefore analyzed most intensively. Initially, various publications (including our own in 2012[4]) using the 2c-ZORA implementation in ADF found 40 % EXX admixture to reproduce different experimental NMR values, e.g. ^{13}C shifts in organometallic uranium complexes[4] and ^{13}C as well as ^{15}N shifts in TM complexes.[113] However, those conclusions were made without considering the XC kernel in the calculation and, thus, reflected partly the compensation of the missing kernel. In contrast, the calibration for the present work was done with ZORA calculations of NMR chemical shifts with the previously neglected terms from the XC response kernel.

For Paper I, Figure 7 shows that the computed ^{1}H shifts at PBE level are systematically too deshielded by ∼3−4 ppm, but excellent agreement with the experimental values is found with the PBE0 functional (green triangles in Figure 7 left, SD = 0.9 ppm, R^2 = 0.99), i. e. with 25 % EXX admixture. This functional does also provide reliable ^{195}Pt shifts.

In Paper III, a more complicated picture was obtained for the revision of shifts in uranium complexes, which do not provide a systematic behavior upon increasing admixture of EXX. The computed shifts exhibit a strong dependence (particularly their SO contributions) on the EXX admixture in the functional, with both examples for increasing and decreasing SO contributions to the shifts with increasing EXX admixture (cf. Figure 7 right). In spite of

some uncertainties concerning the reliability of the relatively scarce experimental data, it turned out that (upon inclusion of the XC response kernel) a conventional PBE0 functional provides reasonable predictive quality (cf. green triangles in Figure 7 right, SD = 64.1 ppm, $R^2 = 0.95$) for the ligand NMR shift calculations of uranium(VI) complexes as well. While this level tends to overestimate the shifts somewhat for most of the complexes, it seemed to be the best compromise for systems with a positive or negative dependence of the shift on EXX admixture (15 % EXX would perform better for the former, 40 % for the latter). Up to now, the rather small experimental database of U(VI)-bound carbon atoms has not allowed a more accurate calibration.

3.2 Role of SO Effects for *trans* Influences on Ligand NMR Shifts in TM Hydrides

The *trans* influence can be described as the general impact of a ligand L in *trans* position to the observed nucleus. Hence, a discussion of the *trans* influence is usually connected to a certain symmetry requirement for the investigated systems. For Paper I, square-planar Pt(II) hydrides were chosen due to their general importance, particularly in catalysis, and extensive previous available studies. Paper II provides an even more general picture of such *trans* effects. While the most detailed analyses are done for linear Au(I) hydrides, square planar d^8 as well as (pseudo-)octahedral d^6 hydride complexes can be better understood as well (cf. Figure 8).

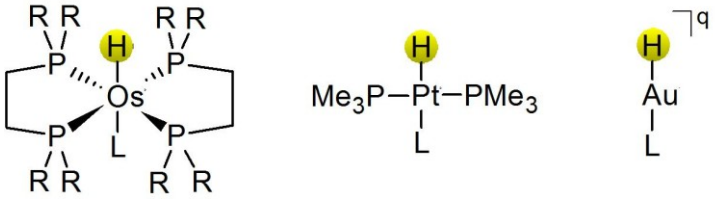

Figure 8. Investigated *trans* ligand sets of d^6 (Os^{II}), d^8 (Pt^{II}), and d^{10} (Au^{I}) 5d transition-metal hydride complexes.

The evaluation of NMR methods did already show the need for considering SO effects in the applied calculations to reproduce experimental values for

heavy element systems. Moreover, the following results will illustrate the large impact of ligand effects on the electronic structure and therefore the NMR shifts, which are strongly dominated by SO effects.

3.2.1 General *trans* Ligand Influences on Bonds and NMR Shifts

The *trans* influence is typically defined as the ability of a ligand L to weaken the metal-ligand bond *trans* to itself. It is therefore not surprising, that the bond length in *trans* position correlates with the considered ligand as shown in Figure 9, representing the lengthening of the (computed) Pt–H bond with increasing σ-donor ability of the *trans* ligand in the square-planar d^8 Pt(II) hydrides (Paper I). In addition, Figure 9 reveals that also the ^{1}H shifts correlate with the *trans* ligand. In Paper II, both correlations were also found for other TM hydrides like the linear d^{10} HAuL or pseudo-octahedral d^6 HOsL(dhpe)$_2$ cases pointing to surprisingly general effects of *trans* ligands in 5d complexes.

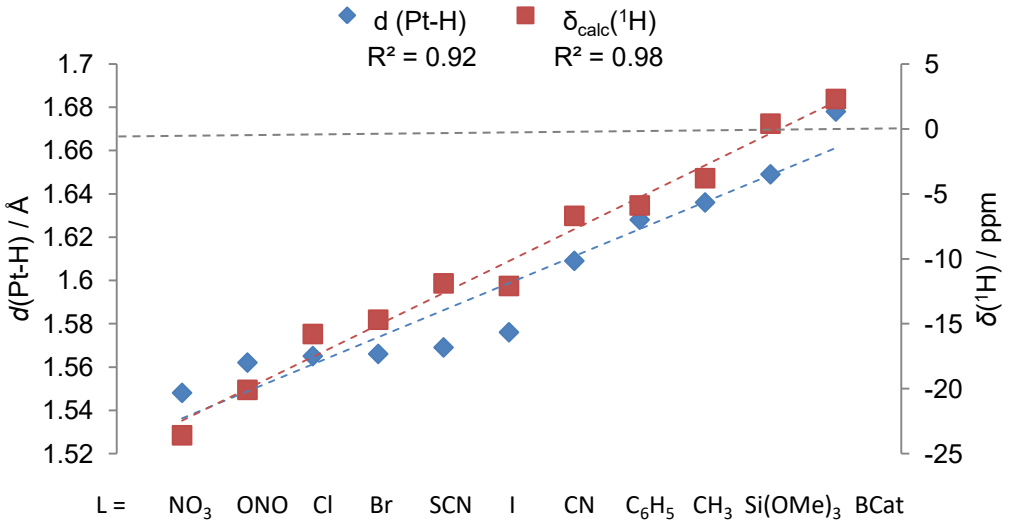

Figure 9. Correlation between optimized Pt–H bond lengths and computed ^{1}H hydride shifts with L in the *trans*-[HPtL(PMe$_3$)$_2$] series (2c-ZORA-SO/PBE0/TZ2P results, adapted from Paper I).

While such plots might suggest a direct causal relationship between bond length and ^{1}H NMR shift, closer analysis showed almost no direct distance dependence of NMR contributions for a given complex. The often observed correlation between measured shielding and M-H distances has an indirect rather than direct origin, as both properties are affected by changes in covalency

and polarization of the metal d (and partly p) orbitals by the *trans* ligand influence.

Table 1. NPA atomic charges (q) at the hydride ligand, the composition of the M-H bonding NLMOs and the SO part of the isotropic shielding ordered by *trans* ligand strength (exemplarily adapted from Paper I and II).[a]

Ligand L	NPA q(H)	NLMO (M-H) %M	M(6s)	M(5d)	$\sigma^{SO}(^1H)$ [ppm]
$HPtL(PMe_3)_2$					
NO_3	-0.11	38	23.5	76.2	14.9
Cl	-0.15	34	25.5	73.8	10
CN	-0.25	27	24.7	74.8	3.1
CH_3	-0.31	21	23.7	75.4	1.2
BCat	-0.38	13	30.6	68.3	-2.8
HAuL					
H_2O	-0.18	43	80.5	19.3	10.3
NH_3	-0.25	41	80.0	19.8	4.7
AsH_3	-0.28	41	86.2	13.6	-2.5
PH_3	-0.31	40	86.3	13.5	-6.6

[a] ZORA-SR/PBE0/TZ2P results.

Table 1 gives insight into the electronic structure from a localized point of view by providing the composition of the M-H bonding NLMOs for some ligands from Papers I and II. It demonstrates that the metal character in the M-H bond is significant and larger for systems with weaker *trans* ligands. For the d^8 Pt hydrides this metal character is dominated by the 5d orbitals whereas for the d^{10} Au hydrides the 6s contribution is predominant. Stronger ligands tend to lead to a rehybridization of the metal atom towards more 6s and less 5d character. The more covalently bound ligands with strong *trans* influence polarize the relevant metal atomic orbitals away from the M−H bond, which is accompanied by a decrease of the M−H bond covalency (cf. increasing NPA atomic charges).

Remarkably, σ-donating/π-accepting ligands with a very strong *trans* influence are shown to even invert the sign of the ^1H shifts (cf. Figure 9 for Pt hydrides). This influence of the *trans* ligand was found to be even more pro-

nounced for the Au hydrides in Paper II and can be mainly traced back mainly to the SO shielding contribution (cf. Table 1), which will be analyzed in the following chapter. The *trans* ligand affects also the shift of the metal center itself, although to a lesser extent, as was shown for the Pt hydrides in Paper I (see below).

While this was not analyzed in as much detail, a similar influence of the *trans* ligand holds also for ^{13}C NMR shifts in square-planar d^8 Pt(II) and Au(III) complexes, where the change of the *trans* ligand appeared to be even more important for the ^{13}C NMR signal than the metal center (cf. Figure 10).

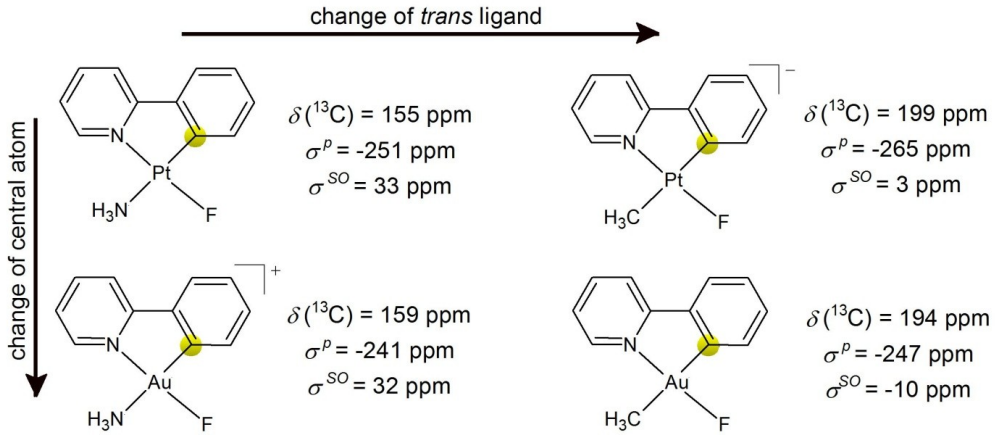

Figure 10. Computed ^{13}C NMR shifts (together with paramagnetic and SO shielding contributions) for isoelectronic d^8 Pt(II) and Au(III) complexes with a weak (NH_3) and strong (CH_3^-) *trans* ligand (2c-ZORA-SO/PBE0/TZ2P results, adapted from Paper II). The relevant carbon nucleus is indicated.

3.2.2 Analysis of Shielding Tensor Contributions and Components

In Papers I and II, a clear and strong dependence of the nuclear hydride ^{1}H NMR shift on the nature of the *trans* ligand was obtained for 5d metal hydrides. The separation of the calculated shielding tensors into the well-known diamagnetic (σ^d) and paramagnetic (σ^p) terms and into a spin−orbit (σ^{SO}) term gave insights regarding the question, which part is affected most.

In Figure 11 it can be seen that the isotropic σ^d remains almost constant across the series of *trans* ligands whereas the paramagnetic and SO shielding contributions vary more pronouncedly and go roughly in parallel. It is obvious, that the σ^d and σ^p contributions alone explain neither the large low-frequency hydride shifts for complexes involving ligands with weak *trans* influence nor the positive ^{1}H shift values recorded for complexes with strong *trans*-influence

ligands. Thus, overall the *trans* ligand influence on hydride NMR shifts tends to be dominated by SO effects, which can change sign from appreciably shielding for "weak" *trans* ligands to appreciably deshielding for "strong ones". The sign and magnitude of the overall SO effects on the ^{1}H shieldings depends fundamentally on the *trans* ligand not only for these d^{10} complexes but in a similar way also for d^{8} complexes, while SO effects and thus the overall trends are less pronounced for d^{6} systems.

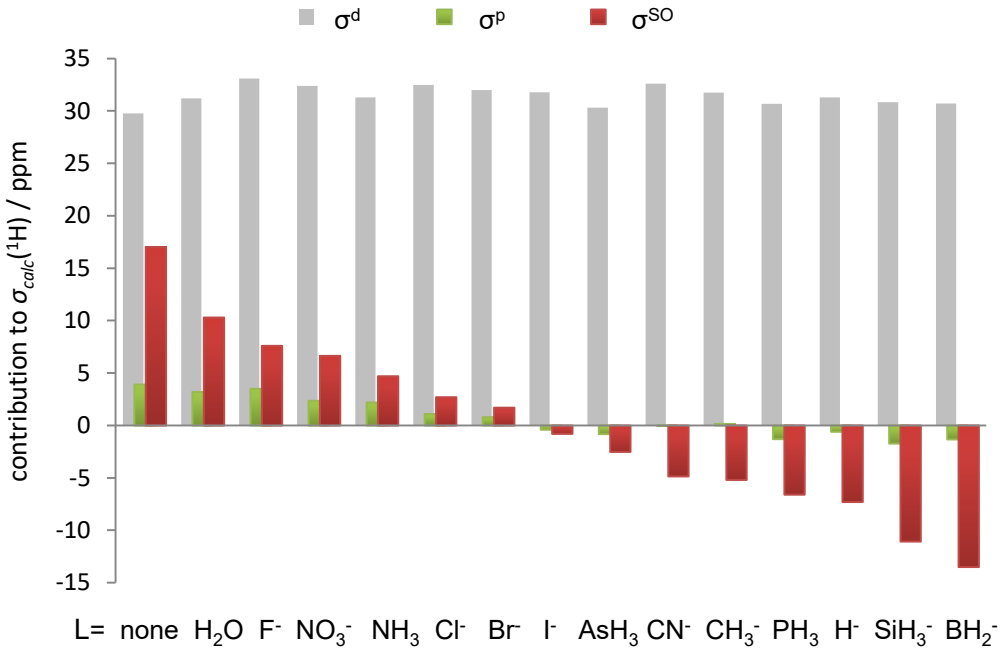

Figure 11. Calculated diamagnetic (σ^{d}), paramagnetic (σ^{p}) and spin-orbit (σ^{SO}) contributions to the ^{1}H NMR isotropic shielding in the $HAuL^{q}$ (q=0, -1) series (2c-ZORA-SO/PBE0/TZ2P results, adapted from Paper II).

The dominance of SO contributions can be used to explain the poor (inverse) correlation of hydride ^{1}H shifts and the corresponding ^{195}Pt shifts that was obtained in Paper I. Based on the Buckingham-Stephens model,[63,64,67] the paramagnetic ring currents within the incomplete metal d-shell that cause the well-known shielding of the hydride atom due to a diatropic current in this off-center position, should lead to a deshielding of the metal nucleus. However, in contrast to the ^{1}H shifts which are attributed to a HALA effect and, thus, determined by the SO shifts arising from SO coupling of the metal, the metal itself experiences a HAHA effect. These are essentially atomic in nature and thus largely cancel for relative shift trends (cf. section 2.5.5).[114–116] Thus, in comparison with their total shifts, ^{195}Pt shifts are not that much affected by SO

effects (about 7 ppm) and they therefore experience less dramatic changes with the ligand L in the investigated Pt hydrides (but they were, interestingly, found to be influenced by HALA effects for heavier halide *trans* ligands, Paper I).

A separation of the shielding contribution into tensor components was made, with $\sigma_{\parallel}$ parallel and $\sigma_{\perp}$ perpendicular to the M-H bond (cf. Figure 12). All shielding contributions were found to be highly anisotropic and the components are affected quite differently by the *trans* ligand: Whereas all components of the diamagnetic part remain almost constant by changing the *trans* ligand, the main trends of the isotropic paramagnetic and SO shieldings were found to be dominated almost exclusively by the perpendicular shielding tensor components. The parallel component does not change as much for the different ligands. Overall, the perpendicular σ^{SO} components dominate the trend of the ^{1}H hydride shifts. The general importance of the perpendicular σ^{SO} components is exemplary presented in Figure 12.

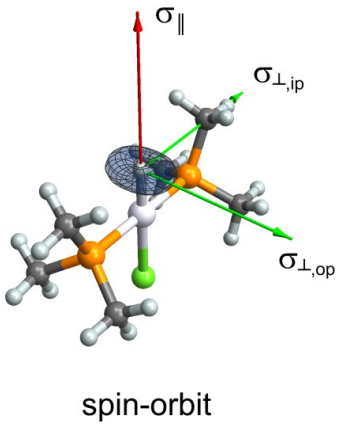

Figure 12. Spin-orbit hydride shielding tensors in *trans*-[HPtCl(PMe$_3$)$_2$], represented as polar plot of functions (a green arrow indicates a shielding contribution, a red one a deshielding contribution). Adapted from Paper I.

3.2.3 Analysis of the Electronic Structure

In Paper II, *trans* ligand effects on electronic structure were analyzed in detail, particularly for linear d^{10} Au(I) hydrides. Figure 13 summarizes the results.

The most notable and by far most important trend among the molecular orbitals (MOs) along the series with increasing *trans* influence is the strong destabilization of the 2σ MO at scalar relativistic level (cf. Figure 13). The destabilization of this σ-type MO in turn, translates into very different σ-/π-

mixing if SO coupling (SOC) is included. It was possible to transfer atomic spinor considerations, which are well understood, to an understanding of the molecular spinors, as the SOC in the investigated complexes is clearly dominated by the metal orbitals. SO effects for a given spinor depend strongly on a) relative energies between the scalar-relativistic MOs contributing to a given spinor, and on b) the Au(5d)/Au(6p) character of the spinor, as the ligand orbitals and the Au 6s-orbital do not contribute to the SOC. While many occupied and virtual MOs are affected by SOC, the largest impact regarding the *trans* influence was connected to the 2σ MO. 2σ has significant Au(5d) [and some Au(6p)] character and is energetically close to the almost pure 5d-type 3π/4π MOs (cf. Figure 13). Due to SOC, 2σ mixes extensively with these π-type MOs, and it contributes mainly to two spinors (cf. Figure 13), which both exhibit metal-AO $m_j = \pm 1/2$ character. The energetically lower of the resulting spinors may be interpreted as having more $d_{3/2}$ participation, whereas $d_{5/2}$ character should dominate in the energetically higher-lying one. The degree of SO-mixing, and thus the dominance of σ- or π-character in each of those spinors, is correlated with the energy position of the involved SR-MOs. SO-mixing benefits not only from a small energy gap between the relevant SR-MOs but also from an MO order where the π-orbitals are above the corresponding σ-orbital. This is due to the fact, that the σ component of the $m_j=\pm 1/2$ metal orbitals remains constant in energy, whereas the π components are SO-stabilized on average. In case of the Au(I) hydrides, the mixing of 2σ into the π-MOs becomes more pronounced due to the destabilization caused by stronger *trans* ligands, but once the 2σ has moved above those π-levels, mixing becomes less favorable, resulting in a HOMO-3 with increasing σ-character. Thus, the high-lying HOMO-3 (expected to exhibit mainly $5d_{5/2}$ character) changes its symmetry properties from π- to σ-character with increasing *trans* influence, whereas the lower-lying parental spinor (expected to exhibit mainly $5d_{3/2}$ character), experiences the reverse effect (cf. Figure 13). As exemplary shown in Figure 13 this parental spinor is the HOMO-5 for complexes with a weak *trans* ligand and the HOMO-4 for stronger ones.

Similar *trans* influences on electronic structure were also observed for other TM hydrides, namely the Pt(II) and Os(II) hydrides shown in Figure 11.

The most striking similarity is the dramatic destabilization of one σ-type SR-MO by a stronger *trans* ligand. The effects of energetic destabilization, together with an enhanced M($6p_z$) character, translates into changes for the SOC-mixing in the 2-component framework, where spinors with large σ-character are shifted above π-type spinors by strong *trans* ligands.

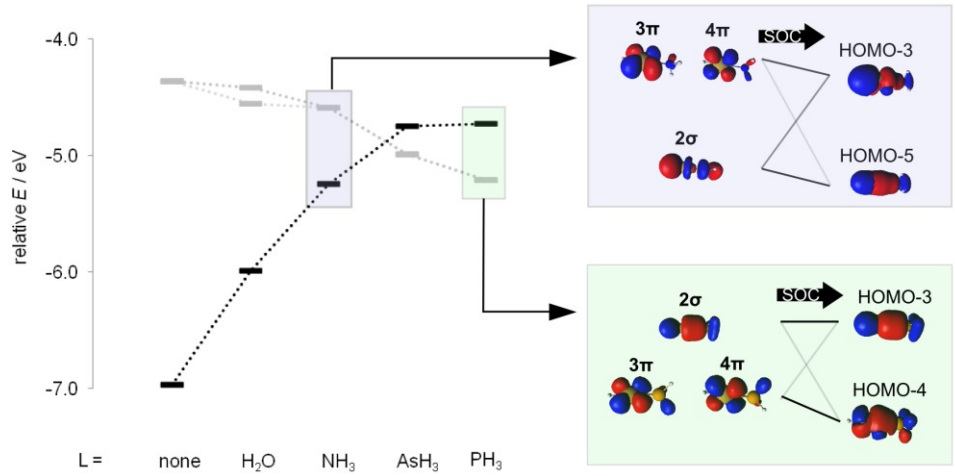

Figure 13. Energies for the most important scalar-relativistic frontier MOs for the neutral HAuL series (ZORA-SR/PBE0/TZ2P results), together with their isosurface plots (±0.03 a. u.) and their SOC-induced mixing to 2-component spinors for one weak (NH_3) and one strong ligand (PH_3).

3.2.4 MO Analysis of σ^{p+SO} Contributions to ^{1}H Shielding

Based on relativistic ZORA-GIAO calculations, that separate the SO- (and paramagnetic) shielding term σ^{p+SO} into contributions from individual couplings between occupied and virtual canonical spinors, a bridge between the electronic structure and the computed NMR signals can be built. The preliminary analyses in Paper I were significantly improved upon in Paper II, where we noted that large SO-mixing causes notable differences between the basic character of SR-MOs and SO-spinors (see above). Therefore the σ^{p+SO} contributions that are calculated within the MO analysis in ADF cannot be separated easily into a paramagnetic and SO term. Moreover, due to the large SO-mixing, the symmetry labels of the original SR-MOs are not always suitable to characterize a given spinor. These considerations led to a more detailed and improved analysis in Paper II, on which we will focus in the following.

The σ^{p+SO} values arise from numerous contributions, but there are only a few that stand out by being larger or by dictating the main trends and differences between the complexes with different *trans* ligands. In case of the Au(I) hydride complexes, those contributions were found to arise mainly from mixed σ/π-type spinors, namely the HOMO-3 and its parental spinor (cf. Table 2), that were discussed in the previous chapter (cf. Figure 13).

Table 2. Composition of the most relevant occupied 2-c spinors, and spinor contributions to ^{1}H shieldings for two ligands of the HAuL series (adapted from Paper II).[a]

L	MO (spinor)	σ character [%]	π character [%]	1s(H) [%]	5d(Au) [%]	6s(Au) [%]	6p(Au) [%]	σ^{p+SO} contr. [ppm]
NH_3	HOMO-3	9	90	12	70	2	2	20.3
	HOMO-5	66	32	22	49	0	3	-11.8
PH_3	HOMO-3	86	13	17	33	5	6	-0.5
	HOMO-4	16	82	3	79	2	1	-1.0

[a] 2c-ZORA-SO/PBE0/TZ2P results.

These spinors exhibit significant Au(5d) [and some Au(6p)] character, giving rise to large SOC, but they also contain a reasonable amount of 1s(H) character. The latter is important for promoting an effective FC mechanism for the transfer of the SOC effects. As high-lying occupied spinors provide a smaller energy denominator (cf. equation (40)) for coupling with virtual spinors, the HOMO-3 has a pronounced effect in comparison with its lower-lying parental spinor . While it has been known for a relatively long time, that the 1s(H) character and the energy differences between occupied and virtual spinors crucially influence the SO shielding contributions,[83] Vícha *et al.* first emphazised the d-orbital participation to be decisive in 2014.[117]

The large shielding SO contribution of about 20 ppm from the HOMO-3 of $HAuNH_3$ (cf. Table 2) is not compensated by any of the other MO couplings and therefore causes mainly the overall positive ^{1}H SO shielding. This can be traced back in particular to a combination of the large 5d-π-character permitting non-zero Zeeman matrix elements (providing the coupling to the external magnetic field) with SO-induced σ-character giving rise to FC hyperfine matrix elements (coupling the nuclear and electronic spins at the

hydrogen atom). Surprisingly, these large SO contributions to shielding diminish for the strong *trans* ligands, as shown for PH_3 in Table 2. The absence of a strongly positive contribution allows the eventual change of sign for σ^{SO}, and thus of the total ^1H shift, with the strong *trans* ligand (cf. Figure 11). While HOMO-4 also exhibits a strong 5d-π-character, it does not provide a comparable shielding contribution. This can be traced back to a combination of the following aspects:

1) At scalar relativistic level the 2σ MO exhibits notably smaller 1s(H) character upon going from weak to strong *trans* ligands resulting in 2c spinors with smaller 1s(H) character as well (cf. Table 2). This prohibits an effective FC mechanism. The missing 1s(H) contribution for the HOMO-4 of $HAuPH_3$ can be nicely seen in the isosurface plots in Figure 13.
2) The energy gap to the virtual spinors is significantly larger for the stronger ligands, which is partly caused by an increased HOMO-LUMO gap but mainly by the reordering of the spinors due to the destabilization of the 2σ-MO at SR-level.
3) In addition to the occupied spinors, the character of the virtual spinors involved in occupied-to-virtual couplings from the σ/π-type spinors affects the shielding contributions.
4) Additionally, also the predominant angular momentum character of the spinors seems to be decisive. Stronger ligands provide more $5d_{3/2}$ participation to the occupied spinor with dominant π-character whereas the weaker ones give more $5d_{5/2}$ participation.

These angular momentum aspects provide further understanding of SO effects. While the total angular momentum participation for the 2c-spinors is difficult to quantify, even qualitative trends offer valuable clues on the size and sign of SO contributions of individual couplings. As all abovementioned aspects work together to influence the SO contributions to shielding, very simple rules have been elusive so far. However, in the analyses of Papers I and II, recurring patterns where found that point to this connection to total angular momentum of the main participating metal orbitals in the occupied and virtual spinors.

Similar results were found for the *trans* ligand effects in the d^8 series, to a lesser extent also for d^6 complexes In contrast to the linear Au hydrides, for the square-planar Pt hydrides (and for the octahedral Os hydrides), a larger number of relevant couplings were found that contribute significantly to the changes in the ^{1}H NMR shifts. This can be understood as the (SO-affected) metal orbitals participate in more interactions due to the additional *cis* ligands. However, in agreement with the already mentioned results, again the occupied π- or π/σ-type MOs/spinors were found to be responsible for most of the observed trends. As mentioned in the previous chapter, the high-lying σ/π mixed spinors exhibit more π-character in the higher-lying occupied spinors for weaker ligands, and their (shielding) σ^{p+SO} contributions are overall always larger compared to the investigated ligands with larger *trans* influence.

Besides, a previous empirical observation[66,85] suggesting that occupied MOs with σ- and π-character relative to the bond between heavy atom and nucleus of interest provide deshielding and shielding SO-contributions, respectively, did not fully hold anymore. On one hand the large SO-mixing renders such symmetry labels inaccurate. On the other hand several occupied (predominantly σ-type and π-type) spinors were found, that each gave rise to both positive and negative contributions depending on the virtual spinor involved in the coupling. The first analysis where a π-type occupied MO was linked to shielding and a σ-type MO to deshielding HALA effects has been done for hydrogen halides and used a four-component, relativistically parametrized Extended Hückel method (REX).[85] For Paper II, a comparison for HI at 1c, 2c and 4c levels data differed by exhibiting a nominally σ-type spinor with slightly positive SO contributions, rather than negative ones as in the REX analysis. Thus, the assumption of especially deshielding contributions from σ-type occupied MOs does not seem to be general and depends also on the virtual orbitals involved in the magnetic couplings with the given σ-type MO, and to some extent on the analysis method.

3.2.5 Relations to Magnetically Induced Current Loops

In 2015, Berger *et al.*[118] presented pictures of magnetically induced probability currents in molecules derived from relativistic theory. The two investi-

gated d^{10} systems, namely HAu and HHgH, can be connected to the analyses of the *trans* influence series, with the former representing the extreme case of no *trans* ligand (= weak *trans* influence) and the latter illustrating the example of a strong σ-donor *trans* ligand (= strong *trans* influence). Accordingly, HAu exhibits a strongly shielding ^{1}H σ^{SO} whereas for HHgH it is deshielding. Consistently, difference plots displaying only the SO-induced currents, showed diatropic (clockwise) current loops around the hydride in HAu and small localized paratropic (anti-clockwise) current loops for HHgH.

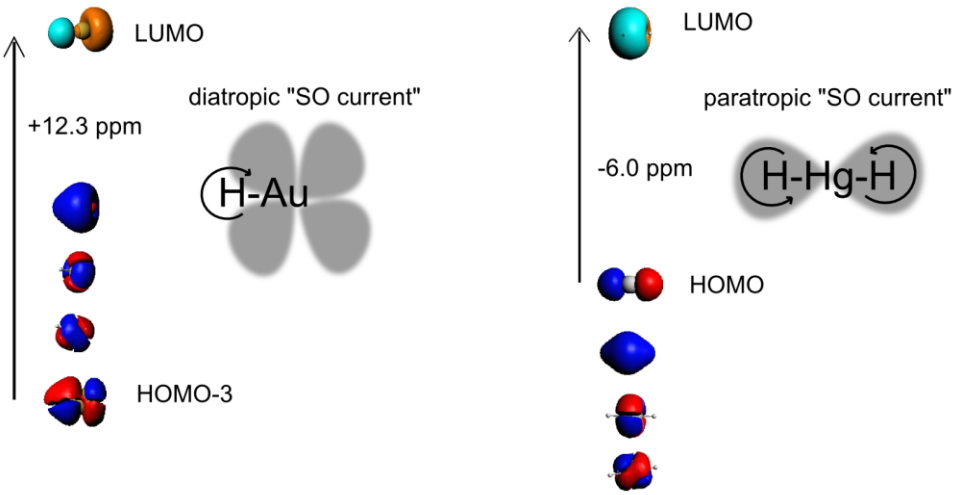

Figure 14. Illustration of the predominant ^{1}H σ^{p+SO} couplings (indicated by an arrow) in HAu and HHgH from 2-component spinors, in relation to the direction of SO-induced currents. Spinors are shown as isosurface plots (±0.03 a. u.). Taken from Paper II.

In Paper II, those relativistic current plots could be related to the shapes of the spinors being responsible for the dominant shielding contributions (cf. Figure 14). Similar to the case of $HAuNH_3$ described above, for HAu a π-type spinor, namely HOMO-3, leads to a strongly positive ^{1}H σ^{p+SO} contribution. In agreement, the corresponding SO-induced current loops create a picture resembling a π-type orbital with the diatropic current loop around the hydride *between* the lobes of this orbital. For HHgH, in contrast, the σ-type HOMO is mainly responsible for the overall deshielding SO contribution. Accordingly, the SO-induced current loops resemble a σ-type orbital. Again, the diatropic current loops appear *between* the lobes but the paratropic loops are *on* the lobes and thus, on the hydride position.

Consistent with an earlier study for NMR shifts of agostic protons[119] it seem reasonable to conclude, that high-lying π-type occupied MOs tend to create diatropic induced current loops at the position of the hydride which lies *outside* the main lobes of this MO and thus, in a charge-depletion zone. High-lying σ-type MOs, in contrast, create a paratropic current around the hydride, which in this case lies *on* the lobe of this MO, which is a charge-concentration zone. The charge distribution, on the other hand, is appreciably influenced (or shaped) by the *trans* ligand.

3.3 Role of SO Effects for Ligand NMR Shifts in Uranium(VI) Complexes

Already in 2012, we predicted spectacular SO-induced high-frequency ^{1}H and ^{13}C shifts in actinide complexes with $5f^{0}$ configuration, in particular for uranium(VI) species.[4] As mentioned in the evaluation part (section 3.1), those results were obtained using the 2c-ZORA implementation in ADF without considering the XC kernel, and about 40 % EXX admixture gave the best agreement with experiment for a number of ^{13}C shifts in organometallic U(VI) complexes. Upon revisiting these systems in Paper III, it was found that upon including the kernel, the conventional PBE0 functional with 25 % EXX admixture provides reasonable results and can be used to predict and analyse NMR shifts in such systems. PBE0 was only a compromise as finding a generally well-performing method was hampered by a non-systematic dependence of calculated ^{13}C shifts on EXX admixture, and by a general scarcity of available experimental data. The EXX dependences can be traced back to ligand effects that will be discussed in the following. Before, the “best” methods identified will be used to predict unknown shifts in organometallic uranium complexes and uranium hydrides.

3.3.1 Predictions of ^{13}C and ^{1}H Shifts

In Paper III, several experimentally known organometallic U(VI) complexes were studied. However, not for all of them the ^{13}C shifts have been detected to date. All of the so far elusive actinide-bonded ^{13}C shifts correspond to car-

bon atoms without hydrogen substituents, such that the missing signals could also be rationalized by their lower sensitivity (impossibility of direct ^{1}H decoupling). In some cases, the experimental lack of the signals may be attributed to unexpected spectral regions in the ^{13}C NMR shifts where they can appear, sometimes beyond the usual measurement area. In an attempt to guide the search for such signals in the right spectral range, predictions for several carbon atoms bonded to a uranium(VI) were presented in Paper III. In addition, ^{1}H chemical shifts of suitable target U(VI) hydride complexes were predicted, exhibiting signals between 30 ppm and more than 200 ppm and thus, clearly outside the known ^{1}H shift range for diamagnetic systems. Those large shifts are to a large extent dominated by SO contributions. A selection of the results is shown in Figure 15. Based on the detailed evaluations for similar systems (section 3.1), the figure shows predictions for those functionals expected to perform best for a given complex.

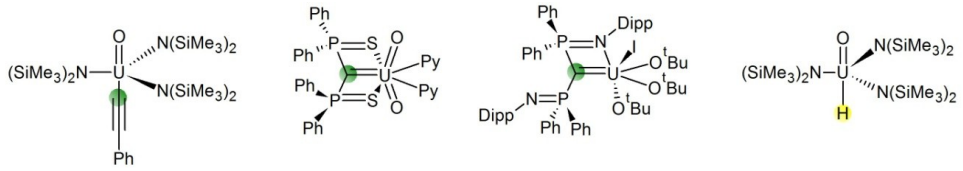

Figure 15. Calculated NMR shifts with the most promising method, respectively, for some experimentally known organometallic uranium(VI) complexes with undetermined ^{13}C NMR shifts for uranium-bound carbon nuclei (highlighted in green) as well as for a promising target uranium(VI) hydride (hydride highlighted in yellow).

The U(VI) alkinyl complex (1st complex in Figure 15) is predicted to exhibit a high-frequency shift of about 400 ppm. This is about 100 ppm higher than the value for the analogous U(VI) methyl complex which was found at about 300 ppm[120] and was excellently reproduced at PBE0 level. The predicted value for the 2nd complex in Figure 15 does not look impressive at the first sight, but in comparison with a structurally closely related methanide complex, whose ^{13}C NMR signal was found at 21 ppm, it is notable. The much stronger U-C interaction in the carbene complex leads to a predicted shift of about 150 ppm, clearly dominated by SO effects. For the 2nd carbene complex (3rd

complex in Figure 15) a ^{13}C shift in the 550-620 ppm range seems likely, but the measurement only went up to 400 ppm. Here, the prediction would not only be outside the measurement range but also provide a value at the very high-frequency end of known ^{13}C shifts for diamagnetic compounds, with up to half of the shift caused by SO contributions. However, we found that the triplet U(IV) structure lies energetically lower than the corresponding closed-shell U(VI) structure. It also gave better agreement between computed and experimental structures. Based on the small energetic gap, it is reasonable to assume the diamagnetic U(VI) complex in an equilibrium with the U(IV) species, whereas the X-Ray structure is expected to describe the U(IV) system.

The hypothetical U(VI) hydride in Figure 15 was adapted from closely related complexes (cf. the 1st complex in Figure 15), where experimental values were excellently reproduced at PBE0 level. Given the inverse *trans* influence (ITI) provided by the *trans* U=O group,[120] this system may be a particularly promising target system for a U(VI) hydride, and its computed ^{1}H shift of about 170 ppm (almost completely due to SOC) would already extend the known ^{1}H shift range dramatically.

3.3.2 General Ligand Influences

While no systematical analysis of ligand influences in uranium complexes was done for this work, the analysis of experimentally known complexes in Paper III already revealed some interesting trends. Figure 16 shows an example for each of the three types of U(VI) complexes that should be distinguished. The first group exhibits a carbon atom in equatorial position to a uranyl UO_2^{2+} unit, for the second the carbon is in *trans* position to a U=O bond, and the third group lacks any strong π-donor ligands.

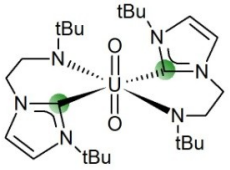

d(U-C) = 2.63 Å
δ (^{13}C) = 287 ppm
δ^{SO}(^{13}C) = 78 ppm

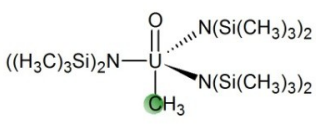

d(U-C) = 2.30 Å
δ (^{13}C) = 300 ppm
δ^{SO}(^{13}C) = 171 ppm

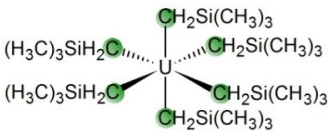

d(U-C) = 2.32 Å
δ (^{13}C) = 537 ppm
δ^{SO}(^{13}C) = 363 ppm

Figure 16. U-C bond lengths and ^{13}C NMR shifts for some organometallic U(VI) complexes representing each a group of complexes with the carbon atom in equatorial position to a uranyl UO_2^{2+} unit (group 1, left), the carbon in *trans* position to a U=O bond (group 2, center) and no strong π-donor ligands (group 3, right).

In Paper III, it was found that the U-C bond lengths correlate with the position of the carbon atom in the molecule. The longest U–C bonds pertain generally to the first group, whereas they are much shorter for the second (caused by ITI[120]) and the third (cf. Figure 16). Additionally, a correlation with the ^{13}C shift was observed: particularly large shifts were found in the absence of strong π-donor ligands in the complex, lower shifts for U-C bonds in *trans* position to a U=O bond and the lowest values appeared usually for the carbon atoms in equatorial position. Again, those trends are dominated by SO contributions to the NMR shifts. The correlations could be connected to the covalency of the U-C bonds rationalized by the percentage uranium character (%U) in the corresponding σ-bonding NLMO (cf. Table 5). The first group has less covalent bonds with clearly diminished 5f-orbital character and larger 6d contributions. The more covalent complexes of the 2nd and 3rd group clearly exhibit dominant 5f-orbital character of the U-C σ-bond, whereas the 6d-orbital character is comparably small here. The main aspects that enhance the SO contributions to the NMR shielding were similar to those found for the TM hydrides: a small energy difference between occupied and virtual orbitals, a high uranium 5f-character in the U-C bond and in the high-lying occupied and low-lying virtual MOs, a large covalency, and also a high C(2s) character in the U-C bond. While the latter aspect may be rationalized by the known Fermi-contact-type mechanisms for SO-induced shifts, the 5f-participation is crucial due to SO matrix elements.

Interestingly, the position of the carbon atom in the complex is also connected to the dependence of computed shifts (particularly their SO contributions) on the EXX admixture in the functional: positions equatorial to an uranyl (or related) unit lead to a negative dependence, positions *trans* to a U=O bond or the absence of competing strong π-donor ligands in the system give a positive dependence. Hence, the observed correlations provided a tentative rationalization of the at first sight non-systematic dependence of the ^{13}C (and ^{1}H

shifts) in uranium complexes on EXX admixture. In general, increasing EXX admixture renders the metal-ligand bonds less covalent. For the already only slightly covalent cases (group 1), increasing EXX admixture diminishes the SO contributions to the ^{13}C shifts by interrupting the Fermi-contact pathway that transmits the SO-induced spin polarization from the heavy uranium center to the carbon nucleus. For the more covalent cases with dominant uranium 5f-orbital contributions to the bond, the larger EXX admixture increases the polarization and thus, the SO terms, which was probed by a computational experiment in which a finite Fermi-contact perturbation was placed at the carbon nucleus, and the delocalization of the induced spin density throughout the system was monitored as a function of EXX admixture.

Table 5. Compositions of the U–C σ-bonding NLMOs for the complexes in Figure 16.[a]

Example of group	%U	%U(d)	%U(f)	%C	%C(s)	%C(p)
1	16.4	49	32	79.9	44	56
2	28.5	24	73	66.0	25	75
3	28.7	25	68	69.2	22	78

[a] PBE0/ECP/TZVP results.

4 Conclusion

"I saw in a dream a Table where all elements fell into place as required. Awakening, I immediately wrote it down on a piece of paper, only in one place did a correction later seem necessary."

Dmitri Mendeleev

In 1869, Dmitri Mendeleev stated to have had a dream in which he envisioned the Periodic Table of elements.[121] While he claimed that only one correction was required, we know today, that there are a few more displacements in his tabular arrangement. The most striking examples are the heavy elements such as platinum, gold and uranium. Several *unusual* features in heavy element chemistry are well known to be caused by relativistic effects that can have a drastic influence on a wide scale of properties complicating not only the tabular arrangement for Mendeleev.

This work focused on the influence of SO coupling, which is one of the most common manifestations of relativistic effects in the molecular sciences. Based on four- and particularly two-component relativistic density functional methods the influence of SO effects on NMR shifts, notably for ^{1}H and ^{13}C nuclei, was under consideration for several diamagnetic 5d TM complexes, uranium hydrides and organometallic uranium complexes. The extensive evaluation of computational methods concentrated in particular on the influence of the EXX admixture in the (hybrid) DFT functional and the linear response of the exchange-correlation (XC) potential. It turned out, that the XC kernel has a large effect for systems where substantial SO effects are involved, and that it has to be taken into account for accurate NMR calculations, both at the 2c and 4c level. In the presence of the kernel the PBE0 functional with 25 % EXX provides excellent agreement with experimental shifts for TM hydrides and reasonable predictive quality for organometallic uranium complexes. Based on this computational level a strikingly general correlation of the *trans* ligand influence series and the NMR shifts of metal-bound nuclei in 5d transition-metal complexes was observed, encompassing especially $5d^8$ and $5d^{10}$ configurations, with related effects also for $5d^6$ complexes. The effect was

shown to be dominated by SO coupling, noting that it is the perpendicular shift tensor components that mainly determine the trend. While it has been concentrated on ^{1}H shifts of hydride ligands, where SO-induced shielding effects are most prominent, similar effects are operative also for other nuclei as shown for example for ^{13}C NMR shifts. For square-planar Pt(II) and linear Au(I) systems a sign change from shielding to deshielding of the dominant SO-induced shifts was found upon going from weak to strong *trans* ligands. This changes the current assumption that highly deshielded hydride chemical shifts are implicated only for d^0 and d^{10} systems, whereas intermediate electron counts are linked to characteristic low-frequency shifts. Very recently, a similar deviation was observed for pseudo-octahedral d^6 Ru(II) hydride complexes in which the hydride ligand displays not always highly shielded ^{1}H NMR shifts but for some *trans* ligands also deshielded values (about +5 ppm).[122] Similar as for the d^6 Os(II) hydride complexes discussed in this work, those trends are dominated by paramagnetic shielding terms which, however, were found to go roughly in parallel with the SO contributions.

While also the M-H distances correlate with the *trans* ligand influence series, this change does not cause the changes for NMR signals. However, both properties are linked to the same patterns in the electronic structure. Based on detailed canonical and localized MO analyses it was shown that variations in the polarization of metal 5d orbitals, changes in the covalency of the metal−hydrogen bond and the destabilization of a specific σ-type MO may be responsible for both correlations. The latter translates into a very different σ–/π-mixing for weak and for strong *trans* ligands once SO coupling is included. The effects of SO-mixing are in turn related to angular-momentum admixture from atomic spinors at the metal center.

In general, it can be concluded that high-lying π-type occupied MOs or spinors are connected with an overall shielding SO contribution, which in contrast, are diminished or even deshielding for strong *trans* ligands where specific occupied σ-type levels are higher in energy. The position of the NMR nucleus outside the main lobes of a metal's SO-active π-type spinor may be linked to diatropic SO currents at the position of the NMR nucleus causing the shielding effect by inducing an magnetic field, which opposes the applied field.

The position on a lobe of a SO-active σ-type spinor, in contrast, is associated with paratropic SO currents and thus, deshielding effects. While this observation matches to the earlier considerations on the shielding role of π-type occupied and the deshielding role of σ-type occupied MOs for such SO-induced shifts, it turned out that this behavior does not seem to be general. Having a look at individual couplings, σ- and π-type spinors can cause either shielding or deshielding contributions. Although a complete understanding of the different signs of the SO shielding contributions still have to be found, the deviations may be attributed mainly to the extensive SO-induced σ/π-mixing (presumably connected with angular momentum mixing) of the occupied and virtual spinors.

In extension to previous relativistic quantum-chemical predictions, unusually large ^{1}H and ^{13}C NMR chemical shifts for ligand atoms directly bonded to a diamagnetic uranium(VI) center have been revisited and deeper analyzed in this work. The revised approach with XC kernel still predicts ^{1}H hydride shifts between 30 ppm and to about 170 ppm, which clearly extends the known ^{1}H shift range for diamagnetic systems. Among the predictions for uranium-bonded ^{13}C NMR shifts for some known organometallic U(VI) complexes, for which no corresponding signals have been detected to date, an extremely large ^{13}C shift above 550 ppm, near the upper end of the diamagnetic ^{13}C shift spectrum, is predicted for a pincer carbene complex. Based on bonding analyses, the magnitude of SO contributions, which clearly dominate the uranium-bonded ^{1}H and ^{13}C NMR shifts, could be linked to the ligand position in the complex, the covalency of the U-C bond, the metal 5d- and 5f-orbital character and the carbon 2s-orbital character.

The understanding of the molecular and electronic structure in chemistry is crucial for the insights into reaction mechanisms and the rational design of complexes, for instance of more efficient catalysts. The insights in the SO-induced trends for transition-metal and actinide systems should allow qualitative as well as quantitative predictions of a wide range of complexes. Experimentally, NMR chemical shifts provide a valuable source of structural information, as they reflect the electronic structure and bonding pattern at the metal center. In addition, ^{1}H NMR spectroscopy is frequently the only experimental

technique that indicates unambiguously the presence of a metal-hydrogen bond in a complex. The obtained data in this work could be used to rationalize certain trends and to find concepts that may be useful beyond explicit calculations. The findings enable the estimation of ligand effects also for unknown complexes, a more meaningful design of (target) complexes, and an improved characterization by NMR spectroscopy.

5 Implications for further research

Until recently the largest experimentally confirmed high-frequency ^{1}H NMR shifts were for transition metal hydrides with d^{10} and d^{0} configurations, ranging up to about +25 ppm for some Ta(V) hydride complexes.[123,124] The size of the standard ^{13}C shift range goes typically up to about +300 ppm for organometallics. Both limits are relatively low compared to the recently predicted (and in this work bolstered) spectacular SO induced high-frequency shifts in f^{0} uranium complexes up to about +200 ppm for ^{1}H and above +550 ppm for the ^{13}C NMR shifts. This leads to the problem of possibly overlooking certain NMR signals, which lie outside the usual spectral area. Hence, not only from a theoretical point of view, it could be interesting to search for the limits of NMR spectra. Certainly, using the results of this thesis in combination with other recent results could be used to design complexes that exhibit signals beyond the known borders of the known spectral ranges for various nuclei and guide the experimentalist's search in the right spectral area, particularly for so far unknown species.

Next to uranium complexes which could be one candidate extending the known NMR spectral ranges, also main group elements seem to be promising. Very recently, the role of relativistic effects on ^{1}H NMR chemical shifts of Sn(II) and Pb(II) hydrides[125] and ^{13}C and ^{29}Si NMR signals of ligand atoms directly bonded to Tl(I) or Pb(II)[126] were investigated by using fully relativistic DFT calculations. Those complexes are predicted to resonate at very high frequencies, up to 90 ppm for Pb(II) hydrides, up to 400 ppm for ^{13}C and over 1000 ppm for ^{29}Si, outside the typical experimental NMR chemical-shift ranges for the given type of nuclei. Even more recently, the existence of Pb(II) hydrides was confirmed by Schneider *et al.*.[127] In agreement with the predicted high-frequency shifts for such complexes a hydride ^{1}H NMR signal of about +36 ppm was observed for the first low-valent organolead hydride, which is at the lowest field observed so far for a diamagnetic compound. In analogy to the present work, those shifts are dictated by sizable relativistic contributions due to spin-orbit coupling at the heavy atom.[125] In addition, Vícha *et al.*[126] mapped the trends for the ^{13}C NMR shifts in a series of $M(Ph)Cl_n$ model com-

plexes along the sixth period of the periodic table, from platinum to astatine, and found about 15 time larger SO contributions in the subvalent species, like Tl(I) and Pb(II), than for those in full-valence species, Tl(III) and Pb(IV). It would be interesting to analyze whether this is really due to the oxidation states or rather the p orbital occupation of the metal or is again related to ligand effects, as the number n of chloride ligands changes in their model systems. Replacing chloride by stronger and weaker ligands could change the results dramatically. In general, there should be a closer look also on other ligand influences on the SO NMR shift, as this thesis mainly focused on the *trans* ligand only (e.g. *cis* ligand influences).

At least theoretically, also TM complexes could re-capture their throne of providing the highest known ^{1}H and ^{13}C NMR shifts.[124,128] It could be shown in the present work that SO effects can have a crucial impact already for the 5d elements and their complexes, while the Periodic Table of elements also provides 6d elements. Although those *super-heavy* transactinide elements (Z = 104-120) are radioactive (with extremely short half-lives) and have only been obtained synthetically in laboratories, one can expect very interesting effects for their complexes. Special relativity should have a decisive impact on all properties of 6d complexes which prevents an extrapolation of specific effects for those systems.

Nevertheless, until now it seems that the SO effects for these super-heavy complexes will not outperform the results theoretically found for Pb(II) hydrides or U(VI) hydrides, even though the metal centers have smaller atomic numbers Z. The spectacular SO contributions were traced back to efficient coupling of the frontier or nearby spinors containing sufficiently large 6p or 5f character of the heavy metal atom, respectively.[4,125] Further investigations along these lines would be very interesting. Analyzing the influences of the metal atom and thus the corresponding metal orbitals (i.e. 5d vs. 6p vs. 5f couplings) could be helpful to get better insights into the interplay of electronic structure and SO chemical shifts. Especially, the links to differences in angular momenta and symmetry would be very helpful. They could add an additional explanation to the differences between 5d and analogous 5f complexes. The model $5f^0$ HUF_5 complex is predicted to exhibit a large ^{1}H shift of over

200 ppm whereas the shift of the analogous $5d^0$ complex HWF_5 is only about 30 ppm. Analysis with a perturbational treatment of the SO coupling showed, that the energetically low-lying vacant spinors with dominating f character are responsible for the extremely high SO contributions of the uranium compound.[4] Another factor could be the overall higher symmetry of the octahedral U(VI) complex in comparison with the distorted W(VI) analogue,[129] experiencing no *trans* (and *cis*) ligand influence. A similar effect can be seen for WMe_6 and UMe_6, where only the latter is octahedral and exhibits SO contributions which are about 10 times larger than for the TM complex. Even if the 5d metal tungsten is replaced by its analogue 6d element, seaborgium, which is significantly heavier than uranium, this observation remains. It would be interesting to analyze more closely whether mainly the low-lying f orbitals, the higher symmetry or another feature of the f orbitals is crucial here.

Bibliography

[1] D. Mendeleev, *Zeitschrift für Chemie* **1869**, *12*, 405–406.
[2] P. Pyykkö, *Annu. Rev. Phys. Chem.* **2012**, *63*, 45–64.
[3] D. Mendeleev, *Annalen der Chemie und Pharmacie* **1872**, *8*, 133–229.
[4] P. Hrobárik, V. Hrobáriková, A. H. Greif, M. Kaupp, *Angew. Chem. Int. Ed.* **2012**, *51*, 10884–10888.
[5] Y. Nomura, Y. Takeuchi, N. Nakagawa, *Tetrahedron Lett.* **1969**, *10*, 639–642.
[6] P. Hrobárik, V. Hrobáriková, F. Meier, M. Repiský, S. Komorovský, M. Kaupp, *J. Phys. Chem. A* **2011**, *115*, 5654–5659.
[7] P. Pyykko, J. P. Desclaux, *Acc. Chem. Res.* **1979**, *12*, 276–281.
[8] M. Planck, *Ann. Phys.* **1901**, *309*, 553–563.
[9] M. Planck, *Ann. Phys.* **1900**, *306*, 69–122.
[10] A. Einstein, *Ann. Phys.* **1905**, *322*, 132–148.
[11] W. Heisenberg, *Z. Für Phys.* **1927**, *43*, 172–198.
[12] M. Born, *Z. Für Phys.* **1926**, *37*, 863–867.
[13] M. Born, R. Oppenheimer, *Ann. Phys.* **1927**, *389*, 457–484.
[14] P. A. M. Dirac, *Proc. R. Soc. Math. Phys. Eng. Sci.* **1929**, *123*, 714–733.
[15] W. Pauli, *Z. Für Phys.* **1927**, *43*, 601–623.
[16] C. C. J. Roothaan, *Rev. Mod. Phys.* **1951**, *23*, 69–89.
[17] G. G. Hall, *Proc. R. Soc. Math. Phys. Eng. Sci.* **1951**, *205*, 541–552.
[18] P. Hohenberg, W. Kohn, *Phys. Rev.* **1964**, *136*, B864–B871.
[19] W. Kohn, L. J. Sham, *Phys. Rev.* **1965**, *140*, A1133–A1138.
[20] J. C. Slater, *Phys. Rev.* **1951**, *81*, 385–390.
[21] F. Weinhold, in *Encyclopedia of Computational Chemistry* (Eds.: N.L. Allinger, J. Gasteiger, P.A. Kollman, H.F. Schaefer, P.R. Schreiner), John Wiley & Sons, Ltd, Chichester, UK, **2002**.
[22] F. Weinhold, C. R. Landis, *Chem Educ Res Pr.* **2001**, *2*, 91–104.
[23] A. Einstein, *Ann. Phys.* **1905**, *322*, 891–921.
[24] A. Einstein, *Ann. Phys.* **1905**, *323*, 639–641.
[25] O. Klein, *Z. Für Phys.* **1927**, *41*, 407–442.
[26] W. Gordon, *Z. Für Phys.* **1926**, *40*, 117–133.
[27] W. H. E. Schwarz, in *Relativistic Methods for Chemists* (Eds.: M. Barysz, Y. Ishikawa), Springer Netherlands, Dordrecht, **2010**, pp. 1–62.
[28] R. E. Stanton, S. Havriliak, *J. Chem. Phys.* **1984**, *81*, 1910.
[29] E. van Lenthe, E. J. Baerends, J. G. Snijders, *J. Chem. Phys.* **1993**, *99*, 4597.
[30] C. Chang, M. Pelissier, P. Durand, *Phys. Scr.* **1986**, *34*, 394–404.
[31] V. Arcisauskaite, J. I. Melo, L. Hemmingsen, S. P. A. Sauer, *J. Chem. Phys.* **2011**, *135*, 44306–11.
[32] J. Autschbach, *Philos. Trans. R. Soc. Math. Phys. Eng. Sci.* **2014**, *372*, 20120489–20120489.
[33] D. Andrae, U. Häußermann, M. Dolg, H. Stoll, H. Preuß, *Theor. Chem. Acta* **1990**, *77*, 123–141.

[34] J. Vaara, O. L. Malkina, H. Stoll, V. G. Malkin, M. Kaupp, *J. Chem. Phys.* **2001**, *114*, 61–71.
[35] M. Kaupp, in *Anorganische Chemie Prinzipien von Struktur und Reaktivität* (Ed.: R. Steudel), De Gruyter, Berlin/Boston, **2012**, pp. 1043–1097.
[36] P. Pyykkö, *Chem. Rev.* **1988**, *88*, 563–594.
[37] M. Dolg, X. Cao, *Chem. Rev.* **2012**, *112*, 403–480.
[38] P. Schwerdtfeger, *ChemPhysChem* **2011**, *12*, 3143–3155.
[39] R. E. Powell, *J. Chem. Educ.* **1968**, *45*, 558.
[40] K. S. Pitzer, *Acc. Chem. Res.* **1979**, *12*, 271–276.
[41] P. Pyykkö, in *Adv. Quantum Chem.*, Elsevier, **1978**, pp. 353–409.
[42] J. Autschbach, *J. Chem. Phys.* **2012**, *136*, 150902.
[43] M. Kaupp, M. Dolg, H. Stoll, H. G. von Schnering, *Inorg. Chem.* **1994**, *33*, 2122–2131.
[44] W. H. E. Schwarz, E. M. van Wezenbeek, E. J. Baerends, J. G. Snijders, *J. Phys. B At. Mol. Opt. Phys.* **1989**, *22*, 1515–1529.
[45] J. Autschbach, S. Siekierski, M. Seth, P. Schwerdtfeger, W. H. E. Schwarz, *J. Comput. Chem.* **2002**, *23*, 804–813.
[46] P. Romaniello, P. L. de Boeij, *J. Chem. Phys.* **2005**, *122*, 164303.
[47] P. Romaniello, P. L. de Boeij, *J. Chem. Phys.* **2007**, *127*, 174111.
[48] H. Häkkinen, M. Moseler, U. Landman, *Phys. Rev. Lett.* **2002**, *89*, 33401.
[49] B. D. El-Issa, P. Pyykko, H. M. Zanati, *Inorg. Chem.* **1991**, *30*, 2781–2787.
[50] F. Calvo, E. Pahl, M. Wormit, P. Schwerdtfeger, *Angew. Chem. Int. Ed.* **2013**, *52*, 7583–7585.
[51] X. Wang, L. Andrews, S. Riedel, M. Kaupp, *Angew. Chem. Int. Ed.* **2007**, *46*, 8371–8375.
[52] S. Riedel, M. Kaupp, *Coord. Chem. Rev.* **2009**, *253*, 606–624.
[53] T. Ziegler, J. G. Snijders, E. J. Baerends, *Chem. Phys. Lett.* **1980**, *75*, 1–4.
[54] W. H. E. Schwarz, *Phys. Scr.* **1987**, *36*, 403–411.
[55] V. Saltykov, J. Nuss, U. Wedig, M. Jansen, *Z. anorg. allg. Chem.* **2011**, *637*, 357–361.
[56] H. Schwarz, *Angew. Chem. Int. Ed.* **2003**, *42*, 4442–4454.
[57] R. Ahuja, A. Blomqvist, P. Larsson, P. Pyykkö, P. Zaleski-Ejgierd, *Phys. Rev. Lett.* **2011**, *106*, 18301.
[58] W. E. Lamb, *Phys. Rev.* **1941**, *60*, 817–819.
[59] N. F. Ramsey, *Phys. Rev.* **1950**, *77*, 567–567.
[60] N. F. Ramsey, *Phys. Rev.* **1950**, *78*, 699–703.
[61] C. J. Jameson, J. Mason, in *Multinuclear NMR* (Ed.: J. Mason), Plenum Press, New York, **1987**, pp. 3–83.
[62] J. S. Griffith, L. E. Orgel, *Trans. Faraday Soc.* **1957**, *53*, 601.
[63] A. D. Buckingham, P. J. Stephens, *J. Chem. Soc. Resumed* **1964**, 4583.
[64] A. D. Buckingham, P. J. Stephens, *J. Chem. Soc. Resumed* **1964**, 2747.
[65] J. Vaara, *Phys. Chem. Chem. Phys.* **2007**, *9*, 5399.
[66] M. Kaupp, in *Relativistic Electronic Structure Theory II Applications* (Ed.: P. Schwerdtfeger), Elsevier, Amsterdam, **2004**, pp. 552–597.
[67] Y. Ruiz-Morales, G. Schreckenbach, T. Ziegler, *Organometallics* **1996**, *15*, 3920–3923.

[68] K. Wolinski, J. F. Hinton, P. Pulay, *J. Am. Chem. Soc.* **1990**, *112*, 8251–8260.
[69] R. Ditchfield, *J. Chem. Phys.* **1972**, *56*, 5688–5691.
[70] G. A. Aucar, T. Saue, L. Visscher, H. J. A. Jensen, *J. Chem. Phys.* **1999**, *110*, 6208–6218.
[71] W. Kutzelnigg, *J. Comput. Chem.* **1999**, *20*, 1199–1219.
[72] S. Komorovský, M. Repiský, O. L. Malkina, V. G. Malkin, I. Malkin Ondík, M. Kaupp, *J. Chem. Phys.* **2008**, *128*, 104101–15.
[73] S. Komorovský, M. Repiský, O. L. Malkina, V. G. Malkin, *J. Chem. Phys.* **2010**, *132*, 154101.
[74] S. K. Wolff, T. Ziegler, E. van Lenthe, E. J. Baerends, *J. Chem. Phys.* **1999**, *110*, 7689–7698.
[75] M. Krykunov, T. Ziegler, E. van Lenthe, *J. Phys. Chem. A* **2009**, *113*, 11495–11500.
[76] J. Autschbach, *Mol. Phys.* **2013**, *111*, 2544–2554.
[77] J. Vaara, K. Ruud, O. Vahtras, *J. Chem. Phys.* **1999**, *111*, 2900–2909.
[78] S. Zheng, J. Autschbach, *Chem. - Eur. J.* **2011**, *17*, 161–173.
[79] M. Repiský, S. Komorovský, O. L. Malkina, V. G. Malkin, *Chem. Phys.* **2009**, *356*, 236–242.
[80] J. Autschbach, *J. Chem. Phys.* **2008**, *129*, 94105.
[81] J. Autschbach, *J. Chem. Phys.* **2009**, *130*, 209901.
[82] G. Schreckenbach, *Inorg. Chem.* **2002**, *41*, 6560–6572.
[83] M. Kaupp, O. L. Malkina, V. G. Malkin, P. Pyykkö, *Chem. Eur. J.* **1998**, *4*, 118–126.
[84] A. . Cheremisin, P. Schastnev, *J. Magn. Reson. 1969* **1980**, *40*, 459–468.
[85] P. Pyykkö, A. Görling, N. Rösch, *Mol. Phys.* **1987**, *61*, 195–205.
[86] G. Schreckenbach, T. Ziegler, *J. Phys. Chem.* **1995**, *99*, 606–611.
[87] G. Schreckenbach, T. Ziegler, *Int. J. Quantum Chem.* **1997**, *61*, 899–918.
[88] S. K. Wolff, T. Ziegler, *J. Chem. Phys.* **1998**, *109*, 895–905.
[89] V. G. Malkin, O. L. Malkina, D. R. Salahub, *Chem. Phys. Lett.* **1996**, *261*, 335–345.
[90] M. Kaupp, O. L. Malkina, *J. Chem. Phys.* **1998**, *108*, 3648–3659.
[91] M. Hyvärinen, J. Vaara, A. Goldammer, B. Kutzky, K. Hegetschweiler, M. Kaupp, M. Straka, *J. Am. Chem. Soc.* **2009**, *131*, 11909–11918.
[92] L. A. Truflandier, E. Brendler, J. Wagler, J. Autschbach, *Angew. Chem. Int. Ed.* **2011**, *50*, 255–259.
[93] *Turbomole, Version 6.3.1*, A Development Of University Of Karlsruhe And Forschungszentrum Karlsruhe GmbH, 1989-2007, TURBOMOLE GmbH, Since 2007; available from http://www.turbomole.com.
[94] F. Weigend, R. Ahlrichs, *Phys. Chem. Chem. Phys.* **2005**, *7*, 3297.
[95] X. Cao, M. Dolg, *J. Mol. Struct. THEOCHEM* **2004**, *673*, 203–209.
[96] K. Eichkorn, F. Weigend, O. Treutler, R. Ahlrichs, *Theor Chem Acta* **1997**, *97*, 119–124.
[97] J. P. Perdew, K. Burke, M. Ernzerhof, *Phys. Rev. Lett.* **1997**, *78*, 1396–1396.
[98] J. P. Perdew, Y. Wang, *Phys. Rev. B* **1992**, *45*, 13244–13249.
[99] A. D. Becke, *Phys. Rev. A* **1988**, *38*, 3098–3100.
[100] C. Lee, W. Yang, R. G. Parr, *Phys. Rev. B* **1988**, *37*, 785–789.

[101] S. Grimme, J. Antony, S. Ehrlich, H. Krieg, *J. Chem. Phys.* **2010**, *132*, 154104–19.
[102] S. Grimme, S. Ehrlich, L. Goerigk, *J. Comput. Chem.* **2011**, *32*, 1456–1465.
[103] A. Klamt, G. Schüürmann, *J. Chem. Soc. Perkin Trans. 2* **1993**, 799.
[104] A. Klamt, *J. Phys. Chem.* **1995**, *99*, 2224–2235.
[105] A. Klamt, V. Jonas, *J. Chem. Phys.* **1996**, *105*, 9972–9981.
[106] *Amsterdam Density Functional (ADF) Version 2012.01*, SCM, Theoretical Chemistry, Vrije Univeriteit, Amsterdam, Netherlands, 2012; available from http://www.scm.com.
[107] E. Van Lenthe, E. J. Baerends, *J. Comput. Chem.* **2003**, *24*, 1142–1156.
[108] *ReSpect, Version 3.3.0 (Beta), 2013* and *Version 3.5.0, 2016*, Relativistic Spectroscopy DFT Program; M. Repisky, S. Komorovsky S., V. G. Malkin, O. L. Malkina, M. Kaupp, K. Ruud, with contributions from R. Bast, U. Ekstrom, S. Knecht, I. Malkin Ondik, E. Malkin; available from www.respectprogram.org.
[109] K. G. Dyall, *Theor. Chem. Acc.* **2004**, *112*, 403–409.
[110] K. G. Dyall, *Theor. Chem. Acc.* **2007**, *117*, 491–500.
[111] W. Kutzelnigg, U. Fleischer, M. Schindler, in *NMR Basic Principles and Progress*, Springer Verlag, Berlin, **1991**, p. 165.
[112] S. H. Vosko, L. Wilk, M. Nusair, *Can. J. Phys.* **1980**, *58*, 1200–1211.
[113] J. Vícha, J. Novotný, M. Straka, M. Repisky, K. Ruud, S. Komorovsky, R. Marek, *Phys Chem Chem Phys* **2015**, *17*, 24944–24955.
[114] P. Manninen, P. Lantto, J. Vaara, K. Ruud, *J. Chem. Phys.* **2003**, *119*, 2623.
[115] P. Manninen, K. Ruud, P. Lantto, J. Vaara, *J. Chem. Phys.* **2005**, *122*, 114107.
[116] P. Manninen, K. Ruud, P. Lantto, J. Vaara, *J. Chem. Phys.* **2006**, *124*, 149901.
[117] J. Vícha, M. Straka, M. L. Munzarová, R. Marek, *J. Chem. Theory Comput.* **2014**, *10*, 1489–1499.
[118] R. J. F. Berger, M. Repisky, S. Komorovsky, *Chem Commun* **2015**, *51*, 13961–13963.
[119] J. E. Barquera-Lozada, A. Obenhuber, C. Hauf, W. Scherer, *J. Phys. Chem. A* **2013**, *117*, 4304–4315.
[120] A. J. Lewis, P. J. Carroll, E. J. Schelter, *J. Am. Chem. Soc.* **2013**, *135*, 13185–13192.
[121] J. B. Arden, *Science, Theology and Consciousness*, Praeger Frederick A., **1998**.
[122] L. J. L. Häller, E. Mas-Marzá, M. K. Cybulski, R. A. Sanguramath, S. A. Macgregor, M. F. Mahon, C. Raynaud, C. A. Russell, M. K. Whittlesey, *Dalton Trans* **2017**, *46*, 2861–2873.
[123] B. C. Parkin, J. R. Clark, V. M. Visciglio, P. E. Fanwick, I. P. Rothwell, *Organometallics* **1995**, *14*, 3002–3013.
[124] S. A. Strazisar, P. T. Wolczanski, *J. Am. Chem. Soc.* **2001**, *123*, 4728–4740.
[125] J. Vícha, R. Marek, M. Straka, *Inorg. Chem.* **2016**, *55*, 10302–10309.
[126] J. Vícha, R. Marek, M. Straka, *Inorg. Chem.* **2016**, *55*, 1770–1781.
[127] J. Schneider, C. P. Sindlinger, K. Eichele, H. Schubert, L. Wesemann, *J. Am. Chem. Soc.* **2017**, DOI 10.1021/jacs.7b01856.

[128] S. Takemoto, J. Ohata, K. Umetani, M. Yamaguchi, H. Matsuzaka, *J. Am. Chem. Soc.* **2014**, *136*, 15889–15892.
[129] M. Kaupp, *Angew. Chem. Int. Ed.* **2001**, *40*, 3534–3565.

Original Papers

I

Inorganic Chemistry

Article

pubs.acs.org/IC

A Relativistic Quantum-Chemical Analysis of the trans Influence on ^{1}H NMR Hydride Shifts in Square-Planar Platinum(II) Complexes

Anja H. Greif,[†] Peter Hrobárik,*[,†] Veronika Hrobáriková,[†] Alexei V. Arbuznikov,[†] Jochen Autschbach,[‡] and Martin Kaupp*[,†]

[†]Institut für Chemie, Technische Universität Berlin, Strasse des 17. Juni 135, 10623 Berlin, Germany

[‡]Department of Chemistry, University at Buffalo, State University of New York, Buffalo, New York 14260, United States

Supporting Information

ABSTRACT: Empirical correlations between characteristic ^{1}H NMR shifts in Pt(II) hydrides with trans ligand influence series, Pt−H distances, and ^{195}Pt shifts are analyzed at various levels of including relativistic effects into density-functional calculations. A close examination of the trans ligand effects on hydride NMR shifts is shown to be dominated by spin−orbit shielding σ^{SO}. A rather complete understanding of the trends has been obtained by detailed molecular orbital (MO)-by-MO and localized MO analyses of the paramagnetic and spin−orbit (SO) contributions to the chemical shifts, noting that it is the perpendicular shift-tensor components that determine the trend of the ^{1}H hydride shifts. In contrast to previous assumptions, the change of the Pt−H distance in given complexes does not allow correlations between hydride shifts and metal−hydrogen bond length to be understood. Instead, variations in the polarization of metal 5d orbitals by the trans ligand affects the SO (and partly paramagnetic) shift contributions, as well as the Pt−H distances and the covalency of the metal−hydrogen bond (quantified, e.g., by natural atomic charges and delocalization indices from quantum theory atoms-in-molecules), resulting in a reasonable correlation of these structural/electronic quantities with hydride σ^{SO} shieldings. Our analysis also shows that specific σ^{P}- and σ^{SO}-active MOs are not equally important across the entire series. This explains some outliers in the correlation for limited ranges of trans-influence ligands. Additionally, SO effects from heavy-halide ligands may further complicate trends, indicating some limitations of the simple one-parameter correlations. Strikingly, σ-donating/π-accepting ligands with a very strong trans influence are shown to invert the sign of the usually shielding σ^{SO} contribution to the ^{1}H shifts, by a substantial reduction of the metal 5d orbital involvement in Pt−H bonding, and by involvement of metal 6p-type orbitals in the magnetic couplings, in violation of the Buckingham−Stephens "off-center ring-current" picture.

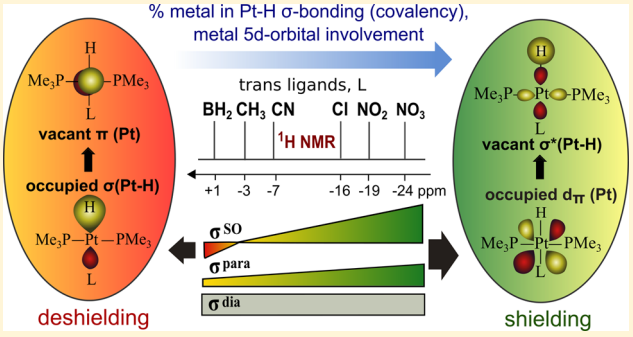

INTRODUCTION

The distinction between the trans influence as the ability of a ligand to weaken the metal−ligand bond trans to itself, which is thermodynamic in origin, and the kinetic trans effect on ligand substitution reactivity was introduced by Pidcock in 1960s.[1] Square-planar Pt(II) complexes have been studied most intensively in this context.[2] In addition to the bond length and binding energy of the trans metal−ligand bond, some spectroscopic parameters, such as vibrational frequencies, NMR chemical shifts, or nuclear spin−spin couplings, also tend to correlate with standard trans-influence series, and might thus serve as indicators. Chatt and Shaw showed some correlation between the trans-influence series and the ^{1}H NMR shifts for Pt(II) hydrides already in 1962.[3] For example, the hydride ligand has a more negative chemical shift when it is trans to a nitrate rather than a cyanide ligand. That is, a stronger trans donor ligand causes a less pronounced ^{1}H shielding. Buckingham and Stephens introduced an off-center ring-current model to explain the sometimes drastic low-frequency ^{1}H shifts of transition-metal hydride complexes.[4,5] They suggested that larger shielding should be caused mainly by a shorter M−H bond, related to the competition of the two trans ligands for the same sd-hybrid orbital of the metal center. Atkins et al. supported this assumption by reporting an almost linear correlation between ^{1}H NMR shifts and Pt−H IR stretching frequencies.[6] They excluded largely the ligand-field splitting (position of the trans ligand within the spectrochemical series) as a possible cause of the correlations. Birnbaum emphasized the position of the trans ligand in the nephelauxetic series and brought metal−ligand covalency into play.[7] The Buckingham−Stephens model was subsequently confirmed by density-functional theory (DFT) calculations.[8]

We have recently shown by fully relativistic DFT calculations of ^{1}H shifts in a wide variety of transition-metal hydride complexes that for 4d and in particular for 5d complexes spin−

Received: March 6, 2015
Published: July 16, 2015

DOI: 10.1021/acs.inorgchem.5b00446
Inorg. Chem. 2015, 54, 7199−7208

Table 1. Quasi-Relativistically Optimized Pt−H Distances, QTAIM Delocalization Indices (DI), NPA Atomic Charges (q) at the Hydride Ligand and Compositions (in %) of the Pt−H σ-Bonding NLMOs in *trans*-[HPtL(PMe_3)$_2$] Series along with Computed and Experimental ^{1}H NMR Hydride Shifts (in ppm vs TMS). The Spin−Orbit Part of the Isotropic Shielding (σ^{SO}) Is Given as well[a]

ligand	d(Pt−H)	DI(Pt↔H)	NPA	NLMO (Pt−H)			σ^{SO}(^{1}H)	δ_{calcd}(^{1}H)[b]	δ_{expt}(^{1}H)
L	[Å]		q(H)	%Pt	Pt(s)	Pt(d)	[ppm]	[ppm]	[ppm]
NO_3	1.548	1.004	−0.109	38.1	23.5	76.2	14.9	−23.6	−23.8[c]
ONO	1.562	0.990	−0.155	36.2	23.4	76.2	12.6	−20.1	−19.7[c,d]
Cl	1.565	0.987	−0.149	34.2	25.5	73.8	10.0	−15.8	−16.9[c]
Br	1.566	0.980	−0.147	33.8	25.5	73.8	9.6	−14.7	−15.6[c]
I	1.569	0.966	−0.149	32.7	25.4	73.8	8.3	−11.9	−12.7[c]
SCN	1.576	0.956	−0.156	32.2	23.5	76.0	7.8	−12.1	−13.3[c]
NO_2	1.582	0.968	−0.196	32.4	23.5	76.1	11.4	−19.0	−19.7[c,d]
CN	1.609	0.946	−0.251	26.6	24.7	74.8	3.1	−6.7	−7.8[c]
C_6H_5	1.628	0.923	−0.285	22.7	25.5	74.1	3.0	−5.9	−5.7[e]
CH_3	1.636	0.907	−0.305	20.8	23.7	75.4	1.2	−3.8	−3.8[e]
$Si(OMe)_3$	1.649	0.880	−0.328	15.5	23.6	75.1	−1.2	0.4	+0.7[f]
BCat	1.678	0.860	−0.377	13.1	30.6	68.3	−2.8	2.3	+0.4[g]

[a]See Computational Methods. [b]^{1}H NMR hydride shifts calculated at the 2c-ZORA(SO)/PBE0/TZ2P level including exchange-correlation kernel (cf. Figure 1 and Table S2 in Supporting Information for comparison of various computational methods). [c]Reference 3. The experimental values belong to *trans*-[HPtL(PEt_3)$_2$] measured in C_6D_6 (the τ values given in ref 3 were converted to the conventional NMR shift scale as $\delta = 10.0 - \tau$). [d]Doubtful assignment; see text. [e]Reference 43. The experimental values belong to *trans*-[HPtL(PPh_3)$_2$] measured in CD_2Cl_2. [f]Reference 44. The experimental value of *trans*-[HPt{Si(OMe)$_3$}(PEt_3)$_2$] in C_6D_6. [g]Reference 17a. The experimental value of *trans*-[HPt(BCat){P(CH_2Cy)$_3$}$_2$] in C_6D_6 (Cat = catecholate, 1,2-$O_2C_6H_4$).

orbit (SO) effects are important.[9] Note that in contrast to transition-metal complexes with a partially filled d-shell, d^0 and d^{10} hydrides, and even more so f^0 actinide hydrides, exhibit characteristic ^{1}H shifts in the very high-frequency range, and SO effects play a decisive role here as well.[10] The Buckingham−Stephens model thus must be augmented by sizable SO contributions, which may amount to roughly two-thirds of the observed low-frequency ^{1}H shifts in certain iridium and platinum hydride complexes.[9] In some of the analyzed systems, more negative ^{1}H shifts did not correlate well with larger ligand-field strength of the trans ligand, and it is thus desirable to revisit these correlations carefully. Here we apply quantitative relativistic DFT methodology to unravel the relations between electronic structure and ^{1}H shifts in transition-metal hydride complexes in much more detail than has hitherto been possible. In view of their general importance, particularly in catalysis, and of extensive previous studies, we focus our attention on square-planar Pt(II) d^8 hydride complexes.

COMPUTATIONAL METHODS AND THEORETICAL BACKGROUND

Gas-phase PBE0/def2-TZVP[11−13] (with quasi-relativistic, energy-adjusted small-core ECP for Pt and I)[14,15] structure optimizations were performed with the Turbomole program package.[16] The quality of the optimized structures was assessed by comparing salient bond lengths with X-ray structure data of some related square-planar platinum(II) hydride complexes[17] (cf. Table S1 in Supporting Information). Note that the popular B3LYP functional[18] provides noticeably longer bond lengths between the Pt center and non-hydrogen ligand atoms (by ∼0.05 Å), and it is thus not the best choice for this type of complex (cf. Table S1).

Quasi-relativistic DFT single-point calculations were performed using the Amsterdam density functional (ADF) program[19] at the generalized-gradient-approximation (GGA) level, using the Perdew−Burke−Ernzerhof (PBE) exchange-correlation functional,[11] as well as its one-parameter hybrid form (PBE0),[12] employing Slater-type orbital basis sets of triple-ζ doubly polarized (TZ2P)[20] quality and an integration accuracy parameter of 5.0. Relativistic effects were treated by the two-component (2c) zeroth-order regular approximation (ZORA)[21,22] to the Dirac equation, and gauge including atomic orbitals (GIAOs)[23] were used for the shielding calculations. The implementation of the ADF program used here includes the response of the first order exchange-correlation potential (xc kernel) for the calculated shielding implemented recently.[24]

Fully relativistic DFT calculations were performed at the four-component (4c) matrix Dirac−Kohn−Sham (mDKS) level of theory with the ReSpect program package.[25] The method combines GIAOs with restricted magnetically balanced (RMB) orbitals for the small component (this includes an xc kernel).[26,27] For comparison with the ADF results, the mDKS calculations were performed with the PBE functional as well. For the heavy atomic centers (Pt, Br, I), Dyall's all-electron valence-double-ζ (Dyall VDZ) basis sets[28] were employed. Fully uncontracted Huzinaga−Kutzelnigg-type IGLO-III basis sets[29] were used for the lighter ligand atoms ($Z < 18$). The calculated nuclear shieldings σ were converted to chemical shifts δ (in parts per million) relative to the shielding of tetramethylsilane (TMS) for ^{1}H and relative to *trans*-[HPtNO_3(PMe_3)$_2$] for ^{195}Pt, computed at the same level. These are also the reference standards used in the experiments we compare to.

Molecular orbital (MO) analyses of contributions to the shieldings were performed at two different levels: (a) using the analysis tools in the ADF code, both scalar relativistic and two-component ZORA results were broken down into MO (spinor) contributions; (b) additionally, one-component (1c) GIAO calculations of ^{1}H shieldings were done, based on combining Gaussian 09[30] to obtain the Kohn−Sham MOs and the local MAG property code[31] to compute both scalar-relativistic shifts and SO corrections. For the latter, Kohn−Sham orbitals with a Fermi-contact finite-perturbation at the nucleus of interest (finite-perturbation parameter $\lambda = 0.001$) were obtained, using the PBE functional, IGLO-III basis sets for the lighter ligand atoms, and Stuttgart relativistic small-core (RSC) effective core potentials (ECPs) with corresponding valence basis sets[14] for platinum and iodine. The perturbed MOs were transferred to MAG, which used RSC spin−orbit ECPs[32] to compute the SO corrections within the mixed finite perturbation approach of ref 33.

Analyses of atomic charges and of scalar relativistic natural localized molecular orbitals (NLMOs) were done with the NBO 5.0 module by Weinhold et al. in the ADF package.[34,35] Partially ionic natural-bond-orbital (NBO) Lewis structures with a lone pair on the hydride atom

DOI: 10.1021/acs.inorgchem.5b00446
Inorg. Chem. 2015, 54, 7199−7208

were selected via the Choose keyword to invoke Lewis structures with equivalent phosphine ligands in the studied complexes with a C_{2v} symmetric *trans*-[$HPtP_2X$] core. NLMOs based on such a Lewis structure were analyzed. The lone pair NLMO on the hydride atom, with appreciable metal contribution, is denoted as BD(Pt−H). A corresponding shielding tensor analysis in terms of the full NLMO set was performed with the method reported in ref 36. Atomic contributions to the SO operators were obtained by selecting individual atomic contributions to individual ECP SO operators (for Pt, I, as well as an all-electron atomic-mean field SO operator for Br) in MAG. The delocalization index δ(A↔B), as a quantitative measure for the sharing of electrons in the context of the quantum theory of atoms-in-molecules (QTAIM),[37,38] was evaluated in the DGrid program[39] on the basis of single-point calculations performed with Gaussian09 using an all-electron Dyall VDZ basis set on Pt and def2-TZVP basis set on ligand atoms and employing a Douglas−Kroll−Hess second-order scalar relativistic Hamiltonian.[40] To distinguish this index from chemical shifts, we denote it as "DI" throughout this work. Bulk solvent effects on computed NMR shieldings were simulated via the conductor-like screening model (COSMO),[41] as implemented self-consistently in ADF.

RESULTS AND DISCUSSION

Correlation between Pt−H Distances and ^{1}H Chemical Shifts. The bond length in trans position to the considered ligand is often taken as a measure of the trans influence of a ligand.[42] As the precise position of the hydrogen atom near a heavy metal center is difficult to obtain experimentally, we may evaluate the correlation between Pt−H distances and ^{1}H shifts based on our optimized structures. In Table 1 the ligands were listed in the order of increasing Pt−H bond length, which is also the sequence of increasing trans influence, as found in many inorganic chemistry textbooks:

$$NO_3^- < ONO^- < Cl^- < Br^- < I^- < SCN^- < NO_2^- < CN^- < C_6H_5^- < CH_3^- < SiR_3^- < BR_2^-$$

The data confirm the well-known trend of a lengthening of the Pt−H bond with increasing σ-donor ability of the trans ligand, particularly for methanide, silanide, and boranide ligands.

The two- and four-component relativistic results for the ^{1}H hydride shifts of the same series of *trans*-[$HPtL(PMe_3)_2$] complexes are given in Table S2 in Supporting Information and are compared with experiment in Figure 1. Note that the experimental values sometimes belong to complexes with differently substituted phosphine ligands.[3,17,43,44] This may influence the hydride shifts but only moderately, as demonstrated for the *trans*-[$HPtCN(PR_3)_2$] series (R = H, Me, Et, Cy, Ph) in Table S3 in Supporting Information. Here, the largest difference is observed between complexes with PPh_3 and PCy_3 ligands (with $\delta(^1H)$ = −6.3 ppm and −7.6 ppm, respectively), while hydride shifts in Pt(II) complexes with methyl- and ethyl-substituted phosphine ligands differ only by 0.2 ppm. The generally somewhat more shielded hydride shifts for the [$HPtL(PCy_3)_2$] series are also evident by comparing experimental data from Table 1 with those in ref 45.

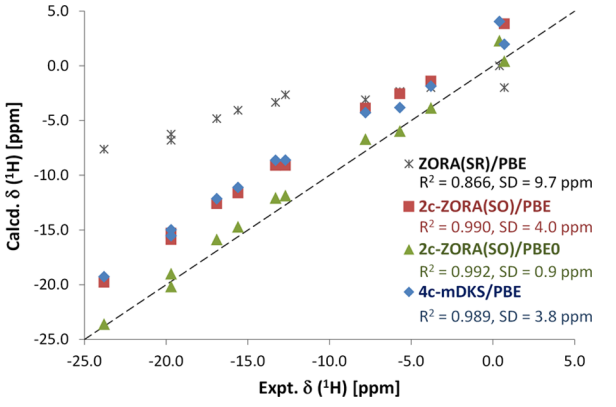

Figure 1. Computed vs experimental ^{1}H NMR hydride shifts (in ppm vs TMS) in *trans*-[$HPtL(PMe_3)_2$] complexes (cf. Table S2 in Supporting Information for numerical data). The dashed line represents the ideal agreement with experiment.

From Figure 1 it is particularly obvious that the scalar relativistic ZORA(SR) results for ^{1}H NMR hydride shifts tend to be insufficiently negative. In keeping with our previous findings,[9] this is improved significantly by inclusion of SO effects. The two-component relativistic ZORA(SO) (including SO coupling) and the four-component mDKS results with the PBE functional agree well with each other, and both reproduce the experimental trend in hydride shifts very well (R^2 > 0.98), although the computed shifts are systematically too deshielded by ∼3−4 ppm. Excellent agreement between theory and experiment (with R^2 = 0.992 and a standard deviation of 0.9 ppm) is achieved by using the 2c-ZORA(SO) method in conjunction with the hybrid PBE0 functional. This method is thus preferred in further discussion and analysis. Note that the current 4c-mDKS ReSpect implementation of chemical shifts does not yet allow for GIAO calculations with hybrid functionals, and it is under development. Furthermore, it is clear that inclusion of the kernel in the modified ADF implementation[24] is important for good agreement. Table S2 in Supporting Information demonstrates that the previous 2c-ZORA implementation of nuclear shieldings in ADF without kernel provides insufficiently negative ^{1}H shifts, particularly for systems with larger σ^{SO} contribution (with a maximum deviation of 4.4 ppm from experiment for the nitrato complex when using the PBE0 functional). Indeed, if we delete the kernel contributions in the 4c-mDKS ReSpect calculations, we see the same deterioration (see the PBE results in Table S2). Inclusion of bulk solvent effects by the COSMO solvation model (assuming benzene and CH_2Cl_2 as solvent, respectively) leads to only a marginal improvement of computed hydride shifts, reducing the standard deviation by 0.1 ppm (Table S4 in Supporting Information).

Figure 2 shows that more negative ^{1}H shifts are indeed roughly correlated to shorter Pt−H bonds, as emphasized early on by Buckingham and Stephens.[4] A trans influence series for the ^{1}H hydride shifts is

$$NO_3^- < ONO^- < NO_2^- < Cl^- < Br^- < SCN^- \approx I^- < CN^- < Ph^- < Me^- < SiR_3^- \approx BR_2^-$$

The N-nitrito complex at first sight provides the clearest outlier, as had been noted already by Chatt and Shaw.[3] The measured and computed proton shift is at less negative value than expected from the usual trans effect series. It had been suggested that the nitrito group is actually bound to platinum by one of its oxygen atoms. However, our computations show that this would affect the hydride shift only marginally—the O-nitrito complex exhibits a very similar computed value (cf. Table 1). Moreover, measured spin−spin coupling constants later confirmed an N-nitrito complex.[46]

While the N-nitrito complex with its "too negative" shift is the most apparent outlier, the halide complexes deviate in the

DOI: 10.1021/acs.inorgchem.5b00446
Inorg. Chem. 2015, 54, 7199−7208

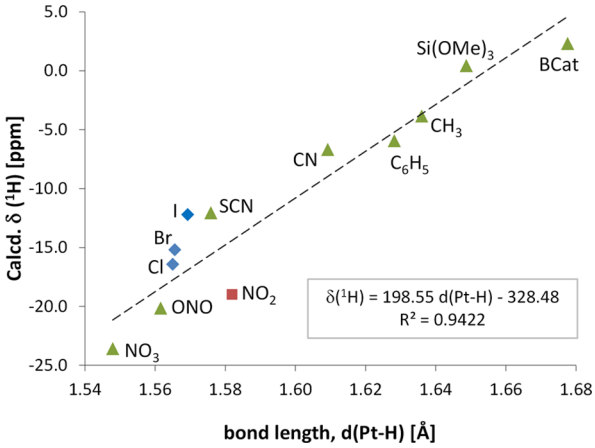

Figure 2. Correlation between computed ^{1}H NMR hydride shifts (2c-ZORA(SO)/PBE0/TZ2P results) and optimized Pt−H bond lengths in *trans*-[HPtL(PMe$_3$)$_2$] series (cf. Table 1). The dashed line represents the linear-regression line of the values represented by triangles.

positive direction (cf. Figure 2 and discussion below). The nitrite ligand is in any case an example that shows previous interpretations to be incomplete: while the N- and O-nitrito compounds exhibit very similar ^{1}H shifts, the N-nitrito complex clearly has a longer Pt−H bond (cf. Table 1). On the other hand, the N-nitrito and S-thiocyanato complexes exhibit similar Pt−H distances but rather different hydride shifts. These cases indicate that a rationalization of the shifts via the Pt−H distances does not cover all aspects of the problem. A more detailed theoretical analysis is thus desirable.

Shielding-Tensor Contributions. We separate the shielding (both isotropic value and tensor components) into the well-known diamagnetic (σ^d) and paramagnetic (σ^p) terms and into a spin−orbit (σ^{SO}) term. Table 2 shows such a breakdown obtained at the 2c-ZORA-GIAO-PBE0/TZ2P level. We note that the separation into σ^d and σ^p is not unique but depends on the chosen gauge of the magnetic vector potential. Here we followed the previous convention for definition of diamagnetic and paramagnetic terms at DFT-GIAO level by Ziegler and co-workers.[22,47] Separation of the SO terms also follows the standard procedure for the 2c-ZORA-GIAO-PBE0/TZ2P level.[48]

We see that the isotropic σ^d remains almost constant (within less than 2.2 ppm) across the series of trans ligands. This constancy is usually assumed for all nuclei except hydrogen (or helium). For proton shifts it is not self-evident, as hydrogen has no (spherical) core−shell, and we show below that the diamagnetic contribution to the shielding tensor is in fact highly anisotropic. Nevertheless, for the purpose of analyzing the trans influence on the isotropic ^{1}H hydride shifts, we may concentrate on σ^p and σ^{SO} (Figure 3).

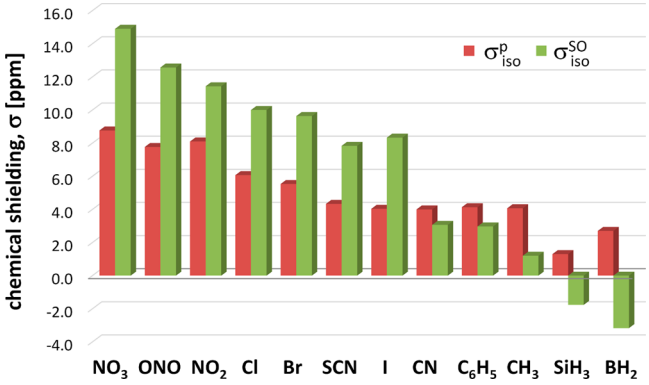

Figure 3. Dependence of the computed paramagnetic and SO contributions to isotropic hydride ^{1}H shielding on trans ligand L in the [HPtL(PMe$_3$)$_2$] series (2c-ZORA(SO)/PBE0/TZ2P results; cf. Table 2 and Table S5 for numerical data).

Across the entire series, the isotropic σ^p varies by up to 7.5 ppm, σ^{SO} by ∼18 ppm! Furthermore, the σ^d and σ^p contributions alone explain neither the large low-frequency hydride shifts for complexes involving ligands with weak trans influence nor the positive ^{1}H shift values recorded for some silyl and boryl complexes. It is thus clear that σ^{SO} dominates the dependence of the shielding on the trans ligand. While the σ^p and σ^{SO} trends go roughly parallel for "weak" trans ligands (suggesting related electronic-structure origins), notable differences between the two terms are seen for strong σ-donor ligands. For example, we see that the isotropic σ^p remains relatively unchanged for the ligands SCN$^-$, CN$^-$, CH$_3^-$, and BH$_2^-$ (within less than 1.5 ppm), whereas σ^{SO} still drops significantly along the same series and changes from positive to negative sign for the strongest σ-donors (Figure 3).

In addition, bromine and particularly iodine are both sufficiently heavy to contribute noticeably to the SO effects on the ^{1}H shifts.[49] Analyses at the one-component perturbational level (by removing individual SO-ECPs) show contributions of −0.3 ppm for Br and of −1.3 ppm for I to the ^{1}H shieldings. Converted into shifts, halogen SO contributions hence provide an explanation for the "too positive" shifts in Figure 2 for L = Br, I.

Table 2. Calculated Components of the Hydride ^{1}H Shielding Tensors (in ppm) in Selected *trans*-[HPtL(PMe$_3$)$_2$] Complexes and Their Separation into Diamagnetic (σ^d), Paramagnetic (σ^p) and Spin−Orbit (σ^{SO}) Terms[a]

L	$\sigma^d_{\parallel}$	$\sigma^d_{\perp,ip}$	$\sigma^d_{\perp,op}$	σ^d_{iso}	$\sigma^p_{\parallel}$	$\sigma^p_{\perp,ip}$	$\sigma^p_{\perp,op}$	σ^p_{iso}	$\sigma^{SO}_{\parallel}$	$\sigma^{SO}_{\perp,ip}$	$\sigma^{SO}_{\perp,op}$	σ^{SO}_{iso}
NO_3	58.7	23.7	12.2	31.5	−4.9	13.1	18.1	8.8	−2.2	22.2	24.7	14.9
Cl	58.2	23.1	12.7	31.3	−3.8	7.5	14.5	6.1	−2.1	14.2	17.9	10.0
NO_2	57.0	23.4	12.8	31.1	−5.0	12.2	17.1	8.1	−2.5	15.4	21.4	11.4
CN	55.9	23.6	14.0	31.2	−3.7	5.2	10.5	4.0	−3.0	0.3	11.9	3.1
CH_3	54.1	23.2	13.0	30.1	−2.7	4.4	10.5	4.1	−3.6	−2.9	10.1	1.2
SiH_3	53.8	23.2	13.3	30.1	−4.4	0.7	7.6	1.3	−3.8	−11.1	9.6	−1.8
BH_2	51.2	23.1	13.7	29.3	−6.1	0.2	14.0	2.7	−5.0	−17.8	13.3	−3.2

[a]2c-ZORA(SO)/PBE0/TZ2P results; isotropic shielding $\sigma_{iso} = \sigma^d_{iso} + \sigma^p_{iso} + \sigma^{SO}_{iso}$, where $\sigma^k_{iso} = (\sigma^k_{\parallel} + \sigma^k_{\perp,ip} + \sigma^k_{\perp,op})/3$ (k = d, p, SO). Data for all Pt(II) hydride complexes are given in Table S5 in Supporting Information. Model complexes with SiH_3 and BH_2 trans ligands possess similar hydride shifts as their Si(OMe)$_3$ and BCat congeners and are therefore used in further analysis.

DOI: 10.1021/acs.inorgchem.5b00446
Inorg. Chem. 2015, 54, 7199−7208

Molecular Orbital Analysis of σ^{p}. While σ^{SO} dominates the overall trends, we start our closer MO analysis with σ^{p} for a number of complexes (at the scalar-relativistic ZORA level). For closer analysis it is important to distinguish the individual components of the $\boldsymbol{\sigma}^{p}$ tensor, which is clearly anisotropic (cf. Table 2). That is, we obtain $\sigma^{p}_{\parallel}$ parallel to the Pt−H bond, $\sigma^{p}_{\perp,ip}$ perpendicular to the Pt−H bond but in the plane of the complex, and the out-of-plane perpendicular component, $\sigma^{p}_{\perp,op}$ (cf. Figure 4). As predicted by the Buckingham−Stephens model,[4] it is the two perpendicular components that provide an overall shielding contribution, while the parallel component is deshielding. This had been confirmed by DFT calculations, which, however, gave much lower shielding anisotropies than the original Buckingham−Stephens model predictions.[8]

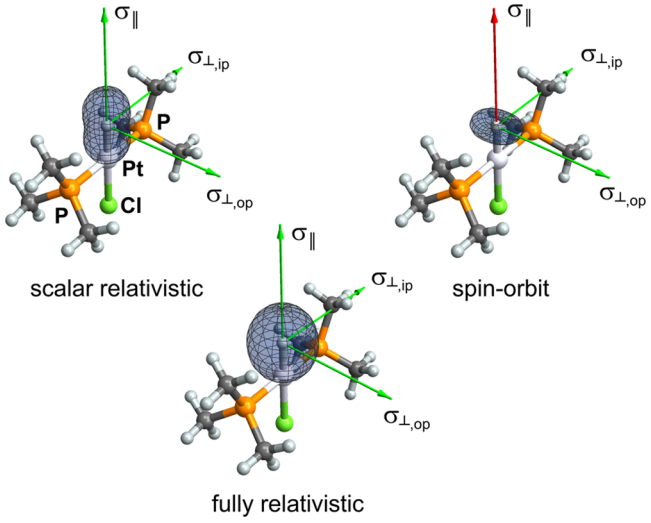

Figure 4. Scalar-relativistic ($\boldsymbol{\sigma}^{d}$ + $\boldsymbol{\sigma}^{p}$), spin−orbit ($\boldsymbol{\sigma}^{SO}$), and fully relativistic hydride shielding tensors in *trans*-[HPtCl(PMe$_3$)$_2$], represented as polar plots of functions^{S0} $\sum_{ij} r_i r_j \sigma_{ij}$ (a green arrow indicates a shielding contribution; a red one indicates a deshielding contribution).

The comparison in Table 2 reveals (a) very anisotropic but closely similar diamagnetic shielding tensors for all complexes; (b) the main changes of the isotropic σ^{p} are clearly due to the two perpendicular paramagnetic shielding tensor contributions (e.g., $\sigma^{p}_{\perp,ip}$ decreases by ∼13 ppm with increasing trans influence), whereas the parallel contributions differ much less ($\sigma^{p}_{\parallel}$ changes overall by ca. 3.5 ppm).

To what extent are changes in the Pt−H distance the direct *cause* of the trends in paramagnetic shieldings, as implied by previous studies?[S1] This is probed in Table 3 for the chloro and cyano complexes as examples, by contracting or expanding, respectively, the Pt−H distance by 0.05 Å from its optimized value. We first of all note that the overall changes in shielding tensor components (and isotropic values as well) upon elongation/shortening of Pt−H bonds are significantly less than the range covered by complexes with different trans ligands (cf. Tables 2 and 3), although they show a comparable range of Pt−H distances [cf. d(Pt−H) values in Tables 1 and 3]. That is, the direct distance dependence of the perpendicular paramagnetic shieldings is quite small and does not support the original interpretations by Buckingham and Stephens.[4]

The main trans effects on σ^{p} arise from the perpendicular components (Table 2). We separate these components into contributions from individual couplings between occupied and virtual canonical MOs obtained from scalar relativistic ZORA-GIAO calculations. We focus here on the comparison between the CN and BH$_2$ complexes as examples with strong trans influence and small σ^{p} values, on the Cl complex with a medium trans influence, and on the NO$_3$ complex as a case with weak trans influence and large shielding contributions. The analysis shows that σ^{p} values arise from numerous contributions, but there are only a few that stand out by being larger and by differing more between the complexes (cf. Table 4; the main MOs contributing to σ^{p} and σ^{SO} are shown in Figure 5).

In agreement with the Buckingham−Stephens model[4] and previous DFT analyses,[8] these contributions are mainly caused by couplings between (in-plane and out-of-plane) d_{π}-type occupied MOs and the σ^{*}(Pt−H)-type unoccupied MO(s) with some d-metal character and s orbital contribution from the hydride atom (cf. Figure 5). While coupling of the in-plane d_{π}-type MO to the σ^{*}(Pt−H)-type MO dominates the out-of-plane perpendicular component of $\boldsymbol{\sigma}^{p}$, the out-of-plane d_{π}-type MO contributes to the in-plane perpendicular component. These contributions are significantly larger for the NO$_3$ than for the CN and BH$_2$ complexes, thus also explaining differences in the isotropic σ^{p} contributions for these systems.

Analogous dominant occupied-virtual MO couplings, which originate from in-plane or out-of-plane d_{π}-type MOs, are found to be largely responsible also for the trans ligand influences on σ^{p} of the other complexes (see Table S8 and Figure S1 in Supporting Information for analyses on more complexes). Overall, these few contributions from d_{π}-type MOs reflect the entire σ^{p} trend in the trans influence series.

MO Analysis of σ^{SO}. We showed above that the trans influence is largely dictated by σ^{SO}. Table 2 shows that the two perpendicular components of $\boldsymbol{\sigma}^{SO}$ are responsible for the important SO shielding (as well as for the small SO deshielding in the case of silyl and boryl complexes), and these components are both significantly smaller for ligands with strong trans influence than for weak trans-influence ones. The trends for the

Table 3. Computed Hydride ^{1}H NMR Shielding Tensor Components (in ppm) in *trans*-[HPtL(PMe$_3$)$_2$] (L = Cl, CN) Complexes as a Function of Pt−H Distance[a]

L	d(Pt−H)[Å]	$\sigma^{d}_{\parallel}$	$\sigma^{d}_{\perp,ip}$	$\sigma^{d}_{\perp,op}$	σ^{d}_{iso}	$\sigma^{p}_{\parallel}$	$\sigma^{p}_{\perp,ip}$	$\sigma^{p}_{\perp,op}$	σ^{p}_{iso}	$\sigma^{SO}_{\parallel}$	$\sigma^{SO}_{\perp,ip}$	$\sigma^{SO}_{\perp,op}$	σ^{SO}_{iso}
Cl	1.505	61.5	23.7	13.0	32.7	−4.2	7.5	15.2	6.2	−2.0	13.4	16.2	9.2
	1.565	58.2	23.1	12.7	31.3	−3.8	7.5	14.5	6.1	−2.1	14.2	17.9	10.0
	1.605	55.2	22.6	12.6	30.1	−3.5	7.4	13.9	5.9	−2.2	15.2	19.8	10.9
CN	1.559	59.0	24.1	14.2	32.4	−4.0	5.2	11.1	4.1	−2.9	0.4	10.7	2.7
	1.609	55.9	23.6	14.0	31.2	−3.7	5.2	10.5	4.0	−3.0	0.3	11.9	3.1
	1.659	53.2	23.2	13.9	30.1	−3.4	5.2	10.0	3.9	−3.0	0.2	13.2	3.5

[a] 2c-ZORA(SO)/PBE0/TZ2P results (cf. Computational Methods and footnotes in Table 2).

DOI: 10.1021/acs.inorgchem.5b00446
Inorg. Chem. 2015, 54, 7199−7208

Table 4. Selected Contributions from Occupied MOs with d_π Character to the Paramagnetic Part of the ^{1}H NMR Hydride Shielding Tensor, σ^p, in Pertinent *trans*-[HPtL(PMe$_3$)$_2$] Complexes[a]

L	molecular orbitals	σ^p_{iso} [ppm]	$\sigma^p_{\parallel}$ [ppm]	$\sigma^p_{\perp,ip}$ [ppm]	$\sigma^p_{\perp,op}$ [ppm]	ΔE [eV]
NO_3	HOMO−2	3.2	−0.7	10.2	0.0	
	(HOMO−2→LUMO+1)	(2.0)	(0.0)	(6.0)	(0.0)	6.80
	HOMO−3	3.0	−0.5	0.4	9.0	
	(HOMO−3→LUMO+1)	(1.2)	(0.0)	(0.0)	(3.6)	7.25
	HOMO−6	1.6	−1.4	−0.6	6.8	
	(HOMO−6→LUMO+1)	(1.9)	(0.0)	(0.0)	(5.6)	8.03
Cl	HOMO	1.4	−0.1	4.0	0.0	
	(HOMO→LUMO+1)	(0.6)	(0.0)	(1.8)	(0.0)	6.41
	HOMO−2	2.1	0.0	0.4	5.9	
	(HOMO−2→LUMO+1)	(1.0)	(0.0)	(0.0)	(3.0)	6.61
	HOMO−6	1.2	−0.3	4.2	−0.4	
	(HOMO−6→LUMO+1)	(1.0)	(0.0)	(3.0)	(0.0)	8.10
	HOMO−7	1.6	−0.7	−0.2	5.7	
	(HOMO−7→LUMO+1)	(1.8)	(0.0)	(0.0)	(5.5)	8.57
CN	HOMO−1	1.4	−0.2	4.4	0.0	
	(HOMO−1→LUMO+2)	(0.5)	(0.0)	(1.5)	(0.0)	7.37
	HOMO−2	2.2	0.0	0.3	6.2	
	(HOMO−2→LUMO+2)	(1.0)	(0.0)	(0.1)	(2.9)	7.65
BH_2	HOMO−5	1.1	0.5	1.0	1.7	
	(HOMO−5→LUMO+4)	(0.4)	(0.2)	(0.4)	(0.6)	8.65

[a]Individual contributions from couplings of the given occupied MOs to σ^*(Pt−H) virtual MOs are given in parentheses. ZORA(SR)/PBE0/TZ2P results. See Figure 5 for plots of the relevant MOs.

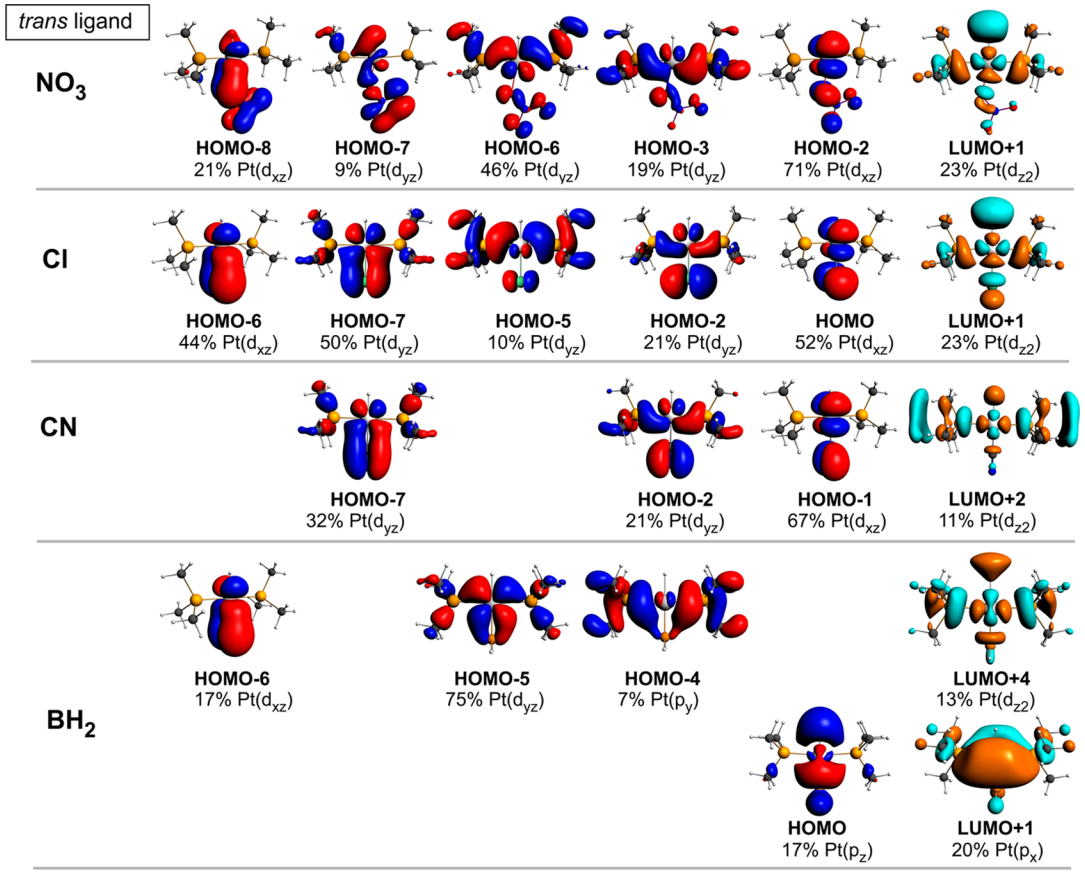

Figure 5. Isosurface plots (±0.03 au) of the dominant occupied and virtual MOs contributing to the $\boldsymbol{\sigma}^p$ and $\boldsymbol{\sigma}^{SO}$ tensors in selected *trans*-[HPtL(PMe$_3$)$_2$] complexes (cf. Tables 4 and 5). Contributions from the Pt d-orbitals (and p-orbitals where applicable) in percent are indicated. The symmetry of the dominant Pt(5d)/Pt(6p) atomic orbitals is indicated in parentheses (*z* corresponds to a twofold rotation axis along the Pt−H bond; *y* and *x* axes lie in-plane and out-of-plane, respectively).

DOI: 10.1021/acs.inorgchem.5b00446
Inorg. Chem. 2015, 54, 7199−7208

out-of-plane component go roughly parallel to the two perpendicular components of $\boldsymbol{\sigma}^{p}$ (Table 2), whereas the trend for the in-plane component of $\boldsymbol{\sigma}^{SO}$ is more pronounced. This indicates that the SO shieldings in these hydride complexes may be viewed as an extension of the Buckingham−Stephens model,[9] but with some modifications (see below). The SO contributions in Table 3 show, furthermore, that there is almost no direct distance dependence of these contributions. This may be attributed to the almost constant metal 5d-orbital involvement in the Pt−H bonds upon their elongation/shortening when keeping the trans ligand unchanged. That is, the correlation between measured shieldings and Pt−H distances has an indirect rather than direct origin also for the SO contributions (see above). In fact, the shorter Pt−H bond length provides even the smaller isotropic σ^{SO} shielding contribution, although only by a small margin (cf. Table 3).

Note that due to the large anisotropy of $\boldsymbol{\sigma}^{d}$ compared to $\boldsymbol{\sigma}^{p}$ (with a dominant parallel $\sigma_{\parallel}^{d}$ component), the "scalar relativistic" hydride shielding tensor ($\boldsymbol{\sigma}^{d} + \boldsymbol{\sigma}^{p}$) has its largest shielding component along the Pt−H bond. The SO-induced shielding ($\boldsymbol{\sigma}^{SO}$), which contributes predominantly to the two perpendicular components, makes the "fully relativistic" shielding tensor less anisotropic in most cases (cf. Figure 4 and Table S6 in Supporting Information). This contrasts, for example, to some five-coordinate square-pyramidal Ir(III) and Rh(III) complexes, where SO effects give rise to highly anisotropic shielding tensors.[9] The predicted anisotropies in the latter systems have very recently been confirmed by solid-state $^{1}H/^{2}H$ NMR experiments.[52]

MO analyses of the SO contributions may be obtained by subtraction of MO contributions obtained in scalar-relativistic calculations from the corresponding MO (spinor) contributions of two-component ZORA-SO calculations. Table 5 shows

Table 5. Dominant Occupied-MO Contributions to the Spin-Orbit Part of the ^{1}H NMR Hydride Shielding Tensor, $\boldsymbol{\sigma}^{SO}$, in Pertinent *trans*-[HPtL(PMe_3)$_2$] Complexes[a]

ligand L	MO contributions	σ_{iso}^{SO} [ppm]	$\sigma_{\parallel}^{SO}$ [ppm]	$\sigma_{\perp,ip}^{SO}$ [ppm]	$\sigma_{\perp,op}^{SO}$ [ppm]
NO_3	HOMO−3 (→LUMO+1)	3.1	−0.9	1.0	9.3
	HOMO−6 (→LUMO+1)	2.3	−1.1	−1.2	9.2
	HOMO−7 (→LUMO+1)	2.3	−0.2	1.8	5.3
	HOMO−8 (→LUMO+1)	5.8	0.4	17.4	−0.5
Cl	HOMO−5 (→LUMO+1)	6.2	−0.1	2.2	16.5
	HOMO−7 (→LUMO+1)	3.5	−0.9	1.3	10.2
CN	HOMO−7 (→LUMO+2)	4.0	−0.7	1.0	11.7
BH_2	HOMO (→LUMO+1)	−7.2	−9.5	−7.4	−4.7
	HOMO−4 (→LUMO+4)	2.1	0.9	2.0	3.5
	HOMO−5 (→LUMO+4)	1.7	0.2	1.5	3.4
	HOMO−6 (→LUMO+4)	1.4	2.6	1.4	0.1

[a]2c-ZORA(SO)/PBE0/TZ2P results (cf. Computational Methods). The dominant occupied-virtual MO couplings are indicated in parentheses.

the dominant contributions to the $\boldsymbol{\sigma}^{SO}$ tensor, which stem in most cases from coupling between the occupied in-plane and out-of-plane d_{π}-type and virtual σ^{*}(Pt−H) MOs (note that σ and π-type symmetry is given here with respect to the Pt−H bond). Although the platinum d_{π}-type MO contributions reflect the overall trend when considering only ligands with weak and medium trans influence, the dominant contributors to σ^{p} are not equally important for σ^{SO} (cf. Table S7 in Supporting Information). Note also that other couplings contribute to σ^{SO} as well, in particular, for the strongest σ-donors (L = alkyl, SiR_3, BR_2). Here, magnetic couplings from occupied σ(Pt−H)-type MOs into vacant π-type MOs (both involving platinum 6p orbitals) come into play and are responsible for the deshielding (negative σ^{SO}) contribution, which counteracts the shielding SO effect from $5d_{\pi} \rightarrow 5d_{\sigma}^{*}$-based couplings (cf. Table 5 and Table S9 in Supporting Information for more data). Now the magnitude and the sign of the hydride σ^{SO} is based on a balance between various shielding (predominantly $5d_{\pi} \rightarrow 5d_{\sigma}^{*}$) and deshielding ($5d/6p_{\sigma} \rightarrow 6p_{\pi}$) magnetic couplings. This results, for example, in a substantial reduction of σ^{SO} for *trans*-[HPtMe(PMe_3)$_2$] (still with slightly predominant d_{π}(Pt) → σ^{*}(Pt−H) transitions) and in a change to negative σ^{SO} for silyl and boryl complexes (with a dominant deshielding contribution from the magnetic coupling between the σ-type highest occupied molecular orbital (HOMO), with appreciable Pt($6p_z$) character and the vacant π-type second lowest unoccupied molecular orbital (LUMO+1) with 20% Pt($6p_x$) character).

In Supporting Information, we also provide an analysis of SO shieldings obtained at one-component perturbation level based on a scalar relativistic calculation (see Tables S15 and S16 and Figure S2), which gives a qualitatively similar MO picture.

Recently, Vicha et al.[53] have studied the influence of electronic and structural effects on the σ^{SO} contributions to ^{15}N NMR shifts for a series of d^6 iridium complexes by stretching trans bonds and modifying trans ligands. They found correlations with the nitrogen s-orbital character of the Ir−N bond, with energy gaps and, most importantly, with the iridium d-orbital character in the Ir−N bond. Notably, these authors argued not only via the FC matrix elements, as is often done,[54,55] but emphasized the SO matrix elements as decisive. Consistent with the present work, those authors also recognized the shielding and deshielding SO contributions coming from 5d → 5d* and 6p → 6p* magnetic couplings, respectively, on ^{13}C and ^{15}N NMR shifts in some 2-phenylpyridine d^8 complexes of platinum(II) and gold(III).[56] We show here additionally, that a deshielding SO effect due to $6p_{\sigma} \rightarrow 6p_{\pi}$-based magnetic couplings may be induced in Pt(II) complexes by introducing ligands with a strong trans influence, without changing the transition-metal center (Pt(II) → Au(III) in ref 56).

As the hydrogen s-orbital character in the Pt−H bond (relevant for the Fermi-contact interaction) is largely constant within the present series, it is the SO coupling of platinum 5d orbitals that dominates the hydride σ^{SO}. It is thus to be expected that the trans ligand influence on σ^{SO} may indeed reflect the metal d-orbital contributions to the relevant MOs. Using the relativistic NMR shielding analysis method based on NLMOs,[36] it can be shown that the percentage of Pt character (and thus the metal d-orbital involvement) in the Pt−H bond goes parallel with the σ^{SO} contribution due to this NLMO, which causes almost the entire σ^{SO} term (cf. Table S11 in Supporting Information). Together, these observations suggest that the more covalently bound ligands with strong trans influence polarize the relevant Pt(5d) atomic orbitals away from the Pt−H bond, which is accompanied by a decrease of the Pt−H bond covalency (cf. NPA atomic charges and QTAIM delocalization indices in Table 1). Such ligands thus diminish the relevant matrix elements, both for σ^{SO} and σ^{p}. This is demonstrated in Figure 6, which shows a very good correlation of the hydride σ^{SO} term with the metal percentage contribution to the Pt−H σ-bonding NLMO as well as with the

DOI: 10.1021/acs.inorgchem.5b00446
Inorg. Chem. 2015, 54, 7199−7208

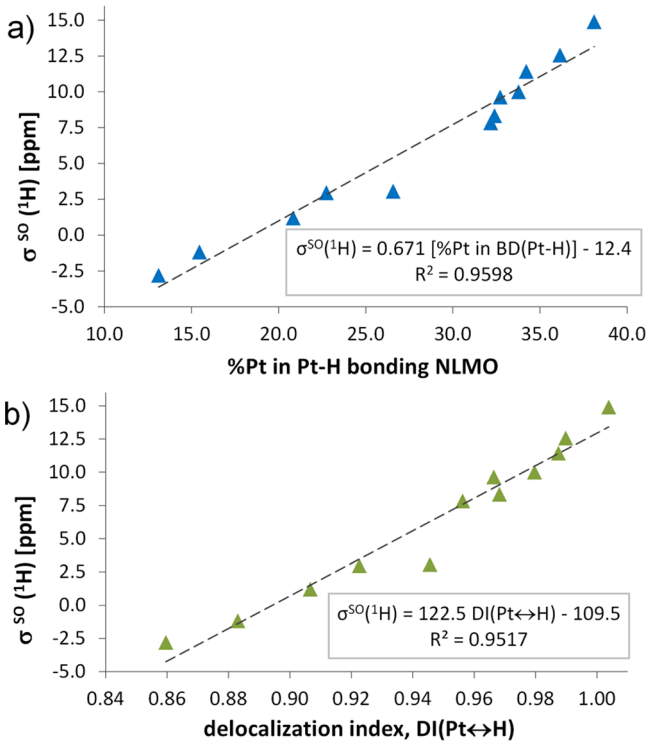

Figure 6. Correlation of the SO-induced isotropic hydride shielding σ^{SO} with a) the percentage of metal character in the Pt−H σ-bonding NLMO and b) the QTAIM delocalization index.

QTAIM delocalization index DI(Pt↔H), as a measure of the covalency of the Pt−H bond.

Somewhat poorer but still reasonable linear plots are also found for correlations of σ^{SO} with the optimized Pt−H bond lengths (R^2 = 0.9148) and with the hydride atomic charges (R^2 = 0.9443; see Figures S3 and S4 in Supporting Information).

Correlation between ^{1}H and ^{195}Pt NMR Shifts. The Buckingham−Stephens off-center ring-current model[4] would suggest that the same paratropic ring currents within the incomplete metal d-shell will lead to a deshielding of the metal nucleus and the well-known shielding of the hydride proton. Indeed, already in 1968 Dean and Green found a moderately good correlation between ^{195}Pt and ^{1}H NMR chemical shifts for a series of platinum hydride complexes.[51] Deviations from ideal correlation were attributed to the dependence of the ^{1}H shifts on the Pt−H distance (see above), in contrast to the ^{195}Pt shifts, which should be affected less.

The above results for the proton shifts suggest a different interpretation for the incomplete correlation: the hydride ^{1}H shifts are to a large extent determined by the SO shifts arising from platinum SO coupling. This is often termed a heavy-atom effect on the light atom shielding (HALA effect).[54,55] In contrast, platinum SO effects on the ^{195}Pt shieldings belong to the heavy-atom effects on the heavy-atom shielding (HAHA effects), which were shown to be essentially atomic in nature and to thus largely cancel for relative shift trends.[57−59] The ^{195}Pt shift trends are thus expected to be dominated by the σ^p term,[60] unless heavy atoms are bonded to platinum, which could give rise to HALA SO effects. The latter should apply only to the halide ligands.

We thus computed also the ^{195}Pt shifts, both at 2c-ZORA-SO and at 4c-mDKS levels (Table 6). Note again that the experimental values are for compounds with ethyl-substituted phosphine ligands, while we compute the methyl-substituted complexes for consistency with the ^{1}H chemical shifts. Both methods give closely comparable relative shifts, even though larger differences are observed for absolute ^{195}Pt shieldings (cf. Tables S12 and S13 in Supporting Information). The effect of the substituents on the ^{195}Pt shifts is more pronounced than for the ^{1}H hydride shifts, in particular when replacing trialkylphosphine ligands for aryl analogues (cf. Table S3 in Supporting Information), but it is anticipated to have a marginal impact on relative shift trends. The calculated ^{195}Pt chemical shifts at 2c-ZORA-SO as well as at 4c-mDKS levels agree very well with experiment, given the known sensitivity of ^{195}Pt shifts to a variety of factors, including solvent effects.[61,62] Note that the bulk solvent effects on ^{195}Pt NMR shifts simulated by the COSMO solvation model are only marginal (cf. Table S14 in Supporting Information), but some specific interactions (such as a coordination of solvent molecules) may play a role as well.

Figure 7 plots the obtained ^{1}H hydride shifts against the ^{195}Pt data. A good inverse correlation (lower proton shifts with larger platinum shifts) is found only for the Pt(II) complexes, where L = NO_3, ONO, SCN, CN (green triangles), and for the chloro complex. The bromo and iodo complexes deviate considerably from the correlation line, due to the large negative halogen HALA SO contributions to the platinum shift, in particular of course for the iodo complex. Indeed, if we artificially switch off

Table 6. Calculated and Experimental ^{195}Pt NMR Shifts in the *trans*-[HPtL(PMe_3)$_2$] Series[a]

ligand L	δ^{Pt}_{2c} (PBE) [ppm]	δ^{Pt}_{4c} (PBE) [ppm]	δ^{Pt}_{2c} (PBE0) [ppm]	expt[b] [ppm]
NO_3	0.0	0.0	0.0	0.0
ONO	43.2	57.3	8.9	−60.3
Cl	−161.2	−163.7	−168.5	−137.4
Br	−250.7	−273.0	−267.6	−249.3
I	−421.7	−443.7	−452.5	−442.9
SCN	−200.3	−184.9	−262.9	−248.9
CN	−268.8	−239.6	−362.0	−408.3

[a]NMR shifts in parts per million vs *trans*-[HPtNO$_3$(PMe_3)$_2$] as the primary reference standard. δ^{Pt}_{2c}: 2c-ZORA(SO) results with TZ2P basis set; δ^{Pt}_{4c}: 4c-mDKS results using a Dyall VDZ/IGLO III basis set (cf. Computational Methods). [b]Reference 51. The experimental values for *trans*-[HPtL(PEt_3)$_2$] were measured in acetone-d_6.

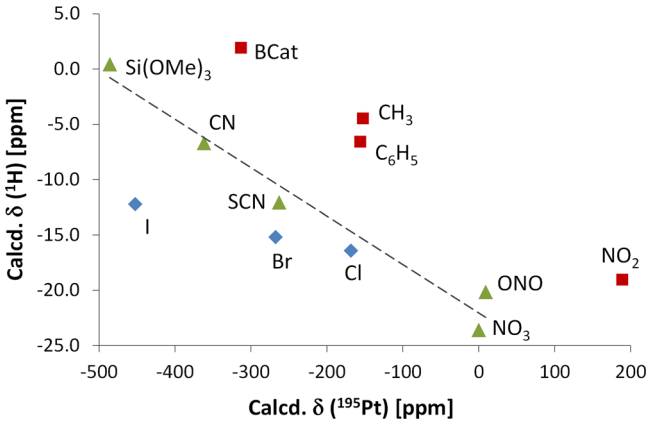

Figure 7. Correlation of computed ^{1}H and ^{195}Pt chemical shifts within the *trans*-[HPtL(PMe_3)$_2$] series (2c-ZORA(SO)/PBE0/TZ2P results). See data in Tables 1 and 6. The dashed line represents the linear-regression line of the values represented by green triangles.

DOI: 10.1021/acs.inorgchem.5b00446
Inorg. Chem. 2015, 54, 7199−7208

the halogen contributions, the points for the bromo and iodo complex fall closer to the correlation line (data not shown).

Including also computed shifts for the other trans platinum hydrides (L = NO_2, C_6H_5, CH_3, $Si(OMe_3)_3$, BCat), where no experimental ^{195}Pt values are available, provides still much poorer correlation with the hydride shifts (Figure 7). This is most striking for the N-nitrito complex, which exhibits a comparably more deshielded ^{195}Pt signal, whereas the other Pt(II) complexes are shielded relative to *trans*-$[HPtNO_3(PMe_3)_2]$. Indeed, the very limited correlation between the shifts of the two nuclei should not be too surprising, given the various SO and non-SO contributions we have identified, in particular, for the proton shifts.

CONCLUSIONS

We have recently demonstrated the often appreciable importance of SO effects for the strikingly negative ^{1}H shifts of heavy transition-metal hydride complexes with d^6 or d^8 configurations.[9] This observation has prompted the present study, which has revisited the long-appreciated correlations of these ^{1}H hydride shifts with the trans ligand influence series, with Pt−H distances, and with ^{195}Pt shifts in a series of square-planar Pt(II) complexes.

We find that the paramagnetic and SO shielding contributions go roughly in parallel for "weak" and "medium" trans ligands and tend to be dominated by magnetic couplings between the d_π-type occupied and σ^*(Pt−H) virtual MOs. In general, it is, however, the SO shifts that dominate the observed trans ligand dependencies. The correlations between σ^p and σ^{SO} may break down, for example, due to SO effects arising from heavy halide substituents or due to additional magnetic couplings between occupied σ(Pt−H) and vacant π-type MOs (both with an appreciable platinum 6p character). The latter are deshielding and become pronounced for ligands with the strongest trans influence (they are, however, not operative for σ^p).

In agreement with some recent work for other types of metal-bonded ligand-atom shifts in 5d transition-metal complexes, trans ligand-dependent trends in the SO shifts are affected relatively little by ligand-field energy splittings and more noticeably by changes in the matrix elements of the SO and magnetic-field operators, due to variations in the polarization of the metal d-orbitals by the ligand in trans position. Both σ^p and σ^{SO} contributions to the ^{1}H hydride shielding tensors tend to be dominated by contributions perpendicular to the M−H bond. Overall, the trans ligand affects the covalency of the Pt−H bond but even more decisively the polarization of the metal d-orbitals. For example, good π-acceptor ligands draw the metal orbitals toward them and thereby diminish relevant matrix elements of the ^{1}H hydride shielding tensor. As this influences both paramagnetic and SO contributions to the ^{1}H shieldings in a roughly comparable way, it appears reasonable to view the observed trends in terms of an extended Buckingham−Stephens model that emphasizes the importance of SO effects. Interestingly, ligands with the strongest trans influence (SiR_3, BR_2) are shown to revert the sign of the usually shielding σ^{SO} contribution to the ^{1}H shifts in complexes with partially filled d-shell (by a substantial reduction of the metal 5d-orbital involvement in Pt−H bonding, and by involvement of metal 6p-type orbitals in the magnetic couplings), which counteracts the shielding effect from Pt(d_π) → σ^*(Pt−H)-based couplings and may cause an overall small deshielding of the hydride proton.

Previously observed correlations between the ^{1}H shifts and Pt−H distances arise indirectly from the effect of the trans ligand on the polarization of the metal d orbitals, which in turn affects both the structures and the shifts. For a given complex, changes in the Pt−H distance do not lead to comparable changes in the shift. Correlations between ^{1}H and ^{195}Pt shifts start to break down once more and more systems are included in the comparison. This is due, for example, to much larger SO effects on ^{195}Pt than ^{1}H shifts for heavy halide ligands.

We furthermore noticed a large effect of the exchange-correlation kernel on NMR chemical shifts when substantial SO effects are involved. Clearly, the kernel must be taken into account for accurate relativistic shielding computations, both at the two- and at the four-component level.

ASSOCIATED CONTENT

Supporting Information

Bond lengths in optimized and X-ray structures; Cartesian coordinates of the optimized structures; additional ^{1}H and ^{195}Pt NMR shifts with different methods with and without the exchange-correlation kernel; main contributions from separate excitations to σ^p and σ^{SO} at 2c-ZORA(SO)/PBE0/TZ2P and 1c-PBE/ECP level as well as the appropriate MO plots; background to analysis at one-component perturbation level; absolute ^{195}Pt shieldings. The Supporting Information is available free of charge on the ACS Publications website at DOI: 10.1021/acs.inorgchem.5b00446.

AUTHOR INFORMATION

Corresponding Authors

*E-mail: peter.hrobarik@tu-berlin.de. (P.H.)
*E-mail: martin.kaupp@tu-berlin.de. (M.K.)

Notes

The authors declare no competing financial interest.

ACKNOWLEDGMENTS

Funding from the Berlin DFG excellence cluster on Unifying Concepts in Catalysis (UniCat) is gratefully acknowledged. A.H.G. thanks Fonds der chemischen Industrie for a Ph.D. scholarship. J.A. acknowledges support from Grant No. CHE-1265833 of the National Science Foundation.

REFERENCES

(1) Pidcock, A.; Richards, R. E.; Venanzi, L. M. *J. Chem. Soc. A* **1966**, 1707.
(2) Hartley, F. R. *The chemistry of platinum and palladium: with particular reference to complexes of the elements;* Applied Science Publishers: London, U.K., 1973.
(3) Chatt, J.; Shaw, B. L. *J. Chem. Soc.* **1962**, 5075.
(4) Buckingham, A. D.; Stephens, P. J. *J. Chem. Soc.* **1964**, 4583.
(5) Buckingham, A. D.; Stephens, P. J. *J. Chem. Soc.* **1964**, 2747.
(6) Atkins, P. W.; Green, J. C.; Green, M. L. H. *J. Chem. Soc. A* **1968**, 2275.
(7) Birnbaum, E. R. *Inorg. Nucl. Chem. Lett.* **1971**, *7*, 233.
(8) Ruiz-Morales, Y.; Schreckenbach, G.; Ziegler, T. *Organometallics* **1996**, *15*, 3920.
(9) Hrobárik, P.; Hrobáriková, V.; Meier, F.; Repiský, M.; Komorovský, S.; Kaupp, M. *J. Phys. Chem. A* **2011**, *115*, 5654.
(10) Hrobárik, P.; Hrobáriková, V.; Greif, A. H.; Kaupp, M. *Angew. Chem., Int. Ed.* **2012**, *51*, 10884.
(11) (a) Perdew, J. P.; Burke, K.; Ernzerhof, M. *Phys. Rev. Lett.* **1996**, *77*, 3865. (b) Perdew, J. P.; Burke, K.; Ernzerhof, M. *Phys. Rev. Lett.* **1997**, *78*, 1396.
(12) Adamo, C.; Barone, V. *Chem. Phys. Lett.* **1998**, *298*, 113.

DOI: 10.1021/acs.inorgchem.5b00446
Inorg. Chem. 2015, 54, 7199−7208

(13) Weigend, F.; Ahlrichs, R. *Phys. Chem. Chem. Phys.* **2005**, *7*, 3297.
(14) Andrae, D.; Häußermann, U.; Dolg, M.; Stoll, H.; Preuß, H. *Theor. Chim. Acta* **1990**, *77*, 123.
(15) Peterson, K. A.; Figgen, D.; Goll, E.; Stoll, H.; Dolg, M. *J. Chem. Phys.* **2003**, *119*, 11113.
(16) Turbomole, version 6.3.1, a Development of University of Karlsruhe and Forschungszentrum Karlsruhe GmbH, 1989−2007, Turbomole GmbH, since 2007; available from http://www.turbomole.com.
(17) See, for example, (a) Braunschweig, H.; Brenner, P.; Dewhurst, R. D.; Guethlein, F.; Jimenez-Halla, J. O. C.; Radacki, K.; Wolf, J.; Zöllner, L. *Chem. - Eur. J.* **2012**, *18*, 8605. (b) Cowan, R. L.; Trogler, W. C. *J. Am. Chem. Soc.* **1989**, *111*, 4750. (c) Languérand, A.; Barnes, S. S.; Bélanger-Chabot, G.; Maron, L.; Berrouard, P.; Audet, P.; Fontaine, F. G. *Angew. Chem., Int. Ed.* **2009**, *48*, 6695.
(18) (a) Becke, A. D. *J. Chem. Phys.* **1993**, *98*, 5648. (b) Lee, C.; Yang, W.; Parr, R. G. *Phys. Rev. B: Condens. Matter Mater. Phys.* **1988**, *37*, 785. (c) Stephens, P. J.; Devlin, F. J.; Chabalowski, C. F.; Frisch, M. J. *J. Phys. Chem.* **1994**, *98*, 11623.
(19) *Amsterdam Density Functional (ADF)*, version 2012.01; SCM, Theoretical Chemistry, Vrije Univeriteit: Amsterdam, Netherlands, 2012; available from http://www.scm.com.
(20) van Lenthe, E.; Baerends, E. J. *J. Comput. Chem.* **2003**, *24*, 1142.
(21) Wolff, S. K.; Ziegler, T. *J. Chem. Phys.* **1998**, *109*, 895.
(22) Wolff, S. K.; Ziegler, T.; van Lenthe, E.; Baerends, E. J. *J. Chem. Phys.* **1999**, *110*, 7689.
(23) Wolinski, K.; Hinton, J. F.; Pulay, P. *J. Am. Chem. Soc.* **1990**, *112*, 8251.
(24) Autschbach, J. *Mol. Phys.* **2013**, *111*, 2544.
(25) ReSpect-mDKS, version 3.3.0, 2013; Repisky, M.; Komorovsky, S.; Malkin, V. G.; Malkina, O. L.; Kaupp, M.; Ruud, K., with contributions from Bast, R.; Ekstrom, U.; Knecht, S.; Malkin-Ondik, I.; Malkin, E. (see http://rel-qchem.sav.sk).
(26) Aucar, G. A.; Saue, T.; Visscher, L.; Jensen, H. J. A. *J. Chem. Phys.* **1999**, *110*, 6208.
(27) Kutzelnigg, W. *J. Comput. Chem.* **1999**, *20*, 1199.
(28) Dyall, K. G. *Theor. Chem. Acc.* **2004**, *112*, 403.
(29) Kutzelnigg, W.; Fleischer, U.; Schindler, M. In *NMR—Basic Principles and Progress;* Springer Verlag: Berlin,Germany, p 165.
(30) , Frisch, M. J.; Trucks, G. W., et al. *Gaussian 09,* Revision D.01; Gaussian, Inc.: Wallingford, CT, 2009.
(31) Malkin, V. G.; Malkina, O. L.; Reviakine, R.; Arbuznikov, A. V.; Kaupp, M.; Schimmelpfennig, B.; Malkin, I.; Repisky, M.; Komorovsky, S.; Hrobarik, P.; Malkin, E.; Helgaker, T.; Ruud, K. *MAG-ReSpect,* version 2.3; 2010.
(32) Dolg, M.; Wedig, U.; Stoll, H.; Preuss, H. *J. Chem. Phys.* **1987**, *86*, 866.
(33) Vaara, J.; Malkina, O. L.; Stoll, H.; Malkin, V. G.; Kaupp, M. *J. Chem. Phys.* **2001**, *114*, 61.
(34) Reed, A. E.; Curtiss, L. A.; Weinhold, F. *Chem. Rev.* **1988**, *88*, 899.
(35) Glendening, E. D.; Badenhoop, J. K.; Reed, A. E.; Carpenter, J. E.; Bohmann, J. A.; Morales, C. M.; Weinhold, F. *NBO 5.0;* Theoretical Chemistry Institute, University of Wisconsin: Madison, WI, 2001; available from http://nbo.chem.wisc.edu.
(36) Autschbach, J. *J. Chem. Phys.* **2008**, *128*, 164112.
(37) Bader, R. F. W.; Stephens, M. E. *J. Am. Chem. Soc.* **1975**, *97*, 7391.
(38) Fradera, X.; Austen, M. A.; Bader, R. F. W. *J. Phys. Chem. A* **1999**, *103*, 304.
(39) Kohout, M. *DGrid*, version 4.6; Springer: Germany, 2011; available from http://www2.cpfs.mpg.de/~kohout/dgrid.html.
(40) Nakajima, T.; Hirao, K. *Chem. Rev.* **2012**, *112*, 385.
(41) Klamt, A.; Schüürmann, G. *J. Chem. Soc., Perkin Trans. 2* **1993**, 799.
(42) Hartley, F. R. *Chem. Soc. Rev.* **1973**, *2*, 163.
(43) Engesser, T. A.; Hrobárik, P.; Trapp, N.; Eiden, P.; Scherer, H.; Kaupp, M.; Krossing, I. *ChemPlusChem* **2012**, *77*, 643 and references therein .
(44) Voigt, J.; Braun, T. *Dalton Trans.* **2011**, *40*, 12699.
(45) Stahl, S. S.; Labinger, J. A.; Bercaw, J. E. *Inorg. Chem.* **1998**, *37*, 2422.
(46) Appleton, T. G.; Chisholm, M. H.; Clark, H. C.; Manzer, L. E. *Inorg. Chem.* **1972**, *11*, 1786.
(47) Schreckenbach, G. *Theor. Chem. Acc.* **2002**, *108*, 246.
(48) van Lenthe, E.; Snijders, J. G.; Baerends, E. J. *J. Chem. Phys.* **1996**, *105*, 6505.
(49) For halogen dependence of NMR shifts, see, for example: Engesser, T. A.; Hrobárik, P.; Trapp, N.; Eiden, P.; Scherer, H.; Kaupp, I. *ChemPlusChem* **2012**, *77*, 643 and references therein. .
(50) Autschbach, J.; Zheng, S.; Schurko, R. W. *Concepts Magn. Reson., Part A* **2010**, *36A*, 84.
(51) Dean, R. R.; Green, J. C. *J. Chem. Soc. A* **1968**, 3047.
(52) Garbacz, P.; Terskikh, V. V.; Ferguson, M. J.; Bernard, G. M.; Kędziorek, M.; Wasylishen, R. E. *J. Phys. Chem. A* **2014**, *118*, 1203.
(53) Vícha, J.; Straka, M.; Munzarová, M. L.; Marek, R. *J. Chem. Theory Comput.* **2014**, *10*, 1489.
(54) Kaupp, M. In *Relativistic Electronic Structure Theory II: Applications;* Schwerdtfeger, P., Ed.; Elsevier: Amsterdam, 2004; p 552.
(55) Pyykkö, P.; Görling, A.; Rösch, N. *Mol. Phys.* **1987**, *61*, 195.
(56) Vícha, J.; Foroutan-Nejad, C.; Pawlak, T.; Munzarová, M. L.; Straka, M.; Marek, R. *J. Chem. Theory Comput.* **2015**, *11*, 1509.
(57) Manninen, P.; Ruud, K.; Lantto, P.; Vaara, J. *J. Chem. Phys.* **2005**, *122*, 114107.
(58) Manninen, P.; Ruud, K.; Lantto, P.; Vaara, J. *J. Chem. Phys.* **2006**, *124*, 149901.
(59) Manninen, P.; Lantto, P.; Vaara, J.; Ruud, K. *J. Chem. Phys.* **2003**, *119*, 2623.
(60) Autschbach, J.; Zheng, S. *Magn. Reson. Chem.* **2008**, *46*, S45.
(61) Sterzel, M.; Autschbach, J. *Inorg. Chem.* **2006**, *45*, 3316.
(62) Truflandier, L. A.; Sutter, K.; Autschbach, J. *Inorg. Chem.* **2011**, *50*, 1723.

DOI: 10.1021/acs.inorgchem.5b00446
Inorg. Chem. 2015, 54, 7199−7208

A Relativistic Quantum-Chemical Analysis of the *Trans* Influence on ^{1}H NMR Hydride Shifts in Square-Planar Platinum(II) Complexes

Anja H. Greif,[a] *Peter Hrobárik,*[a,*] *Veronika Hrobáriková,*[a] *Alexey V. Arbuznikov,*[a] *Jochen Autschbach,*[b] *Martin Kaupp* [a,*]

[a] Institute of Chemistry, Technical University of Berlin, Strasse des 17. Juni 135, D-10623 Berlin, Germany; [b] Department of Chemistry, University at Buffalo, State University of New York, Buffalo, NY, 14260, USA

Corresponding authors:

peter.hrobarik@tu-berlin.de

martin.kaupp@tu-berlin.de

Supporting Information

Table S1. Pertinent bond lengths (in Ångstroms) in optimized and X-ray structures of some square-planar Pt(II) hydride complexes. Assessment of DFT methods. [a]

Complex	B3LYP/def2-TZVP (ECP)			PBE0/def2-TZVP (ECP)			X-ray structure			ref.
	d(Pt–H)	d(Pt–P)	d(Pt–X)[b]	d(Pt–H)	d(Pt–P)	d(Pt–X)[b]	d(Pt–H)	d(Pt–P)	d(Pt–X)[b]	
trans-[HPt**Cl**(P^iPr_3)$_2$]	1.568	2.339	2.465	1.565	2.307	2.412	(1.846)	2.286	2.395	[S1]
trans-[HPt**Cl**(PCy_3)$_2$]	1.567	2.338	2.467	1.566	2.306	2.415	(1.385)	2.285	2.404	[S2]
trans-[HPt**Br**(PEt_3)$_2$]	1.571	2.319	2.602	1.565	2.290	2.551	–	2.256	2.562	[S3]
trans-[HPt(**C**$_6H_5$)(P^iPr_3)$_2$]	1.635	2.297	2.144	1.628	2.270	2.111	1.621	2.273	2.098	[S4]
trans-[HPt(**B**$O_2C_6H_4$)(PCy_3)$_2$]	1.678	2.325	2.104	1.672	2.291	2.082	–	2.286	2.071	[S5]
trans-[HPt(**O**C_6H_5)(PEt_3)$_2$]	1.569	2.319	2.154	1.565	2.290	2.120	–	2.272	2.098	[S6]
trans-[HPt(**N**HC_6H_5)(PEt_3)$_2$]	1.588	2.317	2.153	1.582	2.287	2.121	–	2.273	2.126	[S6]

[a] See Computational Methods in main text. [b] X atom of trans ligand is given in bold.

Table S2. Calculated ^{1}H NMR hydride shifts (in ppm vs. TMS) for *trans*-[HPtL(PMe$_3$)$_2$] series (listed in the order of increasing Pt–H distance) with and without (noXC) exchange-correlation kernel, using GGA-type PBE and hybrid PBE0 functionals [a]

Ligand L	δ_{SR} (PBE) [ppm]	δ_{2c}^{noXC} (PBE) [ppm]	δ_{2c} (PBE) [ppm]	δ_{4c}^{noXC} (PBE) [ppm]	δ_{4c} (PBE) [ppm]	δ_{2c}^{noXC} (PBE0) [ppm]	δ_{2c} (PBE0) [ppm]
NO_3	–7.6	–16.9	–19.8	–15.7	–19.3	–19.4	–23.6
ONO	–6.2	–13.9	–15.9	–12.6	–15.5	–16.8	–20.1
Cl	–4.8	–11.2	–12.6	–9.8	–12.1	–13.1	–15.8
Br	–4.1	–10.2	–11.6	–8.9	–11.1	–12.0	–14.7
I	–2.6	–7.9	–9.1	–6.7	–8.6	–9.4	–11.9
SCN	–3.3	–8.1	–9.1	–6.9	–8.6	–9.7	–12.1
NO_2	–6.8	–13.8	–15.3	–12.3	–15.0	–15.9	–19.0
CN	–3.1	–5.1	–3.9	–3.6	–4.3	–5.8	–6.7
C_6H_5	–2.4	–5.5	–2.5	–3.1	–3.8	–5.4	–5.9
CH_3	–2.0	–3.4	–1.4	–1.6	–1.9	–3.7	–3.8
$Si(OMe)_3$	–2.0	–1.1	3.8	1.5	2.0	–0.1	0.4
BCat	0.0	0.1	6.1	3.1	4.1	1.0	2.3
R^2	**0.8664**	**0.9784**	**0.9902**	**0.9880**	**0.9889**	**0.9883**	**0.9922**
RMSD	**9.7**	**4.5**	**4.0**	**5.6**	**3.8**	**2.9**	**0.9**

[a] See Computational Methods in main text. δ_{SR} stands for scalar relativistic ZORA results with TZ2P basis set; δ_{2c} stands for 2c-ZORA-SO results with TZ2P basis set; δ_{4c} stands for 4c-mDKS results with Dyall VDZ/IGLO-III basis set. Root-mean-square-deviation (RMSD) of the calculated data from experiment is given as well.

Table S3. Selected bond lengths and calculated isotropic hydride ^{1}H NMR and ^{195}Pt NMR shifts in *trans*-[HPtCN(PR_3)$_2$] series with different phosphine ligands [a,b]

Phosphine	d(Pt–H) [Å]	d(Pt–P) [Å]	d(Pt–C) [Å]	δ(^{1}H) [c] [ppm]	δ(^{195}Pt) [d] [ppm]
PH_3	1.615	2.255	2.029	–6.9	–306.0
PMe_3	1.609	2.281	2.034	–6.7	–362.0
PEt_3	1.611	2.289	2.031	–6.9	–314.1
PCy_3	1.615	2.308	2.025	–7.6	–376.4
PPh_3	1.617	2.303	2.024	–6.3	–599.3

[a] Structures optimized at the PBE0/def2-TZVP/ECP level. [b] NMR chemical shifts calculated at the 2c-ZORA(SO)/PBE0/TZ2P level (cf. Computational Methods in main text). [c] ^{1}H NMR shifts with respect to TMS. [d] ^{195}Pt NMR shifts with respect to *trans*-[HPtNO_3(PMe_3)$_2$] as a primary reference standard.

Table S4. Effect of solvent polarity on ^{1}H NMR hydride shifts (in ppm vs. TMS) within *trans*-[HPtL(PMe$_3$)$_2$] series [a]

Ligand L	*in vacuo*	benzene (ε_r=2.3)	CH_2Cl_2 (ε_r=8.9)
NO_3	–23.6	–23.6	–23.6
ONO	–20.1	–20.5	–20.7
Cl	–15.8	–16.2	–16.4
Br	–14.7	–15.0	–15.2
I	–11.9	–12.1	–12.2
SCN	–12.1	–12.2	–12.3
NO_2	–19.0	–19.0	–19.0
CN	–6.7	–6.7	–6.7
C_6H_5	–5.9	–6.3	–6.6
CH_3	–3.8	–4.2	–4.5
Si(OMe)$_3$	0.4	0.3	0.2
BCat	2.3	2.1	1.9
R^2	**0.9922**	**0.9912**	**0.9901**
RMSD	**0.9**	**0.8**	**0.8**

[a] 2c-ZORA(SO)/PBE0/TZ2P results. Bulk solvent effects were simulated by the COSMO solvation model (cf. Computational Methods in main text).

Table S5. Calculated components of the hydride ^{1}H shielding tensors (in ppm) within the *trans*-[HPtL(PMe$_3$)$_2$] series (listed according to increasing ^{1}H NMR shifts) and their separation into diamagnetic (σ^d), paramagnetic (σ^p) and spin-orbit (σ^{SO}) terms [a]

	diamagnetic				paramagnetic				spin-orbit			
L	$\sigma^d_{\parallel}$	$\sigma^d_{\perp,ip}$	$\sigma^d_{\perp,op}$	σ^d_{iso}	$\sigma^p_{\parallel}$	$\sigma^p_{\perp,ip}$	$\sigma^p_{\perp,op}$	σ^p_{iso}	$\sigma^{SO}_{\parallel}$	$\sigma^{SO}_{\perp,ip}$	$\sigma^{SO}_{\perp,op}$	σ^{SO}_{iso}
NO_3	58.7	23.7	12.2	31.5	–4.9	13.1	18.1	8.8	–2.2	22.2	24.7	14.9
ONO	58.1	23.5	12.6	31.4	–5.3	10.6	18.0	7.8	–2.2	17.3	22.6	12.6
NO_2	57.0	23.4	12.8	31.1	–5.0	12.2	17.1	8.1	–2.5	15.4	21.4	11.4
Cl	58.2	23.1	12.7	31.3	–3.8	7.5	14.5	6.1	–2.1	14.2	17.9	10.0
Br	58.3	22.8	12.2	31.1	–3.8	6.7	13.7	5.5	–1.9	13.1	17.7	9.6
SCN	57.6	24.0	12.8	31.5	–4.5	5.3	12.2	4.3	–1.8	9.3	16.0	7.8
I	58.5	22.8	12.1	31.1	–3.9	4.5	11.5	4.0	–1.7	10.1	16.6	8.3
CN	55.9	23.6	14.0	31.2	–3.7	5.2	10.5	4.0	–3.0	0.3	11.9	3.1
C_6H_5	55.9	22.9	12.7	30.5	–5.3	5.5	12.2	4.1	–3.8	1.4	11.3	3.0
CH_3	54.1	23.2	13.0	30.1	–2.7	4.4	10.5	4.1	–3.6	–2.9	10.1	1.2
$Si(OMe)_3$	54.5	22.3	12.3	29.7	–4.1	3.1	8.8	2.6	–4.2	–8.5	9.2	–1.2
SiH_3	53.8	23.2	13.3	30.1	–4.4	0.7	7.6	1.3	–3.8	–11.1	9.6	–1.8
BCat	53.4	21.8	13.1	29.4	–4.5	2.4	10.0	2.6	–4.4	–13.0	9.0	–2.8
BH_2	51.2	23.1	13.7	29.3	–6.1	0.2	14.0	2.7	–5.0	–17.8	13.3	–3.2

[a] 2c-ZORA(SO)/PBE0/TZ2P results (cf. Computational Methods in main text). $\sigma_{\parallel}$ stands for a principal component along the Pt–H bond; $\sigma_{\perp,ip}$ and $\sigma_{\perp,op}$ stand for principal components perpendicular to the Pt–H bond, lying in- and out-of-plane of the square complex, respectively. Isotropic shielding $\sigma_{iso} = \sigma^d_{iso} + \sigma^p_{iso} + \sigma^{SO}_{iso}$, where $\sigma^k_{iso} = (\sigma^k_{\parallel} + \sigma^k_{\perp,ip} + \sigma^k_{\perp,op})/3$ ($k = d, p, SO$).

Table S6. Anisotropy of the hydride ^{1}H shielding tensors (in ppm) within the *trans*-[HPtL(PMe$_3$)$_2$] series [a]

	scalar-relativity				scalar-relativity + spin-orbit			
L	$\sigma_{\parallel}$	$\sigma_{\perp,ip}$	$\sigma_{\perp,op}$	Ω [b]	$\sigma_{\parallel}$	$\sigma_{\perp,ip}$	$\sigma_{\perp,op}$	Ω [b]
NO_3	53.8	36.8	30.3	23.5	51.6	59.0	55.0	7.4
ONO	52.8	34.1	30.6	22.2	50.6	51.4	53.2	2.6
NO_2	52.0	35.6	29.9	22.1	49.5	51.0	51.3	1.8
Cl	54.4	30.6	27.2	27.2	52.3	44.8	45.1	7.5
Br	54.5	29.5	25.9	28.6	52.6	42.6	43.6	10.0
SCN	53.1	29.3	25.0	28.1	51.3	38.6	41.0	12.7
I	54.6	27.3	23.6	31.0	52.9	37.4	40.2	15.5
CN	52.2	28.8	24.5	27.7	49.2	29.1	36.4	20.1
C_6H_5	50.6	28.4	24.9	25.7	46.8	29.8	36.2	17.0
CH_3	51.4	27.6	23.5	27.9	47.8	24.7	33.6	23.1
$Si(OMe)_3$	50.4	25.4	21.1	29.3	46.2	16.9	30.3	29.3
SiH_3	49.4	23.9	20.9	28.5	45.6	12.8	30.5	32.8
BCat	48.9	24.2	23.1	25.8	44.5	11.2	32.1	33.3
BH_2	45.1	23.3	27.7	21.8	40.1	5.5	41.0	35.5

[a] 2c-ZORA(SO)/PBE0/TZ2P results (cf. Computational Methods in main text).

[b] Span $\Omega = \max(\sigma_{\parallel}, \sigma_{\perp,ip}, \sigma_{\perp,op}) - \min(\sigma_{\parallel}, \sigma_{\perp,ip}, \sigma_{\perp,op})$

Table S7. Main MO contributions to isotropic σ^{p} and σ^{SO} components of the hydride (^{1}H) shielding tensor in pertinent *trans*-[HPtL(PMe$_3$)$_2$] complexes [a]

Ligand L	MO	σ^{p}_{iso} [ppm]	σ^{SO}_{iso} [ppm]
NO_3	HOMO–2	3.2	
	HOMO–3	3.0	3.1
	HOMO–6	1.6	2.3
	HOMO–7		2.3
	HOMO–8		5.8
	Σ main MO contributions	**7.8**	**13.5**
	Σ all contributions	**8.8**	**14.9**
NO_2	HOMO–2	2.8	1.1
	HOMO–3	2.9	1.6
	HOMO–6		2.9
	HOMO–7	1.1	4.1
	Σ main MO contributions	**6.8**	**9.7**
	Σ all contributions	**8.1**	**11.4**
Cl	HOMO	1.4	
	HOMO–2	2.1	
	HOMO–5		6.2
	HOMO–6	1.2	
	HOMO–7	1.6	3.5
	Σ main MO contributions	**6.3**	**9.7**
	Σ all contributions	**6.1**	**10.0**
CN	HOMO–1	1.4	
	HOMO–2	2.2	
	HOMO–7		4.0
	Σ main MO contributions	**3.6**	**4.1**
	Σ all contributions	**4.0**	**3.1**

Ligand L	MO	σ_{iso}^{p} [ppm]	σ_{iso}^{SO} [ppm]
CH_3	HOMO		2.7
	HOMO–1		–9.5
	HOMO–2	1.9	
	HOMO–3	2.3	6.5
	Σ main MO contributions	**4.2**	**–0.3**
	Σ all contributions	**4.1**	**1.2**
BH_2	HOMO		–7.2
	HOMO–4		2.1
	HOMO–5	1.1	1.7
	HOMO–6		1.4
	Σ main MO contributions	**1.1**	**–2.0**
	Σ all contributions	**2.7**	**–3.2**

[a] ZORA(SR)/PBE0/TZ2P results (cf. Computational Methods in main text). See Figure S1 for plots of the relevant MOs.

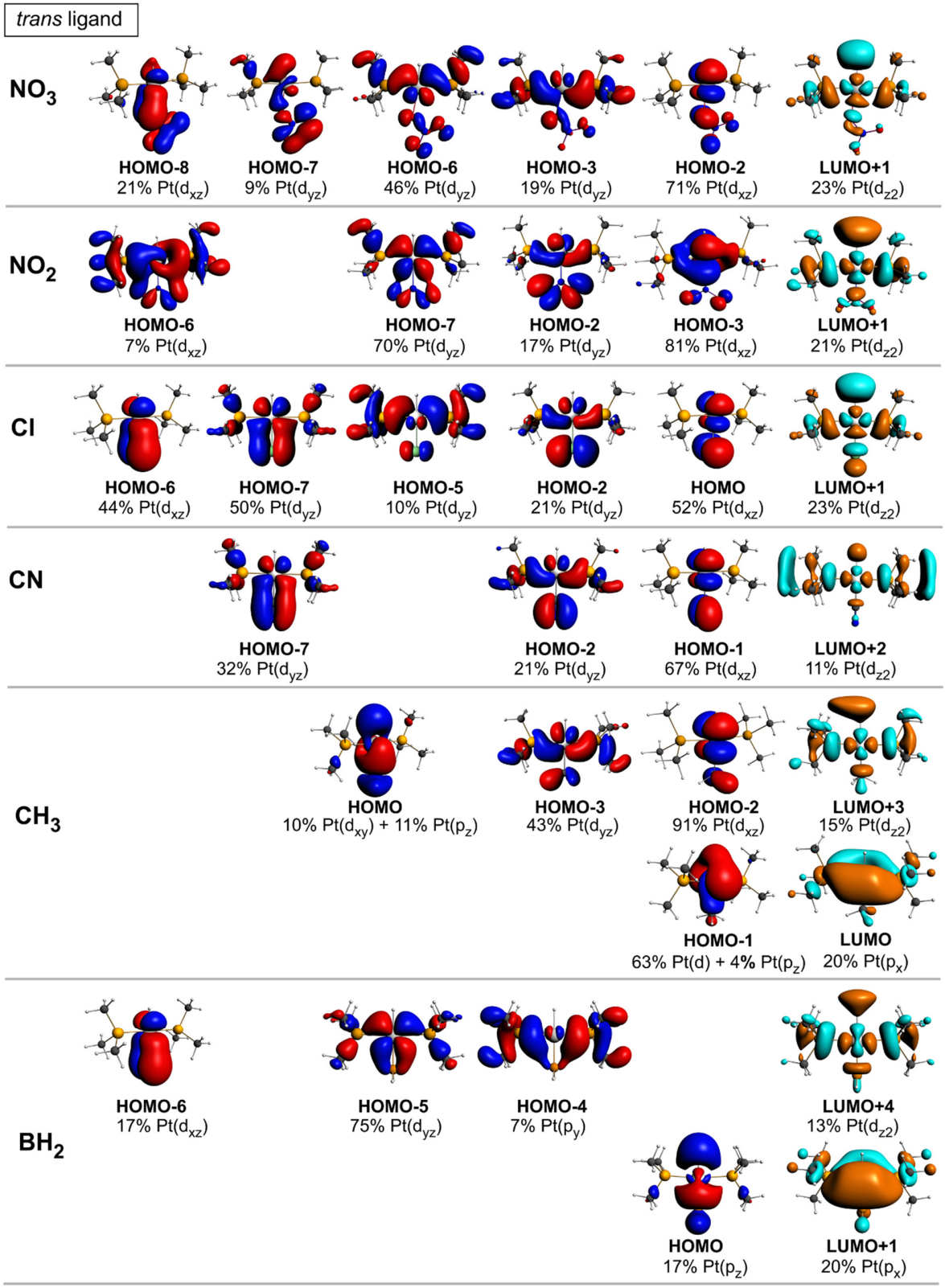

Figure S1. Isosurface plot (+/- 0.03 au) of the dominant occupied and virtual MOs contributing to $\boldsymbol{\sigma}^{p}$ and $\boldsymbol{\sigma}^{SO}$ tensors (ZORA(SR)/PBE0/TZ2P results; cf. Tables S7 and S10 for more data).

Table S8. Most important contributions from individual occupied-virtual MO couplings to $\boldsymbol{\sigma}^p$ of the hydride (^{1}H) shielding tensor in pertinent *trans*-[HPtL(PMe$_3$)$_2$] complexes [a]

Ligand L	MO (main excitation)	σ^p_{iso} [ppm]	$\sigma^p_{\parallel}$ [ppm]	$\sigma^p_{\perp,ip}$ [ppm]	$\sigma^p_{\perp,op}$ [ppm]	ΔE [eV]
NO_3	HOMO–2	3.2	–0.7	10.2	0.0	
	(HOMO–2→LUMO+1)	(2.0)	(0.0)	(6.0)	(0.0)	6.80
	HOMO–3	3.0	–0.5	0.4	9.0	
	(HOMO–3→LUMO+1)	(1.2)	(0.0)	(0.0)	(3.6)	7.25
	HOMO–6	1.6	–1.4	–0.6	6.8	
	(HOMO–6→LUMO+1)	(1.9)	(0.0)	(0.0)	(5.6)	8.03
NO_2	HOMO–2	2.8	0.6	0.6	7.1	
	(HOMO–2→LUMO+1)	(1.4)	(0.0)	(0.0)	(4.3)	6.90
	HOMO–3	2.9	–0.6	8.2	1.2	
	(HOMO–3→LUMO+1)	(1.5)	(0.0)	(3.9)	(0.6)	7.48
	HOMO–7	1.1	–2.0	1.8	3.6	
	(HOMO–7→LUMO+1)	(1.6)	(0.0)	(1.7)	(3.2)	8.40
Cl	HOMO	1.4	–0.1	4.0	0.0	
	(HOMO→LUMO+1)	(0.6)	(0.0)	(1.8)	(0.0)	6.41
	HOMO–2	2.1	0.0	0.4	5.9	
	(HOMO–2→LUMO+1)	(1.0)	(0.0)	(0.0)	(3.0)	6.61
	HOMO–6	1.2	–0.3	4.2	–0.4	
	(HOMO–6→LUMO+1)	(1.0)	(0.0)	(3.0)	(0.0)	8.10
	HOMO–7	1.6	–0.7	–0.2	5.7	
	(HOMO–7→LUMO+1)	(1.8)	(0.0)	(0.0)	(5.5)	8.57
CN	HOMO–1	1.4	–0.2	4.4	0.0	
	(HOMO–1→LUMO+2)	(0.5)	(0.0)	(1.5)	(0.0)	7.37
	HOMO–2	2.2	0.0	0.3	6.2	
	(HOMO–2→LUMO+2)	(1.0)	(0.0)	(0.1)	(2.9)	7.65
CH_3	HOMO–2	1.9	–0.3	3.5	2.5	
	(HOMO–2→LUMO+3)	(0.8)	(0.0)	(1.4)	(1.0)	7.05
	HOMO–3	2.3	0.7	2.5	3.8	
	(HOMO–3→LUMO+3)	(0.8)	(0.3)	(0.9)	(1.2)	7.63
BH_2	HOMO–5	1.1	0.5	1.0	1.7	
	(HOMO–5→LUMO+4)	(0.4)	(0.2)	(0.4)	(0.6)	8.65

[a] ZORA(SR)/PBE0/TZ2P results (cf. Computational Methods in main text). MOs are depicted in Figure S1.

Table S9. Most important contributions from individual occupied MOs to $\boldsymbol{\sigma}^{SO}$ of the hydride (^{1}H) shielding tensor in pertinent *trans*-[HPtL(PMe$_3$)$_2$] complexes [a]

Ligand L	MO (dominant transition)	σ_{iso}^{SO} [ppm]	$\sigma_{\parallel}^{SO}$ [ppm]	$\sigma_{\perp,ip}^{SO}$ [ppm]	$\sigma_{\perp,op}^{SO}$ [ppm]
NO_3	HOMO–3 (→LUMO+1)	3.1	–0.9	1.0	9.3
	HOMO–6 (→LUMO+1)	2.3	–1.1	–1.2	9.2
	HOMO–7 (→LUMO+1)	2.3	–0.2	1.8	5.3
	HOMO–8 (→LUMO+1)	5.8	0.4	17.4	–0.5
NO_2	HOMO–2 (→LUMO+1)	1.1	–0.4	–0.6	4.2
	HOMO–3 (→LUMO+1)	1.6	–1.7	7.6	–1.2
	HOMO–6 (→LUMO+1)	2.9	–3.4	7.7	4.4
	HOMO–7 (→LUMO+1)	4.1	–1.8	3.4	10.6
Cl	HOMO–5 (→LUMO+1)	6.2	–0.1	2.2	16.5
	HOMO–7 (→LUMO+1)	3.5	–0.9	1.3	10.2
CN	HOMO–7 (→LUMO+2)	4.0	–0.7	1.0	11.7
CH_3	HOMO (→LUMO+3)	2.7	–1.3	6.1	3.4
	HOMO–1 (→LUMO)	–9.5	–2.4	–13.3	–12.8
	HOMO–3 (→LUMO+3)	6.5	1.4	7.0	11.2
BH_2	HOMO (→LUMO+1)	–7.2	–9.5	–7.4	–4.7
	HOMO–4 (→LUMO+4)	2.1	0.9	2.0	3.5
	HOMO–5 (→LUMO+4)	1.7	0.2	1.5	3.4
	HOMO–6 (→LUMO+4)	1.4	2.6	1.4	0.1

[a] 2c-ZORA(SO)/PBE0/TZ2P results (cf. Computational Methods in main text). MOs are depicted in Figure S1.

Table S10. NPA atomic charges and selected AO contributions to specific MOs [a]

Complex / MOs	q(Pt)	q(H)	5d (Pt)	6p (Pt)	1s (H)
trans-**[HPtNO$_3$(PMe$_3$)$_2$]**	0.096	–0.109			
LUMO+1			23% (d_{z2})	< 1%	25%
HOMO–2			71% (d_{xz})	< 1%	< 1%
HOMO–3			19% (d_{yz})	4% (p_y)	< 1%
HOMO–6			46% (d_{yz})	1% (p_y)	< 1%
HOMO–7			9% (d_{yz})	2% (p_z)	7%
HOMO–8			21% (d_{xz})	< 1%	< 1%
trans-**[HPtNO$_2$(PMe$_3$)$_2$]**	0.056	–0.196			
LUMO+1			21% (d_{z2})	< 1%	19%
HOMO–2			17% (d_{yz})	< 1%	< 1%
HOMO–3			81% (d_{xz})	< 1%	< 1%
HOMO–6			7% (d_{xz})	4% (p_y)	< 1%
HOMO–7			70% (d_{yz})	< 1%	< 1%
trans-**[HPtCl(PMe$_3$)$_2$]**	0.016	–0.149			
LUMO+1			23% (d_{z2})	1% (p_z)	27%
HOMO			52% (d_{xz})	< 1%	< 1%
HOMO–2			21% (d_{yz})	< 1%	< 1%
HOMO–5			10% (d_{yz})	5% (p_y)	< 1%
HOMO–6			44% (d_{xz})	< 1%	< 1%
HOMO–7			50% (d_{yz})	< 1%	< 1%
trans-**[HPtCN(PMe$_3$)$_2$]**	0.054	–0.251			
LUMO+2			11% (d_{z2})	< 1%	9%
HOMO–1			67% (d_{xz})	< 1%	< 1%
HOMO–2			21% (d_{yz})	2% (p_y)	< 1%
HOMO–7			32% (d_{yz})	< 1%	< 1%

Complex / MOs	q(Pt)	q(H)	5d (Pt)	6p (Pt)	1s (H)
***trans*-[HPtCH$_3$(PMe$_3$)$_2$]**	0.059	–0.305			
LUMO+3			15% (d_{z2})	< 1%	10%
LUMO			< 1%	20% (p_x)	< 1%
HOMO			10% (d_{xy})	11% (p_z)	23%
HOMO–1			63% (d_{xy})	4% (p_z)	10%
HOMO–2			91% (d_{xz})	< 1%	< 1%
HOMO–3			43% (d_{yz})	2% (p_y)	< 1%
***trans*-[HPtBH$_2$(PMe$_3$)$_2$]**	–0.012	–0.420			
LUMO+4			13% (d_{z2})	< 1%	10%
LUMO+1			< 1%	20% (p_x)	< 1%
HOMO			1% (d_{xy})	17% (p_z)	35%
HOMO–4			< 1%	7% (p_y)	< 1%
HOMO–5			75% (d_{yz})	< 1%	< 1%
HOMO–6			17% (d_{xz})	< 1%	< 1%

[a] ZORA(SR)/PBE0/TZ2P results (cf. Computational Methods in main text). Only the total 5d/6p participation is given. The symmetry of the dominant 5d/6p atomic orbital (AO) is indicated in parentheses.

Table S11. Analysis of contributions to hydride (^{1}H) σ^{SO} in terms of NLMOs for selected *trans*-[HPtL(PMe$_3$)$_2$] complexes [a]

L	σ^{SO}	BD (Pt–H)	BD (Pt–L)	LP (Pt)	Σ other	%Pt in BD (Pt–H) [b]
NO_3	14.9	11.4	0.0	1.3	2.2	38.1%
NO_2	11.4	8.6	0.1	0.9	1.8	32.4%
Cl	10.0	7.2	0.4	1.1	1.3	34.2%
CN	3.1	1.7	0.3	0.4	0.7	26.6%
CH_3	1.2	–0.4	1.0	0.5	0.1	20.8%
BH_2	–3.2	–4.0	0.8	0.2	–0.2	11.7%

[a] 2c-ZORA(SO)/PBE0/TZ2P results. [b] Atomic contribution of the Pt atom in the Pt–H σ-bonding NLMO.

Table S12. Computed isotropic ^{195}Pt NMR chemical shieldings in *trans*-[HPtL(PMe$_3$)$_2$] series using different methods [with and without (noXC) exchange-correlation kernel] [a]

L	σ_{2c}^{noXC}(PBE) [ppm]	σ_{2c}(PBE) [ppm]	σ_{4c}^{noXC}(PBE) [ppm]	σ_{4c}(PBE) [ppm]	σ_{2c}^{noXC}(PBE0) [ppm]	σ_{2c}(PBE0) [ppm]
NO_3	5743.8	6240.6	8031.9	8041.6	5935.4	6417.2
ONO	5683.4	6197.4	7955.5	7984.3	5911.4	6408.2
Cl	5883.1	6401.8	8173.1	8205.3	6082.9	6585.6
Br	5971.4	6491.3	8278.7	8314.6	6181.2	6684.8
I	6132.8	6662.4	8439.0	8485.3	6356.9	6869.7
SCN	5906.6	6440.9	8181.9	8226.5	6164.4	6680.1
NO_2	5411.5	5932.7	7662.1	7694.0	5724.5	6228.5
CN	5965.1	6509.4	8226.2	8281.2	6254.2	6779.1
C_6H_5	5753.2	6299.7	7988.5	8049.3	6039.3	6573.5
CH_3	5696.1	6251.8	7939.5	8004.9	6030.2	6570.0
$Si(OMe)_3$	6006.2	6581.6	8265.6	8336.8	6360.7	6903.2
BCat	5842.6	6403.8	8071.1	8142.9	6190.5	6730.5

[a] σ_{2c} stands for chemical shieldings calculated at the 2c-ZORA(SO) level with a TZ2P basis set; σ_{4c} stands for chemical shieldings calculated at the 4c-mDKS level using a Dyall VDZ/IGLO-III basis set (cf. Computational Methods in main text).

Table S13. Computed isotropic ^{195}Pt NMR shifts in *trans*-[HPtL(PMe$_3$)$_2$] series using different methods [with and without (noXC) exchange-correlation kernel] [a,b]

L	δ_{2c}^{noXC} (PBE) [ppm]	δ_{2c} (PBE) [ppm]	δ_{4c}^{noXC} (PBE) [ppm]	δ_{4c} (PBE) [ppm]	δ_{2c}^{noXC} (PBE0) [ppm]	δ_{2c} (PBE0) [ppm]	Expt.[c] [ppm]
NO_3	0.0	0.0	0.0	0.0	0.0	0.0	0.0
ONO	60.4	43.2	76.3	57.3	23.9	8.9	–60.3
Cl	–139.3	–161.2	–141.3	–163.7	–147.6	–168.5	–137.4
Br	–227.6	–250.7	–246.9	–273.0	–245.9	–267.6	–249.3
I	–389.0	–421.7	–407.2	–443.7	–421.5	–452.5	–442.9
SCN	–162.8	–200.3	–150.1	–184.9	–229.1	–262.9	–248.9
NO_2	332.3	307.9	369.8	347.6	210.9	188.7	*n.a.*
CN	–221.3	–268.8	–194.3	–239.6	–318.8	–362.0	–408.3
C_6H_5	–9.4	–59.1	43.4	–7.7	–103.9	–156.3	*n.a.*
CH_3	47.7	–11.2	92.4	36.7	–94.9	–152.8	*n.a.*
Si(OMe)$_3$	–262.4	–340.9	–233.7	–295.2	–425.3	–486.0	*n.a.*
BCat	–98.9	–163.2	–39.2	–101.3	–255.2	–313.4	*n.a.*

[a] δ_{2c} stands for 2c-ZORA(SO) results with a TZ2P basis set; δ_{4c} stands for 4c-mDKS results using a Dyall VDZ/IGLO-III basis set (cf. Computational Methods in main text). [b] ^{195}Pt NMR shifts given in ppm with respect to *trans*-[HPtNO$_3$(PMe$_3$)$_2$] as a primary reference standard. [c] See ref. [S7] and Table 6 in the main text for more details.

Table S14. Bulk solvent effects on computed ^{195}Pt NMR shifts in *trans*-[HPtL(PMe_3)$_2$] series [a]

Ligand L	δ(^{195}Pt) [ppm]		
	in vacuo	CH_2Cl_2 (ε_r=8.9)	acetone (ε_r=20.7)
NO_3	0.0	0.0	0.0
ONO	8.9	13.4	12.0
Cl	–168.5	–170.1	–171.4
Br	–267.6	–260.3	–260.3
I	–452.5	–433.3	–433.0
SCN	–262.9	–269.8	–271.5
NO_2	188.7	207.8	212.8
CN	–362.0	–359.7	–358.3
C_6H_5	–156.3	–166.4	–166.6
CH_3	–152.8	–165.2	–166.9
$Si(OMe)_3$	–486.0	–469.1	–466.9
BCat	–313.4	–306.9	–306.9

[a] 2c-ZORA(SO)/PBE0/TZ2P results (cf. Computational Methods in main text). ^{195}Pt NMR shifts in ppm vs. *trans*-[$HPtNO_3(PMe_3)_2$] as an internal reference standard.

Analysis of the hydride shielding tensors at one-component perturbation level

While most of the calculations in this work are performed within two- and four-component relativistic approaches, some of the analyses were done at one-component perturbational level. In this context it is important to recall that (disregarding temporarily the intricacies of defining dia- and paramagnetic shielding terms within a GIAO-based approach)[S8], paramagnetic shielding may be obtained within a linear-response approach from coupling between occupied and virtual MOs, including for each such coupling products of the matrix elements of the external magnetic field and the nuclear magnetic moment, divided by the energy difference between occupied and virtual MO of interest (see Eq. 1).

$$\sigma_{uv}^{p} = 2\alpha^2 \sum_{i=1}^{occ}\sum_{a=1}^{virt} \frac{\left\langle \varphi_i | l_{0,v} | \varphi_a \right\rangle \left\langle \varphi_a | l_{N,u}\, r_N^{-3} | \varphi_i \right\rangle}{\varepsilon_i - \varepsilon_a}; \quad u,v = x,y,z\,. \tag{1}$$

Here the matrix elements in the numerator correspond to those of the external magnetic field (orbital Zeeman, OZ) and nuclear magnetic moment (paramagnetic spin-orbit, PSO) operators, respectively, i.e., $\mathbf{l}_0 = -i\left(\mathbf{r}\times\nabla\right)$, $\mathbf{l}_N = -i\left[\left(\mathbf{r}-\mathbf{R}_N\right)\times\nabla\right]$ ($\mathbf{R}_N$ is the position of nucleus N of interest), and α is the fine structure constant. Atomic units based on the SI system are used throughout this work.

We also provide a decomposition of the dominant SO corrections obtained from scalar-relativistic wave functions within the framework of a mixed third-order perturbation treatment, where the Fermi-contact hyperfine term is included in the Kohn-Sham SCF calculation as a finite perturbation, and subsequently the influence of the OZ and SO operators is obtained at second order:[S9]

$$\sigma_{N,uv}^{SO-I} = \frac{\pi}{12}\frac{\alpha^4 g_e^2}{\lambda_N}\Bigg[\sum_{i=1}^{occ(\alpha)}\sum_{a=1}^{virt(\alpha)} \frac{\left\langle \varphi_i^{\alpha}(\lambda_N) | l_{0,u} | \varphi_a^{\alpha}(\lambda_N)\right\rangle \left\langle \varphi_a^{\alpha}(\lambda_N) | h_{SO,v} | \varphi_i^{\alpha}(\lambda_N)\right\rangle}{\varepsilon_i^{\alpha} - \varepsilon_a^{\alpha}} - \sum_{i=1}^{occ(\beta)}\sum_{a=1}^{virt(\beta)} \frac{\left\langle \varphi_i^{\beta}(\lambda_N) | l_{0,u} | \varphi_a^{\beta}(\lambda_N)\right\rangle \left\langle \varphi_a^{\beta}(\lambda_N) | h_{SO,v} | \varphi_i^{\beta}(\lambda_N)\right\rangle}{\varepsilon_i^{\beta} - \varepsilon_a^{\beta}}\Bigg] \tag{2}$$

Here λ_N is the finite-perturbation parameter (taken as 0.001 au), and the sums run over α and β spin orbitals; g_e=2.002319 is the free-electron *g*-value, and $\mathbf{h}_{SO}$ is the spatial part of the SO

operator: $\mathbf{h}_{SO} = \sum_K Z_K \frac{\mathbf{l}_K}{r_K^3}$ + two-electron terms. This expression fails to show the quadratic energy denominator that would come into play through the hyperfine operator if the latter would be included in an analytical quadratic response equation (see below). A method for the decomposition of eq. (2) into contributions from occupied and virtual MOs is given below.

Background to analysis of separate contributions to the p_1 term of SO corrections to NMR chemical shielding tensor

We start from the closed-shell system, where $n_\alpha = n_\beta = n_{\text{occ}}$, and, initially $\varphi_i^\alpha = \varphi_i^\beta$, $\varepsilon_i^\alpha = \varepsilon_i^\beta = \varepsilon_{i,0}$, $i = 1, \ldots, N$. Upon applying a small finite Fermi-contact perturbation due to nucleus *K* (controlled by the perturbation parameter λ_N), a system is slightly spin-polarized: i.e., $\varphi_i^\alpha \neq \varphi_i^\beta$ but still $\varphi_i^\alpha \approx \varphi_i^\beta$ with a very small deviation from each other, and also $\varepsilon_i^\alpha \approx \varepsilon_i^\beta$. At a given order of perturbation theory, one is allowed to employ unperturbed one-electron energies $\left(\varepsilon_{i,0}\right)$ in the denominators of perturbational expressions. The main contributions to the components of the SO-shielding tensor can be rewritten as:

$$\begin{aligned}\sigma_{N,uv}^{SO-I} &= \frac{\pi\alpha^4 g_e^2}{12\lambda_N}\sum_{k=1}^{n_{\text{occ}}}\sum_{a=n_{\text{occ}}+1}^{n}\left\{\frac{\left\langle\varphi_k^\alpha\left|l_{O,u}\right|\varphi_a^\alpha\right\rangle\left\langle\varphi_a^\alpha\left|h_{SO,v}\right|\varphi_k^\alpha\right\rangle}{\varepsilon_{k,0}-\varepsilon_{a,0}} - \frac{\left\langle\varphi_k^\beta\left|l_{O,u}\right|\varphi_a^\beta\right\rangle\left\langle\varphi_a^\beta\left|h_{SO,v}\right|\varphi_k^\beta\right\rangle}{\varepsilon_{k,0}-\varepsilon_{a,0}}\right\} \\ &= \frac{\pi\alpha^4 g_e^2}{12\lambda_N}\sum_{k=1}^{n_{\text{occ}}}\sum_{a=n_{\text{occ}}+1}^{n}\frac{\left(l_{O,u}\right)_{ka}^{\alpha}\left(h_{SO,v}\right)_{ak}^{\alpha} - \left(l_{O,u}\right)_{ka}^{\beta}\left(h_{SO,v}\right)_{ak}^{\beta}}{\varepsilon_{k,0}-\varepsilon_{a,0}},\end{aligned} \tag{3}$$

or, for the trace of this tensor,

$$\begin{aligned}\mathrm{Tr}\left[\boldsymbol{\sigma}_N^{SO-I}\right] = \sum_{u=x,y,z}\sigma_{N,uu}^{SO-I} &= \frac{\pi\alpha^4 g_e^2}{12\lambda_N}\sum_{k=1}^{n_{\text{occ}}}\sum_{a=n_{\text{occ}}+1}^{n}\sum_{u=x,y,z}\frac{\left(l_u\right)_{ka}^{\alpha}\left(h_{SO,u}\right)_{ak}^{\alpha} - \left(l_u\right)_{ka}^{\beta}\left(h_{SO,u}\right)_{ak}^{\beta}}{\varepsilon_{k,0}-\varepsilon_{a,0}} \\ &= \frac{\pi\alpha^4 g_e^2}{12\lambda_N}\sum_{k=1}^{n_{\text{occ}}}\sum_{a=n_{\text{occ}}+1}^{n}\frac{\vec{l}_{ka}^{\,\alpha}\cdot\vec{h}_{SO,ak}^{\,\alpha} - \vec{l}_{ka}^{\,\beta}\cdot\vec{h}_{SO,ak}^{\,\beta}}{\varepsilon_{k,0}-\varepsilon_{a,0}}.\end{aligned} \tag{4}$$

In Equations (3) and (4), only excitations from formally doubly occupied to virtual MOs (before application of the FC perturbation) survive. In spite the near identity of φ_i^α and φ_i^β (and therefore of the corresponding matrix elements), the terms in the double sum give sizeable contributions to

$\sigma_{N,uv}^{SO-I}$ because of the small parameter λ_N in the denominator. We introduce small differences ("proportional" to λ_N):

$$\delta\vec{l}_{ka} = \vec{l}_{ka}^{\alpha} - \vec{l}_{ka}^{\beta} \ \left[\sim O(\lambda_N)\right]; \qquad \delta\vec{h}_{SO,ak} = \vec{h}_{SO,ak}^{\alpha} - \vec{h}_{SO,ak}^{\beta} \ \left[\sim O(\lambda_N)\right], \tag{5}$$

Then, Eq. (4) can be rewritten as follows

$$\begin{aligned}
\mathrm{Tr}\left[\boldsymbol{\sigma}_N^{SO-I}\right] &= \frac{\pi\alpha^4 g_e^2}{12\lambda_N}\sum_{k=1}^{n_{\mathrm{occ}}}\sum_{a=N_{\mathrm{occ}}+1}^{n}\frac{\left(\vec{l}_{ka}^{\beta}+\delta\vec{l}_{ka}\right)\cdot\left(\vec{h}_{SO,ak}^{\beta}+\delta\vec{h}_{SO,ak}\right)-\vec{l}_{ka}^{\beta}\cdot\vec{h}_{SO,ak}^{\beta}}{\varepsilon_{k,0}-\varepsilon_{a,0}} \\
&= \frac{\pi\alpha^4 g_e^2}{12\lambda_N}\sum_{k=1}^{n_{\mathrm{occ}}}\sum_{a=N_{\mathrm{occ}}+1}^{n}\frac{\delta\vec{l}_{ka}\cdot\vec{h}_{SO,ak}^{\beta}+\delta\vec{h}_{SO,ak}\cdot\vec{l}_{ka}^{\beta}+O\left(\lambda_N^2\right)}{\varepsilon_{k,0}-\varepsilon_{a,0}} \\
&= \frac{\pi\alpha^4 g_e^2}{12}\sum_{k=1}^{n_{\mathrm{occ}}}\sum_{a=N_{\mathrm{occ}}+1}^{n}\frac{\left(\delta\vec{l}_{ka}/\lambda_N\right)\cdot\vec{h}_{SO,ak}^{\beta}+\left(\delta\vec{h}_{SO,ak}/\lambda_N\right)\cdot\vec{l}_{ka}^{\beta}+O\left(\lambda_N^2\right)}{\varepsilon_{k,0}-\varepsilon_{a,0}}
\end{aligned} \tag{6}$$

$$= \frac{\pi\alpha^4 g_e^2}{12} \times\sum_{k=1}^{n_{\mathrm{occ}}}\sum_{a=N_{\mathrm{occ}}+1}^{n}\frac{\left|\frac{\delta\vec{l}_{ka}}{\lambda_N}\right|\left|\vec{h}_{SO,ak}^{\beta}\right|\cos\left[\angle\left(\delta\vec{l}_{ka},\vec{h}_{SO,ak}^{\beta}\right)\right]+\left|\frac{\delta\vec{h}_{SO,ak}}{\lambda_N}\right|\left|\vec{l}_{ka}^{\beta}\right|\cos\left[\angle\left(\delta\vec{h}_{SO,ak},\vec{l}_{ka}^{\beta}\right)\right]+O\left(\lambda_N^2\right)}{\varepsilon_{k,0}-\varepsilon_{a,0}}.$$

An analysis of all of these the six *objects* (four lengths of vectors and two cosines of angles) is mandatory. Here the question of the mutual orientation of vectors becomes important. Even if, for instance, vectors $\vec{l}_{ka}^{\sigma}$ and $\vec{h}_{SO,ak}^{\sigma}$ are collinear, this is not necessarily the case for the differences ($\delta\vec{l}_{ka}$ and $\vec{h}_{SO,ak}^{\beta}$ or/and $\delta\vec{h}_{SO,ak}$ and $\vec{l}_{ka}^{\beta}$). The following contributions are analyzed in Table S16 below:

Column G: $\left|\delta\vec{l}_{ka}/\lambda_N\right|$;

Column H: $\left|\vec{h}_{SO,ak}^{\beta}\right|$;

Column I: $\cos\left[\angle\left(\delta\vec{l}_{ka},\vec{h}_{SO,ak}^{\beta}\right)\right]$;

Column J: $\left(\delta\vec{l}_{ka}/\lambda_N\right)\cdot\vec{h}_{SO,ak}^{\beta} = \left|\delta\vec{l}_{ka}/\lambda_N\right|\left|\vec{h}_{SO,ak}^{\beta}\right|\cos\left[\angle\left(\delta\vec{l}_{ka},\vec{h}_{SO,ak}^{\beta}\right)\right]$;

Column K: $\left|\delta\vec{h}_{SO,ak}/\lambda_N\right|$;

Column L: $\left|\vec{l}_{ka}^{\beta}\right|$;

Column M: $\cos\left[\angle\left(\delta\vec{h}_{SO,ak}, \vec{l}^{\,\beta}_{ka}\right)\right]$;

Column N: $\left(\delta\vec{h}_{SO,ak}/\lambda_N\right)\cdot\vec{l}^{\,\beta}_{ka} = \left|\delta\vec{h}_{SO,ak}/\lambda_N\right|\left|\vec{l}^{\,\beta}_{ka}\right|\cos\left[\angle\left(\delta\vec{h}_{SO,ak}, \vec{l}^{\,\beta}_{ka}\right)\right]$;

Column O: $10^6\,\dfrac{\pi\alpha^4 g_e^2}{12}\,\dfrac{\left(\delta\vec{l}_{ka}/\lambda_N\right)\cdot\vec{h}^{\,\beta}_{SO,ak} + \left(\delta\vec{h}_{SO,ak}/\lambda_N\right)\cdot\vec{l}^{\,\beta}_{ka}}{\varepsilon_{k,0}-\varepsilon_{a,0}} \approx$

$$\approx \sigma^{SO-I}_{N,xx} + \sigma^{SO-I}_{N,yy} + \sigma^{SO-I}_{N,zz} \quad \left(\text{up to } O\left(\lambda_N^2\right)\right).$$

Note that only relative changes of numbers presented in columns *G, H, J, K, L,* and *M* (rather than their absolute values) make sense.

Table S15. Main contributions from separate excitations to $\boldsymbol{\sigma}^{p}$ of the hydride (^{1}H) shielding tensor in pertinent *trans*-[HPtL(PMe$_3$)$_2$] complexes [a,b]

L	Excitation	σ^{p}_{iso} [ppm]	$\sigma^{p}_{\parallel}$ [ppm]	$\sigma^{p}_{\perp,ip}$ [ppm]	$\sigma^{p}_{\perp,op}$ [ppm]	ΔE [eV]	OZ $\left[\frac{\text{mHartree}}{\text{Zeeman}}\right]$	PSO [mZeeman]
NO_3	HOMO–2→LUMO+1	2.0	0.2	5.8	0.0	4.52	0.900	0.278
	HOMO–3→LUMO+1	3.1	0.0	0.0	9.4	5.24	1.795	0.253
	HOMO–7→LUMO+1	0.9	0.0	0.0	2.7	6.03	0.845	0.179
	HOMO–8→LUMO+1	0.5	0.0	1.6	0.0	6.25	0.697	0.134
NO_2	HOMO–1→LUMO+2	0.9	0.0	0.6	2.2	4.30	1.178	0.098
	HOMO–3→LUMO+2	0.9	0.0	2.5	0.2	5.15	0.677	0.195
	HOMO–6→LUMO+2	0.5	0.0	0.0	1.5	5.71	0.629	0.130
	HOMO–7→LUMO+2	1.0	0.0	0.0	2.9	6.11	0.966	0.168
Cl	HOMO–2→LUMO+1	0.7	0.0	0.0	2.1	4.45	0.494	0.172
	HOMO–6→LUMO+1	0.9	0.0	2.8	0.0	5.72	0.993	0.150
	HOMO–7→LUMO+1	2.1	0.0	0.0	6.2	6.28	1.651	0.217
CN	HOMO–1→LUMO+2	0.7	0.0	2.2	0.0	5.33	0.709	0.153
	HOMO–2→LUMO+2	1.1	0.0	0.0	3.3	5.76	1.106	0.158
	HOMO–7→LUMO+2	0.7	0.0	0.0	2.0	7.36	1.207	0.114
CH_3	HOMO–2→LUMO+2	0.9	0.0	2.8	0.0	4.81	0.779	0.162
	HOMO–3→LUMO+2	1.1	0.0	0.0	3.3	5.61	0.921	0.186
BH_2	HOMO–2→LUMO+3	0.5	0.0	1.4	0.0	5.04	0.615	0.104
	HOMO–5→LUMO+3	0.5	0.0	0.0	1.4	6.72	1.124	0.073

[a] One-component scalar relativistic GIAO calculations at the PBE/ECP/IGLO-III level (cf. Computational Methods in main text). [b] The absolute value of the contribution to the NMR shielding = $4\left|\mathrm{OZ}\right|\left|\mathrm{PSO}\right|/\Delta E$, where orbital Zeeman (OZ) and paramagnetic spin-orbit (PSO) terms are given in mHartree/Zeeman and mZeeman units, respectively, and energy denominator in atomic units.

Table S16. Main contributions from separate excitations to $\boldsymbol{\sigma}^{SO}$ of the hydride (^{1}H) shielding tensor in pertinent *trans*-[HPtL(PMe$_3$)$_2$] complexes [a,b]

L	Excitation	σ_{iso}^{SO} [ppm]	$\sigma_{\parallel}^{SO}$ [ppm]	$\sigma_{\perp,ip}^{SO}$ [ppm]	$\sigma_{\perp,op}^{SO}$ [ppm]	ΔE [eV]	G	H	I	J	K	L	M	N	O
NO_3	HOMO–2→LUMO+1	3.2	0.0	9.7	0.0	4.52	0.439	368	1.00	162	881	0.13	0.98	108	9.7
	HOMO–3→LUMO+1	3.5	0.0	0.0	10.5	5.24	0.351	618	0.99	216	625	0.20	1.00	124	10.5
	HOMO–7→LUMO+1	4.3	0.0	0.0	13.0	6.03	0.636	454	0.99	287	1400	0.14	1.00	199	13.0
	HOMO–8→LUMO+1	0.9	–0.1	2.9	–0.2	6.25	0.475	232	0.60	66	993	0.09	0.39	37	2.6
	Σ all excitations	11.8													
NO_2	HOMO–1→LUMO+2	1.9	0.0	0.8	4.9	4.30	0.355	225	0.98	78	413	0.18	0.96	72	5.7
	HOMO–3→LUMO+2	2.1	0.0	5.8	0.4	5.14	0.374	301	1.00	113	805	0.11	0.96	84	6.2
	HOMO–7→LUMO+2	2.9	0.0	0.0	8.8	6.10	0.340	563	1.00	191	978	0.14	1.00	140	8.8
	Σ all excitations	8.5													
Cl	HOMO→LUMO+1	1.4	0.0	4.2	0.0	4.14	0.407	243	1.00	99	944	0.01	1.00	9	4.2
	HOMO–2→LUMO+1	2.3	0.0	0.0	6.8	4.45	0.353	407	1.00	144	780	0.05	1.00	43	6.8
	HOMO–6→LUMO+1	2.0	0.0	6.0	0.0	5.72	0.410	264	1.00	108	783	0.14	1.00	106	6.1
	HOMO–7→LUMO+1	4.3	0.0	0.0	13.0	6.29	0.478	586	1.00	280	1050	0.22	1.00	224	13.0
	Σ all excitations	8.8													

L	Excitation	σ_{iso}^{SO} [ppm]	$\sigma_{\parallel}^{SO}$ [ppm]	$\sigma_{\perp,ip}^{SO}$ [ppm]	$\sigma_{\perp,op}^{SO}$ [ppm]	ΔE [eV]	G	H	I	J	K	L	M	N	O
CN	HOMO–1→LUMO+2	1.3	0.0	3.8	0.0	5.33	0.260	297	1.00	77	495	0.10	1.00	48	3.8
	HOMO–2→LUMO+2	0.3	0.0	0.0	1.0	5.76	0.050	403	1.00	20	118	0.15	1.00	17	1.0
	HOMO–6→LUMO+2	0.3	0.0	1.0	0.0	7.00	0.156	173	1.00	27	210	0.09	1.00	18	1.0
	HOMO–7→LUMO+2	0.7	0.0	0.0	2.2	7.36	0.216	408	1.00	88	86	0.16	1.00	14	2.2
	Σ all excitations	4.9													
CH_3	HOMO–1→LUMO+2	1.0	0.0	2.8	0.3	4.78	1.540	35	0.83	45	4560	0.03	0.38	50	3.1
	HOMO–3→LUMO+2	1.1	0.0	0.0	3.3	5.61	0.107	509	1.00	55	433	0.14	1.00	60	3.3
	Σ all excitations	2.8													
BH_2	HOMO→LUMO+1	–3.3	–0.1	–10.6	0.9	3.56	0.296	417	0.73	–90	578	0.25	0.85	125	–9.8
	Σ all excitations	–5.2													

[a] One-component GIAO calculations at the PBE/ECP/IGLO-III level (cf. Computational Methods in main text). [b] For headers and units corresponding to columns G–O, see the text above.

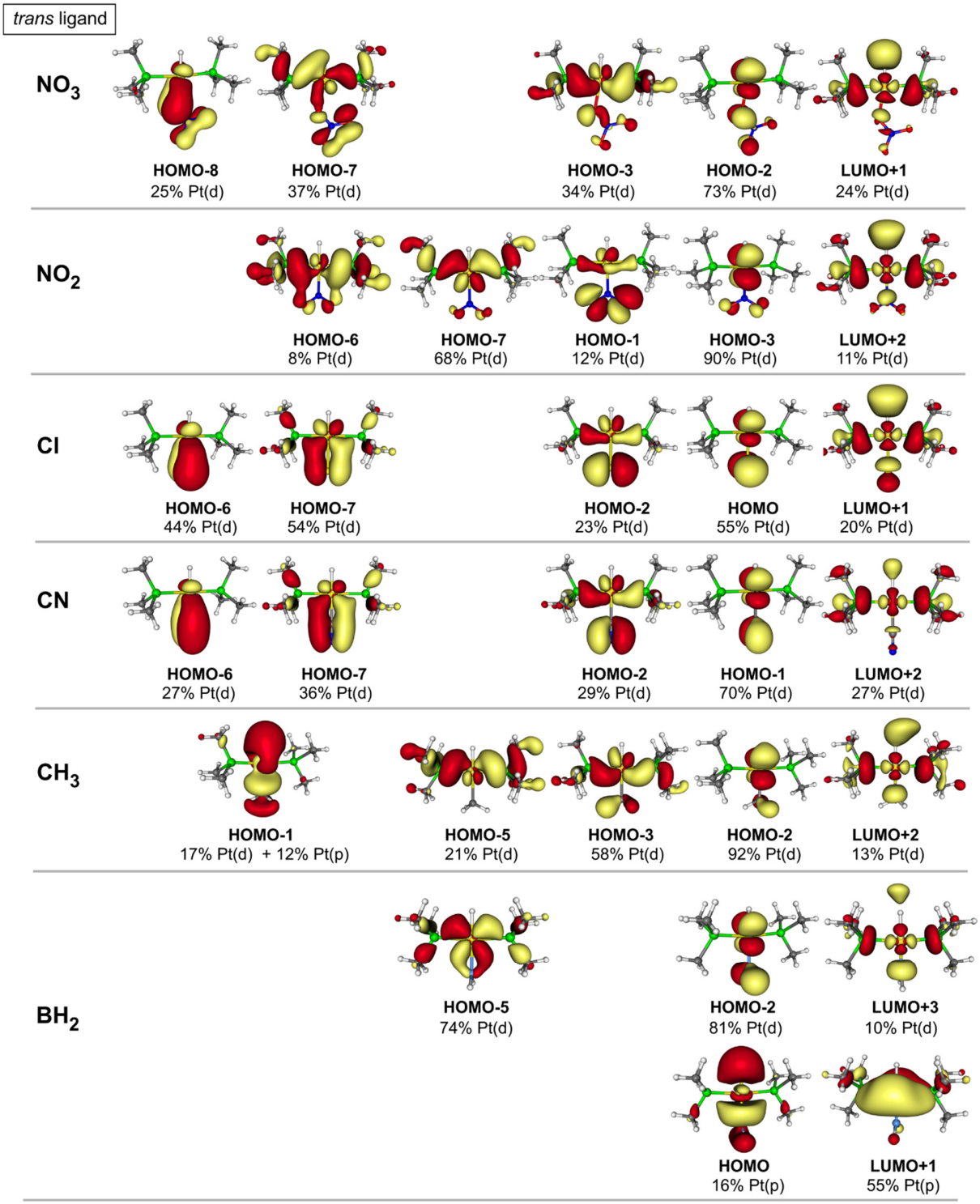

Figure S2. Isosurface plot (+/- 0.03 au) of the dominant occupied and virtual MOs contributing to $\boldsymbol{\sigma}^{p}$ and $\boldsymbol{\sigma}^{SO}$ tensors (1c-PBE/ECP/IGLO-III results; cf. Tables S15 and S16).

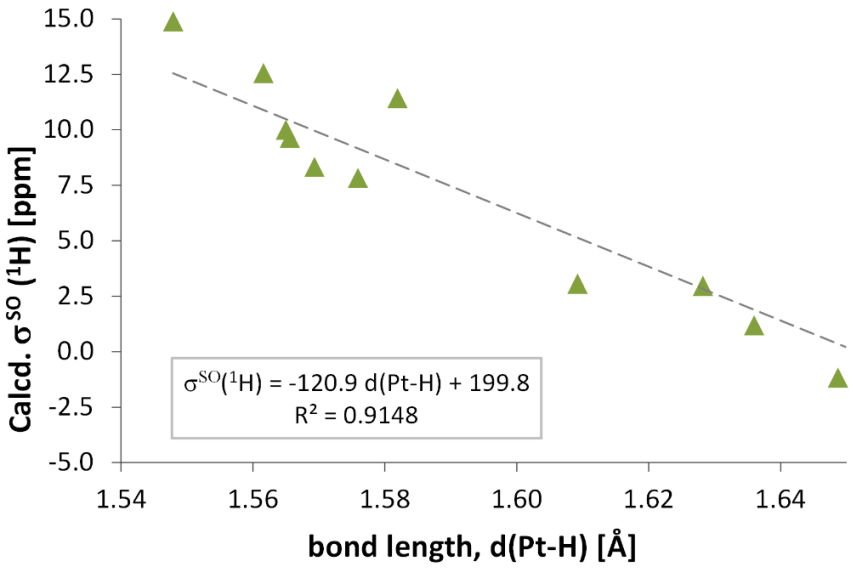

Figure S3. Correlation of the SO-induced hydride shielding (σ^{SO}) within *trans*-[HPtL(PMe$_3$)$_2$] series with the Pt–H bond length.

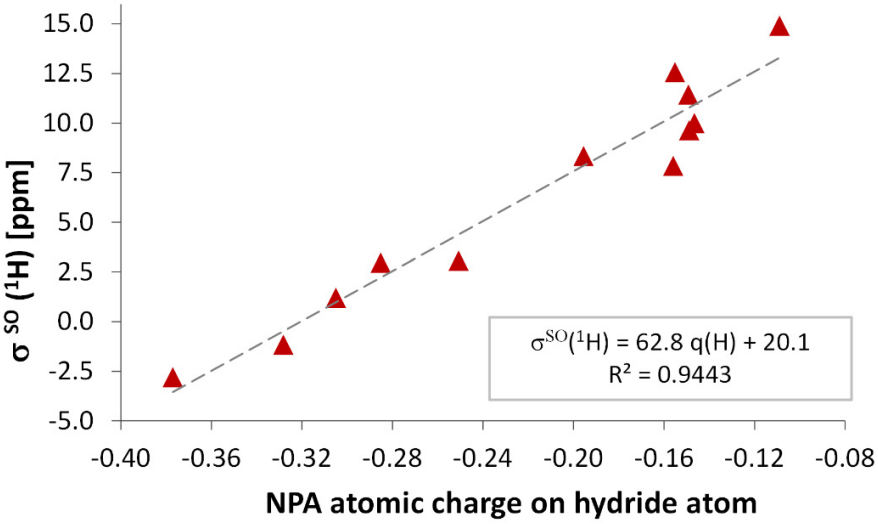

Figure S4. Correlation of the SO-induced hydride shielding (σ^{SO}) within *trans*-[HPtL(PMe$_3$)$_2$] series with the hydride NPA atomic charge.

Cartesian Coordinates of *trans*-[HPtL(PMe$_3$)$_2$] Complexes

(optimized at the PBE0/def2-TZVP/ECP level)

trans-**[HPtNO$_3$(PMe$_3$)$_2$]**

Pt	-0.00284	0.05250	0.19635
H	-0.00629	-0.08922	1.73770
P	0.20987	2.32310	0.41219
P	-0.20468	-2.23565	0.22664
O	0.03070	0.58535	-1.88495
N	-0.02953	-0.20787	-2.90970
O	-0.14268	-1.41420	-2.72277
C	-0.25577	-2.91992	1.91483
C	-1.71366	-2.92607	-0.51199
C	1.15530	-3.17489	-0.52674
C	0.27021	3.00042	2.09597
C	1.70510	2.97162	-0.38727
C	-1.13311	3.23994	-0.39465
O	0.03020	0.30461	-4.00600
H	-0.34786	-4.00866	1.89422
H	2.09077	-2.90907	-0.03166
H	1.22288	-2.91559	-1.58202
H	-1.10455	-2.49583	2.45303
H	-1.18509	2.91291	-1.43420
H	-1.72735	-4.01347	-0.40381
H	1.11594	2.56462	2.62954
H	1.73730	4.06280	-0.34103
H	0.37228	4.08804	2.08072
H	-2.58467	-2.50484	-0.00717
H	2.59051	2.56057	0.09980
H	-2.08129	3.00602	0.09160
H	0.65591	-2.64485	2.44699
H	-0.64351	2.73019	2.62714
H	-1.74662	-2.65646	-1.56632
H	1.69758	2.64473	-1.42819
H	0.98349	-4.24849	-0.41608
H	-0.95853	4.31768	-0.35218

trans-**[HPtONO(PMe$_3$)$_2$]**

Pt	0.06040	-0.11327	0.03279
H	0.06340	-1.61593	-0.39224
P	2.33811	-0.07453	-0.02566
P	-2.21993	-0.31080	0.03939
O	0.25793	1.92071	0.71856
N	-0.44653	2.87426	0.24125
O	-1.25644	2.57394	-0.60739
C	-2.81384	-1.98467	0.44682
C	-3.15016	0.72342	1.21016
C	-3.00655	0.02374	-1.56267
C	3.06721	0.47406	1.54478
C	3.20493	-1.62687	-0.39993
C	3.01283	1.09999	-1.23726
H	4.28897	-1.49060	-0.38873
H	2.83758	-0.25267	2.32524
H	2.60896	1.42678	1.81462
H	2.89382	-1.98272	-1.38312
H	-2.78308	1.05142	-1.84687
H	4.10395	1.13692	-1.18967
H	-2.45077	-2.26721	1.43600
H	-4.21550	0.48315	1.17173
H	-3.90560	-2.03119	0.43592
H	2.70249	0.80784	-2.24136
H	-2.77876	0.55150	2.22157
H	-2.59252	-0.64849	-2.31552
H	2.92544	-2.38075	0.33724
H	-2.41182	-2.69470	-0.27693
H	2.60242	2.08830	-1.02494
H	-2.99961	1.77187	0.95592
H	4.15061	0.58915	1.46225
H	-4.08794	-0.12267	-1.50192

trans-**[HPtCl(PMe$_3$)$_2$]**

Pt	0.00000	0.00000	0.08476
H	0.00000	0.00000	1.64974
P	0.32364	2.25618	0.07645
P	-0.32364	-2.25618	0.07645
Cl	0.00000	0.00000	-2.33290

C	-0.99862	3.15563	-0.78399
C	0.46295	3.10844	1.67651
C	1.82563	2.75372	-0.81506
C	-0.46295	-3.10844	1.67651
C	0.99862	-3.15563	-0.78399
C	-1.82563	-2.75372	-0.81506
H	-0.61489	-4.18234	1.54438
H	1.94083	-3.01513	-0.25205
H	1.09858	-2.72685	-1.78263
H	-1.30174	-2.68897	2.23391
H	-1.09858	2.72685	-1.78263
H	-1.90537	-3.84131	-0.88510
H	1.30174	2.68897	2.23391
H	1.90537	3.84131	-0.88510
H	0.61489	4.18234	1.54438
H	-2.70238	-2.35655	-0.30135
H	2.70238	2.35655	-0.30135
H	-1.94083	3.01513	-0.25205
H	0.44652	-2.93815	2.25418
H	-0.44652	2.93815	2.25418
H	-1.78198	-2.31426	-1.81301
H	1.78198	2.31426	-1.81301
H	0.77479	-4.22295	-0.85305
H	-0.77479	4.22295	-0.85305

trans-**[HPtBr(PMe$_3$)$_2$]**

Pt	0.00000	0.00000	0.02740
H	0.00000	0.00000	1.59304
P	0.00000	2.28157	0.05699
P	0.00000	-2.28157	0.05699
Br	0.00000	0.00000	-2.52204
C	-1.42764	3.01991	-0.78899
C	0.00000	3.09323	1.68474
C	1.42764	3.01991	-0.78899
C	0.00000	-3.09323	1.68474
C	1.42764	-3.01991	-0.78899
C	-1.42764	-3.01991	-0.78899
H	0.00000	-4.18149	1.58726
H	2.34517	-2.72535	-0.27732
H	1.45915	-2.62663	-1.80633

H	-0.88313	-2.77859	2.24266
H	-1.45915	2.62663	-1.80633
H	-1.35536	-4.11000	-0.80911
H	0.88313	2.77859	2.24266
H	1.35536	4.11000	-0.80911
H	0.00000	4.18149	1.58726
H	-2.34517	-2.72535	-0.27732
H	2.34517	2.72535	-0.27732
H	-2.34517	2.72535	-0.27732
H	0.88313	-2.77859	2.24266
H	-0.88313	2.77859	2.24266
H	-1.45915	-2.62663	-1.80633
H	1.45915	2.62663	-1.80633
H	1.35536	-4.11000	-0.80911
H	-1.35536	4.11000	-0.80911

trans-**[HPtI(PMe$_3$)$_2$]**

Pt	0.00000	0.00000	-0.04167
H	0.00000	0.00000	1.52758
P	0.00000	2.28298	0.03419
P	0.00000	-2.28298	0.03419
I	0.00000	0.00000	-2.75590
C	-1.42870	3.06072	-0.77460
C	0.00000	3.03319	1.69196
C	1.42870	3.06072	-0.77460
C	0.00000	-3.03319	1.69196
C	1.42870	-3.06072	-0.77460
C	-1.42870	-3.06072	-0.77460
H	0.00000	-4.12441	1.63483
H	2.34560	-2.73697	-0.27969
H	1.46181	-2.72599	-1.81247
H	-0.88319	-2.69809	2.23767
H	-1.46181	2.72599	-1.81247
H	-1.35795	-4.15040	-0.73391
H	0.88319	2.69809	2.23767
H	1.35795	4.15040	-0.73391
H	0.00000	4.12441	1.63483
H	-2.34560	-2.73697	-0.27969
H	2.34560	2.73697	-0.27969
H	-2.34560	2.73697	-0.27969

H	0.88319	-2.69809	2.23767
H	-0.88319	2.69809	2.23767
H	-1.46181	-2.72599	-1.81247
H	1.46181	2.72599	-1.81247
H	1.35795	-4.15040	-0.73391
H	-1.35795	4.15040	-0.73391

trans-**[HPtNO$_2$(PMe$_3$)$_2$]**

Pt	0.00000	0.00000	0.09906
H	0.00000	0.00000	1.68092
P	-1.45393	1.76969	0.19015
P	1.45393	-1.76969	0.19015
N	0.00000	0.00000	-2.02544
O	0.24832	-1.03309	-2.64220
O	-0.24832	1.03309	-2.64220
C	-2.15081	2.13364	1.82920
C	-0.70306	3.33950	-0.32448
C	-2.92012	1.62053	-0.87095
C	2.15081	-2.13364	1.82920
C	0.70306	-3.33950	-0.32448
C	2.92012	-1.62053	-0.87095
H	-2.82873	2.98959	1.78814
H	-3.49832	0.74361	-0.57572
H	-2.58506	1.49304	-1.90066
H	-1.33919	2.34407	2.52652
H	2.58506	-1.49304	-1.90066
H	-1.43299	4.15235	-0.29393
H	1.33919	-2.34407	2.52652
H	1.43299	-4.15235	-0.29393
H	2.82873	-2.98959	1.78814
H	0.13275	3.57740	0.33504
H	-0.13275	-3.57740	0.33504
H	3.49832	-0.74361	-0.57572
H	-2.69189	1.25925	2.19363
H	2.69189	-1.25925	2.19363
H	-0.32801	3.20851	-1.34019
H	0.32801	-3.20851	-1.34019
H	-3.54815	2.51111	-0.79187
H	3.54815	-2.51111	-0.79187

trans-**[HPtSCN(PMe$_3$)$_2$]**

Pt	0.10124	0.08542	0.10002
H	-0.33348	0.02130	1.61339
P	0.24059	2.35225	0.33879
P	-0.17607	-2.19454	0.12341
S	0.84261	0.32540	-2.19403
C	0.02724	-0.85056	-3.05050
N	-0.52539	-1.67838	-3.65026
C	-0.16663	-2.92313	1.78993
C	1.08266	-3.16624	-0.75278
C	-1.74687	-2.76538	-0.58276
C	1.78160	3.11122	-0.25790
C	-1.05102	3.23541	-0.58350
C	0.08506	2.99967	2.02938
H	0.14783	4.09043	2.04418
H	-2.03203	2.92542	-0.22092
H	-0.97292	2.96018	-1.63653
H	0.87888	2.58166	2.64995
H	1.05950	-2.91314	-1.81285
H	1.74893	4.19806	-0.15128
H	-0.97778	-2.49000	2.37623
H	-1.83449	-3.85113	-0.49440
H	-0.28807	-4.00803	1.74288
H	2.62486	2.71700	0.31095
H	-2.57565	-2.28945	-0.05650
H	2.06907	-2.92649	-0.35366
H	-0.87243	2.68372	2.44541
H	0.77594	-2.68513	2.28494
H	1.92645	2.85595	-1.30909
H	-1.78342	-2.48397	-1.63704
H	-0.94680	4.31762	-0.47374
H	0.89057	-4.23512	-0.63174

trans-**[HPtCN(PMe$_3$)$_2$]**

Pt	0.00000	0.00000	0.15108
H	0.00000	0.00000	1.76028
P	0.00000	2.28134	0.15984
P	0.00000	-2.28134	0.15984
C	0.00000	0.00000	-1.88253

N	0.00000	0.00000	-3.04278
C	-1.42598	-2.99734	-0.70744
C	1.42598	-2.99734	-0.70744
C	0.00000	-3.12312	1.76985
C	-1.42598	2.99734	-0.70744
C	0.00000	3.12312	1.76985
C	1.42598	2.99734	-0.70744
H	0.00000	4.20935	1.65223
H	-2.34695	2.69658	-0.20583
H	-1.44327	2.60252	-1.72459
H	0.88245	2.81621	2.33288
H	1.44327	-2.60252	-1.72459
H	1.36551	4.08799	-0.73250
H	-0.88245	-2.81621	2.33288
H	-1.36551	-4.08799	-0.73250
H	0.00000	-4.20935	1.65223
H	2.34695	2.69658	-0.20583
H	-2.34695	-2.69658	-0.20583
H	2.34695	-2.69658	-0.20583
H	-0.88245	2.81621	2.33288
H	0.88245	-2.81621	2.33288
H	1.44327	2.60252	-1.72459
H	-1.44327	-2.60252	-1.72459
H	-1.36551	4.08799	-0.73250
H	1.36551	-4.08799	-0.73250

trans-**[HPtPh(PMe$_3$)$_2$]**

Pt	0.00000	0.00000	1.00609
H	0.00000	0.00000	2.63428
P	-1.29649	1.86245	1.04383
P	1.29649	-1.86245	1.04383
C	0.00000	0.00000	-1.10532
C	0.98209	0.66558	-1.85332
C	0.98845	0.66975	-3.24394
C	0.00000	0.00000	-3.95032
C	-0.98845	-0.66975	-3.24394
C	-0.98209	-0.66558	-1.85332
C	2.92056	-1.66146	0.24905
C	1.72321	-2.54370	2.67592
C	0.59196	-3.29748	0.17532

C	-1.72321	2.54370	2.67592
C	-2.92056	1.66146	0.24905
C	-0.59196	3.29748	0.17532
H	-2.34846	3.43622	2.59091
H	-3.48306	0.88435	0.76880
H	-2.76971	1.34419	-0.78385
H	-0.80308	2.78915	3.20794
H	2.76971	-1.34419	-0.78385
H	-1.27670	4.14887	0.19852
H	0.80308	-2.78915	3.20794
H	1.27670	-4.14887	0.19852
H	2.34846	-3.43622	2.59091
H	0.35046	3.58008	0.64711
H	-0.35046	-3.58008	0.64711
H	3.48306	-0.88435	0.76880
H	-2.24741	1.77964	3.25142
H	2.24741	-1.77964	3.25142
H	-0.38709	3.01596	-0.85862
H	0.38709	-3.01596	-0.85862
H	-3.48920	2.59426	0.26993
H	3.48920	-2.59426	0.26993
H	-1.77363	-1.20253	-1.33549
H	-1.77121	-1.19992	-3.77849
H	0.00000	0.00000	-5.03482
H	1.77121	1.19992	-3.77849
H	1.77363	1.20253	-1.33549

trans-**[HPtCH$_3$(PMe$_3$)$_2$]**

Pt	0.03856	0.03605	0.11888
H	0.47213	0.49822	1.62717
P	-1.31182	1.84942	0.17571
P	1.44467	-1.72596	0.25737
C	-0.54607	-0.54663	-1.85687
C	2.75814	-1.75258	-1.00456
C	2.38025	-1.93548	1.80446
C	0.64924	-3.35233	0.05597
C	-2.50946	1.84119	1.54772
C	-2.37257	2.21630	-1.25978
C	-0.43215	3.42545	0.41941
H	-3.11125	2.75366	1.55726

H	-3.03850	1.37216	-1.44411
H	-1.75112	2.34880	-2.14650
H	-1.96517	1.74638	2.48775
H	2.30383	-1.71706	-1.99539
H	-1.12900	4.26519	0.48443
H	1.67525	-2.02782	2.63166
H	1.38286	-4.16209	0.08281
H	3.02854	-2.81509	1.77274
H	0.15490	3.36017	1.33580
H	-0.07601	-3.49632	0.85830
H	3.38397	-0.86696	-0.88520
H	-3.16690	0.97629	1.44733
H	2.98045	-1.04114	1.97674
H	0.25372	3.58933	-0.41306
H	0.11428	-3.37359	-0.89399
H	-2.96685	3.11821	-1.09505
H	3.37796	-2.64831	-0.91659
H	-0.04665	-1.43708	-2.25503
H	-1.62237	-0.75667	-1.89869
H	-0.35285	0.25828	-2.57665

trans-**[HPt{Si(OMe)$_3$}(PMe$_3$)$_2$]**

Pt	0.28346	0.23775	1.29773
H	0.63924	0.57613	2.87163
P	-0.99326	2.12020	1.31423
P	1.63722	-1.57756	1.49037
Si	-0.23842	-0.22533	-0.97644
C	3.19680	-1.45221	0.56623
C	2.19768	-1.96255	3.17989
C	0.94178	-3.16970	0.95095
C	-1.39198	2.77881	2.96477
C	-2.63188	2.04044	0.52777
C	-0.20339	3.53246	0.48664
H	-1.99471	3.68841	2.89805
H	-3.20456	1.22092	0.96419
H	-2.49717	1.84379	-0.53598
H	-0.46206	2.98675	3.49467
H	2.95682	-1.32247	-0.48942
H	-0.83521	4.42258	0.54196
H	1.32677	-2.13610	3.81331

H	1.65579	-3.98132	1.11166
H	2.84524	-2.84321	3.19742
H	0.75737	3.73948	0.96009
H	0.03024	-3.37327	1.51489
H	3.74980	-0.57791	0.91323
H	-1.93688	2.02106	3.52972
H	2.73355	-1.10047	3.57837
H	-0.03345	3.25830	-0.55496
H	0.68480	-3.10631	-0.10598
H	-3.17524	2.97839	0.66591
H	3.80790	-2.34673	0.70978
O	0.94526	-1.08633	-1.80501
O	-1.63402	-1.12865	-1.15026
O	-0.48897	1.15684	-1.90205
C	0.71477	-1.97318	-2.86682
H	1.62627	-2.55050	-3.04966
H	-0.09705	-2.67397	-2.64032
H	0.45993	-1.44795	-3.79600
C	-0.13382	1.32573	-3.24760
H	-0.16892	2.39161	-3.49230
H	0.87954	0.96129	-3.44649
H	-0.82504	0.80393	-3.92262
C	-2.57739	-1.02791	-2.17917
H	-3.51695	-1.47699	-1.84415
H	-2.77445	0.01513	-2.45338
H	-2.25543	-1.55942	-3.08489

trans-**[HPtSiH$_3$(PMe$_3$)$_2$]**

Pt	0.04030	0.03848	0.14118
H	0.47228	0.50492	1.66414
P	-1.30926	1.86433	0.21201
P	1.45844	-1.72590	0.28943
Si	-0.62488	-0.58748	-2.07881
C	2.79325	-1.75474	-0.94671
C	2.37074	-1.88813	1.85693
C	0.68596	-3.36394	0.11481
C	-2.47703	1.83702	1.60743
C	-2.39265	2.27206	-1.19172
C	-0.39425	3.41746	0.46172
H	-3.07805	2.74940	1.63626

H	-3.07409	1.44065	-1.37797
H	-1.78772	2.41288	-2.08890
H	-1.91585	1.73162	2.53614
H	2.35587	-1.79594	-1.94488
H	-1.07633	4.26779	0.54055
H	1.65393	-1.97469	2.67453
H	1.42811	-4.15945	0.21848
H	3.03200	-2.75860	1.85246
H	0.20142	3.33396	1.37088
H	-0.08013	-3.48423	0.88226
H	3.38010	-0.83895	-0.86274
H	-3.13752	0.97438	1.50740
H	2.95516	-0.98176	2.02031
H	0.28323	3.57643	-0.37855
H	0.20991	-3.43239	-0.86390
H	-2.96901	3.17909	-0.99420
H	3.44659	-2.61761	-0.79638
H	0.01612	-1.81008	-2.68586
H	-2.09157	-0.88402	-2.24287
H	-0.37510	0.45744	-3.13341

trans-**[HPtBCat(PMe$_3$)$_2$]**

Pt	0.00000	0.00000	-1.41852
H	0.00000	0.00000	-3.09615
P	-2.17847	0.60377	-1.55667
P	2.17847	-0.60377	-1.55667
B	0.00000	0.00000	0.66322
O	0.02947	-1.13909	1.50489
C	0.01714	-0.69396	2.78950
C	-0.01714	0.69396	2.78950
C	-0.03455	1.41900	3.96013
C	-0.01696	0.69445	5.15195
C	0.01696	-0.69445	5.15195
C	0.03455	-1.41900	3.96013
O	-0.02947	1.13909	1.50489
C	-3.19037	-0.50337	-2.58693
C	-2.41290	2.23263	-2.33263
C	-3.17227	0.74325	-0.03706
C	3.17227	-0.74325	-0.03706
C	3.19037	0.50337	-2.58693

C	2.41290	-2.23263	-2.33263
H	-0.05958	2.50191	3.95056
H	-0.02961	1.22703	6.09585
H	0.02961	-1.22703	6.09585
H	0.05958	-2.50191	3.95056
H	-4.22364	-0.15264	-2.64879
H	-2.75226	-0.55154	-3.58408
H	-3.17554	-1.50704	-2.15934
H	-3.47391	2.48062	-2.41792
H	-1.91221	2.99203	-1.73022
H	-1.95352	2.22151	-3.32125
H	-4.19699	1.05564	-0.25354
H	-3.18844	-0.22297	0.47046
H	-2.70207	1.46682	0.63082
H	4.22364	0.15264	-2.64879
H	2.75226	0.55154	-3.58408
H	3.17554	1.50704	-2.15934
H	3.47391	-2.48062	-2.41792
H	1.91221	-2.99203	-1.73022
H	1.95352	-2.22151	-3.32125
H	4.19699	-1.05564	-0.25354
H	3.18844	0.22297	0.47046
H	2.70207	-1.46682	0.63082

trans-**[HPtBH$_2$(PMe$_3$)$_2$]**

Pt	-0.00979	-0.00887	-0.01041
H	0.98570	0.75086	1.14254
P	-1.26025	1.87309	0.04202
P	1.41103	-1.76164	0.13145
B	-1.21441	-0.91923	-1.39887
C	3.13204	-1.33989	-0.27956
C	1.53751	-2.46062	1.80611
C	1.11632	-3.24204	-0.89011
C	-1.89799	2.28203	1.69595
C	-2.75677	1.98363	-0.99256
C	-0.34380	3.37023	-0.43589
H	-2.46716	3.21504	1.68193
H	-3.43829	1.17542	-0.72079
H	-2.47599	1.85052	-2.03904
H	-1.05532	2.36862	2.38219

H	3.18071	-0.99179	-1.31237
H	-0.97393	4.26024	-0.36009
H	0.55867	-2.82715	2.11843
H	1.87729	-4.00976	-0.72779
H	2.25896	-3.28117	1.84005
H	0.52388	3.47076	0.21634
H	0.13329	-3.65117	-0.64895
H	3.45586	-0.52657	0.37022
H	-2.54025	1.47194	2.04444
H	1.83994	-1.66864	2.49145
H	0.01022	3.26471	-1.46239
H	1.11222	-2.95351	-1.94293
H	-3.26697	2.94286	-0.87385
H	3.79147	-2.20285	-0.15685
H	-1.05381	-0.82336	-2.59932
H	-2.17037	-1.61172	-1.11134

References

[S1] Robertson, G. B.; Tucker, P. A.; Wickramasinghe, W. A. *Austr. J. Chem.* **1986**, *39*, 1495.

[S2] Languérand, A.; Barnes, S. S.; Bélanger-Chabot, G.; Maron. L.; Berrouard, P.; Audet, P.; Fontaine, F. G. *Angew. Chem. Int. Ed.* **2009**, *48*, 6695.

[S3] Owston, P. G.; Partridge, J. M.; Rowe, J. M. *Acta Crystallogr.* **1960**, *13*, 246.

[S4] Robertson, G. B.; Tucker, P. A. *Acta Crystallogr.* **1983**, C39, 1354.

[S5] Braunschweig, H.; Brenner, P.; Dewhurst, R. D.; Guethlein, F.; Jimenez-Halla, J. O. C.; Radacki, K.; Wolf, J.; Zöllner, L. *Chem. Eur. J.* **2012**, *18*, 8605.

[S6] Cowan, R. L.; Trogler, W. C. *J. Am. Chem. Soc.* **1989**, *111*, 4750.

[S7] Dean, R. R.; Green, J. C. *J. Chem. Soc. A* **1968**, 3047.

[S8] Schreckenbach, G. *Theor. Chem. Acc.* **2002**, *108*, 246.

[S9] Vaara, J.; Malkina, O.; Stoll, H.; Malkin, V.; Kaupp, M. *J. Chem. Phys.* **2001**, *114*, 61.

Full citation of ref. (30):

Gaussian 09, revision A.02, M. J. Frisch, G. W. Trucks, H. B. Schlegel, G. E. Scuseria, M. A. Robb, J. R. Cheeseman, G. Scalmani, V. Barone, B. Mennucci, G. A. Petersson, H. Nakatsuji, M. Caricato, X. Li, H. P. Hratchian, A. F. Izmaylov, J. Bloino, G. Zheng, J. L. Sonnenberg, M. Hada, M. Ehara, K. Toyota, R. Fukuda, J. Hasegawa, M. Ishida, T. Nakajima, Y. Honda, O. Kitao, H. Nakai, T. Vreven, J. A. Montgomery, Jr., J. E. Peralta, F. Ogliaro, M. Bearpark, J. J. Heyd, E. Brothers, K. N. Kudin, V. N. Staroverov, R. Kobayashi, J. Normand, K. Raghavachari, A. Rendell, J. C. Burant, S. S. Iyengar, J. Tomasi, M. Cossi, N. Rega, J. M. Millam, M. Klene, J. E. Knox, J. B. Cross, V. Bakken, C. Adamo, J. Jaramillo, R. Gomperts, R. E. Stratmann, O. Yazyev, A. J. Austin, R. Cammi, C. Pomelli, J. W. Ochterski, R. L. Martin, K. Morokuma, V. G. Zakrzewski, G. A. Voth, P. Salvador, J. J. Dannenberg, S. Dapprich, A. D. Daniels, Ö. Farkas, J. B. Foresman, J. V. Ortiz, J. Cioslowski, and D. J. Fox, Gaussian, Inc., Wallingford CT, **2009**.

II

ChemPubSoc Europe

DOI: 10.1002/chem.201700844

CHEMISTRY A European Journal Full Paper

Ligand NMR Shifts | *Hot Paper*

Insights into *trans*-Ligand and Spin-Orbit Effects on Electronic Structure and Ligand NMR Shifts in Transition-Metal Complexes

Anja H. Greif,[a] Peter Hrobárik,*[a, b] and Martin Kaupp*[a]

Abstract: Surprisingly general effects of *trans* ligands L on the ligand NMR shifts in third-row transition-metal complexes have been found by quasi-relativistic computations, encompassing $5d^{10}$, $5d^{8}$, and to some extent even $5d^{6}$ situations. Closer analysis, with emphasis on ^{1}H shieldings in a series of linear $HAu^{I}L^{q}$ complexes, reveals a dominance of spin-orbit (SO) effects, which can change sign from appreciably shielding for weak *trans* ligands to appreciably deshielding for ligands with strong *trans* influence. This may be traced back to increasing destabilization of a σ-type MO at scalar relativistic level, which translates into very different σ-/π-mixing if SO coupling is included. For the strongest *trans* ligands, the σ-MO may move above the highest occupied π-type MOs, thereby dramatically reducing strongly shielding contributions from predominantly π-type spinors. The effects of SO-mixing are in turn related to angular momentum admixture from atomic spinors at the metal center. These SO-induced trends hold for other nuclei and may also be used to qualitatively predict shifts in unknown complexes.

Introduction

Research on NMR shifts and electronic structure in heavy transition-metal complexes has in recent years benefitted greatly from improved four-component relativistic and two-component quasi-relativistic methodologies. In particular, the role of spin-orbit (SO) effects on ligand chemical shifts (a "heavy atom effect on the light-atom shielding", HALA) has been exposed in several studies.[1–6] Earlier studies suggested that SO shieldings on directly neighboring atoms induced by occupied MOs with σ symmetry with respect to the bond between the heavy neighboring atom and that nucleus are generally negative, whereas those induced by π orbitals are positive.[7] Our recent analysis of *trans* ligand effects on ^{1}H shifts in a series of square-planar Pt^{II} complexes,[1] and a comparison between ^{13}C and ^{14}N shifts in square-planar Au^{III} and Pt^{II} complexes by Vicha et al.,[4] gave a somewhat more varied picture, whereby seemingly similar bonding arrangements may give rise to either shielding or deshielding SO effects depending on the *trans* ligand or the central metal. Adding the also frequently important paramagnetic contributions (σ^{p}) to the shifts further complicates the situation and makes general predictions without explicit quantitative calculations more difficult. For example, the long-established Buckingham–Stephens[8] effect (based on an off-center diatropic current loop) contributes in a shielding way to the ^{1}H shifts of d^{6} or d^{8} transition-metal hydride complexes, whereas the σ^{p} contributions in d^{10} or d^{0} hydride complexes (as well as in actinide $6d^{0}5f^{0}$ complexes) typically tend to be deshielding.[2,3]

In order to understand the interrelations between molecular and electronic structure and ligand NMR shifts in transition metal complexes in a more fundamental way, in the present study we have striven to analyze the origins of the ligand shifts for some of the simplest building blocks of such complexes, with an emphasis on ^{1}H hydride shifts of linear $HAu^{I}L$ complexes. The choice of hydride ^{1}H shifts was motivated by their extreme dependence on SO effects, due to the large hydrogen 1s character of the bond that facilitates the underlying Fermi-contact (FC) SO-shift mechanism.[9] Gold hydride complexes have been postulated as key reagents or intermediates in many gold-catalyzed reactions, such as homogeneous hydrogenation, hydrodefluorination, or activation of O_2,[10] but our choice of the $HAu^{I}L$ series was also influenced by a recent study of SO-induced ring currents in the diatomic HAu molecule by Berger et al.[11] They found a shielding SO contribution to the ^{1}H shift of this molecule, whereas it is well known that the SO shifts in closely related linear complexes $HAu^{I}L$ (L = NHC ligand)[12,13] or for isoelectronic organomercury hydrides $HHg^{II}R$ are, sometimes strongly, deshielding,[2,14] and the shifts for the hydride ligands in bridging positions in multinuclear silver and gold hydrides are also at high frequencies.[13] Strikingly, we find here that the sign and magnitude of the overall SO effects on the ^{1}H shieldings depend fundamentally on the *trans* ligand, not only for these d^{10} complexes, but in a similar

[a] *A. H. Greif, Dr. P. Hrobárik, Prof. Dr. M. Kaupp*
Technische Universität Berlin
Institut für Chemie, Theoretische Chemie/Quantenchemie
Sekr. C7, Strasse des 17. Juni 135, 10623 Berlin (Germany)
E-mail: peter.hrobarik@tu-berlin.de
martin.kaupp@tu-berlin.de

[b] *Dr. P. Hrobárik*
Faculty of Natural Sciences, Comenius University
Department of Inorganic Chemistry
Mlynská dolina CH-2, 84215 Bratislava (Slovakia)

Supporting information and the ORCID identification number for the author of this article can be found under: https://doi.org/10.1002/chem.201700844.

way for d^8 complexes, whereas it is less pronounced for d^6 systems. Our analyses consequently show that these large *trans* ligand effects have a common explanation, shining new light on the interrelations between electronic structure and ligand NMR shifts in transition-metal complexes in a broader way. In addition, we emphasize the differences between the scalar relativistic (SR) MO picture and a spinor-based spin-dependent one, with notable consequences for interpretation of the NMR shielding tensor.

Computational Details

We performed gas-phase def2-TZVP[15–18] structure optimizations with the PBE0 functional[19,20] using the TURBOMOLE program package.[21] During the optimizations, DFT-D3 dispersion corrections[22] were added with Becke–Johnson damping.[23] This computational level includes a small-core (60-core-electron) quasi-relativistic effective core potential (ECP) for the 5d transition metal.[24,25]

Two-component quasi-relativistic ZORA[26,27] all-electron DFT calculations of nuclear shieldings were carried out using the Amsterdam Density Functional (ADF) program[28] with the PBE0 functional,[29,30] all-electron Slater-type orbital basis sets of triple-ζ doubly-polarized (TZ2P)[31] quality, and an integration accuracy of 5.0. The calculations used gauge-including atomic orbitals (GIAOs).[32] ZORA calculations of NMR chemical shifts were performed with the previously neglected terms from the exchange-correlation (XC) response kernel.[33] The calculated ^{1}H and ^{13}C nuclear shieldings σ were converted into chemical shifts $\delta = \sigma(\mathrm{TMS}) - \sigma$ (in ppm) relative to the shielding of tetramethylsilane (TMS; σ(TMS) = 31.6 ppm). This computational level reproduces excellently the available experimental ^{1}H NMR shifts for *trans*-[HOsL(dhpe)$_2$] (L = Cl, CN), *trans*-[HPtL(PMe$_3$)$_2$] (L = NO$_3$, Cl, CH$_3$, BH$_2$), and HAuNHC (NHC = 1,3-bis(2,6-diisopropylphenyl)imidazol-2-ylidene); see Table S1 in the Supporting Information.

Molecular orbital (MO) analyses of the NMR shifts and natural localized molecular orbital (NLMO) analyses were carried out using the NBO 5.0 module[34] in the ADF code. The (two identical) shielding contributions of degenerate MOs or spinors were summed and are reported as contributions of one parental MO or spinor. When discussing the effect of a given occupied MO, the sum of the so-called U1 (first-order changes in MO coefficients) and S1 (first-order changes in overlap matrix) contributions reported by ADF are given, together with gauge contributions for the σ^p and σ^{p+SO} contributions. In contrast, the individual MO-MO couplings (Table 4 and Table S6 in the Supporting Information) and shielding contributions in Table 5 include only the U1 contributions.

One-component (1c) MO contributions to the nuclear shielding were analyzed at the PBE[20] level with the TZVP basis set for hydrogen and quasi-relativistic small-core Stuttgart ECPs and valence basis sets for iodine and gold,[35,36] using the in-house ReSpect-MAG program[37] interfaced to Gaussian 09.[38] MO analysis of SO shielding was based on a sum-over-states finite-field third-order perturbation theory ansatz[39] using a finite Fermi-contact perturbation parameter of 0.01 a.u. at the hydride position and RSC spin-orbit ECPs[36] on heavy atoms.

The four-component ReSpect program package[40] was used to perform fully relativistic DFT calculations at the four-component (4c) matrix Dirac–Kohn–Sham (mDKS) level, using the PBE functional. The method combines GIAOs with restricted magnetically balanced (RMB) orbitals for the small component.[24,25] For the heavy atom, the Dyall TZ[41] basis set was used, along with fully uncontracted IGLO-III basis sets for the ligand atoms.

Detailed MO or spinor analyses of nuclear shieldings always depend on the choice of gauge. In the relativistic case, further ambiguities may arise. Our analyses here are mainly based on the tools provided by the ADF program for one-component (scalar relativistic) and two-component ZORA results. In the Appendix, we compare the outcome of such ADF-based analyses with those from other approaches (including the fully relativistic four-component mDKS method) for two small molecules (HI and HAu).

For better readability, we use a notation for the complexes starting with the central H-M-L$_{trans}$ unit, followed by the other ligands if present.

Results and Discussion

Strong ligand effects on the ^{1}H shifts for a wide variety of hydride complexes: Our recent analysis[1] of a series of square-planar d^8 *trans*-HPtL(PMe$_3$)$_2$ complexes indicated that the *trans* ligand can affect the hydride ^{1}H NMR shifts to the extent that the usual high-field shift for such nuclei may vanish for ligands with the strongest *trans* influences (Figure 1, yellow squares),

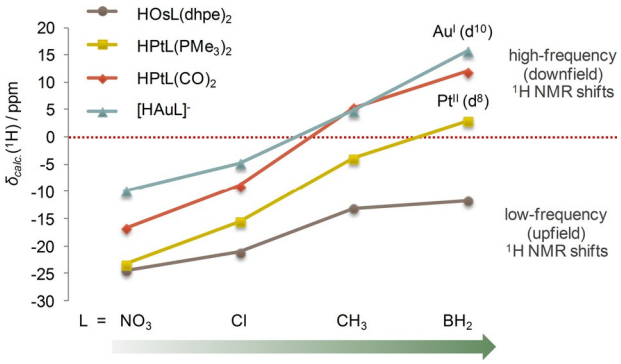

Figure 1. Dependence of hydride ^{1}H shifts (in ppm vs. TMS) on the *trans* ligand effect in widely different sets of d^6 (Os^{II}), d^8 (Pt^{II}), and d^{10} (Au^I) 5d transition-metal hydride complexes (2c-ZORA-SO/PBE0/TZ2P results; cf. Figure 2 for schematic structures and Table S1 in the Supporting Information for numerical data).

which is related to the strong σ-donor and partly π-acceptor character. The effect can even be enhanced by a different choice of the *cis* ligand: the red diamonds in Figure 1 give the ^{1}H shifts if the relatively strong *cis* influence of phosphane ligands in the Pt complexes is replaced by the weaker influence of carbonyl ligands (cf. data for *trans*-HPtL(CO)$_2$ and *trans*-HPtL(PMe$_3$)$_2$). This leads in particular to overall larger shifts and a sign change of the ^{1}H shifts even for L$_{trans}$ = CH$_3^-$ (Figure 1).

Strikingly, almost the same overall ^{1}H hydride shift trends are computed for linear anionic d^{10} Au^{I} hydride complexes (blue triangles in Figure 1), which have neither a *cis* ligand set nor the shielding Buckingham–Stephens contributions of the Pt^{II} d^{8} case.

These trends might be of assistance, for example, in the delineation of transition-metal hydride intermediates in catalytic mechanisms using ^{1}H NMR spectroscopy.[42] To understand them more thoroughly, we decomposed the total hydride shieldings into a diamagnetic, a paramagnetic, and a spin-orbit contribution: $\sigma = \sigma^{d} + \sigma^{p} + \sigma^{SO}$ (see Figure 2). Whereas the σ^{p}

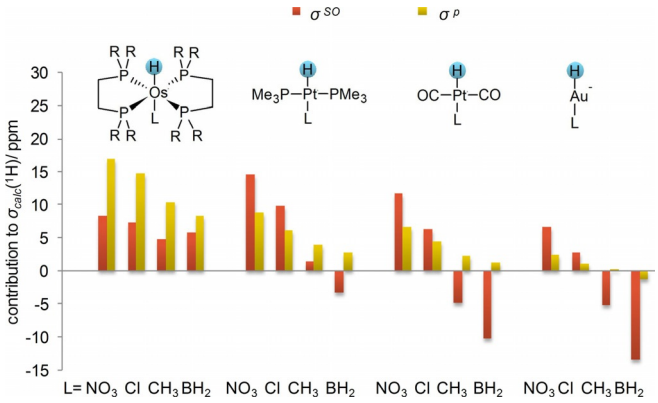

Figure 2. Decomposition of the *trans* ligand effects on the ^{1}H hydride shieldings into spin-orbit (σ^{SO}) and paramagnetic (σ^{p}) contributions for different sets of transition-metal hydride complexes (cf. Figure 1 for computational level and total shifts, and Table S1 for numerical data).

contribution governing the Buckingham–Stephens shielding mechanism[8] is diminished along the series with increasing *trans* influence, it is in particular the dramatic decrease of the spin-orbit contribution (σ^{SO}) that dominates the overall trend and causes the sign change of the ^{1}H shieldings/shifts in d^{8} and d^{10} transition-metal hydride complexes with stronger *trans* ligands (Figure 2). We note in passing that variations in σ^{d} are always much smaller than the trends discussed here (cf. Table S1 in the Supporting Information).

Organomercury hydrides, HHgR, represent another series of linear d^{10} complexes, for which we have previously identified large deshielding σ^{SO} contributions as the origin of the observed large positive hydride ^{1}H shifts.[2,14,39] The dramatic *trans* ligand effect on such ^{1}H shifts is documented in Table S2 in the Supporting Information. Whereas alkyl ligands R give rise to ^{1}H σ^{SO} contributions of about −15 ppm, weaker ligands provide distinctly less negative values, and the predicted σ^{SO} for HHgF is even slightly positive. Complete removal of the *trans* ligand may be viewed as the ultimate weakening of ligand strength, and indeed $[HHg]^{+}$ exhibits a large positive σ^{SO} of 11.5 ppm and an overall negative ^{1}H shift of −3.2 ppm (see Table S2 in the Supporting Information; note the relatively small and almost constant σ^{p} contributions).

To further generalize our observations, we also include a series of pseudo-octahedral d^{6} Os hydride complexes (gray circles in Figure 1). Here, the *trans* ligand effect is less pronounced but still notable. Due to the appreciably lower σ^{SO} contributions for the earlier 5d metal osmium, the trend becomes dominated by the rather large (Buckingham–Stephens) σ^{p} contributions (cf. Figure 2).

Extension to ligand effects on ^{13}C shifts in organometallic complexes: Although ligand effects tend to be magnified for hydride ^{1}H shifts, due to the particularly large SO shieldings involved,[2,3] it is appropriate to widen our view to other nuclei as well.[43] Indeed, previous calculations have already provided indications of such *trans* ligand effects, even for the ^{13}C shifts in organomercury complexes: for example, in ref. [39] we obtained $\sigma^{SO} = -15$ ppm for the methyl carbon atoms in $Hg(CH_3)_2$, but only $\sigma^{SO} = -5$ ppm for CH_3HgCl. The ^{13}C and ^{15}N shifts of square-planar isoelectronic d^{8} Au^{III} and Pt^{II} 2-phenylpyridine (2-ppy) complexes recently studied by Vicha et al.[4] are a case in point. In that work, the deshielding σ^{SO} contribution to the ^{13}C shift of the metal-bound aryl carbon nucleus in the $[Au(CH_3)F(2\text{-ppy})]$ complex was contrasted to the shielding σ^{SO} contribution in the closely related $[Pt(NH_3)F(2\text{-ppy})]$ complex (see upper-left and lower-right structures in Figure 3).

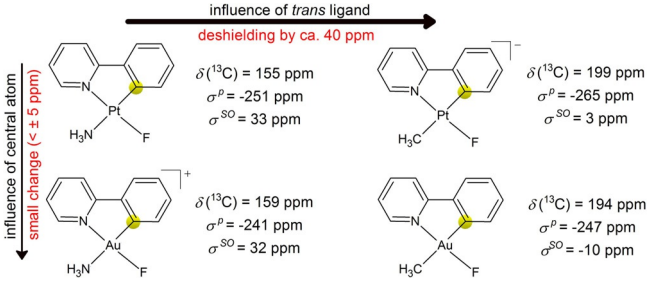

Figure 3. Computed ^{13}C NMR shifts (together with paramagnetic and SO shielding contributions) for isoelectronic d^{8} Pt^{II} and Au^{III} complexes with a weak (NH_3) or a strong (CH_3^{-}) *trans* ligand (2c-ZORA-SO/PBE0/TZ2P results). The relevant carbon nucleus is indicated.

The authors argued that contracted Au 6s and 6p orbitals are responsible for the negative σ^{SO} in the $[Au(CH_3)F(2\text{-ppy})]$ complex, whereas π-type Pt 5d contributions dominate for $[Pt(NH_3)F(2\text{-ppy})]$. However, it should be noted that not only the metal center, but also the *trans* ligand has changed here, from the strong donor CH_3^{-} in the gold complex to the much weaker donor NH_3 in the platinum system. Our present calculations confirm the negative σ^{SO} for the Au complex and the positive one for the Pt complex (see upper-left and lower-right complexes in Figure 3). However, simply replacing CH_3^{-} by neutral NH_3 in the Au^{III} complex gives rise to essentially the same ^{13}C shift change (cf. Figure 3). Replacing NH_3 by CH_3^{-} in the Pt^{II} complex reduces σ^{SO} slightly less markedly, but sufficiently so to give only a very small positive σ^{SO}. Thus, while the argument regarding 6s/6p vs 5d contributions as the origin of the different SO shifts in the two complexes is undoubtedly correct (see also below), it appears that the change of the *trans* ligand may be the more important reason for these bonding changes rather than exchange of the metal center. This brings these trends into the realm of the cases discussed above.

Extended analysis of ligand effects on ^{1}H shifts in the HAuL^q series: Returning to the linear d^{10} gold hydride complexes, we may put the distinct sign change of the ^{1}H shifts in Figure 1 into a broader context. Although our calculations predict "hydridic" high-field (low-frequency) shifts for HAuL complexes with the weakest *trans* ligands (L = NO_3^- and Cl^-, and, in particular, for the unligated HAu; see below), in spite of a lack of shielding Buckingham–Stephens σ^P contributions, the few experimentally observed gold(I) hydride complexes feature stronger ligand sets and thus downfield (high-frequency) ^{1}H hydride shifts. The experimentally characterized linear HAuNHC complex[12] (NHC = 1,3-bis(2,6-diisopropylphenyl)imidazol-2-ylidene) has been computed[2] to exhibit an appreciably deshielding σ^{SO} contribution, and consequently a positive ^{1}H shift (expt. +5.1 ppm in C_6D_6)[12] that may be placed into a trend of increasing shifts along the d^{10} series HCuNHC, HAgNHC, and HAuNHC.[13] A similar monotonous increase of hydride shifts is computed for the small anionic model complexes $[HMCH_3]^-$ (Figure 4). The slope can even be enhanced by the stronger BH_2^- ligand, whereas weaker ligands such as NO_3^- or Cl^- give rise to distinctly shielding σ^{SO} contributions, leading to the typical "Λ-shape" trend down a given group of transition metals (Figure 4), as previously observed for d^6 and d^8 transition metal hydride complexes.[2] We note in passing that no mononuclear Ag^I or Au^I phosphine hydride complexes are known, but bridging hydride ligands in multinuclear coinage-metal complexes exhibit distinctly positive ^{1}H shifts.[13]

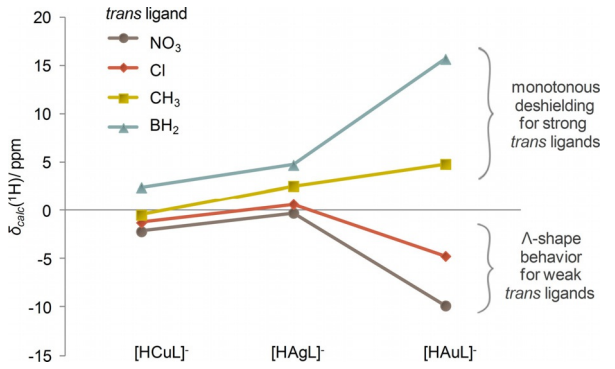

Figure 4. Divergent *trans* ligand effects on hydride ^{1}H shifts (in ppm vs. TMS) for the linear d^{10} $[HML]^-$ series (M = Cu, Ag, Au; L = NO_3^-, Cl^-, CH_3^-, BH_2^-). 2c-ZORA-SO/PBE0/TZ2P results (cf. Table S1 for numerical data).

Figure 5 extends the ligand set covered for linear Au^I complexes. It reveals a clear and strong dependence of the shielding contributions on the *trans* ligand. As for the more restricted ligand set discussed above, we see that the overall trend is dominated by σ^{SO}, but even σ^P changes sign as a function of the ligand (Figure 5). The latter point contrasts with our earlier observations for Pt^{II} hydride complexes.[1] We note in passing that the paramagnetic and SO shieldings are dominated by the shielding tensor components perpendicular to the H-Au-L bonding axes, whereas the parallel component does not change as much for the different ligands (cf. Table S3 in the Supporting Information).

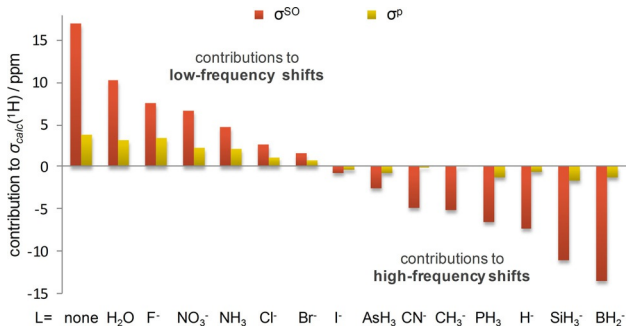

Figure 5. Calculated spin-orbit (σ^{SO}) and paramagnetic (σ^P) contributions to the ^{1}H NMR isotropic shielding in the HAuL^q (q = 0, −1) series (see Table S1 for numerical data).

Electronic structure in the HAuL^q series: The increasing *trans* ligand influence is also reflected by increasing Au–H bond lengths, which tend to correlate with increasing hydride ^{1}H shifts (cf. Figure 6 for neutral ligands; different correlation lines are obtained for neutral and anionic complexes; Figure S2 in the Supporting Information[44]). However, similarly as found in our previous study of Pt^{II} hydride complexes,[1] the observed correlations between hydride shifts and Au-H distances arise indirectly from the effect of the *trans* ligand on the polarization of the metal d (and p) orbitals, which in turn affects both the structures and the hydride shifts (see below).

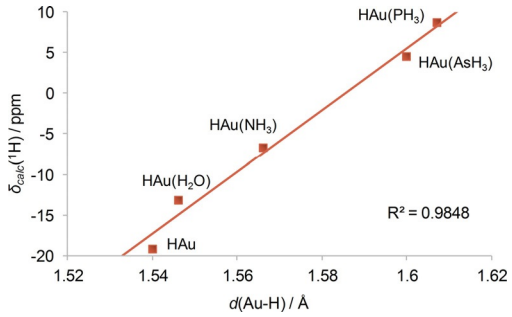

Figure 6. Correlation between hydride ^{1}H NMR shift and Au–H bond length in the selected neutral HAuL complexes (see Table S1 for numerical data).

As a prerequisite for a closer analysis of the shielding trends below, we need to have a closer look at the energies and compositions of the molecular orbitals (MOs) for different *trans* ligands, initially for the HAuL^q series. A frontier MO diagram at scalar relativistic level for a series of neutral complexes (q = 0) is shown in Figure 7, covering the range of scenarios from no *trans* ligand (i.e., unligated HAu) on the left to a strong phosphine ligand on the right. The Au–H bond length increases along the series (cf. Figure 6). Au^I may be considered a soft Lewis acid, and consequently the strongest Au–L bonds are with soft ligands such as PH_3.[45] In addition, Table 1 gives the fragment orbital contributions for the occupied MOs. For better comparison with the HAuL series, MO labels for "unligat-

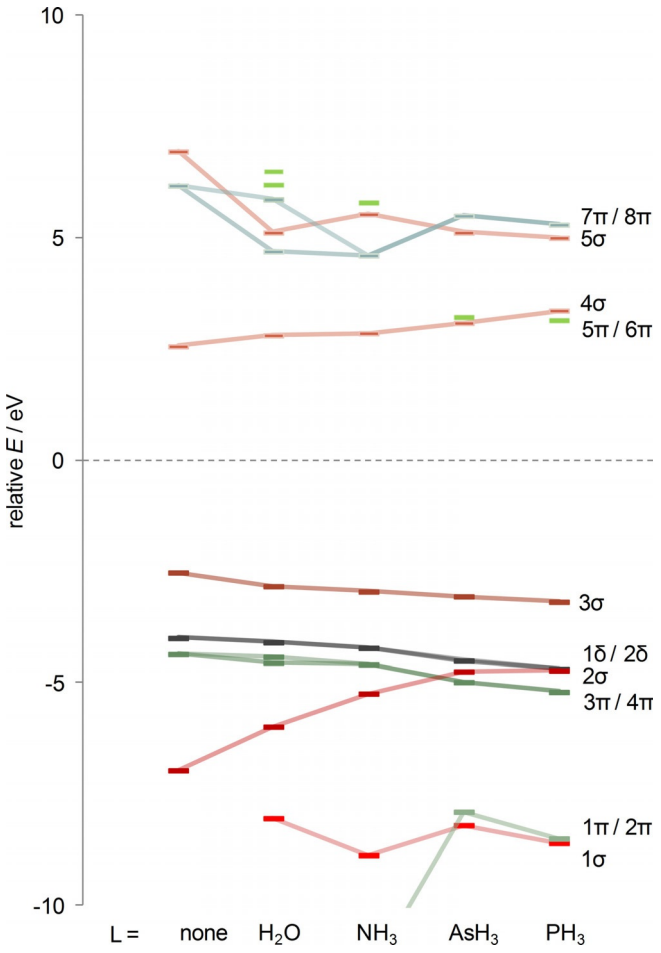

Figure 7. Scalar-relativistic frontier MO diagram for the neutral HAuL series (ZORA-SR/PBE0/TZ2P results).

Table 1. Main percentage AO contributions to the scalar relativistic frontier σ- and π-type MOs for the neutral HAuL series, and σ^p contributions (in ppm) to hydride ^{1}H shielding.[a]

L	1s(H)	5d(Au)	6s(Au)	6p(Au)	s(L) [b]	p(L) [b]	σ^p
3σ							
none	15	32	53	0	0	0	−1.5
H_2O	16	29	55	0	0	0	−1.6
NH_3	18	27	54	0	0	0	−1.5
AsH_3	27	23	47	3	0	0	−0.1
PH_3	31	20	43	4	0	0	0.3
2σ							
none	39	54	5	0	0	0	1.0
H_2O	36	34	0	3	0	21	1.4
NH_3	34	27	0	5	3	25	1.5
AsH_3	19	22	4	7	7	31	−0.7
PH_3	20	25	5	7	7	29	1.2
1σ							
none	–	–	–	–	–	–	–
H_2O	4	11	0	0	3	75	−0.4
NH_3	9	27	6	0	4	45	−0.5
AsH_3	16	39	4	0	2	28	2.0
PH_3	12	39	8	0	2	27	0.3
3π/4π							
none	0	99	0	0	0	0	−0.3
H_2O	0	95	0	0	0	3	−1.3
NH_3	0	96	0	0	0	0	−1.4
AsH_3	0	93	0	0	2	0	−3.3
PH_3	0	91	0	0	4	0	−2.1

[a] ZORA-SR/PBE0/TZ2P results. [b] Contributions from AOs of the coordinating atom of the *trans* ligand.

ed" HAu are adopted to denote the lowest σ-type valence MO 2σ, as HAu has one fewer occupied σ-type (frontier) MO than the other complexes.

Figure 7 indicates that the energies of the 3σ as well as of the 1δ/2δ and the 3π/4π MOs are relatively insensitive to the *trans* ligand, which, of course, can be related to the small *trans* ligand participation in these orbitals (cf. Table 1). The 3σ MO is Au–H bonding with dominant Au(6s) and H(1s) contributions and displays essentially no *trans* ligand character (cf. Table 1). Relativistic d orbital expansion and s orbital contraction lead to significant s-d mixing in this orbital. The π- and δ-type MOs have predominant nonbonding Au(5d) character as well as very low ligand contributions, and, consequently, are less affected by the *trans* ligand (Figure 7). The most notable and by far most important trend among the occupied MOs along the series is the strong destabilization of the 2σ level (Figure 7). Its energy first moves closer to those of the 3π/4π MOs, whereas for the strongest *trans* ligands (L = AsH_3 and PH_3) 2σ resides above the 3π/4π MOs. The destabilization of the 2σ MO is connected to the increasing Au–H bond length along the series. It reflects decreased Au–H bonding but enhanced Au–L antibonding for the stronger *trans* ligands, accompanied by a loss of H(1s) and Au(5d) character and an increase in contributions from the coordinating atom of the *trans* ligand (Table 1). The Au(6p) character of 2σ also increases somewhat along the series. Note that a similar destabilization of a 2σ-type MO with stronger *trans* ligands was also found for anionic $[HAuL]^-$ complexes (Figure S3 in the Supporting Information). Indeed, a closely related σ(M-H)-type MO was seen to be important in our previous analyses of d^8 square-planar Pt^{II} complexes, pointing to a general origin of the observed trends.[1]

In contrast to the major changes for 2σ, the Au–H and Au–L bonding 1σ MO shows a non-monotonous and less pronounced trend and cannot be responsible for the monotonous trends in the Au–H bond length or in the shielding components. The contributions of the *trans* ligand coordinating atom to 1σ decrease along the series (Table 1).

Among the virtual MOs, the largest effect is the stabilization of π-type MOs by stronger *trans* ligands, causing near-degeneracy or even a change in order of 4σ and these π MOs.

In view of the overriding importance of SO effects for the shifts, we now turn to the two-component spinor framework. To understand SO coupling (SOC) in the complexes, we start with Au atomic energy levels within a linear complex. Figure 8 exemplifies how SOC leads to spinors with total angular momentum $j = l \pm 1/2$ for p and d orbitals, using a characterization in $C_{\infty v}$ symmetry (i.e., by σ, π, δ labels). We keep in mind that SOC leaves the degeneracy-weighted midpoint of a given set of scalar-relativistic orbital energies unchanged. Considering, for example, the (σ-type) p_z AO ($l = 1$, $m_l = 0$), it contributes to the $p_{1/2}$ and $p_{3/2}$ spinors with $m_j = \pm 1/2$ (because $m_j = m_l \pm 1/2$). As the $p_{1/2}$ level is stabilized by 2/3 Δ^{SO} compared to the

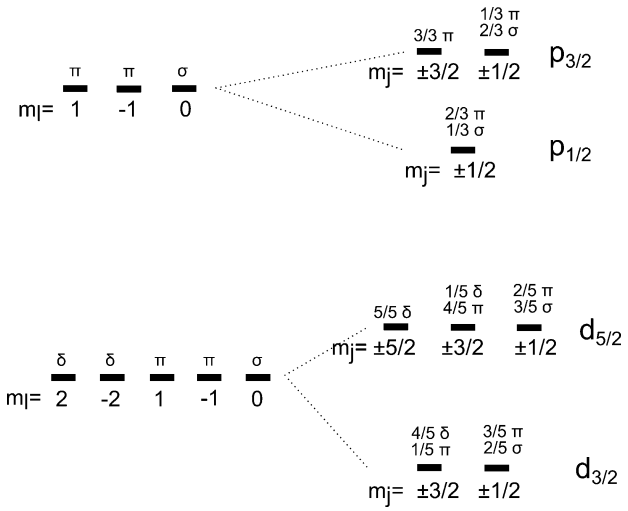

Figure 8. Representation of scalar-relativistic metal AOs (left, with $C_{\infty v}$ symmetry labeling) in the final relativistic AO spinors (right).

scalar-relativistic p AOs, the original p_z (σ-type) AO is represented only to one-third. To retain the energy midpoint at the $p_{3/2}$ ($j=3/2$, $m_j=\pm1/2$) level, destabilized by 1/3 Δ^{SO}, p_z (σ) is represented by two-thirds. The $m_j=\pm3/2$ level, also destabilized by 1/3 Δ^{SO}, is only possible for $m_l=\pm1$. It can thus only accommodate p_π orbitals and is of pure π character (Figure 8). The remaining p_π character emerges by two-thirds in the $p_{1/2}$ and by only one-third in the $p_{3/2}$ spinors with $m_j=\pm1/2$. Similar conjectures can be drawn for the other AOs, providing us with the percentage σ, π, and δ characters of the SO-stabilized ($j=l-1/2$; $p_{1/2}$, $d_{3/2}$) and SO-destabilized ($j=l+1/2$; $p_{3/2}$, $d_{5/2}$) AO-type spinors (Figure 8). Spinors with mixed σ/π character will be most important for the SO effects on NMR shielding[7] (see below), and the $m_j=\pm1/2$ levels are thus very relevant in this context.

As the SOC in our complexes is clearly dominated by the metal orbitals, we can transfer these considerations to an understanding of the metal character of our MO spinors (Figure 9). In contrast to the AO case in Figure 8, the energy

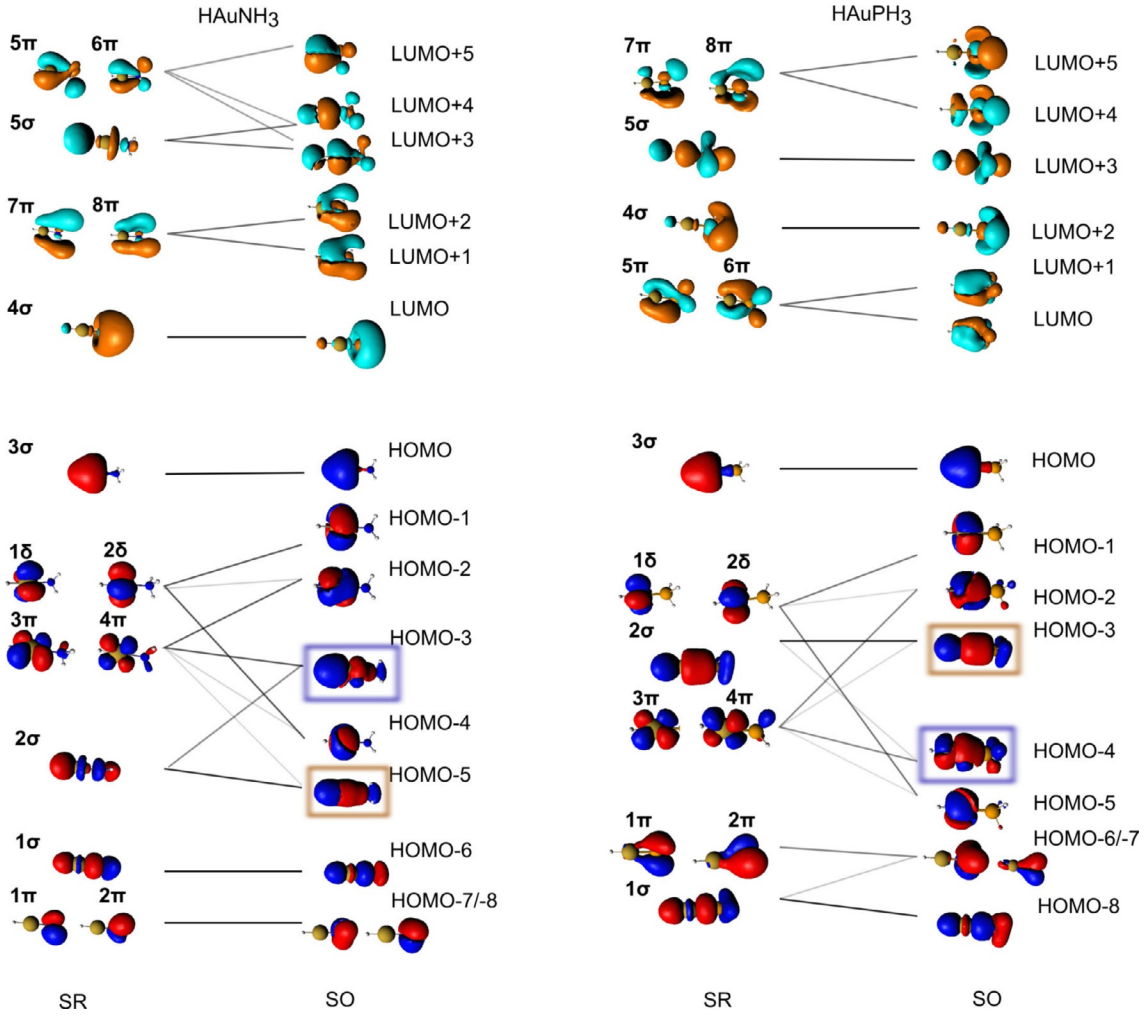

Figure 9. Frontier MOs at scalar-relativistic (SR) level and their mixing to two-component spinors (SO) (isosurface plots, ±0.03 a.u.). The opacity of the lines indicates the mixing percentages of SR MOs in SO MOs (see Table 2 for numerical data). Only one of two degenerate spinors is shown. The spinors mainly responsible for the overall differences in the ^{1}H shifts with different *trans* ligands are highlighted. They exhibit $m_j=\pm1/2$ AO spinor character. ZORA/PBE0/TZ2P results.

Table 2. Composition of selected occupied two-component spinors in terms of SR-MOs, and spinor contributions to ^{1}H shieldings for the neutral HAuL series. Columns ordered by dominant SR-MO character.[a]

MO (spinor)	L	SR-MO contr. [%]				σ^{P+SO} contr. [ppm]
		3σ	**2σ**	**3π/4π**	**1δ/2δ**	
HOMO	none	96	–	4	–	−6.2
	H_2O	95	–	5	–	−4.4
	NH_3	95	–	5	–	−4.0
	AsH_3	97	–	3	–	−4.2
	PH_3	97	–	3	–	−3.8
HOMO−1	none	–	–	–	100	0.0
	H_2O	–	–	–	100	0.0
	NH_3	–	–	–	100	0.0
	AsH_3	–	–	–	100	0.0
	PH_3	–	–	–	100	0.0
HOMO−2	none	–	–	64	36	3.8
	H_2O	–	–	70	30	3.0
	NH_3	–	–	70	30	2.4
	AsH_3	–	–	67	33	0.9
	PH_3	–	–	66	34	0.0
HOMO−3	none	4	5	90	–	19.8
	H_2O	5	11	82	–	20.5
	NH_3	4	33	62	–	20.3
HOMO−4	AsH_3	2	19	76	–	−2.3
	PH_3	2	14	82	–	−1.0
HOMO−4	none	–	–	36	64	0.0
	H_2O	–	–	30	70	0.0
	NH_3	–	–	30	70	0.0
HOMO−5	AsH_3	–	–	33	67	0.0
	PH_3	–	–	34	66	0.0
HOMO−5	none	–	95	5	–	4.4
	H_2O	–	88	11	–	−6.1
	NH_3	–	66	32	–	−11.8
HOMO−3	AsH_3	1	80	18	–	4.9
	PH_3	1	85	13	–	−0.5

[a] 2c-ZORA-SO/PBE0/TZ2P results.

degeneracy between σ, π, and δ orbitals is lifted, affecting of course the SO mixing. Figure 9 shows a comparison of the relationships between two-component spinors and the underlying SR-MOs for HAuL with one weaker ($L=NH_3$) and one stronger ($L=PH_3$) ligand. The opacity of the connecting lines indicates the importance of a given SR-MO for a spinor (cf. Table 2 for numerical data). The nature and shape of the frontier MOs/spinors are shown as well.

SO effects on the MOs depend strongly on their energies relative to the other MOs and on their Au(5d)/Au(6p) character, as the ligand orbitals and the Au 6s orbital are not affected by SOC. Thus, as the 3σ HOMO is dominated by Au(6s) (Table 1) and has a large energy gap relative to the 5d π orbitals (cf. Figure 7 for energy levels true to scale), it is affected very little by SOC and largely retains its σ character and position as the HOMO. The SO mixing of the 1δ/2δ and 3π/4π SR-MOs, which show very little mixing with ligand orbitals (Table 2, Figure 9), is very close to the atomic picture drawn in Figure 8. This leads to the HOMO−1 (with predominantly $m_j=\pm5/2$, $5d_{5/2}$ character), the HOMO−2 (mainly representing $m_j=\pm3/2$ with $5d_{5/2}$), the HOMO−4 for $L=NH_3$, and accordingly the HOMO−5 for $L=PH_3$ (the latter two MOs mainly have $m_j=\pm3/2$ with $5d_{3/2}$ character). Due to the large SO mixing, the symmetry labels of the SR-MOs cease to be useful in characterizing a given spinor.

As could already be expected from the SR picture, the greatest differences between the complexes with different *trans* ligands appear for those spinors that exhibit 2σ contributions. 2σ has significant Au(5d) [and some Au(6p)] character and is energetically close to the almost pure 5d-type 3π/4π MOs. It therefore mixes extensively with the latter and contributes mainly to two spinors. The first retains the dominant σ character (HOMO−5 for $HAuNH_3$, HOMO−3 for $HAuPH_3$; 6th group of MO spinors in Table 2), whereas the second acquires more π character (HOMO−3 for $HAuNH_3$, HOMO−4 for $HAuPH_3$; 4th group of MO spinors in Table 2). Due to symmetry considerations (see Figure 8), both spinors exhibit $m_j=\pm1/2$ character. The energetically lower one can be interpreted as having stronger $d_{3/2}$ participation, whereas $d_{5/2}$ should dominate in the energetically higher one.

SO mixing benefits from a small energy gap between the SR-MOs involved, but the relative energy order of the MOs is also important: mixing between 2σ and 3π/4π becomes more efficient in the series HAu, $HAu(H_2O)$, $HAuNH_3$ (cf. Table 2) due to the destabilization of 2σ and the associated lower energy gap to 3π/4π (cf. Figure 7). However, σ/π mixing is less efficient for $HAuAsH_3$, for which the energy gap between 2σ and 3π/4π is small, but with 2σ already above 3π/4π, and it decreases further for $HAuPH_3$, again with an increasing energy gap. Apparently, mixing is more efficient if the π orbitals are above the corresponding σ orbital: the σ component itself is constant in energy, whereas the π components are on average SO-stabilized (cf. $m_j=\pm1/2$, Figure 8).

Hence, we see a distinct effect of the destabilization of the 2σ SR-MO by stronger *trans* ligands on the composition of the 2c spinors: initially, mixing of 2σ into π MOs becomes more pronounced, as the energy of 2σ approaches those of 3π/4π from below. However, once 2σ has moved above these π levels, mixing becomes less favorable, resulting in a HOMO−3 with increasing σ character (while the 2σ character is concentrated in the HOMO−5 for the weaker *trans* ligands). This also influences the dominant angular momentum in a given spinor: whereas the higher-lying HOMO−3 in complexes with strong *trans* ligands has more $5d_{5/2}$ character, the lower-lying HOMO−5 in complexes with weaker ligands has more $5d_{3/2}$ character.

We also note appreciable SO mixing for the virtual MOs. For example, for $HAuNH_3$, the 5σ and the 5π/6π orbitals, which exhibit Au(6p) contributions, mix efficiently. This leads to LUMO+5 (with $m_j=\pm3/2$, $6p_{3/2}$ character), LUMO+4 (with $m_j=\pm1/2$, $6p_{3/2}$), and LUMO+3 (with $m_j=\pm1/2$, $6p_{1/2}$). A closely related SO effect can be seen for the 4σ and 5π/6π orbitals of $HAuAsH_3$. The 7π/8π MOs generally contain less Au(6p) character than the 5π/6π MOs and thus mix less efficiently with the corresponding σ orbitals (e.g., only by 3% with 5σ in the case of $HAuPH_3$). Again, mixing appears only to

be effective with the π MO above the σ MO and both having notable Au(5d) or Au(6p) character.

Further insight into the electronic structure from a localized point of view is provided by the compositions of the Au–H and Au–L bonding NLMOs (see Table 3 for neutral complexes).

Table 3. Composition of the Au–H and Au–L bonding NLMOs.[a]

L	q(H)	%Au	%Au(6s)	%Au(6p)	%Au(5d)
Au–H NLMO					
H_2O	−0.18	43	80.5	0.2	19.3
NH_3	−0.25	41	80.0	0.2	19.8
AsH_3	−0.28	41	86.2	0.2	13.6
PH_3	−0.31	40	86.3	0.2	13.5
Au–L NLMO[b]					
H_2O		2	77.9	2.6	19.2
NH_3		4	78.0	2.6	19.1
AsH_3		7	84.8	1.8	13.3
PH_3		8	84.8	1.8	13.3

[a] ZORA-SR/PBE0/TZ2P results. [b] Characterized as ligand lone pair in the NBO Lewis structure.

The metal contributions to both the relatively covalent Au–H bond and the much more ionic Au–L bond are dominated by Au(6s) character, but the Au(5d) character is significant and larger for the weaker *trans* ligands. That is to say, the stronger ligands not only push more negative charge towards the hydride ligand (cf. Table 3), but also lead to a rehybridization of the gold atom towards more 6s and less 5d character, consistent with earlier electronic structure analyses of such complexes.[45] The 6p character in the Au–H NLMO is almost negligible and also relatively small in the Au–L bond.

Electronic structure analysis of σ^{p+SO} contributions to ^{1}H hydride shielding in the HAuL^q series: Having characterized the spinors, we can now analyze their shielding contributions in more detail. As σ^p and σ^{SO} depend in a largely parallel way on the *trans* ligand,[1] and separation of the spinor contributions is difficult due to the appreciable mixing of the SR-MOs by SOC (see above), Table 2 provides an overview of the sums σ^{p+SO} for a given occupied spinor (note that the two identical contributions from degenerate spinors are summed as one contribution). We can nevertheless get an impression of the σ^p contributions of a given SR-MO from Table 1.

One would expect the largest SO contributions to the ^{1}H shielding to arise from: a) spinors with significant Au(5d) and/or Au(6p) character (largest SOC), b) high-lying occupied spinors (smaller energy denominator for coupling with virtual spinors), and c) spinors that also contain a reasonable amount of 1s(H) character, as the main mechanism to transfer the SOC effects is FC-based.[46]

These criteria tend to be fulfilled in particular by mixed σ/π-type spinors.[47] Among them, HOMO−3 and HOMO−5 for weak *trans* ligands, and HOMO−4 and HOMO−3 for strong *trans* ligands (L = AsH_3, PH_3), contribute appreciably and dictate the main trends and differences between the various complexes (cf. Figure 9). The strong dominance of these two mixed σ-/π-spinors for the overall σ^{SO} contributions can be clearly seen in Figure S4. The "3σ-type" HOMO provides negative σ^{p+SO} contributions that follow the σ^p behavior and depend only slightly on the *trans* ligand L (Table 1).[50]

By far the most important contributions for weaker *trans* ligands arise from the predominantly π-type HOMO−3 (Table 2). These contributions of about +20 ppm are clearly dominated by SO effects and are the origin of the overall positive SO contribution for complexes with weaker *trans* ligands. In line with the early interpretation of the ^{1}H shielding in HI by Pyykkö et al.,[7] the large SO contributions from such "$\pi_{1/2}$ spinors" are a combination of the π character permitting non-zero Zeeman matrix elements (providing the coupling to the external magnetic field) with SO-induced σ character giving rise to FC hyperfine matrix elements (coupling of the nuclear and electronic spins at the hydrogen atom). In contrast, the analogous π-type HOMO−4 for L = AsH_3 and PH_3 exhibits not merely small, but even negative (deshielding) σ^{p+SO} contributions (Table 2). Here, we suspect small or negligible σ^{SO} contributions and a dominance of small negative σ^p (cf. Table 1).

The question then arises as to why these large SO contributions to chemical shielding/shift diminish so significantly for strong *trans* ligands. We may trace this back to the character of 2σ at scalar relativistic level, which exhibits notably smaller 1s(H) character upon going from weak to strong *trans* ligands (cf. Table 1). Turning to the two-component analysis, the 2σ admixture to 3π/4π results in 1s(H) character of only about 3% for strong *trans* ligands, prohibiting an effective FC mechanism. The isosurface plots of HOMO−3 for L = NH_3 and HOMO−4 for L = PH_3 (Figure 9) nicely confirm the different participations of the hydride 1s orbitals. In addition, the energy gap to the virtual spinors is significantly larger for the stronger ligands, which is not only caused by the increased HOMO–LUMO gap, but mainly by the reordering of the spinors due to the destabilization of the 2σ MO at SR level. A reordering with 2σ above 3π/4π in such cases not only makes 2σ admixture to HOMO−3 less effective (see above), but also affects the predominant angular momentum character of this spinor, with more $5d_{3/2}$ participation for stronger ligands. This obviously reduces the HOMO−3 SO contributions to shielding. We note in passing that the σ^{p+SO} contribution from the corresponding spinor in the anionic halide complexes decreases from about 12 ppm (L = F) to 2 ppm (L = Br), even though the σ/π mixing remains almost constant (cf. Table S5). In this case, the Au(5d) participation in the π-MOs is significantly reduced along the series (cf. Table S4).

The predominantly "2σ-type" spinors provide a more complicated picture (Table 2). Earlier analyses, either at relativistic extended Hückel level (REX; cf. Table 5 in the Appendix below)[7] or at one-component perturbational levels had suggested σ- and π-type occupied MOs to provide deshielding and shielding SO contributions, respectively.[14,46] Although this is confirmed through large deshielding σ^{p+SO} contributions from the HOMO−5 spinor for the weak *trans* ligands L = H_2O and NH_3, and would be expected to simply diminish for the stronger *trans* ligands, the positive shielding contributions for HAu and for $HAuAsH_3$ contradict this expectation. Closer inspection of the SR-MOs contributing to 2σ for the latter complex (Table 1)

shows, however, that it has only 22% $5d_\sigma$ character, whereas the $3\pi/4\pi$ SR-MOs are almost pure $5d_\pi$. In spite of the 80% σ character and 18% π character of the HOMO−3 spinor (Table 2), the overall Au($5d_\sigma$) and Au($5d_\pi$) contributions to this spinor are thus almost equal, rendering the classification of the spinor as "σ-type" inaccurate. For $HAuPH_3$, the overall distribution represents more Au($5d_\sigma$) character (Tables 1 and 2), thus explaining the overall slightly deshielded σ^{p+SO}.

Additionally, the character of the virtual spinors involved in occupied-to-virtual couplings from the σ/π-type spinors affects the shielding contributions (cf. Table 4 for $HAuNH_3$ and Table S6 in the Supporting Information for the other complexes): we first note that in general only couplings to σ-type or mixed σ/π-type virtual spinors contribute notably to σ^{p+SO}, whereas couplings to pure π-type spinors do not. Usually, the largest contributions arise from coupling to the lowest-lying virtual σ or σ/π spinor. This is often the LUMO, but can also be the LUMO+2 (L = PH_3, Figure 9).

Table 4. Dominant occupied virtual spinor couplings contributing to σ^{p+SO} for the ^{1}H NMR shielding in $HAuNH_3$.[a]

Occupied spinor	Virtual spinor	σ^{p+SO} contribution [ppm]	ΔE (eV)
HOMO−3	→ LUMO	7.0	7.6
	→ LUMO+3	5.8	10.2
	→ LUMO+4	−2.2	10.3
HOMO−5	→ LUMO	−2.6	8.4
	→ LUMO+3	2.0	11.1
	→ LUMO+4	−3.4	11.2

[a] 2c-ZORA-SO/PBE0/TZ2P results.

The counterintuitive positive σ^{p+SO} contribution for HAu (Table 2) is dominated by the HOMO−5→LUMO coupling (Table S6). While this is consistent with the other complexes with weak ligands, the LUMO in HAu has a very different character compared to that of the substituted HAuL species: the underlying 4σ SR-MO (Figure 7) has much larger metal character (≈70%) than in the ligated complexes (ca. 10–15%), and in contrast to the almost exclusive 6s character for the other complexes, these metal contributions also have about one-third $6p_z$ character. These features largely persist in the LUMO spinor and account for the different behavior with respect to the shielding contributions.

The importance of the composition of the virtual spinors for the substituted complexes is also demonstrated in Table 4. For L = NH_3, it gives the main couplings for the HOMO−3 ("π-type") and the HOMO−5 ("σ-type"), which can both give rise to couplings with negative and positive σ^{p+SO} contributions, depending on the virtual spinor involved. Strikingly, couplings from HOMO−3 and HOMO−5 give positive contributions to LUMO+3 and negative contributions to LUMO+4, even though these two virtual spinors appear to have similar compositions (about 50% 5σ and 50% $5\pi/6\pi$; note that Figure 9 presents only one of two degenerate 2c spinors; the second spinor for LUMO+3 resembles the displayed LUMO+4 spinor, and *vice versa*).

The question then arises as to why these apparently so similar virtual spinors have such different influences on the ^{1}H shieldings. Going back to our symmetry-related analysis of the spinor compositions (cf. Figures 8 and S3) we note that, whereas both LUMO+3 and LUMO+4 exhibit Au(6p) contributions with $m_j = \pm 1/2$ character, the lower-lying LUMO+3 has more $j = l-1/2$ ($6p_{1/2}$) contributions, and the higher-lying LUMO+4 has more $j = l+1/2$ ($6p_{3/2}$) character. This leads to a sign change of the SO matrix elements for a given orbital.[7]

Similar patterns can be used to partially rationalize the positive σ^{p+SO} contributions from the HOMO−3 of $HAuAsH_3$: the first and second virtual SR-MOs 4σ and $5\pi/6\pi$ are almost degenerate (Figure 7), resulting in strong SO mixing between them. Thus, both the LUMO and LUMO+1 for this complex have strongly mixed σ/π character (similar to the LUMO+3 and LUMO+4 for $HAuNH_3$; see above). Again, the lower of these two spinors is dominated by metal $j = l-1/2$ AOs and the higher-lying one by $j = l+1/2$ AOs, thereby presumably accounting for the opposite signs of the HOMO−3→LUMO and HOMO−3→LUMO+1 shielding contributions (Table S6). As the former exhibits a larger absolute value, the overall HOMO−3 contribution is one of shielding (Table 2).

Relation to magnetically induced ring currents: We may now relate our MO-based analyses to the shapes (curvatures) of the induced ring currents for HAu and HHgH presented in ref. [11] at four-component relativistic level, which had allowed the extraction of the SO contributions to these current loops. Current plots[11] showed diatropic current loops (see also ref. [8b]) around the hydride in HAu and small SO-induced localized paratropic current loops for HHgH, consistent with shielding ^{1}H σ^{SO} for HAu and a deshielding one for HHgH (cf. Figure 10). Clearly, these two d^{10} systems exemplify extreme cases within our analyses presented above, with HAu representing the weakest ("zero") *trans* ligand and HHgH a strong σ-donor ligand in the *trans* position. Indeed, our above analysis for HAu showed the characteristic shielding contributions from a predominantly π-type spinor (see Figure 10 left, cf. also Table 2). In contrast, HHgH exhibits the typical high-lying, pre-

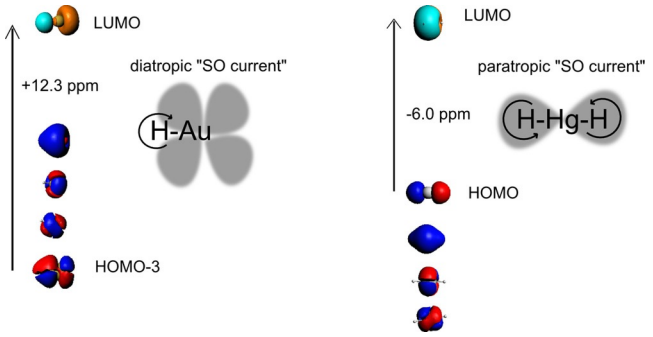

Figure 10. Illustration of the predominant ^{1}H σ^{p+SO} contributions in HAu and HHgH from two-component spinors (the predominant occupied virtual spinor coupling is in both cases indicated by an arrow), in relation to the direction of SO-induced current loops. Spinors are shown as isosurface plots (±0.03 a.u.).

dominantly σ-type spinor caused by the strong *trans* influence (Figure 10, right). It has significant M($6p_z$) character and is responsible for large ^{1}H deshielding.

Indeed, the individual one-component (scalar relativistic) and four-component (fully relativistic) induced current plots from ref. [11] are closely related to the shapes of the 3σ SR-MOs and the associated 2c spinors of both HAu and HHgH (HOMO for HAu, HOMO−1 for HgH_2, Figure 10). In contrast, the difference plots displaying only the SO-induced current loops can be related to the shapes of those spinors responsible for the dominant shielding contributions. That is, the SO-induced current loops of HAu create a picture resembling a π-type MO such as HOMO−3 (Figure 10, left), where the hydride resides *between* the lobes of the orbital and experiences a diatropic current loop. This causes a weakening of the applied magnetic field and thus positive SO contributions. The SO-induced paratropic current loops around the hydride positions of HHgH are consistent with the shape of the σ-type HOMO (Figure 10, right). Here, the hydride position is *on* the orbital lobes of the HOMO, and diatropic current loops appear only *between* these lobes.

We can also relate these analyses to recent rationalizations of ^{1}H shifts of agostic protons in planar d^8 transition-metal complexes.[51] The authors connected the shifts to the position of the monitored hydrogen nucleus relative to features in the Laplacian of the charge density ($\nabla^2\rho$) in the valence shell of the metal center. According to their analyses, diatropic current density is induced in planes that bisect charge depletion (CD) zones ($-\nabla^2\rho<0$; $\sigma>0$), and paratropic current density in planes bisecting charge concentration (CC) zones ($-\nabla^2\rho>0$; $\sigma<0$). Protons pointing to CD zones are thus shielded and those pointing to CC zones are deshielded. That study focused on σ only in nonrelativistic calculations, and on a charge distribution pre-shaped mainly by the covalent bond framework, whereby the agostic protons could approach this charge distribution from different orientations. We may translate this picture into the MO picture of contributions for the covalently bound hydride: as we have seen, high-lying π-type occupied MOs create diatropic induced current loops at the position of the hydride, which lies *outside* the main lobes of this MO ("depletion zone"). In contrast, high-lying σ-type MOs create a paratropic current loop around the hydride, which in this case lies *on* the lobe of this MO ("concentration zone"). This holds for σ^{SO} contributions as well as for σ^{p} contributions, for which the same angular momentum symmetries play a role: for example, π-type occupied MOs are responsible for the Buckingham–Stephens effect[8,52] of hydride shieldings for incomplete metal d shells, related to a diatropic local σ^{p} current loop at the hydride position. As we have seen, the other ligands in the complex may "pre-shape" the charge distribution in either direction and thus modify the current loop around the ligand nucleus in question (hydride protons in particular, but as we have seen, other nuclei may also be affected); strong *trans* ligands may raise the energies of certain σ-type MOs and thus favor paratropic induced local currents. This is more likely for d^{10} systems, for which the π-type MOs are typically lower in energy than, for example, in d^8 cases. Nevertheless, the ligand framework may of course play a dominant role, so that both situations may occur for either d configuration.

Extension of electronic structure analyses to other types of complexes: Figure 11 extends the electronic structure analysis at scalar-relativistic level to the highest occupied MOs from the anionic d^{10} $[HAuL]^-$ series to the d^8 *trans*-$HPtL(PMe_3)_2$ and d^6 *trans*-$HOsL(dhpe)_2$ complexes, generally with $L=Cl^-$ and BH_2^- as examples of weak and strong *trans* ligands, respectively. We recall that we had noticed a change in sign with *trans* ligand for the SO contribution in the Au^I and Pt^{II} complexes, but not in the Os^{II} complex (Figure 2). The most striking similarity between the three sets of complexes is the dramatic destabilization of one σ-type SR-MO by the stronger *trans* ligand BH_2^- (Figure 11). It is again the highest occupied σ-MO, involving the *trans* ligand. For the Os and Pt chlorides, this MO is the HOMO−4. It moves to the HOMO−1 (Os) or the HOMO (Pt) for $L=BH_2^-$. Compared to the complexes discussed so far, the σ-type MOs exhibit a larger $6p_z$ contribution, which increases with the stronger *trans* ligand (already slightly discernible in Table 1). Together with the effects of energetic destabilization (see discussion above for HAuL), the enhanced M($6p_z$) character helps to reduce shielding or even create deshielding SO contributions, as noted previously.[1,4] The percentage $6p_z$ character of the d^6 and d^8 complexes increases from about 10% (Cl) to above 15% (BH_2). In comparison, for $[HAuCl]^-$, the σ-type HOMO−5 has 7% $6p_z$ character, increasing to 13% for the HOMO of $[HAuBH_2]^-$.

As discussed above for the HAuL series, the destabilization of one σ-type SR-MO translates into changes in the SOC mixing in the two-component framework, whereby spinors with high σ character are shifted above π-type spinors by strong *trans* ligands. Indeed, the σ/π mixed spinors exhibit more π character in the more highly occupied spinors for $L=Cl^-$ for all three central metals, and their overall (shielding) σ^{p+SO} contributions are always larger compared to those with $L=BH_2^-$. These analyses confirm similar mechanisms not only for the *trans* ligand effects in the d^{10} and d^8 series, but also for d^6. For the d^6 Os complexes, the destabilization of the σ-type MO is not sufficiently strong to bring it above the highest π-type MO (Figure 11). Overall, the SO effects are consistently smaller for these d^6 complexes.

We furthermore recall that the SO effects are amplified for the ^{1}H shieldings, due to enhancement of the FC-type mechanism by the high H(1s) character. Overall, SO effects are thus diminished for other nuclei (e.g., the ^{13}C examples shown in Figure 3). Nevertheless, we find qualitatively similar effects on SO shifts by strong *trans* ligands in these cases, due to destabilization of one particular σ-type MO (cf. Figure S5 for the highest occupied SR MOs of [Au(2-ppy)(F)L] with $L=NH_3$ and CH_3).

Conclusion

We have found, by relativistic quantum-chemical analyses, a strikingly general *trans* ligand effect on the NMR shifts of metal-bound nuclei in 5d transition-metal complexes, encompassing both $5d^8$ and $5d^{10}$ configurations, with related effects even for $5d^6$ complexes. Although our analyses have concen-

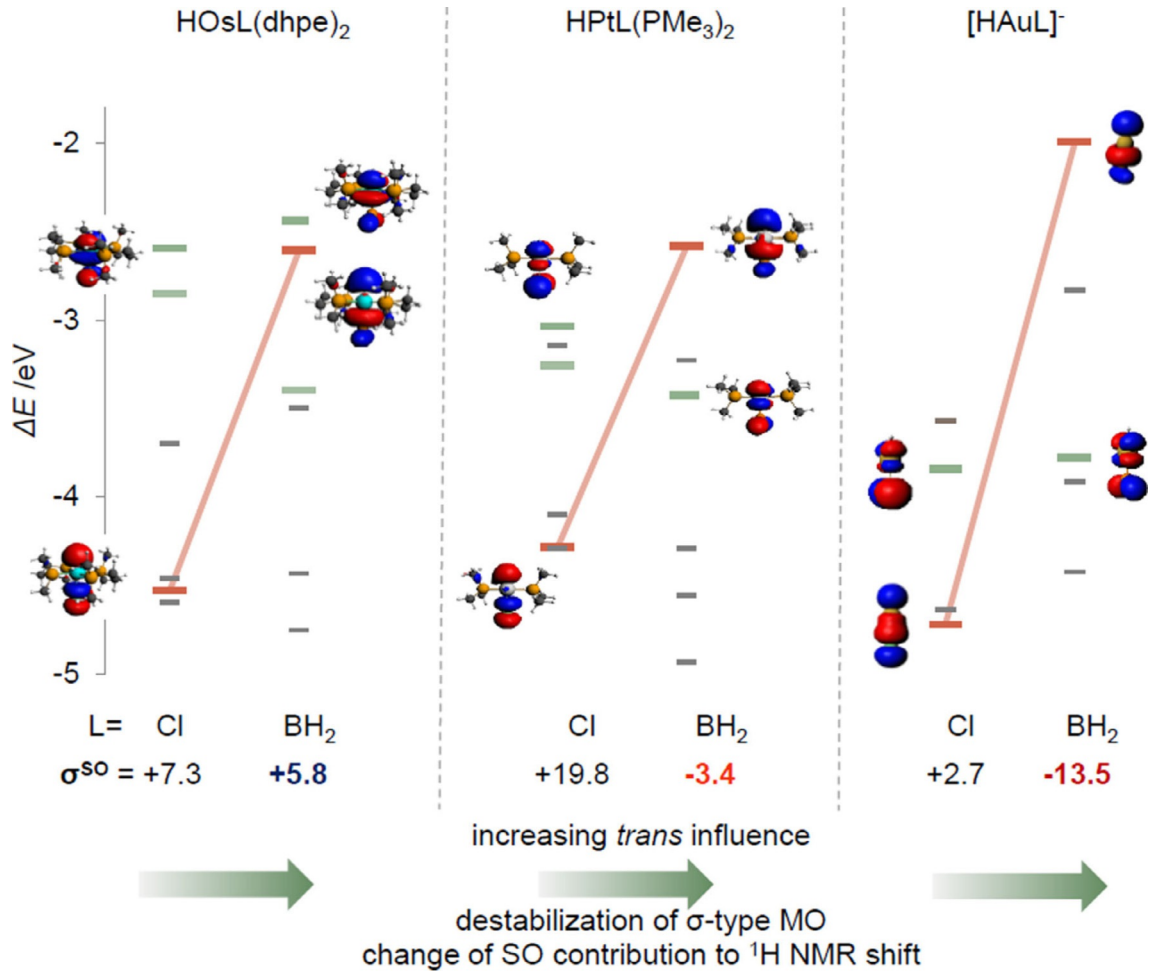

Figure 11. Energies of the highest occupied MOs at SR-ZORA level for the pseudo-octahedral d^6 Os, the square-planar d^8 Pt, and the linear d^{10} Au hydride complexes with a weak (Cl) and a strong (BH_2) *trans* ligand, respectively, and influence of destabilization of σ-type MO on SO shieldings, σ^{SO} (in ppm). The highest occupied π-type MOs are highlighted in green, whereas the highest σ-type MO with significant *trans*-ligand character is highlighted in red. The corresponding MOs are shown as isosurface plots (±0.03 a.u.), with the hydride ligand generally being placed at the top (ZORA-SR/PBE0/TZ2P results).

trated on ^{1}H shifts of hydride ligands, for which SO-induced shielding effects are most prominent, similar effects are also operative for other nuclei. In particular, for both $5d^8$ and $5d^{10}$ systems, we have found a sign change of the dominant SO-induced shifts from shielding to deshielding on going from weak to strong *trans* ligands. Detailed analyses within a two-component quasi-relativistic spinor framework have shown the *trans* ligand effects on the shieldings to be exclusively dominated by two mixed σ-/π-type spinors. Large shielding contributions of the predominantly π-type of these two spinors for weak *trans* ligands are diminished or even lost for strong *trans* ligands due to a destabilization of the occupied σ levels. The latter may even become the highest occupied MOs and alter decisively the composition of the most important valence spinors and thus change the sign of the SO shielding (or overall shift). For hydride complexes, destabilization of this σ level also causes an increasing H–M bond length with stronger *trans* ligands. This explains the correlation between ^{1}H shift and H–M bond length in such complexes.

Our analyses also go beyond earlier considerations by ourselves and others on the shielding role of π-type occupied MOs and the deshielding role of σ-type occupied MOs for such SO-induced shifts. Deviations from this general behavior, albeit relatively small in magnitude, can be attributed to several factors, ranging from contributions by spin-dipolar hyperfine effects (beyond the established predominant Fermi-contact-based mechanism of SO-induced shifts) to extensive SOC-induced σ/π-mixing of both occupied and virtual spinors. The latter may subtly alter the predominant character of these spinors, and thus also the sign of individual shielding contributions. These analyses may also be used to rationalize in detail recent studies of paratropic and diatropic SO-induced ring currents in HAu and HHgH.

APPENDIX: A test of MO (spinor) analyses of NMR shifts in the relativistic case: The observations and trends described above call for deeper insight into shielding or deshielding contributions, both to σ^p and σ^{SO} (diamagnetic shielding contributions tend to be less dependent on ligand effects, even though their changes are not negligible for ^{1}H shifts, cf. Table S1).[1] In view of the ambiguities of MO analyses (gauge dependence, method dependence, see Computational Details above), it is helpful to compare different analysis schemes, in

Table 5. Calculated total hydride ^{1}H isotropic shieldings (σ^{total}), σ^{P}, σ^{SO}, and combined (σ^{P+SO}) parts, and the dominant occupied orbital contributions (in ppm) in HI and HAu obtained by different methods.[a]

	σ^{total}	σ^{P}	σ^{SO}	σ^{P+SO}	MO	σ^{P} contr.	σ^{SO} contr.[g]	σ^{P+SO} contr.[h]	
HI									
Exp.[b]	43.9								
REX[c]	39.2	–	11.1	–	2π[i]	–	19.0	–	($\pi_{1/2}$)
					2σ[i]	–	−7.9	–	
4c-mDKS[d]	44.9	1.9	12.7	14.6	$1\pi/2\pi$[i]	1.6	(0.3)	1.9	($\pi_{3/2}$)
						1.6	(7.0)	8.6	($\pi_{1/2}$)
					2σ[i]	−0.6	(3.0)	2.4	
					1σ	−0.6	(0.5)	−0.1	
2c-ZORA[e]	44.7	1.9	12.9	14.8	$1\pi/2\pi$[i]	1.6	(0.4)	2.0	($\pi_{3/2}$)
						1.6	(7.4)	9.0	($\pi_{1/2}$)
					2σ[i]	0.1	(2.7)	2.8	
					1σ	−0.8	(0.4)	−0.4	
1c-ECP[f]	42.5	2.6	11.1	13.7	$1\pi/2\pi$[i]	1.6	5.6	7.2	
						1.6	5.6	7.2	
					2σ	−0.1	−0.1	−0.2	
					1σ	−0.2	0.0	−0.2	
HAu									
4c-mDKS[d]	52.1	6.3	17.6	23.9	2σ[i]	0.1	(−5.8)	−5.7	
					$1\pi/2\pi$[i]	3.3	(1.2)	4.5	($\pi_{3/2}$)
						3.3	(12.8)	16.1	($\pi_{1/2}$)
					1σ[i]	−0.6	(7.2)	6.6	
					$1\delta/2\delta$[i]	0.0	(1.1)	1.1	($\delta_{3/2}$)
2c-ZORA[e]	52.3	4.7	17.9	22.6	2σ[i]	0.0	(−6.3)	−6.3	
					$1\pi/2\pi$[i]	2.9	(1.5)	4.4	($\pi_{3/2}$)
						2.9	(14.2)	17.1	($\pi_{1/2}$)
					1σ[i]	−1.8	(7.5)	5.7	
					$1\delta/2\delta$	0.0	(1.0)	1.0	($\delta_{3/2}$)
1c-ECP[f]	45.3	5.9	12.2	18.1	2σ	0.7	1.4	2.1	
					$1\pi/2\pi$[i]	2.8	4.5	7.3	
						2.8	4.5	7.3	
					1σ	−0.7	0.7	0.0	

[a] In contrast to the main text, MO labels for "unligated" HAu are adopted to denote the lowest σ-type valence MO as 1σ. [b] Experimental data from ref. [54]. [c] Four-component relativistic extended Hückel results.[7] [d] Four-component mDKS results (PBE/Dyall-TZ/IGLO-III), this work. [e] Two-component ZORA-SO results (PBE/TZ2P) for σ^{SO} and σ^{P+SO}, with one-component ZORA-SR results for σ^{P}, this work. [f] One-component perturbational ECP calculations with third-order perturbation treatment of SO contributions (PBE/RSC/TZVP), this work. [g] Numbers in parentheses obtained by subtraction of SR σ^{P} contributions from the σ^{P+SO} values; note that the SR and SO MOs are not identical. [h] The actual spinor character is given in parentheses, after SO splitting of the degenerate SR-MOs, which are indicated further to the left. [i] Dominated by coupling with the 3σ MO (LUMO).

particular for the case of large SO effects. One of the first studies of ^{1}H SO shieldings (the HALA effect) in hydrogen halides[7] used a four-component, relativistically parametrized extended Hückel method (REX).[53] In spite of the rather approximate nature of the electronic structure method, this work represents the first treatment going beyond leading-order perturbation theory for the SO contributions. For the ^{1}H shielding in HI, Pyykkö et al.[7] identified a dominant shielding contribution from a $\pi_{1/2}$-type spinor (HOMO−1). As SO coupling mixes some σ character into this MO, some hydrogen spin density is created, which is the origin of the dominant shielding contribution (through coupling to a virtual 3σ MO). In contrast, a predominantly σ-bonding MO (2σ spinor, HOMO−2) contributes in a deshielding fashion, facilitated by SO-induced π-admixture. This was probably the first case in which a π-type occupied MO was linked to shielding and a σ-type MO to deshielding HALA effects, an observation that has since been corroborated in many cases, often by perturbational SO treatments.[9] Due to its prototypical nature and simplicity, a detailed comparison of analysis methods for this molecule should provide a good starting point for further studies. From here, we can proceed in a natural way, via the also still simple HAu to more diverse transition-metal cases.

Table 5 shows that the overall shielding and SO contributions from the simple REX calculations are not dissimilar (within 2 ppm for σ^{SO}, within 4 ppm for σ^{total}, due to the missing σ^{P} contributions; see text) to those obtained by more sophisticated four-component (4c) or two-component (2c) treatments at DFT levels (1c perturbation results give almost the same overall σ^{SO} as the REX data), which in turn agree very well with experimental data. However, we see notable differences between the individual MO (spinor) couplings. In the minimal-basis REX calculations, σ^{P} contributions vanish, and the data represent pure SO effects. This is not the case for the 2c-ZORA-SO and 4c-mDKS calculations, in which the spinor couplings correspond to σ^{P+SO} contributions. We carried out additional ZORA-SR and spin-orbit-free 4c-mDKS calculations to extract the σ^{P} contributions, overall and for different occupied MOs, which, however, are not identical in the SR and SO picture (see above).

Keeping this in mind, we see that the shielding contributions from predominantly π-type spinors at the more advanced levels are lower (with the $\pi_{1/2}$ spinor dominating), and those from the nominally 2σ-type spinor become slightly positive, rather than negative as in the REX analysis (Table 5). The 1c third-order perturbational scheme gives almost vanishingly small σ contributions, and the π-type contributions are provided as an average over $\pi_{1/2}$ and $\pi_{3/2}$ spinors. Qualitatively, the analysis agrees well with the 2c-ZORA-SO and 4c-mDKS results, consistent with the overall somewhat lower shieldings. We should furthermore keep in mind the different definitions of σ^p for GIAOs for 2c and 1c calculations compared to the common gauge used in the REX calculations. In any case, we find that the assumption of deshielding contributions from σ-type occupied MOs does not seem to be general and also depends on the virtual orbitals involved in the magnetic couplings with the given σ-type MO and on the analysis method. Due to the numerous approximations employed in simple REX calculations (which result, e.g., in different relative MO energies compared to those with a fully relativistic treatment), we rely here on analyses/data obtained at more sophisticated levels, such as 2c-ZORA and 4c-mDKS, providing a consistent picture for HI. That is to say, slightly positive SO shielding is obtained for σ(H–M)→σ*(H–M) type transitions, whereby both the occupied and virtual spinors display appreciable $p_{1/2}$ character. We note in passing that similar, albeit somewhat more enhanced positive SO shielding contributions for σ-type MOs are also found for HAt (cf. Table S8 in the Supporting Information). Among main group diatomic hydrides, "typical" (but particularly large) negative SO contributions from σ-type MOs are evident, for example, for indium(I) hydride, HIn, and thallium(I) hydride, HTl (Table S8). Similarly to HI, the occupied and virtual spinors possess large M(p)-character, but with different j values ($p_{1/2}$ and $p_{3/2}$ for the HOMO and LUMO, respectively).

Let us turn now to the HAu molecule as our simplest representative of the transition-metal complexes under scrutiny here. The overall ^{1}H shieldings are somewhat larger here as compared to those for HI, consistent with enhanced SO effects. As for HI, the picture provided by the 2c-ZORA-SO and 4c-mDKS analyses confirms large shielding contributions from π-type MOs (in particular from a $\pi_{1/2}$-type spinor), and different SO shieldings for the nominally σ-type frontier spinors, with 1σ shielding and 2σ deshielding. Since both of the latter contributions are dominated by coupling with the same virtual (LUMO) spinor, the different signs of the SO shielding contributions for these two σ-type occupied spinors can be attributed to different j values of the dominantly contributing Au(5d) orbitals ($d_{3/2}$ and $d_{5/2}$ for 1σ and 2σ, respectively). The 1c data suggest that the π-type MOs dominate the SO shielding, with a small additional (positive) contribution from 2σ. Overall, the situation is similar to that for HI. Notably, the agreement between 2c-ZORA and 4c-mDKS analyses is excellent, vindicating our use of the former throughout the present work.

Acknowledgements

AHG thanks the Fonds der chemischen Industrie for a Ph.D. scholarship. Funding from the Berlin DFG excellence cluster on Unifying Concepts in Catalysis is gratefully acknowledged.

Conflict of interest

The authors declare no conflict of interest.

Keywords: electronic structure · ligand effects · NMR shifts · relativistic NMR calculations · spin-orbit effects · *trans* influence · transition metal hydrides

[1] A. H. Greif, P. Hrobárik, V. Hrobáriková, A. V. Arbuznikov, J. Autschbach, M. Kaupp, *Inorg. Chem.* **2015**, *54*, 7199 – 7208.
[2] P. Hrobárik, V. Hrobáriková, F. Meier, M. Repiský, S. Komorovský, M. Kaupp, *J. Phys. Chem. A* **2011**, *115*, 5654 – 5659.
[3] P. Hrobárik, V. Hrobáriková, A. H. Greif, M. Kaupp, *Angew. Chem. Int. Ed.* **2012**, *51*, 10884 – 10888; *Angew. Chem.* **2012**, *124*, 11042 – 11046.
[4] J. Vícha, C. Foroutan-Nejad, T. Pawlak, M. L. Munzarová, M. Straka, R. Marek, *J. Chem. Theory Comput.* **2015**, *11*, 1509 – 1517.
[5] J. Vícha, M. Straka, M. L. Munzarová, R. Marek, *J. Chem. Theory Comput.* **2014**, *10*, 1489 – 1499.
[6] J. Vícha, J. Novotný, M. Straka, M. Repiský, K. Ruud, S. Komorovský, R. Marek, *Phys. Chem. Chem. Phys.* **2015**, *17*, 24944 – 24955.
[7] P. Pyykkö, A. Görling, N. Rösch, *Mol. Phys.* **1987**, *61*, 195 – 205.
[8] a) A. D. Buckingham, P. J. Stephens, *J. Chem. Soc. Res.* **1964**, 4583; b) Y. Ruiz-Morales, G. Schreckenbach, T. Ziegler, *Organometallics* **1996**, *15*, 3920 – 3923.
[9] M. Kaupp, in *Relativistic Electron. Struct. Theory II, Appl.* (Ed.: P. Schwerdtfeger), Elsevier, Amsterdam, **2004**, pp. 552 – 597.
[10] See, for example: a) A. S. K. Hashmi, G. J. Hutchings, *Angew. Chem. Int. Ed.* **2006**, *45*, 7896 – 7936; *Angew. Chem.* **2006**, *118*, 8064 – 8105; b) H. Ito, T. Saito, T. Miyahara, C. Zhong, M. Sawamura, *Organometallics* **2009**, *28*, 4829 – 4840; c) D. A. Roşca, D. A. Smith, D. L. Hughes, M. Bochmann, *Angew. Chem. Int. Ed.* **2012**, *51*, 10643 – 10646; *Angew. Chem.* **2012**, *124*, 10795 – 10798; d) H. B. Lv, J. H. Zhan, Y. B. Cai, Y. Yu, B. W. Wang, J. L. Zhang, *J. Am. Chem. Soc.* **2012**, *134*, 16216 – 16227; e) H. Schmidbaur, H. G. Raubenheimer, L. Dobrzanska, *Chem. Soc. Rev.* **2014**, *43*, 345 – 380; f) D. A. Roşca, J. Fernandez-Cestau, D. L. Hughes, M. Bochmann, *Organometallics* **2015**, *34*, 2098 – 2101.
[11] R. J. F. Berger, M. Repiský, S. Komorovský, *Chem. Commun.* **2015**, *51*, 13961 – 13963.
[12] E. Y. Tsui, P. Müller, J. P. Sadighi, *Angew. Chem. Int. Ed.* **2008**, *47*, 8937 – 8940; *Angew. Chem.* **2008**, *120*, 9069 – 9072.
[13] A. J. Jordan, G. Lalic, J. P. Sadighi, *Chem. Rev.* **2016**, *116*, 8318 – 8372.
[14] M. Kaupp, O. L. Malkina, *J. Chem. Phys.* **1998**, *108*, 3648 – 3659.
[15] K. Eichkorn, F. Weigend, O. Treutler, R. Ahlrichs, *Theor. Chem. Acc.* **1997**, *97*, 119 – 124.
[16] X. Cao, M. Dolg, H. Stoll, *J. Chem. Phys.* **2003**, *118*, 487 – 495.
[17] W. Küchle, M. Dolg, H. Stoll, H. Preuss, *J. Chem. Phys.* **1994**, *100*, 7535 – 7542.
[18] X. Cao, M. Dolg, *J. Mol. Struct.* **2004**, *673*, 203 – 209.
[19] J. P. Perdew, Y. Wang, *Phys. Rev. B* **1992**, *45*, 13244 – 13249.
[20] J. P. Perdew, K. Burke, M. Ernzerhof, *Phys. Rev. Lett.* **1997**, *78*, 1396 – 1396.
[21] *Turbomole*, *version 6.3.1*, A Development of University of Karlsruhe and Forschungszentrum Karlsruhe GmbH, 1989 – 2007, TURBOMOLE GmbH, since 2007; available from http://www.turbomole.com.
[22] S. Grimme, J. Antony, S. Ehrlich, H. Krieg, *J. Chem. Phys.* **2010**, *132*, 154104/1 – 19.
[23] S. Grimme, S. Ehrlich, L. Goerigk, *J. Comput. Chem.* **2011**, *32*, 1456 – 1465.
[24] G. A. Aucar, T. Saue, L. Visscher, H. J. A. Jensen, *J. Chem. Phys.* **1999**, *110*, 6208 – 6218.

[25] W. Kutzelnigg, *J. Comput. Chem.* **1999**, *20*, 1199 – 1219.
[26] S. K. Wolff, T. Ziegler, *J. Chem. Phys.* **1998**, *109*, 895 – 905.
[27] S. K. Wolff, T. Ziegler, E. van Lenthe, E. J. Baerends, *J. Chem. Phys.* **1999**, *110*, 7689 – 7698.
[28] Amsterdam Density Functional (ADF), version 2012.01, SCM, Theoretical Chemistry, Vrije Universiteit, Amsterdam, Netherlands, 2012; available from http://www.scm.com.
[29] M. Ernzerhof, G. E. Scuseria, *J. Chem. Phys.* **1999**, *110*, 5029 – 5036.
[30] S. Grimme, *J. Comput. Chem.* **2004**, *25*, 1463 – 1473.
[31] D. N. Laikov, *Chem. Phys. Lett.* **1997**, *281*, 151 – 156.
[32] A. E. Hansen, T. D. Bouman, *J. Chem. Phys.* **1986**, *84*, 2433.
[33] J. Autschbach, *Mol. Phys.* **2013**, *111*, 2544 – 2554.
[34] E. D. Glendening, J. K. Badenhoop, A. E. Reed, J. E. Carpenter, J. A. Bohmann, C. M. Morales, F. Weinhold, NBO 5.0, Theoretical Chemistry Institute, University of Wisconsin, Madison, 2001. Available at: www.nbo.chem.wisc.edu.
[35] D. Andrae, U. Häußermann, M. Dolg, H. Stoll, H. Preuß, *Theor. Chim. Acta* **1990**, *77*, 123 – 141.
[36] M. Dolg, U. Wedig, H. Stoll, H. Preuss, *J. Chem. Phys.* **1987**, *86*, 866 – 872.
[37] *MAG-ReSpect*, *version 2.3*, *2010*; V. G. Malkin, O. L. Malkina, R. Reviakine, A. V. Arbuznikov, M. Kaupp, B. Schimmelpfennig, I. Malkin, M. Repisky, S. Komorovsky, P. Hrobarik, E. Malkin, T. Helgaker, K. Ruud.
[38] Gaussian 09, Revision D.01, M. J. Frisch, G. W. Trucks, H. B. Schlegel, G. E. Scuseria, M. A. Robb, J. R. Cheeseman, G. Scalmani, V. Barone, B. Mennucci, G. A. Petersson, H. Nakatsuji, M. Caricato, X. Li, H. P. Hratchian, A. F. Izmaylov, J. Bloino, G. Zheng, J. L. Sonnenberg, M. Hada, M. Ehara, K. Toyota, R. Fukuda, J. Hasegawa, M. Ishida, T. Nakajima, Y. Honda, O. Kitao, H. Nakai, T. Vreven, J. A. Montgomery, Jr., J. E. Peralta, F. Ogliaro, M. Bearpark, J. J. Heyd, E. Brothers, K. N. Kudin, V. N. Staroverov, R. Kobayashi, J. Normand, K. Raghavachari, A. Rendell, J. C. Burant, S. S. Iyengar, J. Tomasi, M. Cossi, N. Rega, J. M. Millam, M. Klene, J. E. Knox, J. B. Cross, V. Bakken, C. Adamo, J. Jaramillo, R. Gomperts, R. E. Stratmann, O. Yazyev, A. J. Austin, R. Cammi, C. Pomelli, J. W. Ochterski, R. L. Martin, K. Morokuma, V. G. Zakrzewski, G. A. Voth, P. Salvador, J. J. Dannenberg, S. Dapprich, A. D. Daniels, Ö. Farkas, J. B. Foresman, J. V. Ortiz, J. Cioslowski, D. J. Fox, Gaussian, Inc., Wallingford CT, **2009**.
[39] J. Vaara, O. L. Malkina, H. Stoll, V. G. Malkin, M. Kaupp, *J. Chem. Phys.* **2001**, *114*, 61 – 71.
[40] *ReSpect*, *version 3.5.0*, *2016*, Relativistic Spectroscopy Program; M. Repisky, S. Komorovsky, V. G. Malkin, O. L. Malkina, M. Kaupp, K. Ruud, with contributions from R. Bast, U. Ekström, S. Knecht, L. Konecny, I. Malkin Ondik, E. Malkin, available from www.respectprogram.org.
[41] K. G. Dyall, *Theor. Chem. Acc.* **2004**, *112*, 403 – 409.
[42] See, for example: a) T. T. Metsänen, P. Hrobárik, H. F. T. Klare, M. Kaupp, M. Oestreich, *J. Am. Chem. Soc.* **2014**, *136*, 6912 – 6915; b) T. Stahl, P. Hrobárik, C. D. F. Königs, Y. Ohki, K. Tatsumi, S. Kemper, M. Kaupp, H. F. T. Klare, M. Oestreich, *Chem. Sci.* **2015**, *6*, 4324 – 4334.
[43] See, for example, extremely large ^{13}C spin-orbit-induced deshielding contributions in some actinide organometallic complexes: a) L. A. Seaman, P. Hrobárik, M. F. Schettini, S. Fortier, M. Kaupp, T. W. Hayton, *Angew. Chem. Int. Ed.* **2013**, *52*, 3259 – 3263; *Angew. Chem.* **2013**, *125*, 3341 – 3345; b) A. H. Greif, P. Hrobárik, J. Autschbach, M. Kaupp, *Phys. Chem. Chem. Phys.* **2016**, *18*, 30462 – 30474.
[44] This may be traced back to a larger HOMO–LUMO gap for the anionic (ca. 7–8 eV) compared to the neutral (ca. 5–6 eV) complexes. Larger energy denominators in the perturbation expressions reduce the magnitude of both σ^{P} and σ^{SO} contributions (in particular the latter), and thereby damp ligand effects in the $[HAuL]^{-}$ series.
[45] P. Schwerdtfeger, P. D. W. Boyd, A. K. Burrell, W. T. Robinson, M. J. Taylor, *Inorg. Chem.* **1990**, *29*, 3593 – 3607.
[46] M. Kaupp, O. L. Malkina, V. G. Malkin, P. Pyykkö, *Chem. Eur. J.* **1998**, *4*, 118 – 126.
[47] The pure δ-type and π/δ-type spinors do not include any 1s(H) contribution and contribute only marginally to σ^{SO}. The exception is HOMO−2 with small but notable σ^{P+SO} contributions (cf. Table 2), which do not seem to arise from σ^{P} (cf. Table 1). We suspect this slightly positive contribution to be caused by a spin-dipolar hyperfine term contained in the overall SO shifts[48,49] that cannot readily be separated in a two- or four-component framework.
[48] J. Vaara, K. Ruud, O. Vahtras, *J. Chem. Phys.* **1999**, *111*, 2900 – 2909.
[49] J. I. Melo, M. C. Ruiz de Azua, C. G. Giribet, G. A. Aucar, P. F. Provasi, *J. Chem. Phys.* **2004**, *121*, 6798 – 6808.
[50] The absolute value of this contribution correlates with the energy gap of the occupied and virtual MOs, which causes, in contrast to the situation in the complexes in Table 2, an increasing contribution from the halides as *trans* ligands, in line with the increasing HOMO–LUMO gap (cf. Figure S1 and Table S5).
[51] J. E. Barquera-Lozada, A. Obenhuber, C. Hauf, W. Scherer, *J. Phys. Chem. A* **2013**, *117*, 4304 – 4315.
[52] A. D. Buckingham, P. J. Stephens, *J. Chem. Soc.* **1964**, 2747 – 2759.
[53] L. L. Lohr, P. Pyykkö, *Chem. Phys. Lett.* **1979**, *62*, 333 – 338.
[54] W. G. Schneider, H. J. Bernstein, J. A. Pople, *J. Chem. Phys.* **1958**, *28*, 601 – 607.

Manuscript received: February 22, 2017
Accepted manuscript online: March 24, 2017
Version of record online: May 19, 2017

CHEMISTRY
A European Journal

Supporting Information

Insights into *trans*-Ligand and Spin-Orbit Effects on Electronic Structure and Ligand NMR Shifts in Transition-Metal Complexes

Anja H. Greif,[a] Peter Hrobárik,*[a, b] and Martin Kaupp*[a]

chem_201700844_sm_miscellaneous_information.pdf

Table S1. Computed M-H distances, d(M-H) (in Ångstroms), ^{1}H NMR shielding components (in ppm; diamagnetic σ^{d}, paramagnetic σ^{p}, and spin-orbit σ^{SO}) and comparison of σ^{total} with experiment (where available) for selected TM hydride complexes (with a trans ligand L) [a]

Complex	d(M-H)	σ^{d}	σ^{p}	σ^{SO}	σ^{total}	σ_{exp} [b]
***trans*-[HOsL(dhpe)$_2$]**						
NO_3^-	1.63	30.7	17.0	8.3	56.0	
Cl^-	1.64	30.6	14.8	7.3	52.7	54.4 [c]
CN^-	1.70	30.4	9.6	3.8	43.8	45.6 [d]
CH_3^-	1.69	29.6	10.5	4.7	44.7	
BH_2^-	1.74	29.2	8.2	5.8	43.2	
***trans*-[HPtL(PMe$_3$)$_2$]**						
NO_3^-	1.55	31.5	8.7	14.7	54.9	55.4 [e]
Cl^-	1.56	31.3	6.0	19.8	47.1	48.5 [e]
CH_3^-	1.63	30.2	3.8	1.4	35.4	35.4 [f]
CF_3^-	1.62	30.5	5.0	3.9	39.4	
$HC{\equiv}C^-$	1.62	30.6	4.4	2.5	37.6	
BH_2^-	1.70	29.3	2.6	-3.4	28.6	31.2 [g]
***trans*-[HPtL(CO)$_2$]**						
NO_3^-	1.56	30.1	6.6	11.7	48.4	
Cl^-	1.58	29.9	4.3	6.3	40.5	
CH_3^-	1.63	29.0	2.1	-4.9	26.2	
BH_2^-	1.67	28.7	1.1	-10.2	19.6	
***trans*-[HPtL$_2$Cl]**						
NH_3	1.57	30.7	6.5	13.3	50.5	
py	1.57	32.5	3.0	13.1	48.6	
$As(CH_3)_3$	1.56	30.4	7.8	11.6	49.9	
[HCuL]^{q}						
none	1.49	27.6	3.0	1.8	32.4	
H_2O	1.48	29.0	3.6	1.9	34.5	
F^-	1.51	30.6	3.8	2.2	36.7	
NO_3^-	1.51	30.1	2.3	1.4	33.7	
NH_3	1.49	29.2	3.0	1.2	33.3	
Cl^-	1.53	30.4	1.6	0.8	32.8	
CH_3^-	1.56	30.1	1.3	0.7	32.0	
H^-	1.57	29.8	0.0	0.1	30.0	
BH_2^-	1.60	29.5	-0.4	0.0	29.1	

Complex	d(M-H)	σ^{d}	σ^{p}	σ^{SO}	σ^{total}	σ_{exp} [b]
[HAgL]^{q}						
none	1.62	27.3	0.7	3.1	31.1	
H_2O	1.60	28.4	1.5	1.9	31.8	
F^-	1.62	30.1	1.9	1.7	33.8	
NO_3^-	1.62	29.5	1.1	1.2	31.8	
NH_3	1.61	28.7	1.4	0.9	31.1	
Cl^-	1.64	29.9	0.7	0.4	30.9	
CH_3^-	1.68	29.6	0.3	-0.9	29.0	
H^-	1.70	29.6	-0.5	-1.5	27.5	
BH_2^-	1.73	29.2	-0.4	-1.9	26.8	
[HAuL]^{q}						
none	1.54	29.7	3.9	17.0	50.7	
H_2O	1.55	31.2	3.2	10.3	44.7	
F^-	1.57	33.0	3.5	7.6	44.2	
NO_3^-	1.57	32.4	2.4	6.6	41.4	
py	1.57	31.8	1.6	5.3	38.6	
NH_3	1.57	31.3	2.2	4.7	38.2	
Cl^-	1.59	32.5	1.1	2.7	36.3	
Br^-	1.59	32.0	0.8	1.7	34.5	
I^-	1.60	31.8	-0.4	-0.8	30.6	
AsH_3	1.60	30.3	-0.8	-2.5	27.0	
CN^-	1.62	32.6	0.0	-4.9	27.7	
CH_3^-	1.65	31.8	0.2	-5.2	26.7	
NHC	1.61	31.3	-0.2	-5.4	25.7	26.5 [h]
PH_3	1.61	30.7	-1.3	-6.6	22.8	
CO	1.61	30.9	0.2	-7.0	24.1	
H^-	1.66	31.3	-0.6	-7.3	23.4	
PF_3	1.61	30.6	-1.1	-7.5	22.0	
SiH_3^-	1.67	30.8	-1.7	-11.1	18.0	
BH_2^-	1.71	30.7	-1.3	-13.5	15.9	
[HAu(CNC)]		30.6	-0.1	7.5	38.1	37.3 [i]
$[(PEt_3)Au(H)Pt(PEt_3)_2(C_6Cl_5)]^+$		33.6	2.5	-0.4	35.8	36.3 [j]

[a] 2c-ZORA-SO/PBE0/TZ2P results for PBE0-D3(BJ)/def2-TZVP optimized structures, see Computational Details in main text. [b] σ_{exp}= 31.6 ppm – δ_{exp} [c] See ref. [S1]. The expt. value belongs to [HOsL(depe)$_2$] (depe=1,2-bis(diethylphosphino)ethane). [d] See ref. [S2]. The expt. value belongs to [HOsL(depe)$_2$] (depe=1,2-bis(diethylphosphino)ethane). [e] See ref. [S3]. The expt. value belongs to [HPtX(PEt$_3$)$_2$]. [f] See ref. [S3]. The expt. value belongs to [HPtX(PPh$_3$)$_2$]. [g] See ref. [S4]. The expt. value belongs to [HPt(BCat)(P(CH$_2$Cy)$_3$)$_2$] (Cat= catecholate, 1,2-O$_2$C$_6$H$_4$). [h] See ref. [S5]. [i] See ref. [S6]. [j] See ref. [S7].

Table S2. Quasirelativistically optimized Hg-H distances (in Ångstroms) and calculated ^{1}H NMR shifts (δ^{total}) in linear d^{10} HHgX complexes in comparison with experiment (in ppm). The paramagnetic and SO contribution to the ^{1}H isotropic shielding (in ppm) are given as well. [a]

	d(Hg-H)	σ^{p}	σ^{SO}	δ^{total}	δ_{exp} [b]
[HHgCH_3]	1.65	-1.7	-14.9	19.0	17.2
[HHgCH_2CH_3]	1.65	-1.6	-14.6	18.8	17.1
[HHg$CHCH_2$]	1.64	-1.4	-12.2	15.9	14.4
[HHgPh]	1.64	-1.4	-11.5	15.4	13.3
[HHg(C_6F_6)]	1.62	-1.4	-10.2	14.4	11.9
[HHgH]	1.65	-1.4	-15.1	19.2	–
[HHgCl]	1.60	-1.4	-4.1	8.0	–
[HHgF]	1.58	0.2	1.1	1.4	–
$[HHg]^{+}$	1.61	-0.4	11.5	-3.2	–

[a] 2c-ZORA-SO/PBE0/TZ2P results for PBE0-D3(BJ) optimized structures, see Computational Details in main text. [b] See ref. [S8].

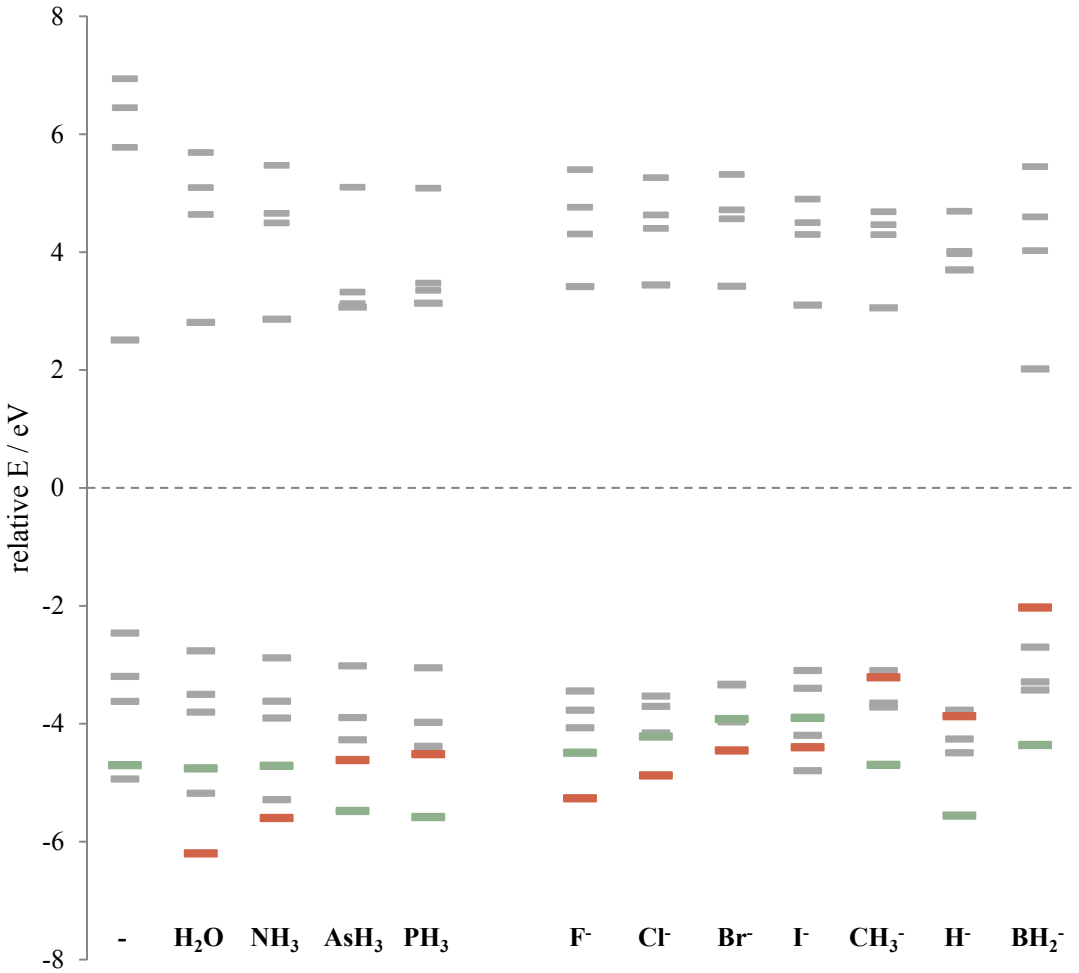

Figure S1. Quasirelativistic energies of the frontier MO spinors for the $HAuL^q$ series (q = 0, −1). The highest occupied π-type spinors with some σ character are highlighted in green, whereas the highest occupied σ-type spinor with significant *trans* ligand character is highlighted in red (2c-ZORA-SO/PBE0/TZ2P results).

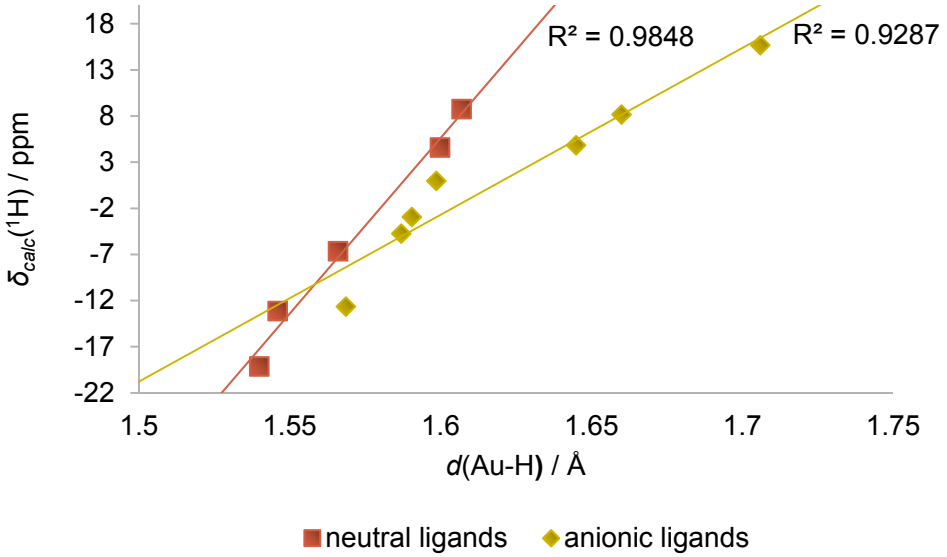

Figure S2. Correlation between hydride ^{1}H NMR shifts and Au-H bond lengths in the $HAuL^{q}$ series (see Table S1 for numerical data), with separate regression lines for neutral (q = 0, red squares) and anionic ligands (q = -1, yellow diamonds).

Table S3. Computed ^{1}H NMR shielding tensor components (in ppm) in HAuL complexes [a]

L	$\sigma_{\parallel}^{d}$	$\sigma_{\perp}^{d}$	$\sigma_{\perp}^{d}$	$\sigma_{\parallel}^{p}$	$\sigma_{\perp}^{p}$	$\sigma_{\perp}^{p}$	$\sigma_{\parallel}^{SO}$	$\sigma_{\perp}^{SO}$	$\sigma_{\perp}^{SO}$
none	58.2	15.5	15.5	0.2	5.8	5.8	-2.4	26.7	26.7
H_2O	60.0	16.7	16.8	0.2	4.7	4.8	-2.0	16.2	16.5
NH_3	59.5	17.2	17.2	0.2	3.2	3.2	-1.9	8.0	8.0
AsH_3	58.0	16.5	16.5	-0.8	-0.8	-0.8	-1.8	-2.9	-2.9
PH_3	57.2	17.5	17.5	-0.9	-1.5	-1.5	-2.3	-8.8	-8.8

[a] 2c-ZORA-SO/PBE0/TZ2P results for PBE0-D3(BJ) optimized structures, see Computational Details in main text.

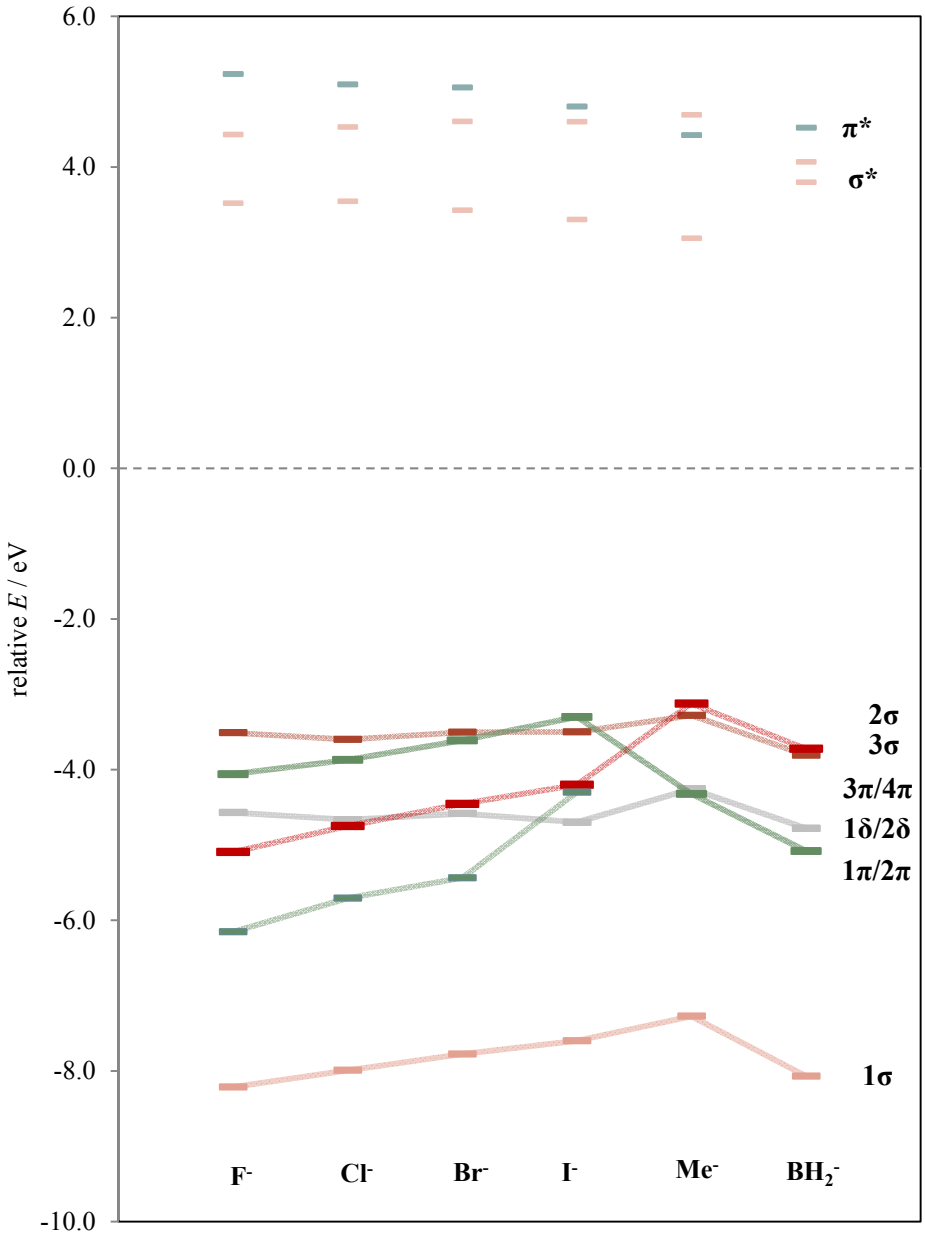

Figure S3. Energies of the scalar-relativistic frontier MOs for the $[HAuL]^-$ series (ZORA-SR/PBE0/TZ2P results).

Table S4. Main percentage AO contributions to the scalar relativistic frontier σ and π MOs for the $[HAuL]^-$ series [a]

L	1s(H)	5d(Au)	6s(Au)	6p(Au)	s(L)	p(L)	σ^p
	3σ						
F	10	35	53	0	0	1	-1.5
Cl	18	33	46	1	0	0	-1.2
Br	21	32	45	2	0	0	-1.1
I	28	28	36	4	0	4	-0.5
	2σ						
F	36	7	0	6	0	52	0.7
Cl	23	7	0	7	0	62	0.0
Br	17	7	3	6	0	67	0.0
I	9	9	11	5	0	66	0.0
	1σ						
F	22	37	3	0	0	36	0.0
Cl	26	42	5	0	0	24	0.9
Br	30	44	4	0	0	19	1.4
I	32	47	4	0	0	14	1.6
	3π/4π						
F	0	60	0	0	0	37	-1.6
Cl	0	35	0	0	0	64	-1.7
Br	0	23	0	0	0	75	-1.0
I	0	13	0	0	0	85	0.0
	1π/2π						
F	0	38	0	0	0	61	-0.7
Cl	0	64	0	0	0	34	-0.8
Br	0	75	0	0	0	24	-1.2
I	0	85	0	0	0	13	-3.0

[a] ZORA-SR/PBE0/TZ2P results.

Table S5. Composition of selected occupied 2-component spinors in terms of SR MOs, and spinor contributions to ^{1}H shieldings for the $[HAuL]^{-}$ series (L = F, Cl, Br, I) [a]

MO (spinor)	L	SR-MO contr. [%]						σ^{p+SO} contr.
		3σ	**2σ**	**1σ**	**3π/4π**	**1π/2π**	**1δ/2δ**	[ppm]
HOMO	F	85	–	–	14	–	–	-2.2
	Cl	80	–	–	18	–	–	-3.6
	Br	78	–	–	19	–	–	-4.3
HOMO-1	I	63	–	–	35	–	–	-5.5
HOMO-1	F	–	–	–	87	–	11	2.7
	Cl	–	–	–	91	–	7	1.8
	Br	–	–	–	95	–	4	1.2
HOMO	I	–	–	–	98	–	0	0.5
HOMO-3	F	14	4	–	79	–	–	11.6
	Cl	17	2	–	79	–	–	5.2
HOMO-2	Br	18	0	–	79	–	–	2.4
	I	29	20	–	48	3	–	-0.2
HOMO-4	F	–	94	–	–	4	–	-1.6
	Cl	–	95	–	–	2	–	-0.8
	Br	–	95	–	–	3	–	2.2
	I	6	74	–	16	3	–	3.4
HOMO-7	F	1	1	2	–	95	–	2.2
	Cl	3	3	2	–	91	–	3.4
	Br	3	3	3	–	90	–	3.7
HOMO-6	I	2	5	-	–	89	–	3.8
HOMO-8	F	–	–	–	–	1	–	-1.4
	Cl	–	–	–	–	3	–	-2.8
	Br	–	–	96	–	3	–	-3.3
	I	–	–	95	–	4	–	-4.4

[a] 2c-ZORA-SO/PBE0/TZ2P results.

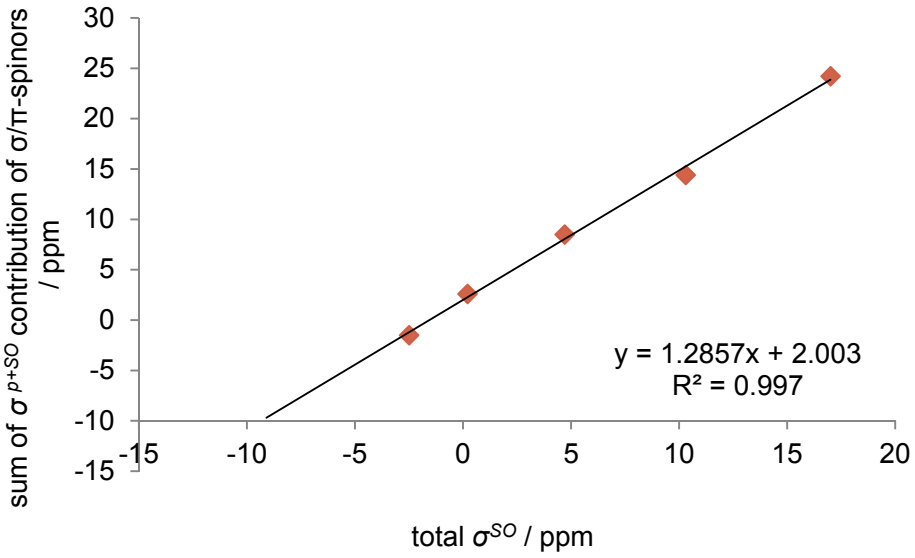

Figure S4. Correlation between the sum of shielding contributions σ^{p+SO} by the HOMO-3 and the other most important spinor with mixed σ/π character (HOMO-4 or HOMO-5, cf. Table 2) and total σ^{SO} in the neutral HAuL series (see Table 2 and Table S1 for numerical data).

Table S6. Dominant occupied-virtual spinor couplings contributing to σ^{p+SO} of the ^{1}H NMR shielding for the neutral HAuL series. Contributions $|\sigma^{p+SO}| < 1$ppm are neglected. [a]

L	occupied spinor	virtual spinor	σ^{p+SO} contribution [ppm]	ΔE (eV)
none	HOMO	→LUMO	-5.0	5.0
	HOMO-2	→LUMO	3.5	6.1
	HOMO-3	→LUMO	12.3	7.2
	HOMO-5	→LUMO	3.7	9.6
H_2O	HOMO	→LUMO	-1.7	5.6
	HOMO-3	→LUMO	7.1	7.6
		→LUMO+2	4.4	9.9
		→LUMO+6	2.2	13.8
	HOMO-5	→LUMO	-0.7	9.0
		→LUMO+2	1.2	11.3
		→LUMO+3	-1.4	11.9
NH_3	HOMO	→ LUMO	-1.1	5.7
	HOMO-3	→ LUMO	7.0	7.6
		→ LUMO+3	5.8	10.2
		→ LUMO+4	-2.2	10.3
		→ LUMO+8	2.1	13.8
	HOMO-5	→ LUMO	-2.6	8.4
		→ LUMO+3	2.0	11.1
		→ LUMO+4	-3.4	11.2
AsH_3	HOMO	→ LUMO+1	-2.2	6.1
		→ LUMO+3	1.8	8.1
	HOMO-3	→ LUMO	7.8	7.7
		→ LUMO+1	-4.0	7.7
		→ LUMO+4	-1.1	10.0
		→ LUMO+6	1.3	10.8
		→ LUMO+8	-1.7	11.3
	HOMO-8	→ LUMO	2.4	11.3
		→ LUMO+1	-1.8	11.4

L	occupied spinor	virtual spinor	σ^{p+SO} contribution [ppm]	ΔE (eV)
PH_3	HOMO	→ LUMO+2	-1.4	6.5
		→ LUMO+3	1.4	8.1
	HOMO-3	→ LUMO+2	2.7	8.0
		→ LUMO+8	-1.2	11.3
	HOMO-7	→ LUMO+2	-3.0	11.9
		→ LUMO+3	1.0	13.5
	HOMO-8	→ LUMO+2	1.5	12.1
		→ LUMO+3	-1.3	13.7
		→ LUMO+8	2.8	18.0

[a] 2c-ZORA-SO/PBE0/TZ2P results.

Table S7. Main SR-MO contributions to selected spinors at 2c-ZORA level for HAu and HHgH along with the paramagnetic and SO contribution to the ^{1}H NMR shielding. [a]

MO		contribution **3σ** to MO [%]	contribution **2σ** to MO [%]	contribution **1σ** to MO [%]	contribution **1π/2π** to MO [%]	contribution **1δ/2δ** to MO [%]	Total σ^{p+SO} of occupied MO [ppm]
HOMO	HHgH	–	–	99	–	–	-10.8
HOMO	HAu	96	–	–	4	–	-6.2
HOMO-1	HHgH	99	–	–	-	–	-1.8
HOMO-2	HAu	–	–	–	64	36	3.8
HOMO-3	HHgH	–	–	–	78	22	–
HOMO-3	HAu	4	5	–	90	–	17.3
HOMO-4	HHgH	1	18	–	81	–	4.4
HOMO-5	HAu	–	95	–	5	–	4.4
HOMO-6	HHgH	–	82	–	18	–	-3.1

[a] 2c-ZORA-SO/PBE0/TZ2P results.

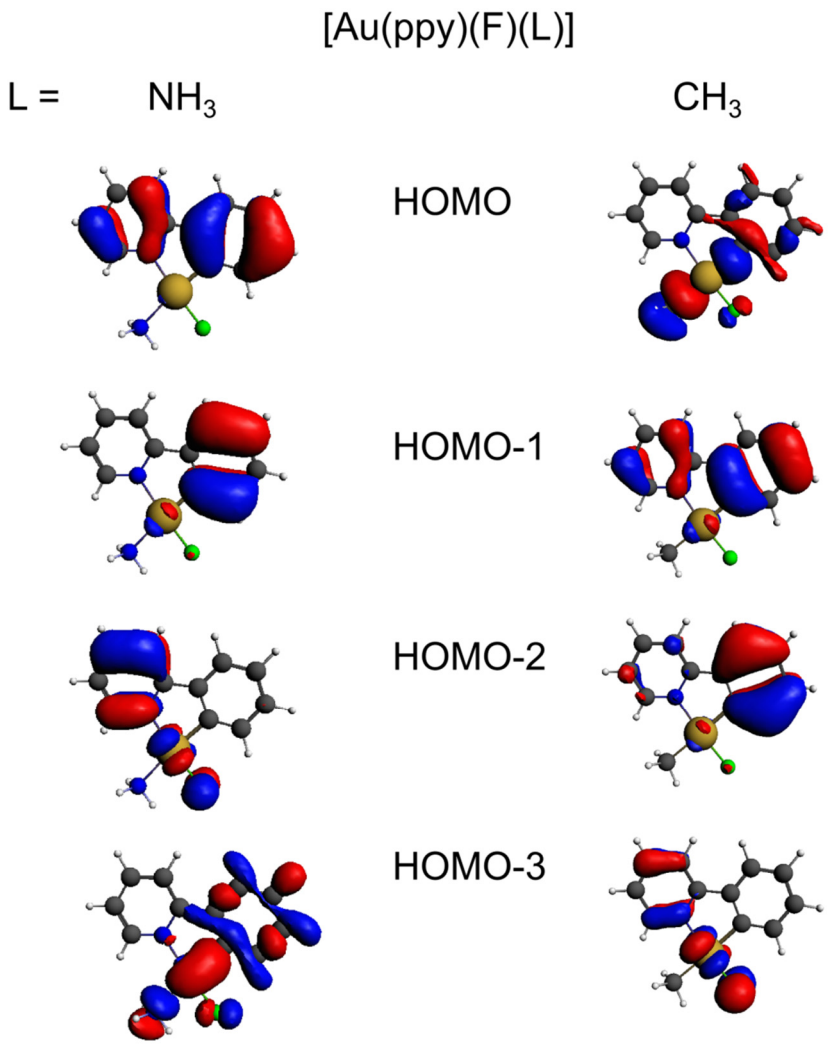

Figure S5. Isosurface plots (±0.03 a. u.) of occupied frontier MOs of [Au(2-ppy)(F)L] at scalar-relativistic (SR) level.

Table S8. Calculated total hydride ^{1}H isotropic shieldings (σ^{total}), σ^{p}, σ^{SO} and combined (σ^{p+SO}) parts, and the dominant occupied-spinor contributions (in ppm) with different methods for HAt, HIn and HTl [a]

	σ^{total}	σ^{p}	σ^{SO}	σ^{p+SO}	MO	σ^{p} contr.	σ^{SO} contr.	σ^{p+SO} contr.	
HAt									
4c-mDKS	59.9	3.8	27.9	31.7	1π/2π	1.9	(1.8)	3.7	($\pi_{3/2}$)
						1.9	(10.2)	12.1	($\pi_{1/2}$)
					2σ	-0.1	(10.0)	9.9	
					1σ	-0.2	(0.6)	0.4	
2c-ZORA	59.5	3.4	26.7	30.1	1π/2π	1.8	(1.9)	3.7	($\pi_{3/2}$)
						1.8	(11.2)	13.0	($\pi_{1/2}$)
					2σ	-0.3	(8.8)	8.5	
					1σ	-0.6	(0.7)	0.1	
HIn									
4c-mDKS	-13.4	-5.1	-35.1	-40.2	2σ	-5.9	(-29.0)	-34.9	
					1σ	0.5	(-4.0)	-3.5	
2c-ZORA	-15.6	-5.3	-37.2	-42.5	2σ	-5.7	(-30.9)	-36.6	
					1σ	0.2	(-4.0)	-3.8	
HTl									
4c-mDKS	-149.5	-4.5	-171.0	-175.5	2σ	-5.2	(-153.1)	-158.3	
					1σ	0.2	(-9.3)	-9.1	
2c-ZORA	-156.2	-4.0	-178.0	-182.0	2σ	-5.1	(-158.8)	-163.9	
					1σ	-0.2	(-9.3)	-9.5	

[a] See Table 5 in main text for comparison with HAu and HI.

REFERENCES

[S1] P. A. Maltby, M. Schlaf, M. Steinbeck, A. J. Lough, R. H. Morris, W. T. Klooster, T. F. Koetzle, R. C. Srivastava, *J. Am. Chem. Soc.* **1996**, *118*, 5396–5407.

[S2] E. Rocchini, P. Rigo, A. Mezzetti, T. Stephan, R. H. Morris, A. J. Lough, C. E. Forde, T. P. Fong, S. D. Drouin, *J. Chem. Soc. Dalton Trans.* **2000**, 3591–3602.

[S3] J. Chatt, B. L. Shaw, *J. Chem. Soc. Resumed* **1962**, 5075.

[S4] H. Braunschweig, P. Brenner, R. D. Dewhurst, F. Guethlein, J. O. C. Jimenez-Halla, K. Radacki, J. Wolf, L. Zöllner, *Chem. - Eur. J.* **2012**, *18*, 8605–8609.

[S5] E. Y. Tsui, P. Müller, J. P. Sadighi, *Angew. Chem. Int. Ed.* **2008**, *47*, 8937–8940.

[S6] A. S. K. Hashmi, *Angew. Chem.* **2012**, *124*, 13109–13110.

[S7] H. Lehner, D. Matt, P. S. Pregosin, L. M. Venanzi, A. Albinati, *J. Am. Chem. Soc.* **1982**, *104*, 6825–6827.

[S8] M. Kaupp, O. L. Malkina, *J. Chem. Phys.* **1998**, *108*, 3648–3659.

III

PCCP

PAPER

View Article Online
View Journal | View Issue

Cite this: *Phys. Chem. Chem. Phys.*, 2016, **18**, 30462

Giant spin–orbit effects on ^{1}H and ^{13}C NMR shifts for uranium(VI) complexes revisited: role of the exchange–correlation response kernel, bonding analyses, and new predictions†

Anja H. Greif,[a] Peter Hrobárik,*[a] Jochen Autschbach[b] and Martin Kaupp*[a]

Received 5th September 2016,
Accepted 18th October 2016

DOI: 10.1039/c6cp06129j

www.rsc.org/pccp

Previous relativistic quantum-chemical predictions of unusually large ^{1}H and ^{13}C NMR chemical shifts for ligand atoms directly bonded to a diamagnetic uranium(VI) center (P. Hrobárik, V. Hrobáriková, A. H. Greif and M. Kaupp, *Angew. Chem., Int. Ed.*, 2012, **51**, 10884) have been revisited by two- and four-component relativistic density functional methods. In particular, the effect of the exchange–correlation response kernel, which had been missing in the previously used two-component version of the Amsterdam Density Functional program, has been examined. Kernel contributions are large for cases with large spin–orbit (SO) contributions to the NMR shifts and may amount to up to ~30% of the total shifts, which means more than a 50 ppm difference for the metal-bonded carbon shifts in some extreme cases. Previous calculations with a PBE-40HF functional had provided overall reasonable predictions, due to cancellation of errors between the missing kernel contributions and the enhanced exact-exchange (EXX) admixture of 40%. In the presence of an exchange–correlation kernel, functionals with lower EXX admixtures give already good agreement with experiments, and the PBE0 functional provides reasonable predictive quality. Most importantly, the revised approach still predicts unprecedented giant ^{1}H NMR shifts between +30 ppm and more than +200 ppm for uranium(VI) hydride species. We also predict uranium-bonded ^{13}C NMR shifts for some synthetically known organometallic U(VI) complexes, for which no corresponding signals have been detected to date. In several cases, the experimental lack of these signals may be attributed to unexpected spectral regions in which some of the ^{13}C NMR shifts can appear, sometimes beyond the usual measurement area. An extremely large uranium-bonded ^{13}C shift above 550 ppm, near the upper end of the diamagnetic ^{13}C shift range, is predicted for a known pincer carbene complex. Bonding analyses allow in particular the magnitude of the SO shifts, and of their dependence on the functional, on the ligand position in the complex, and on the overall electronic structure to be better appreciated, and improved confidence ranges for predicted shifts have been obtained.

Introduction

The presence of a heavy element in a molecule may affect the nuclear magnetic resonance (NMR) chemical shifts of neighbouring atoms through spin–orbit (SO) effects.[1,2] These "SO chemical shifts" or "heavy-atom-effects on the light-atom shift" (HALA)[1] may alter the NMR shifts of certain nuclei in a system dramatically. As the SO shifts are mainly transmitted by a Fermi-contact-type mechanism,[3,4] atoms featuring a high s-orbital character in the bond towards the heavy-atom substituent are affected most significantly. Consequently, ^{1}H shifts are most susceptible to SO-induced effects. Spectacular examples for low-frequency SO ^{1}H shifts include the hydrogen halides[5,6] and in particular 4d or 5d transition-metal hydride complexes with d^6 or d^8 configurations,[7,8] with shifts down to −60 ppm *vs.* tetramethylsilane (TMS) for certain iridium complexes.[9] In contrast, the largest experimentally confirmed high-frequency ^{1}H SO shifts so far are induced for metal hydrides with d^{10} and d^0 configurations,[7,10–12] with measured shift values up to *ca.* +20 ppm.[13] The SO origin of many of these shifts has been confirmed by a large variety of quantum-chemical studies,

[a] *Institut für Chemie, Technische Universität Berlin, Strasse des 17. Juni 135, D-10623 Berlin, Germany. E-mail: peter.hrobarik@tu-berlin.de, martin.kaupp@tu-berlin.de*
[b] *Department of Chemistry, University at Buffalo, State University of New York, Buffalo, NY, 14260, USA*

† Electronic supplementary information (ESI) available: NMR chemical shifts of U(VI)-bound ligand atoms computed at DFT level using various EXX admixtures and different structures, their decomposition into individual (diamagnetic, paramagnetic and spin–orbit) terms, NMR shift tensor anisotropies, detailed bonding analysis and Cartesian coordinates of optimized structures. See DOI: 10.1039/c6cp06129j

ranging from a perturbational treatment of SO coupling *via* two-component quasirelativistic approaches to fully relativistic four-component calculations, using in most cases density functional theory (DFT) methods.[2,3,5,12,14,15]

Using two-component ZORA ("zeroth-order regular approximation")[16,17] relativistic calculations, we have recently predicted spectacular SO-induced high-frequency ^{1}H and ^{13}C shifts in actinide complexes with $5f^0$ configuration, in particular for uranium(VI) species.[12] The predicted ^{1}H chemical shifts of suitable target U(VI) hydride complexes ranged up to clearly beyond +100 ppm, which would considerably extend the known ^{1}H shift range for diamagnetic compounds. As the computed shifts depended strongly on the exact-exchange (EXX) admixture of the DFT exchange–correlation functional, in the absence of experimental ^{1}H data our strategy for the selection of the most suitable functional was based on the parallel study of ^{13}C shifts in uranium(VI) organometallic complexes. In the latter case, some experimental data were available, and the evaluation of functionals on these data suggested best performance for a PBE-based global hybrid functional with 40% EXX admixture (PBE-40HF).[12] Values obtained with this functional were then put forward as predictions for the unknown ^{1}H chemical shifts in U(VI) hydride complexes,[12] and for the ^{13}C NMR shifts in two new U(VI) alkyl complexes.[18] The predictions in the latter cases were subsequently confirmed experimentally, resulting in one case in the drastic revision of a previous experimental assignment.[18]

However, recent findings regarding the two-component ZORA implementation for NMR shifts in the ADF program,[19] which had been used for our studies on actinide systems, suggest that we may have obtained the right answer for not entirely the right reasons: One of us noted that the ADF NMR shielding implementation misses the linear response of the exchange–correlation potential (*i.e.* the shielding contribution from the response XC kernel) to the external perturbation.[20] It was argued by Wolff and Ziegler in the publication preceding the one reporting the original ZORA NMR implementation that this shielding contribution 'even for heavy atoms [is] not large'.[16] This is indeed not a problem in the absence of significant SO effects, as the perturbation operators for external magnetic field and nuclear magnetic moment are imaginary ones that do not create coupling terms for pure (semi-)local functionals. However, due to the impact of the electron spin-dependent part of the hyperfine interaction (a real perturbation) for the SO nuclear shielding effects (see above), the kernel becomes important or even essential in cases of large SO contributions when using spin-polarized calculations.[21] Employing a modified pilot implementation, Autschbach demonstrated significant changes between the standard implementation in ADF and the modified one for ^{1}H shifts in hydrogen halides and for ^{199}Hg shifts in mercury halides were demonstrated.[20] Notable differences between two- and four-component results in a recent study of carbon and nitrogen shifts in transition-metal cyanide complexes also pointed to possible inaccuracies with the previous ZORA implementation in ADF due to the lack of the XC-kernel SO effects on the nuclear magnetic shielding[22] (see also ref. 15 and 23 for other two- *vs.* four-component comparisons). Even more recently, we have compared both the original and the modified implementation to four-component calculations for ^{1}H and ^{195}Pt shifts in a series of platinum hydride complexes.[14] While absolute shieldings at two-component ZORA and four-component levels differed considerably (as has been shown earlier in other cases[24]), the relative shifts agreed rather well, provided the XC-kernel SO contributions were included at both levels, and excellent agreement with the experimental shifts was obtained with PBE0. The effects of the missing XC contributions were large and excellent agreement with the experimental values was found with PBE0. In another recent study of ^{13}C and ^{15}N shifts in similar square-planar transition-metal complexes, the missing kernel in the standard ADF implementation was again successfully compensated for by 40% EXX admixture to the functional.[15]

In view of these observations, in this work we re-evaluate our previous calculations on ^{1}H and ^{13}C shifts in uranium(VI) complexes, using the modified two-component ZORA implementation in ADF in comparison with four-component Dirac–Kohn–Sham (DKS) calculations. In spite of some uncertainties concerning reproducibility of experimental data, it turns out that upon inclusion of the XC response kernel in the NMR calculations, the optimal EXX admixture needed for best agreement with the abovementioned experimental ^{13}C shifts is often considerably lower than the *ca.* 40% needed without kernel (see above). In the end, a conventional PBE0 functional with 25% EXX admixture seems to be a reasonable choice for the NMR shift calculations of uranium(VI) complexes, tending to somewhat overestimate ^{13}C NMR shifts. Calculations using PBE0 or related functionals with inclusion of the exchange–correlation kernel also confirm the overall range of the predicted spectacular high-frequency ^{1}H shifts in U(VI) hydride complexes, although with some modifications of the detailed predicted values in either direction. Moreover, calculated ^{13}C shifts for other recently synthesized organometallic uranium(VI) complexes are reported, extending the spectral range for uranium-bonded carbon shifts from about 20 ppm to above 550 ppm.

Computational details

We have performed gas-phase structure optimizations with the Turbomole program[25] using def2-TZVP basis sets[26,27] and the Perdew–Burke–Ernzerhof (PBE)[28] functional within the generalized gradient approximation (GGA), its hybrid form (PBE0),[28,29] and with B3LYP.[30,31] This computational level includes a small-core (60 core electrons) quasi-relativistic effective-core potential (ECP) for uranium.[26] In addition, atom-pairwise corrections for dispersion forces were simulated *via* Grimme's D3 model with Becke–Johnson (BJ) damping.[32,33] The quality of the optimized structures was evaluated by comparison of metal–ligand bond lengths (in particular U–C bonds) with experiment, where available.

The two-component quasirelativistic ZORA[16,17] DFT calculations have been carried out using the Amsterdam Density Functional (ADF) program[19] with the PBE functional,[28] and with PBE-based hybrids having variable EXX admixture,[34,35] using all-electron Slater-type orbital basis sets of triple-ζ doubly polarized (TZ2P)[36]

quality, and an integration accuracy of 5.0 (Voronoi grids). The calculations used gauge-including atomic orbitals (GIAOs).[37] The ZORA calculations of NMR chemical shifts are done with and without the previously neglected terms from the exchange–correlation (XC) response kernel.[20] We note in passing that the implementation of the PBE functional used here without and with XC kernel differs slightly, as the former uses PW92[29] for the LDA part and the latter VWN.[38] The latter goes back to the initial implementation of PBE in ADF by S. Patchkovskii. However, the differences affect the results negligibly.

Bulk solvent effects on the optimized structures and on the computed NMR shieldings were simulated *via* the conductor-like screening model (COSMO),[39–41] both in Turbomole and in ADF.

For comparison, fully relativistic four-component GIAO-DFT calculations at the matrix Dirac–Kohn–Sham (mDKS) level of theory and Gaussian-type orbital basis sets have been performed with the ReSpect program package.[42] The approach uses restricted magnetically balanced (RMB) orbitals for the small component[43,44] and includes a correct XC kernel treatment (which can be turned off for testing and comparison). The mDKS calculations have been done at generalized-gradient-approximation level with the PBE functional.[28,45] For the uranium center, Dyall's all-electron valence-triple-ζ (Dyall TZ)[46] basis set has been employed, together with fully uncontracted Huzinaga–Kutzelnigg-type IGLO-III basis sets[47] for the ligand atoms.

The calculated ^{1}H and ^{13}C nuclear shieldings σ were converted to chemical shifts δ (in ppm) relative to the shielding of TMS, computed at the same level. The SO contributions to the ^{13}C chemical shift were computed as $\delta^{SO} = 0.9\ \text{ppm} - \sigma^{SO}$, where the value of 0.9 ppm corresponds to the SO part of the isotropic ^{13}C shielding in TMS.

Analysis of natural localized molecular orbitals (NLMOs) at the scalar relativistic level was done with the NBO 5.9 module in Gaussian09 (G09)[48] using def(2)-TZVP[27,49] basis sets and the corresponding small-core ECP for uranium.[26,50] Interestingly, we noted problems with the NBO 5.0 module in the ADF 2012 package[51] when applied to uranium complexes. Without an error message, strongly overestimated f-orbital and underestimated d-orbital contributions to the U–C bonds were found compared to the G09 results, whereas no problems for transition-metal complexes were observed (*cf.* Table S1 in ESI†). In contrast, NBO 6.0 in ADF (2014)[52] gave data in good agreement with the G09 results. We thus suspect erroneous NBO analysis for f-element compounds in the older NBO version that comes with ADF. The delocalization index (DI), as a measure of shared electrons (bond covalency) between two atoms in question in the context of the quantum theory of atoms-in-molecules (QTAIM),[53,54] was calculated with the Multiwfn program,[55,56] at the same level as used for NLMO analyses (the corresponding .wfx files were generated in G09).

Results and discussion

Evaluation of the quality of the optimized structures

As chemical shifts can be very structure-dependent, a meaningful benchmarking of methods for shift calculations relies on accurate input structures. We therefore scrutinize initially the optimized structures of the organometallic complexes used for computation of ^{13}C shifts. Despite the recently described renaissance of non-aqueous uranium chemistry and, thus, of organouranium chemistry,[57] only a few complexes with direct U(VI)–C σ bonds were characterized structurally to date. ^{13}C NMR shifts of these complexes are even scarcer. Thus, our evaluation of structures and carbon NMR shifts uses the same set of recent organometallic complexes investigated in our previous work (complexes **1–3**, **6**, **7**),[12] however, three additional systems are considered here (**4**, **5**, **8**) (*cf.* Fig. 1 for all these structures). The latter include complex **8** as an example for a number of known U(VI) complexes with a methanide ligand and chelating phosphorano (in this case thiophosphorano) arms.[58–60] These systems exhibit clearly smaller (low-frequency) ^{13}C shifts (with a resonance peak at about 20 ppm) than the other complexes.

Fig. 2 plots percentage deviations of optimized uranium-carbon bond lengths from experiment at different theory levels, with and without including dispersion corrections (see Table S2 in ESI† for numerical data). A clear distance trend is found, where B3LYP and PBE give the largest and PBE0 and PBE0-D3 the lowest values (with differences between 0.04 and 0.09 Å). The B3LYP-D3 and PBE0-D3 structures feature the smallest standard deviation (Table S2, ESI†), also for the U–N and U=O bonds (Table S3, ESI†). While the rather short PBE0-D3 distances underestimate the pure σ-bond in **5** (by 0.05 Å), PBE0-D3 structures will be used in the following for the evaluation of ^{13}C shifts. Note that PBE0 structures are known to perform excellently for transition-metal complexes, as has also been found in a recent systematic analysis.[15] Additional NMR shift calculations for the structures optimized at B3LYP-D3 level are also provided to estimate the influence of the structural differences on the chemical shifts (see below). Bulk solvent effects simulated *via* the conductor-like screening model (COSMO)[39–41] are found to be negligible for the structural parameters (Table S4, ESI†). In view of the large SO effects on NMR shifts, we also performed

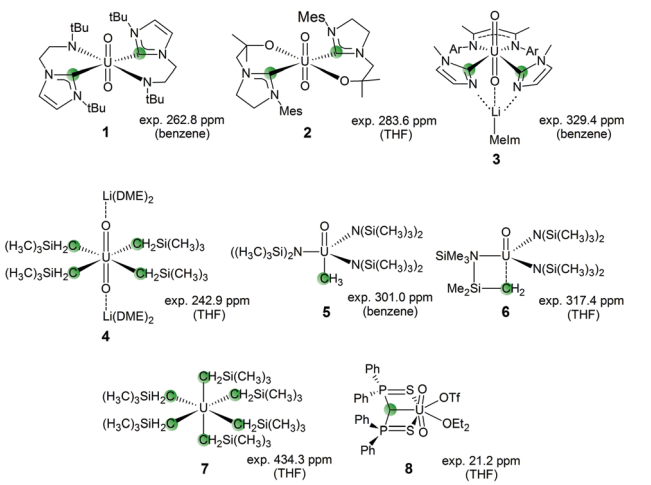

Fig. 1 Organometallic uranium(VI) complexes with known ^{13}C NMR shifts for metal-bound carbon atoms (highlighted in green). See Table 3 for corresponding references.

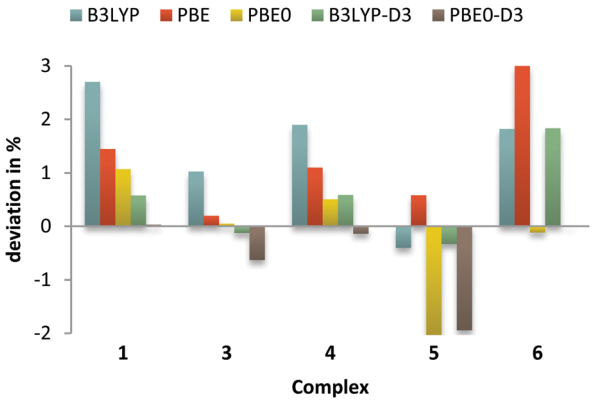

Fig. 2 Deviations from experiment of the U–C bond lengths optimized at different levels. See Table S2 in ESI† for numerical data and standard deviations. Average for two non-equivalent alkyl carbon atoms in **4** shown.

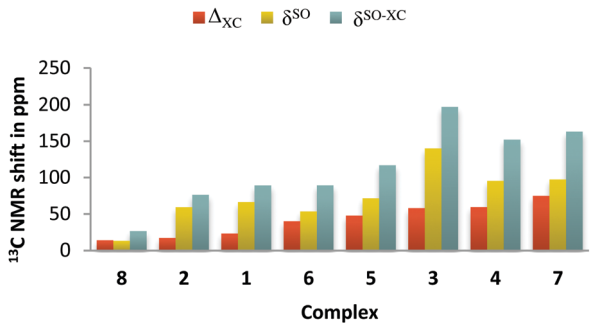

Fig. 3 Total XC-kernel contribution ($\Delta_{XC} = \delta^{xc}_{2c} - \delta_{2c}$) to the calculated ^{13}C NMR shifts for complexes **1–8** in comparison with the SO shift contributions without (δ^{SO}) and with ($\delta^{SO\text{-}XC}$) exchange–correlation kernel at PBE level; ordered by increasing Δ_{XC}.

structure optimizations for selected complexes at the 2c-ZORA/TZ2P level with spin–orbit coupling. These calculations revealed rather minor 5f-SO effects on both U–C and U–H bond lengths, mostly smaller than 0.01 Å (*cf.* Table S5, ESI†).

Interplay of functional and XC kernel contributions for the ^{13}C shifts

Computed ^{13}C NMR shifts of the carbon atoms directly bound to uranium in complexes **1–8** are presented in Table 1 (see also Fig. 1 and Table 3 for experimental data).

Starting with the effect of the kernel at PBE level, we see an appreciable increase of the ^{13}C shifts upon inclusion of the kernel for all systems. The lowest impact (Δ_{XC} = 13.6 ppm) is observed for a methanide complex **8**, which exhibits also the smallest overall SO contribution to the ^{13}C NMR shift. In fact, the influence of the kernel is connected to the magnitude of SO effects (*cf.* Fig. 3). Thus, for the σ-bonded carbon atoms in **4**, **5** and **7** (with δ^{SO} contributions of 115–165 ppm), the kernel contribution increases the shift by *ca.* 30%, which means 45–65 ppm difference for the carbon shift! For the N-heterocyclic carbene complexes **1** and **2** (with δ^{SO} contributions of *ca.* 75–90 ppm) the effect is below 10%. The "ate" complex **3** deviates slightly from this pattern as it exhibits the largest δ^{SO} contribution at PBE level but is only at third place in the XC kernel contribution.

Table 1 Computed isotropic ^{13}C NMR shifts without and with kernel (in ppm *vs.* TMS) for uranium(VI)-bound carbon atoms. δ^{SO} contributions are given in parentheses[a]

Complex	δ_{2c} (PBE)		δ^{xc}_{2c} (PBE)		δ_{2c} (PBE0)		δ^{xc}_{2c} (PBE0)	
1	266.4	(66.2)	289.4	(89.1)	270.6	(62.5)	286.8	(78.6)
2	283.5	(59.1)	300.4	(76.1)	288.5	(52.1)	299.5	(63.1)
3	360.1	(139.9)	417.9	(197.0)	347.6	(130.6)	387.3	(169.9)
4	174.2	(95.3)[b]	233.5	(151.9)[b]	209.3	(134.6)[b]	291.5	(212.9)[b]
5	184.1	(71.4)	231.7	(116.8)	231.6	(107.6)	299.9	(172.8)
6	207.3	(53.3)	247.1	(89.2)	253.7	(82.7)	313.7	(137.4)
7	249.0	(97.2)	323.7	(163.0)	340.5	(181.2)	536.8	(363.5)
8	38.9	(12.9)	52.6	(26.3)	22.1	(7.3)	28.5	(13.4)

[a] 2c-ZORA-SO/TZ2P results using PBE and PBE0 functional, respectively. Superscript "xc" indicates inclusion of the XC kernel. [b] Averaged data for two non-equivalent alkyl carbon atoms.

The total shielding is partitioned in the ADF output into a diamagnetic component that is calculated as an expectation value of a bilinear perturbation operator, and a linear response part that involves the perturbed Kohn–Sham orbitals to first order. The linear response part is further partitioned into a paramagnetic contribution that has a nonrelativistic counterpart, and a SO contribution involving the electron spin-dependent hyperfine operators that vanishes in the absence of SO coupling. The calculations confirm clearly the expectation that the kernel contribution affects almost exclusively the SO part of the nuclear shielding constants (*cf.* Tables S6 and S7 in ESI†). The paramagnetic part is influenced slightly as well (in particular for **7**, by about 10 ppm; see Tables S6 and S7, ESI†), as the first-order perturbed orbitals differ with and without consideration of the kernel.[61]

At first sight one would expect the kernel contribution to diminish when going from the "pure" GGA functional PBE to its hybrid form PBE0, as 25% of the PBE exchange have been replaced by exact exchange, and these 25% thus do not enter the kernel (the exact-exchange contributions are accurately accounted for in both implementations). While this expectation is borne out for the cases with relatively small kernel contributions (**1–3**, **8**), the kernel contribution actually increases with EXX admixture for **4–7**!

Strikingly, the latter four species are those complexes that exhibit a larger (more deshielded) ^{13}C NMR shift with EXX admixture than without. This may be attributed to a mutual enhancement (cross terms) between EXX-derived coupling terms and the PBE kernel contributions within the generalized coupled-perturbed Kohn–Sham scheme used. Closer analysis (Tables S6 and S7, ESI†) confirms that it is mostly the SO contributions that account for these trends (with sizeable paramagnetic contributions for **7**, see above). The differences between XC kernel contributions at PBE and PBE0 levels correlate with the differences in the shifts for the two functionals. That is, large increases of the kernel contributions upon going from pure PBE to the hybrid functional are found for the cases with the overall largest shift increases with EXX admixture, and *vice versa*.

The largest SO effects and thus the largest kernel contributions tend to be found for complexes with the most pronounced

uranium 5f-orbital involvement in bonding (and thus particularly low-lying nonbonding unoccupied 5f-type orbitals).[12] We previously found a similar enhancement of the SO contributions with 5d-orbital contribution in the case of ^{1}H shifts in platinum hydride complexes (in that case the SO effects are shielding, in contrast to the deshielding effects in the present work).[20] More detailed bonding analyses are provided below.

We note in passing that comparison of PBE0-D3 and B3LYP-D3 structures as input for the shift calculations without XC kernel changes the NMR shifts typically by only a few ppm, except for the very sensitive case of **7**, where somewhat larger effects of about 20 ppm (PBE0 shift calculation) are found (Table S8 in ESI†). Notably, these differences are enhanced by the kernel contribution. Use of B3LYP-D3 structures increases the shifts by about 20 ppm for complexes **4–6** but by 154 ppm for uranium(VI)-hexaalkyl **7**, which is also the system with the overall largest SO contributions. Interestingly, the shifts (and SO contributions) for the B3LYP-D3 optimized structures are larger (high-frequency shifted) even though the calculated U–C bonds are longer (*cf.* Fig. 2 and Table S2, ESI†). Intuitively, one might have expected the opposite trend, as the Fermi-contact mechanism for the SO-induced shift contributions should be enhanced for shorter distances.

Since the experimental NMR shifts were measured in organic solvents with varying polarity, such as pyridine-d_5 (**2**), benzene-d_6 (**1**, **3**, **5**) or THF-d_8 (**4**, **6–8**), we also evaluated the bulk solvent effects on computed NMR shifts. In general, these have somewhat larger influence when using functionals with a higher EXX admixture, as also observed in ref. 15. However, even with PBE0 and kernel, solvent effects on the NMR shifts obtained with the COSMO model tend to be below 7 ppm (Table S9 in ESI†).

Table 2 Comparison of computed 2- and 4-component ^{13}C NMR shifts with and without kernel (in ppm *vs.* TMS) of uranium(VI)-bound carbon atoms in model complexes[a,b]

Complex	δ_{2c} (PBE)	δ^{xc}_{2c} (PBE)	δ_{4c} (PBE)	δ^{xc}_{4c} (PBE)
1′	270.3	293.2	275.0	299.7
5	184.1	231.7	184.5	232.8
7′	227.3	317.2	226.3	311.2
8′	15.4	23.3	17.1	26.5

[a] δ_{2c}: 2c-ZORA-SO/TZ2P results; δ_{4c}: 4c-mDKS results with Dyall TZ/IGLO-III basis. [b] **1′**: ^{t}Bu group replaced by H; **7′**: CH_2SiMe_3 ligand replaced by CH_3; **8′**: Ph group replaced by H and OEt_2 replaced by OMe_2.

In addition to the two-component ZORA results discussed so far, Table 2 provides four-component (4c) mDKS results for some complexes. The standard 4c-mDKS implementation includes a correct XC kernel treatment, which can be turned off to get insight into the kernel contribution. 2c-ZORA results with ADF are given for comparison, as bulky substituent groups in **1**, **7**, and **8** had been replaced by smaller ones for the 4c-mDKS calculations (see footnotes in Table 2 for more details; complex **5** was taken without modification). The truncation in **1′** and **7′** has very small effects on the carbon shifts, whereas the ^{13}C shift in **8** is about halved in **8′** (Table 1). The latter is mainly due to the almost 0.1 Å longer U–C distance in **8′** compared to **8** (*cf.* Table S2 in ESI†). The 4c-mDKS results are overall close to the 2c-ZORA results with and without kernel contributions, respectively, differing generally by less than 7 ppm. Thus, the importance of the kernel terms is very similar at 4c- and 2c-levels, consistent with previous results for transition-metal cyanide[22] and hydride complexes,[14] and with ^{199}Hg relative shifts in ref. 23 (notwithstanding the fact that in the latter case absolute shieldings at 4c-mDKS and 2c-ZORA levels differed appreciably). The moderate differences between 2c- and 4c-results reflect technical differences between implementations (basis sets, grids, functionals, spin–orbit operators).

Evaluation of the functional for ^{13}C shift calculations

As seen in Table 1 and from our previous calibration without kernel,[12] the dependence of $\delta(^{13}C)$ on the functional does not provide a very clear-cut picture for the experimentally known uranium(VI) complexes. Table 3 provides the ^{13}C NMR shifts obtained with kernel, using EXX admixtures of 0% (PBE), 10%, 15%, 25% (PBE0) and 40% for complexes **1–8** in comparison with experiment. For the N-heterocyclic carbene (NHC) complexes **1–3**, dependence on EXX admixture is relatively weak (below 10 ppm with a non-monotonous trend for **1** and **2**, up to 60 ppm for **3**). This is mainly caused by a decrease of the absolute value of the SO contributions with increasing EXX admixture (in contrast to the increase for **4–7**) while the paramagnetic contributions increase by comparable amounts for **1** and **2** and remain almost constant for **3** (Tables S6 and S7 in ESI†). The behaviour for the methanide complex **8** is similar as for **3**.

Our previous validation of functionals without kernel in ref. 12, which provided PBE-40HF as the best-performing functional,

Table 3 Dependence of ^{13}C NMR shifts (in ppm *vs.* TMS) of uranium(VI)-bound carbon atoms on EXX admixture for structures optimized on PBE0-D3/def2-TZVP level[a]

Complex	δ^{xc}_{2c} (PBE)	δ^{xc}_{2c} (PBE-10HF)	δ^{xc}_{2c} (PBE-15HF)	δ^{xc}_{2c} (PBE0)	δ^{xc}_{2c} (PBE-40HF)	δ_{2c} (PBE-40HF)	δ_{exp}
1	289.4	290.0	289.4	286.8	280.5	270.3	262.8[62]
2	300.4	300.7	300.4	299.5	297.3	290.5	283.6[63]
3	417.9	409.8	403.6	387.3	360.0	334.2	329.4[64]
4	233.5[b]	257.5[b]	268.5[b]	291.5[b]	306.9[b]	230.6[b]	242.9[18]
5	231.7	257.5	270.6	299.9	362.2	277.4	301.0[65]
6	247.1	271.7	284.3	313.7	373.3	296.8	317.4[66]
7	323.7	377.5	418.0	536.8	936.0	489.0	434.3[18]
8	52.6	41.7	37.1	28.5	17.4	14.8	21.2[59]

[a] 2c-ZORA-SO/TZ2P results. Superscript "xc" indicates inclusion of the exchange–correlation kernel. [b] Averaged data for two non-equivalent alkyl carbon atoms.

was essentially based on the ^{13}C shifts of **1–3** and **6**. As the results for **1** and **2** depend relatively little on the EXX admixture (*cf.* Table 3), the good performance for **3** and **6** was decisive for the choice of "best" functional in that case. Uranium hexaalkyl complex **7** was found to have been misassigned previously,[67] and its actinide-bound carbon shift was predicted in ref. 12. A subsequent re-measurement of **7** reported in ref. 18 showed that PBE-40HF level without kernel had predicted the general spectral region correctly but still overestimated this remarkably high-frequency shift (Table 3) by about 100 ppm (much closer ^{13}C shift value of 436.5 ppm was achieved upon shortening of the U–C bond by 0.01 Å when including dispersion corrections in the structure optimization and using PBE-35HF with 35% EXX instead of PBE-40HF).[18] In that work the new complex **4** was reported, and its "blind test" assignment gave very good agreement between the PBE-40HF carbon shift (using PBE0/def-TZVPP structure) and experiment. The surprisingly good performance of PBE-40HF without kernel for **1–4** and **6** and the overestimate for **7** are documented in Table 3. The rather small experimental database of U(VI)-bound carbon atoms with significant dependence on EXX admixture did not allow a more accurate calibration without kernel contribution in ref. 12, and it hinders also the selection of a best functional in the presence of a kernel. Results for **1** and **2** are slightly deteriorated in the presence of the kernel. In view of the negligible dependence on EXX admixture, simple adjustment of the latter would not allow an improvement. For **3**, the computed shift decreases slightly more with larger EXX values, but good agreement with experiment (<10% deviation) would require 40% or more EXX admixture. Note that modelling of the lithium counter-ion interactions changes the shift only little (below 5 ppm). This contrasts to complex **4**, where the free anion has a much lower shift (by about −140 ppm, Fig. 4). The differences may be traced to an almost negligible change of the U–C bond length for **3** but a large increase for **4** (by 0.12 Å on average, Table S2, ESI†), emphasizing again the importance of structure. Increased shifts with larger EXX admixtures pertain to the more covalently bound complexes **4–7** (see above). While PBE0 provides excellent agreement with experiment for **5** and **6** (in fact better than PBE-40HF without kernel, Table 3), lower admixtures of around 10 and 15% would provide better agreement for **4** and **7**, respectively. The uncertainties of the interactions within the contact-ion pair **4** in the condensed-phase environment (see ref. 68 for solvent effects on ion-pair separation and ^{77}Se and ^{125}Te shifts in some thorium and uranium complexes), and the extreme structure dependence of the ^{13}C shift (along with absence of an experimental structure) for **7** (Fig. 4) make the latter two systems less useful as benchmarks. Finally, the relatively modest SO contributions for **8** decrease with larger EXX admixture, and a value somewhat above the 25% of PBE0 would seem to provide best performance. We see therefore that the few available experimental data and a seemingly non-systematic behaviour render our choice of a functional clearly more difficult than for typical transition-metal hydride complexes.[7,14] A similarly difficult situation regarding the performance of DFT for ligand chemical shifts in actinide complexes has been identified for

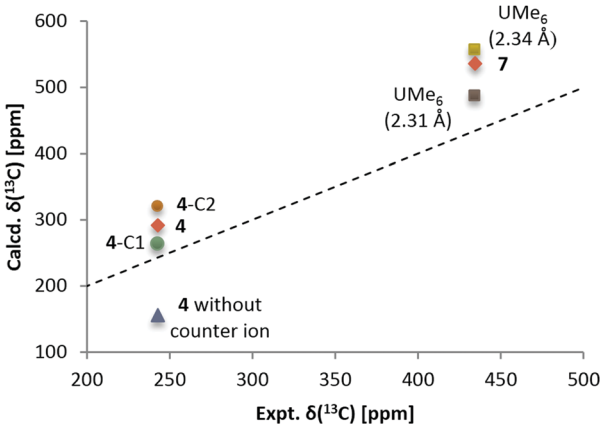

Fig. 4 Calculated ^{13}C shifts with XC kernel and PBE0 functional compared to experiment for **4** and **7**. The dashed line represents ideal agreement with experiment. Cycles represent the two appreciably different calculated ^{13}C shifts in **4** for two non-equivalent carbon atoms (the diamond gives the average). The triangle represents data for an anion-separated species of **4** ($[UO_2(CH_2SiMe_3)_4]^{2-}$), giving a much shielded carbon shift. Squares represent the truncated (hexamethyl) model **7′** with either PBE0-D3 optimized (2.34 Å) or artificially shortened (2.31 Å) U–C bonds. The extreme dependence on bond length may explain the overestimated shifts for the hexaalkyl complex **7** at PBE0 level.

^{19}F shifts of uranium fluoro–chloro complexes where, however, SO effects play no appreciable role.[69] Nevertheless, the standard functional PBE0 seems to perform overall well for the best-documented and -justified experimental values (Table 3, see also Fig. 5). While this level tends to overestimate the shifts somewhat for most of the complexes, it seems to be the best compromise for systems with a positive or negative dependence of the shift on EXX admixture (15% EXX would perform better for the former, 40% for the latter).

Predictions of unknown ^{13}C shift values in known organometallic uranium(VI) complexes

In an attempt to aid in widening the experimental database, Table 4 provides some ^{13}C shift predictions for carbon atoms

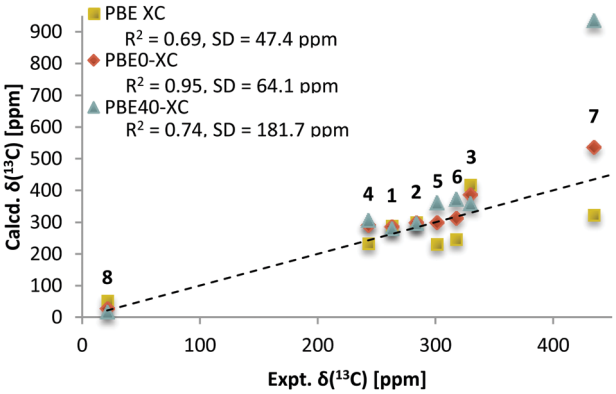

Fig. 5 Calculated ^{13}C shifts with XC kernel and variable EXX admixture (yellow squares: 0%, red diamonds: 25%, blue triangles: 40%) compared to experiment for complexes **1–8** (*cf.* Table 3 for numerical values). The dashed line represents ideal agreement with experiment. Averaged data for two non-equivalent alkyl carbon atoms in **4** are shown.

bonded to a uranium(VI) center for the experimentally known complexes **9–14** (Fig. 6) where, however, the ^{13}C signals so far could not be detected experimentally. As an overestimate is expected at the PBE0 level for those complexes, where the shifts decrease with increasing EXX admixture Table 4 contains also PBE-40HF results for these species. Together with the PBE results, the EXX dependence can again be extracted.

Complex **9** is electronically related to the NHC complexes **1** and **2**, and consequently the predicted ^{13}C NMR shift for the U(VI)-bound carbon atoms is in the same range around 270 ppm (Table 4). It is unclear if attempts to measure this shift have been made.[70] In contrast, complexes **10–14** have been reported during the last 4 years. Together with **5** (*cf.* Fig. 1), Lewis *et al.*[65] also analysed the analogous alkinyl complex **10**. No ^{13}C signal was found for the U(VI)-bound carbon atom. Given the good agreement of PBE0-XC data with experiment for **5** (Table 3), the predicted high-frequency shift of ~400 ppm at this level for **10** should be accurate. The larger value compared to **5** is not due to much larger SO shifts but caused by larger paramagnetic contributions (*cf.* Table S6 in ESI†). In fact, this increase is typical for going from an alkyl to an alkinyl ligand, more or less independently from the metal center.

Carbene complex **11** was analyzed[59] together with the structurally related methanide complex **8** which, however, has a much weaker and less covalent U–C interaction to the central carbon atom (*cf.* Table 5). The two complexes exhibit decreasing shift with increasing EXX admixture (Tables 3 and 4), with significantly larger SO effects and thus a larger shift for the carbene complex **11**. The PBE0 result of about 190 ppm can be expected to be slightly overestimated, our best prediction is thus closer to the PBE-40HF value of about 150 ppm. Increasing SO effects with larger EXX admixture are found for the related carbene complex **12** (Table 4). Due to very large paramagnetic and sizeable SO contributions a relatively high overall shift value of 370 ppm is predicted.

A much shorter U–C bond length in **12** compared to **11** (2.14 Å *vs.* 2.36 Å) is found, attributable to the well-known inverse *trans* influence (ITI) of the U=O bond.[68] No signal has been found experimentally, but the spectral region that was considered is unclear. In case of the related carbene complex **13**,[57] measurement ranged only up to 400 ppm. Here the calculations (on a slightly truncated model with methoxy for *t*-butoxy groups, changing the PBE-level shifts by only 12 ppm) predict a much larger carbon shift at the PBE0 level, with extremely large SO effects and a positive dependence on EXX admixture (Table 4). Even if the PBE0 value may overshoot notably in such cases (*cf.* **7** and **4** in Table 3), a ^{13}C shift in the 550–620 ppm range seems likely. This prediction would not only be outside the measurement range but also provides a value at the very high-frequency end of known ^{13}C shifts for a diamagnetic compound.[73,74] A re-measurement of **13**, possibly with a ^{13}C-enriched carbene ligand, will be very interesting. However, we noted some irregularities for this complex in our computations: all optimized U–L bond-lengths for a singlet U(VI) ground-state differ notably from those found in the X-ray structure (*cf.* Tables S2 and S3 in ESI† and ref. 75), irrespective of the DFT functional, dispersion forces and alkoxy groups used

Table 4 Calculated ^{13}C NMR shifts (in ppm *vs.* TMS; computed with XC kernel) for uranium-bonded carbon atoms in further synthetically known complexes (SO contributions in parentheses)[a]

Complex	δ^{xc}_{2c} (PBE)		δ^{xc}_{2c} (PBE0)		δ^{xc}_{2c} (PBE-40HF)		Exp.
9	298.3	(100.7)	276.7	(73.0)	267.6	(61.6)	[70,c]
10	368.2	(163.6)	426.0	(223.2)	—	—	[65,c]
11	256.5	(96.2)	190.7	(72.3)	146.3	(54.3)	[59,c]
12	296.8	(73.2)	372.5	(100.0)	—	—	[71,c]
13[b]	417.4	(164.5)	702.1	(390.5)	—	—	[58,d]
14	278.0	(76.6)	220.4	(59.0)	179.9	(46.0)	[72,e]

[a] 2c-ZORA-SO results with TZ2P basis sets. See Fig. 6 for the structures of **9–14**. [b] Data computed for slightly truncated complex: O^{t}Bu replaced by OMe. [c] Spectral region of measurements unknown. [d] No signal found in the measurement range up to 400 ppm. [e] No signal found between −200 ppm and +1000 ppm.

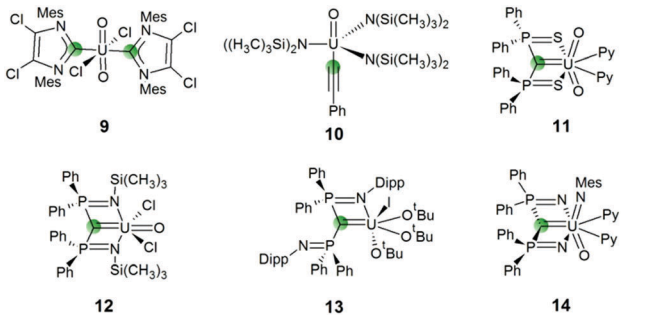

Fig. 6 Further experimentally known organometallic uranium(VI) complexes with undetermined ^{13}C NMR shifts for uranium-bound carbon nuclei (highlighted in green).

Table 5 Quasi-relativistically optimized U–C distances, compositions of the U–C σ-bonding NLMOs, QTAIM delocalization indices (DI), and SO contributions to ^{13}C shielding (σ^{SO}) for **1–14** (complexes are separated into two groups, where increasing EXX admixture decreases or increases the SO contributions to the shifts)[a]

	d(U–C)[b] [Å]	NLMO[c] %U	%U(d)	%U(f)	%C	%C(s)	%C(p)	DI(U–C)[c]	σ^{SO}[d]
1	2.63	16.4	49	32	79.9	44	56	0.366	−77.7
2	2.61	14.9	47	33	80.7	40	60	0.374	−62.2
3	2.48	22.2	43	40	75.0	40	60	0.550	−169.0
8	2.64	15.3	49	43	75.4	8	92	0.420	−12.6
9	2.61	16.3	47	32	80.6	44	56	0.387	−72.1
11	2.36	21.5	52	42	70.2	20	80	0.792	−71.4
14	2.37	20.9	47	49	69.7	18	82	0.779	−58.2
4	2.46	22.1	34	53	74.6	22	78	0.644	−212.0
5	2.30	28.5	24	73	66.0	25	75	0.869	−171.9
6	2.28	27.7	25	72	64.7	20	80	0.937	−136.5
7	2.32	28.7	25	68	69.2	22	78	0.844	−362.7
10	2.29	28.9	34	60	68.2	49	51	0.767	−222.3
12	2.14	30.8	21	77	62.7	18	82	1.224	−99.1
13	2.22	28.2	26	68	67.7	31	69	1.251	−390.0

[a] See Computational methods. The separation of the complexes into two groups is explained in the text. [b] Data for PBE0-D3 structures. [c] PBE0/ECP/TZVP results. [d] 2c-ZORA-SO/PBE0-XC/TZ2P results for U(VI)-bonded carbon atoms.

(*e.g.* the longest U–C bond found at the PBE/def2-TZVP level, d(U–C) = 2.32 Å, is still by 0.13 Å shorter than that found in the solid-state structure of **13**).

Excellent agreement between computed and experimental structure data for **13** was achieved by considering a triplet ground-state, revealing a U(IV) nature of the central metal in the X-ray structure.[75] This is also supported by the fact that the triplet U(IV) structure lies energetically lower than the corresponding closed-shell U(VI) structure by *ca.* 13 kJ mol^{-1}. Based on this small energetic gap, it is reasonable to assume that in solution the diamagnetic U(VI) complex **13** may exist in an equilibrium with the U(IV) species, as also supported by NMR data in ref. 58. The NMR spectra suggest the presence of a uranium-reduced "impurity" (tentatively assigned to a U(V) species) along with the diamagnetic U(VI) complex **13**. More detailed experimental studies might, however, be hindered due to instability of this complex, accompanied by the liberation of iodine.

Finally, the most recent carbene complex **14** in our selection exhibits a behaviour more similar to **11**: SO effects are more moderate and decrease with larger EXX admixture. A ^{13}C shift near 180 ppm, similar to that predicted for **11**, seems most likely. In this case, the spectral range from −200 to +1000 ppm had been scanned without finding a ^{13}C carbene signal.[72] It cannot be excluded that the shift may have fallen into the region of aromatic carbon atoms and thus gone unnoticed. As all of the non-detected actinide-bonded ^{13}C shifts correspond to carbon atoms without hydrogen substituents, the missing signals could also be rationalized by their lower sensitivity (impossibility of direct ^{1}H decoupling) and a ^{13}C enrichment of the ligands would help to detect the corresponding signals.

Rationalization of the observed trends by bonding analyses

To better understand the ^{13}C shifts, their relation to the U–C bond for complexes **1–14**, and also the dependence of computed shifts (particularly their SO contributions) on the EXX admixture in the functional, we have carried out bonding analyses, looking in particular at natural localized molecular orbitals (NLMOs) obtained at scalar relativistic level (Table 5). For convenience, the entries in the Table are separated into those cases, where increasing EXX admixture decreases or increases the SO contributions to the shifts (first and second group of complexes).

The longest U–C bonds (single bonds in **1**, **2**, **4**, **8**, **9**, an NHC "single bond" in **3**, and comparably long carbene double bonds in **11**, **14**) pertain generally to carbon atoms in equatorial position to a uranyl UO_2^{2+} unit (or to an isoelectronic UON^{+} moiety in **14**). Much shorter U–C bonds (Table 5) are found for systems with the carbon ligand in *trans* position with respect to an U=O bond (ITI: **5**, **6**, **10**, particularly the double bond in **12**) or for those, which possess no competing strong π-donor ligand (hexaalkyl complex **7** and carbene complex **13**, where the carbene ligand is the only strong π-donor). The bond lengths correlate closely with covalency, as indicated by the percentage uranium character (%U) in the corresponding σ-bonding NLMO (Table 5, plotted separately for U–C and U=C bonds in Fig. 7).

The separation made in Table 5 between complexes with negative and positive dependence of their (absolute) SO

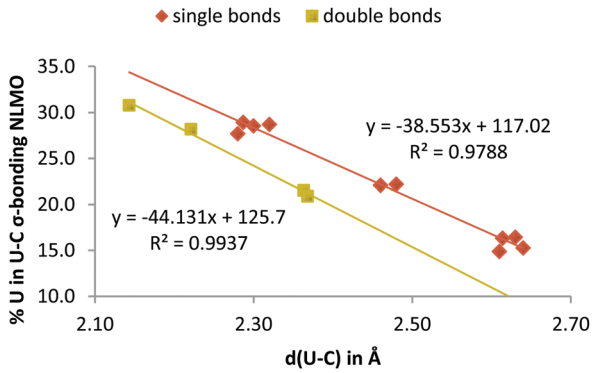

Fig. 7 Correlation between total uranium involvement in the U–C σ-bonding NLMO with U–C bond length, with separate regression lines for U–C single bonds (**1–10**, red diamonds) and carbene U=C double bonds (**11–14**, yellow squares). NHC complex **3** has been plotted with the single-bonded species.

contributions to the ^{13}C shifts on EXX admixture in the functional (*cf.* Tables 1, 3 and 4) can therefore be related to the position of the carbon atom in the complex: positions equatorial to an uranyl (or related) unit lead to a negative dependence, positions *trans* to a U=O bond or the absence of competing strong π-donor ligands in the system give a positive dependence. The recent uranyl-tetraalkyl "ate" complex **4** is the only exception to this rule and provides a borderline case: even though the alkyl ligands are positioned equatorially to a uranyl unit, their U–C bonds still have appreciable covalency (see NLMO composition and QTAIM delocalization index, DI, in Table 5), and the absolute SO contributions exhibit a positive dependence on EXX admixture (Tables 1 and 3).

Further insights are provided by analyzing the overall 5f- *vs.* 6d-orbital involvement in the U–C σ-bonding NLMO. This is shown in Fig. 8, which is ordered by increasing 5f-orbital involvement. Indeed, this ordering separates the investigated complexes into exactly the same groups as we chose for Table 5: the more covalent complexes clearly exhibit dominant 5f-orbital character of the U–C σ-bond (right side of Fig. 8), whereas the 6d-orbital character is comparably small here. In contrast, the less covalent complexes display clearly diminished 5f-orbital character and larger 6d contributions. Uranyl-tetraalkyl complex **4** is just on the borderline where the uranium 5f-orbitals start to make up more than 10% of the overall σ-bonding NLMO.

We may use this observation to provide a tentative rationalization of the at first sight non-systematic dependence of the SO-shifts on EXX admixture. Increasing EXX admixture renders the metal ligand bonds generally less covalent, due to reduction of self-interaction errors ("delocalization errors") in the functional (this is well-known also for transition-metal complexes).[76,77] For the less covalent cases (with predominantly equatorial position to a uranyl unit), the 6d-orbital character dominates the uranium contributions to the U–C σ-bond, and the 5f-orbital involvement is small. In these bonds increasing EXX admixture diminishes the SO contributions to the ^{13}C by interrupting the Fermi-contact pathway that transmits the SO-induced spin polarization from the heavy uranium center to the carbon nucleus.[3] In contrast, for the more covalent cases with dominant uranium 5f-orbital

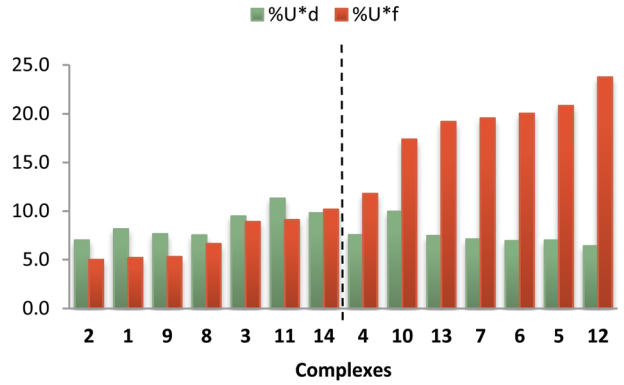

Fig. 8 Total d and f orbital involvement (uranium percentage in the U–C bonding times given orbital type contribution) in the U–C σ-bonding NLMO ordered by increasing f orbital contributions.

contributions to the bond, the possible main effects of larger EXX admixture are (a) increased SO matrix elements due to the larger uranium 5f-character of the MOs, and (b) increased SO terms due to enhanced polarization with larger EXX admixture. We have confirmed these assumptions by a computational experiment in which a finite Fermi-contact perturbation is placed at the carbon nucleus (such perturbations are often used for perturbational computations of SO shifts[5,6,11] or of spin–spin coupling constants[78]), and the delocalization of the induced spin density throughout the system is monitored as a function of EXX admixture (comparing PBE, PBE0, PBE-40HF functionals). The results are provided in ESI† (Table S13 gives Mulliken atomic spin densities and Fig. S1 isosurface plots of the induced spin density). Larger EXX admixture reduces the induced spin density at uranium for **3**, consistent with lowered SO-contributions to the shifts for this complex. In contrast, **4** represents the second class of complexes, where larger EXX admixture enhances the SO shifts, and indeed the induced spin density at uranium increases in this case, consistent with the abovementioned increased polarization.

While these analyses allow us to understand the dependence of SO shifts on EXX admixture, we still need to provide some appreciation of the rather large variations of SO shifts, and of ^{13}C shifts in general, for the different complexes. The 5f-orbital covalency arguments and position of the carbon ligand relative to strong π-donor ligands in a given complex, as discussed above, give a general framework, as roughly speaking the overall SO shifts are larger for the complexes in the second (bottom) half of Table 5 compared to the first (upper) half. However, to understand the trends in more detail, other aspects have to be considered as well: the by far largest SO shifts (and the largest dependence on the functional) are found for carbene complex **13** and hexaalkyl complex **7** (Table 5). These two systems share the absence of other strong π-donor ligands in the complex and are obviously at the limits of stability of U(VI) complexes (see also discussion above). This is for instance reflected by the relatively small HOMO–LUMO gap of **13** (2.1 eV at PBE0/TZ2P level), only half of that for the other complexes. This gives rise to relatively small energy denominators, enhancing the SO contributions as well as the paramagnetic contributions which are particularly large as well (Table 4). **7** does not exhibit a conspicuously small HOMO–LUMO gap but a relatively large uranium 5f-orbital and simultaneously large carbon AO participation in the three highest occupied and also in the low-lying virtual MOs. This enhances in particular the SO contributions to the NMR shielding.

Among the first group of complexes in Table 5, **3** features the by far largest overall SO shifts (even though they decrease with increasing EXX admixture, see above). This seems to be due to a comparably small HOMO–LUMO gap in combination with high uranium 5f-character and equally high carbon 2s-character in the U–C bond to this NHC ligand, in spite of the equatorial position to a uranyl group, which overall diminishes the U–C bond covalency. **3** may be contrasted against the carbene complexes **11** and **14** (the latter two possessing a double-bond U═C character), which feature shorter U–C bonds and even larger covalency but much smaller SO shifts (Table 5). Here the low carbon 2s-character in the U–C bond of only about 20% compared to 40% in **3** is particularly notable. Caused by the large P–C–P angle of this type of pincer carbene ligand (149° and 150° for **11** and **14**, respectively), the low carbon 2s-character in the bond reduces the effectiveness of the Fermi-contact mechanism for transferring SO-induced spin polarization to the carbon nucleus.[3] This effect is even more notable for the methanide complex **8**: while its overall covalency (%U character and DI in Table 5) is not much lower than for the other complexes in the first group in Table 5, the carbon 2s-character of only 8% in the σ-bonding NLMO signals a particularly poor Fermi-contact spin-density transfer and thus explains the smallest SO shifts in the entire set of complexes studied here. The different influences may also compensate to the extent that similar SO shifts arise for rather different bonding situations. For example, the equatorial imidazolyl ligands in **1**, **2**, **9** feature relatively long U–C bonds with low covalency and uranium 5f-character in the bond, but carbon 2s-contributions of about 40%. They have similar SO shifts as the much more covalent complexes **11**, **14** (featuring much larger uranium 5f-character in the σ-bonding NLMO), due to the abovementioned low carbon 2s-character of only about 20% for these pincer carbene complexes.

Most of the complexes of the second group (Table 5) have very large SO shifts in spite of carbon 2s-contributions of only about 20%. Here it is clearly the large covalency and uranium 5f-character in the bond and relatively high-lying occupied MOs that cause the large SO effects. In analogy to complex **8** the carbene complex **12** exhibits comparably low carbon 2s-character due to the pincer-type geometry and consequently has the clearly lowest SO shifts in the second group of complexes. The acetylide complex **10** represents an outlier: it naturally exhibits particularly large carbon 2s-character in the bond but somewhat diminished uranium 5f-character. In fact, the large carbon 2s-character in the C–U bond in **10** causes the associated canonical MOs (mostly HOMO−11, compared to HOMO−3 for **5**) to be very low in energy, leading to relatively large energy denominators in the perturbation expressions, and thus diminished SO contributions.

Revised predictions of ^{1}H shifts in uranium(VI) hydride complexes

The main goal of ref. 12 had been the prediction of ^{1}H shifts of hypothetical uranium(VI) hydride complexes, based on the method calibration done for known ^{13}C values. Using PBE-40HF without kernel as "best functional" then led to the prediction[12] of record high-frequency ^{1}H shifts for so far unknown uranium(VI) hydride complexes, far above the highest-frequency ^{1}H shifts around 20 ppm for diamagnetic compounds.[13] Here we thus have to re-examine these predictions in light of the missing XC kernel in the older ADF implementation (see Fig. 9 for the selected systems, encompassing both unrealistic small models and more realistic target complexes for potential synthesis). We now use consistently PBE0-D3 structures, and thus even PBE-40HF results without kernel deviate somewhat from the values in ref. 12 (by about 4 ppm). Table 6 compares these data with PBE and PBE0 2-component ZORA and PBE 4-component mDKS results, all including a proper kernel treatment. As the U–H bonds exhibit similar covalent bonding character as the σ-bonded U–C bonds above, it is no surprise that the kernel contributions increase the ^{1}H shifts appreciably for a given functional (see Table S14 in ESI†). And as in the abovementioned ^{13}C cases, the effect of the kernel is largest for the overall largest shifts.[12] Dependence of the ^{1}H SO shifts also follows the same patterns as analysed above for the ^{13}C shifts: hydrides in equatorial position to a uranyl or related RN═U═NR moiety exhibit decreasing absolute SO shifts with increasing EXX admixture (**18–22**), whereas the opposite trend is found for complexes with a hydride ligand in *trans* position to a U═O bond (**23**) or in the absence of a strong π-donor ligand (**15–17**). The synthetically less likely model complexes **15–17** without strong π-donors exhibit the same large sensitivity to the input structure (Table S15, ESI†) and EXX admixture as complex **7** above. Here we may expect that PBE0 calculations with kernel may overshoot significantly. However, even if we take the PBE values as lower bound, extremely large ^{1}H shifts between 170 ppm for **16**, **17** and 265 ppm for **15** are predicted far outside the known ^{1}H shift range of diamagnetic compounds.

The hypothetical uranium(VI) hydride **23** is closely related to complexes **5** and **6** (and **10**; *cf.* Fig. 1, 6, and 9), and we may expect similar performance of our methodology as for the ^{13}C

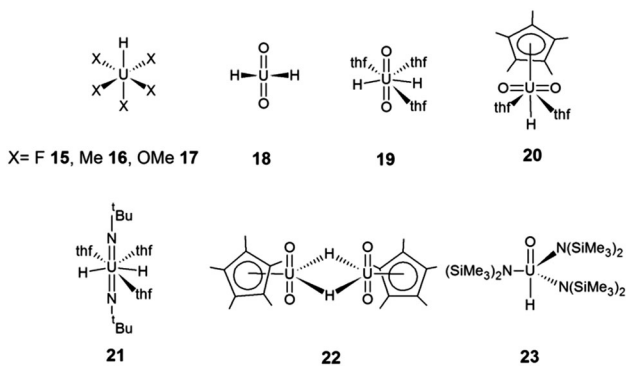

Fig. 9 Model uranium(VI) hydrides.

Table 6 Predicted hydride ^{1}H NMR shifts (*vs.* TMS in ppm) for uranium(VI) hydride complexes. SO contributions are given in parentheses[a]

	δ_{2c} (PBE-40HF)		δ_{2c}^{xc} (PBE)		δ_{2c}^{xc} (PBE0)		δ_{4c}^{xc} (PBE)
15	443.4	(445.6)	265.5	(263.7)	603.7	(606.8)	251.8
16	267.3	(253.8)	171.0	(153.4)	336.6	(321.1)	163.8
17	282.2	(280.2)	178.4	(172.6)	348.8	(346.2)	174.0
18	55.7	(42.3)	132.2	(120.7)	87.3	(74.3)	136.9
19	90.7	(81.6)	212.1	(207.8)	163.4	(156.2)	209.4
20	58.1	(45.3)	93.9	(84.7)	83.2	(71.5)	95.4
21	60.2	(48.7)	124.8	(114.0)	84.1	(72.2)	122.6
22	39.0	(26.6)	55.6	(50.4)	49.8	(39.6)	57.3
23	142.5	(144.5)	117.6	(108.5)	170.5	(169.1)	115.2

[a] 2c-ZORA-SO/TZ2P results (see Computational details).

shifts in these systems, where PBE0 with kernel provided excellent agreement with experiment. We thus regard the predicted ^{1}H shift of about +170 ppm (with almost the same magnitude of the SO contributions; Table 6) as accurate. Given the ITI provided by the *trans* U═O group,[65] **23** may be a particularly promising target system and would already extend the known ^{1}H shift range dramatically!

As **18** and the more realistic target complexes **19–22** exhibit smaller sensitivity to the input structure and decreasing SO-shifts with increasing EXX admixture (comparable to the ^{13}C shifts of **3** above, *cf.* Table 3), we may expect to overshoot the ^{1}H shifts somewhat at PBE0 level, approaching the exact value from above with increased EXX admixture. In keeping with our analyses for the ^{13}C shift cases (**1–3**, **8**, **9**, **11**, **14**) above, less dramatic high-frequency shifts in the range of about 30–70 ppm are expected for these equatorial hydrides, albeit still generally far above the known ^{1}H shift range. Among these five complexes, **19** is a clear outlier, predicted to have a much larger shift than the other four systems.

PBE0 with kernel generally provides larger hydride ^{1}H shifts for all complexes in Table 6 than PBE-40HF without kernel. As the electronic structure of these hydride complexes suggests that PBE0 with kernel may actually overshoot somewhat in most cases, in particular for the equatorial hydrides (**23** may be an exception, where PBE0 with kernel should be more accurate), our previous predictions[12] seem reasonable, even though they had been obtained by a fortuitous compensation between missing kernel and too large EXX admixture. In any case the prediction of unprecedented high-frequency ^{1}H shift ranges for uranium(VI) hydride complexes is upheld, and we can place substantially more confidence into these predictions than hitherto, as we better understand the interplay between molecular and electronic structure and functional. We finally note again the very good agreement between 2-component ZORA and 4-component mDKS results at PBE level when the XC response kernel contributions to the shielding are either included or neglected in both approaches (Table 2).

Chemical-shift anisotropies

Tables S16 and S17 in ESI† provide the computed principal components of ^{13}C and ^{1}H shift tensors (PBE0 level with kernel), respectively, for the complexes studied in this work.

The results confirm our expectation of very large shift anisotropies in many cases, in particular for those species where SO effects lead also to particularly large isotropic shifts (the anisotropy values range from several tens of ppm up to about 700 ppm for both ^{1}H and ^{13}C nuclei).

These shift tensors could be probed by suitable solid-state experiments in the future. Notably, very large chemical-shift anisotropies (CSAs) could lead to fast relaxation processes, in particular in solution.[79,80] This could also explain some of the "non-observed" ^{13}C signals for carbon nuclei directly bound to uranium in some of the synthetically known complexes. Possibly, this could also have been a reason for a lack of observation of ^{1}H signals for uranium(VI) hydride complexes. In any case, CSA-induced relaxation processes may have to be kept in mind in experimental studies of such species.

Conclusions

While our previous predictions of giant ^{1}H NMR shifts in closed-shell uranium(VI) hydride complexes and of also extremely large spin–orbit-induced ^{13}C shifts for uranium(VI)-bound carbon atoms had been obtained without consideration of the exchange–correlation kernel in two-component ZORA DFT calculations, our present study confirms these unusual predictions when the kernel is properly accounted for. The EXX admixture needed to reproduce known spin–orbit-dominated ^{13}C shifts in such species is then reduced considerably, compared to the previous study, from about 40% without kernel to a compromise value closer to 25% with kernel. The overall predicted range for unknown shifts with the revised approach is retained. That is, we still predict ^{1}H hydride shifts in uranium(VI) hydride complexes between 30 ppm and more than 200 ppm, maybe up to 170 ppm for the most realistic target complexes. This is clearly outside the known ^{1}H shift range for diamagnetic systems. Very large spin–orbit induced ^{13}C shifts for uranium-bound carbon atoms are also confirmed, and predictions have been made for complexes that are synthetically known, but where these carbon shifts so far had not been found. In one known pincer carbene complex, an extremely large shift beyond 550 ppm has been predicted.

The present analyses provide much tighter confidence ranges for the predicted shifts than obtained previously, due to improved understanding achieved for dependences on structure, bonding type, and functional. Notably, we find appreciable dependencies on (a) the overall covalency of the U–C bond, (b) the uranium 5f-orbital character in the bond, but also (c) the carbon 2s-contributions to the bonding NLMO. While the latter aspect may be rationalized by known Fermi-contact-type mechanisms for SO-induced shifts, the 5f-participation is crucial due to SO matrix elements. We find furthermore a clear dependence on the position of the carbon atom in question within a given complex: equatorial positions relative to strong π-donor uranyl or related groups lead to a negative dependence of absolute SO-shifts on EXX admixture in the functional (further insights into these aspects have also been provided) and tend to generally reduce covalency and shifts. Particularly large NMR shifts are found in the absence of strong π-donor ligands in the complex (unfortunately for the possible identification of uranium(VI) hydrides, this will likely also render the complexes less stable) and also for U–C or U–H bonds in *trans* position to a U═O bond. These qualitative findings should enable a more meaningful design, and will help also in the experimental characterization of suitable target complexes by NMR spectroscopy.

Acknowledgements

AHG thanks Fonds der chemischen Industrie for a PhD scholarship. Funding from the Berlin DFG excellence cluster on Unifying Concepts in Catalysis is gratefully acknowledged. JA acknowledges support from the U.S. Department of Energy, Office of Basic Energy Sciences, Heavy Element Chemistry program, under grant DE-SC0001136 (formerly DE-FG02-09ER16066).

References

1 P. Pyykkö, A. Görling and N. Rösch, *Mol. Phys.*, 1987, **61**, 195–205.
2 M. Kaupp, in *Relativistic Electronic Structure Theory II: Applications*, ed. P. Schwerdtfeger, Elsevier, Amsterdam, 2004, pp. 552–597.
3 M. Kaupp, O. L. Malkina, V. G. Malkin and P. Pyykkö, *Chem. – Eur. J.*, 1998, **4**, 118–126.
4 Y. Nomura, Y. Takeuchi and N. Nakagawa, *Tetrahedron Lett.*, 1969, **10**, 639–642.
5 O. L. Malkina, B. Schimmelpfennig, M. Kaupp, B. A. Hess, P. Chandra, U. Wahlgren and V. G. Malkin, *Chem. Phys. Lett.*, 1998, **296**, 93–104.
6 V. G. Malkin, O. L. Malkina and D. R. Salahub, *Chem. Phys. Lett.*, 1996, **261**, 335–345.
7 P. Hrobárik, V. Hrobáriková, F. Meier, M. Repiský, S. Komorovský and M. Kaupp, *J. Phys. Chem. A*, 2011, **115**, 5654–5659.
8 P. Garbacz, V. V. Terskikh, M. J. Ferguson, G. M. Bernard, M. Kędziorek and R. E. Wasylishen, *J. Phys. Chem. A*, 2014, **118**, 1203–1212.
9 A. Bagno and G. Saielli, *Phys. Chem. Chem. Phys.*, 2011, **13**, 4285–4291.
10 M. Kaupp and O. L. Malkina, *J. Chem. Phys.*, 1998, **108**, 3648–3659.
11 J. Vaara, O. L. Malkina, H. Stoll, V. G. Malkin and M. Kaupp, *J. Chem. Phys.*, 2001, **114**, 61–71.
12 P. Hrobárik, V. Hrobáriková, A. H. Greif and M. Kaupp, *Angew. Chem., Int. Ed.*, 2012, **51**, 10884–10888.
13 B. C. Parkin, J. R. Clark, V. M. Visciglio, P. E. Fanwick and I. P. Rothwell, *Organometallics*, 1995, **14**, 3002–3013.
14 A. H. Greif, P. Hrobárik, V. Hrobáriková, A. V. Arbuznikov, J. Autschbach and M. Kaupp, *Inorg. Chem.*, 2015, **54**, 7199–7208.
15 J. Vícha, J. Novotný, M. Straka, M. Repisky, K. Ruud, S. Komorovsky and R. Marek, *Phys. Chem. Chem. Phys.*, 2015, **17**, 24944–24955.
16 S. K. Wolff and T. Ziegler, *J. Chem. Phys.*, 1998, **109**, 895–905.
17 S. K. Wolff, T. Ziegler, E. van Lenthe and E. J. Baerends, *J. Chem. Phys.*, 1999, **110**, 7689–7698.

18 L. A. Seaman, P. Hrobárik, M. F. Schettini, S. Fortier, M. Kaupp and T. W. Hayton, *Angew. Chem., Int. Ed. Engl.*, 2013, **52**, 3259–3263.
19 Amsterdam Density Functional (ADF) version 2012.01, SCM, Theoretical Chemistry, Vrije Universiteit, Amsterdam, Netherlands, 2012, available from http://www.scm.com.
20 J. Autschbach, *Mol. Phys.*, 2013, **111**, 2544–2554.
21 S. Komorovský, M. Repiský, O. L. Malkina, V. G. Malkin, I. Malkin Ondík and M. Kaupp, *J. Chem. Phys.*, 2008, **128**, 104101.
22 A. Wodyński, M. Repiský and M. Pecul, *J. Chem. Phys.*, 2012, **137**, 14311.
23 V. Arcisauskaite, J. I. Melo, L. Hemmingsen and S. P. A. Sauer, *J. Chem. Phys.*, 2011, **135**, 44306.
24 S. Komorovsky, M. Repisky, K. Ruud, O. L. Malkina and V. G. Malkin, *J. Phys. Chem. A*, 2013, **117**, 14209–14219.
25 *Turbomole, version 6.3.1*, a development of University of Karlsruhe and Forschungszentrum Karlsruhe GmbH, 1989-2007, TURBOMOLE GmbH, since 2007, available from http://www.turbomole.com.
26 X. Cao and M. Dolg, *THEOCHEM*, 2004, **673**, 203–209.
27 F. Weigend and R. Ahlrichs, *Phys. Chem. Chem. Phys.*, 2005, **7**, 3297–3305.
28 J. P. Perdew, K. Burke and M. Ernzerhof, *Phys. Rev. Lett.*, 1997, **78**, 1396.
29 J. P. Perdew and Y. Wang, *Phys. Rev. B: Condens. Matter Mater. Phys.*, 1992, **45**, 13244–13249.
30 A. D. Becke, *Phys. Rev. A: At., Mol., Opt. Phys.*, 1988, **38**, 3098–3100.
31 C. Lee, W. Yang and R. G. Parr, *Phys. Rev. B: Condens. Matter Mater. Phys.*, 1988, **37**, 785–789.
32 S. Grimme, S. Ehrlich and L. Goerigk, *J. Comput. Chem.*, 2011, **32**, 1456–1465.
33 S. Grimme, J. Antony, S. Ehrlich and H. Krieg, *J. Chem. Phys.*, 2010, **132**, 154104.
34 M. Ernzerhof and G. E. Scuseria, *J. Chem. Phys.*, 1999, **110**, 5029–5036.
35 S. Grimme, *J. Comput. Chem.*, 2004, **25**, 1463–1473.
36 D. N. Laikov, *Chem. Phys. Lett.*, 1997, **281**, 151–156.
37 A. E. Hansen and T. D. Bouman, *J. Chem. Phys.*, 1985, **82**, 5035–5047.
38 S. H. Vosko, L. Wilk and M. Nusair, *Can. J. Phys.*, 1980, **58**, 1200–1211.
39 A. Klamt and V. Jonas, *J. Chem. Phys.*, 1996, **105**, 9972–9981.
40 A. Klamt, *J. Phys. Chem.*, 1995, **99**, 2224–2235.
41 A. Klamt and G. Schüürmann, *J. Chem. Soc., Perkin Trans. 2*, 1993, 799–805.
42 ReSpect, version 3.4.2 (2015) – Relativistic Spectroscopy DFT program of authors M. Repisky, S. Komorovsky, V. G. Malkin, O. L. Malkina, M. Kaupp and K. Ruud, with contributions from R. Bast, U. Ekstrom, M. Kadek, S. Knecht, L. Konečný, E. Malkin and I. Malkin-Ondík, see http://www.respectprogram.org.
43 G. A. Aucar, T. Saue, L. Visscher and H. J. A. Jensen, *J. Chem. Phys.*, 1999, **110**, 6208–6218.
44 W. Kutzelnigg, *J. Comput. Chem.*, 1999, **20**, 1199–1219.
45 C. Adamo and V. Barone, *Chem. Phys. Lett.*, 1998, **298**, 113–119.
46 K. G. Dyall, *Theor. Chem. Acc.*, 2007, **117**, 491–500.
47 W. Kutzelnigg, U. Fleischer and M. Schindler, *NMR—Basic Principles and Progress*, Springer Verlag, Berlin, 23rd edn, 1991, p. 165.
48 M. J. Frisch, G. W. Trucks, H. B. Schlegel, G. E. Scuseria, M. A. Robb, J. R. Cheeseman, G. Scalmani, V. Barone, B. Mennucci, G. A. Petersson, H. Nakatsuji, M. Caricato, X. Li, H. P. Hratchian, A. F. Izmaylov, J. Bloino, G. Zheng, J. L. Sonnenberg, M. Hada, M. Ehara, K. Toyota, R. Fukuda, J. Hasegawa, M. Ishida, T. Nakajima, Y. Honda, O. Kitao, H. Nakai, T. Vreven, J. A. Montgomery, Jr., J. E. Peralta, F. Ogliaro, M. Bearpark, J. J. Heyd, E. Brothers, K. N. Kudin, V. N. Staroverov, R. Kobayashi, J. Normand, K. Raghavachari, A. Rendell, J. C. Burant, S. S. Iyengar, J. Tomasi, M. Cossi, N. Rega, J. M. Millam, M. Klene, J. E. Knox, J. B. Cross, V. Bakken, C. Adamo, J. Jaramillo, R. Gomperts, R. E. Stratmann, O. Yazyev, A. J. Austin, R. Cammi, C. Pomelli, J. W. Ochterski, R. L. Martin, K. Morokuma, V. G. Zakrzewski, G. A. Voth, P. Salvador, J. J. Dannenberg, S. Dapprich, A. D. Daniels, O. Farkas, J. B. Foresman, J. V. Ortiz, J. Cioslowski and D. J. Fox, *Gaussian 09, revision A.02*, Gaussian, Inc., Wallingford CT, 2009.
49 A. Schäfer, C. Huber and R. Ahlrichs, *J. Chem. Phys.*, 1994, **100**, 5829–5835.
50 X. Cao, M. Dolg and H. Stoll, *J. Chem. Phys.*, 2003, **118**, 487–495.
51 E. D. Glendening, J. K. Badenhoop, A. E. Reed, J. E. Carpenter, J. A. Bohmann, C. M. Morales, F. Weinhold, *NBO 5.0*, Theoretical Chemistry Institute, University of Wisconsin, Madison, 2001.
52 E. D. Glendening, J. K. Badenhoop, A. E. Reed, J. E. Carpenter, J. A. Bohmann, C. M. Morales, C. R. Landis and F. Weinhold, *NBO, versions 5.9 and 6.0*, Theoretical Chemistry Institute, University of Wisconsin, Madison, WI, 2013, available from http://nbo.chem.wisc.edu.
53 R. F. W. Bader, *Atoms in molecules: a quantum theory*, Clarendon Press, Oxford University Press, Oxford, New York, 1994.
54 R. F. W. Bader and M. E. Stephens, *J. Am. Chem. Soc.*, 1975, **97**, 7391–7399.
55 T. Lu, Multiwfn*: A Multifunctional Wave Function Analyzer, version 3.3.7*, 2015, available from http://multiwfn.codeplex.com.
56 T. Lu and F. Chen, *J. Comput. Chem.*, 2012, **33**, 580–592.
57 S. T. Liddle, *Angew. Chem., Int. Ed. Engl.*, 2015, **54**, 8604–8641.
58 O. J. Cooper, D. P. Mills, J. McMaster, F. Tuna, E. J. L. McInnes, W. Lewis, A. J. Blake and S. T. Liddle, *Chem. – Eur. J.*, 2013, **19**, 7071–7083.
59 J.-C. Tourneux, J.-C. Berthet, T. Cantat, P. Thuéry, N. Mézailles and M. Ephritikhine, *J. Am. Chem. Soc.*, 2011, **133**, 6162–6165.
60 M. J. Sarsfield, H. Steele, M. Helliwell and S. J. Teat, *Dalton Trans.*, 2003, 3443–3449.
61 J. Autschbach and T. Ziegler, *J. Chem. Phys.*, 2000, **113**, 9410–9418.
62 P. L. Arnold, I. J. Casely, Z. R. Turner and C. D. Carmichael, *Chem. – Eur. J.*, 2008, **14**, 10415–10422.
63 S. A. Mungur, S. T. Liddle, C. Wilson, M. J. Sarsfield and P. L. Arnold, *Chem. Commun.*, 2004, 2738–2739.

64 M. F. Schettini, G. Wu and T. W. Hayton, *Chem. Commun.*, 2012, **48**, 1484–1486.
65 A. J. Lewis, P. J. Carroll and E. J. Schelter, *J. Am. Chem. Soc.*, 2013, **135**, 13185–13192.
66 S. Fortier, N. Kaltsoyannis, G. Wu and T. W. Hayton, *J. Am. Chem. Soc.*, 2011, **133**, 14224–14227.
67 S. Fortier, J. R. Walensky, G. Wu and T. W. Hayton, *J. Am. Chem. Soc.*, 2011, **133**, 11732–11743.
68 D. E. Smiles, G. Wu, P. Hrobárik and T. W. Hayton, *J. Am. Chem. Soc.*, 2016, **138**, 814–825.
69 M. Straka and M. Kaupp, *Chem. Phys.*, 2005, **311**, 45–56.
70 W. J. Oldham Jr., S. M. Oldham, W. H. Smith, D. A. Costa, B. L. Scott and K. D. Abney, *Chem. Commun.*, 2001, 1348–1349.
71 D. P. Mills, O. J. Cooper, F. Tuna, E. J. L. McInnes, E. S. Davies, J. McMaster, F. Moro, W. Lewis, A. J. Blake and S. T. Liddle, *J. Am. Chem. Soc.*, 2012, **134**, 10047–10054.
72 E. Lu, O. J. Cooper, J. McMaster, F. Tuna, E. J. L. McInnes, W. Lewis, A. J. Blake and S. T. Liddle, *Angew. Chem., Int. Ed.*, 2014, **53**, 6696–6700.
73 J. Vícha, R. Marek and M. Straka, *Inorg. Chem.*, 2016, **55**, 1770–1781.
74 S. Takemoto, J. Ohata, K. Umetani, M. Yamaguchi and H. Matsuzaka, *J. Am. Chem. Soc.*, 2014, **136**, 15889–15892.
75 PBE0-D3/def2-TZVP optimized bond-lengths in complex **13** considering a singlet U(VI) ground-state: d(U–C) = 2.22 Å, d(U–N) = 2.26 Å, $d(\mathrm{U–O})_{\mathrm{avg.}}$ = 2.01 Å, d(U–I) = 3.03 Å; PBE0-D3/def2-TZVP optimized bond-lengths in complex **13** considering a triplet U(IV) ground-state: d(U–C) = 2.44 Å, d(U–N) = 2.36 Å, $d(\mathrm{U–O})_{\mathrm{avg.}}$ = 2.04 Å, d(U–I) = 3.10 Å; X-ray structure data: d(U–C) = 2.45 Å, d(U–N) = 2.36 Å, $d(\mathrm{U–O})_{\mathrm{avg.}}$ = 2.05 Å, d(U–I) = 3.11 Å.
76 M. Kaupp, R. Reviakine, O. L. Malkina, A. Arbuznikov, B. Schimmelpfennig and V. G. Malkin, *J. Comput. Chem.*, 2002, **23**, 794–803.
77 J. Autschbach and M. Srebro, *Acc. Chem. Res.*, 2014, **47**, 2592–2602.
78 V. G. Malkin, O. L. Malkina and D. R. Salahub, *Chem. Phys. Lett.*, 1994, **221**, 91–99.
79 R. E. Wasylishen, G. L. Neufeld and K. J. Friesen, *Inorg. Chem.*, 1981, **20**, 637–638.
80 B. E. Eichler, B. L. Phillips, P. P. Power and M. P. Augustine, *Inorg. Chem.*, 2000, **39**, 5450–5453.

Electronic Supplementary Material (ESI) for Physical Chemistry Chemical Physics.

Giant Spin-Orbit Effects on ^{1}H and ^{13}C NMR Shifts for Uranium(VI) Complexes Revisited: Role of the Exchange-Correlation Response Kernel, Bonding Analyses, and New Predictions

Anja H. Greif,[a] Peter Hrobárik,[a,*] Jochen Autschbach,[b] Martin Kaupp [a,*]

[a] *Institut für Chemie, Technische Universität Berlin, Strasse des 17. Juni 135, D-10623 Berlin, Germany.*

[b] *Department of Chemistry, University at Buffalo, State University of New York, Buffalo, NY, 14260, USA.*

peter.hrobarik@tu-berlin.de

martin.kaupp@tu-berlin.de

Electronic Supplementary Information

Table S1. Comparison of the compositions of the U–C σ-bonding NLMOs in selected U(VI) complexes with different NBO modules at PBE0 level [a]

	NBO 5.0 (ADF 2012)			NBO 6.0 (ADF 2014)			NBO 5.9 (G09)		
Complex	%U	%U(d)	%U(f)	%U	%U(d)	%U(f)	%U	%U(d)	%U(f)
1	9.3	12.2	58.8	16.3	49.9	33.8	16.4	49.5	31.5
4	15.3	12.3	71.7	21.0	29.9	56.6	22.1	34.1	53.3
5	28.0	8.6	88.4	28.9	23.5	75.0	28.5	24.5	73.0
6	27.8	8.9	88.3	28.5	26.0	71.4	27.7	25.0	72.3
7	23.1	9.3	82.1	28.7	25.8	67.0	28.7	24.7	68.1

[a] Scalar-relativistic results with def2-TZVP GTO (Gaussian 09) and TZ2P STO (ADF) basis sets at PBE0-D3-optimized structures.

Table S2. Optimized U–C bond lengths (in Ångstroms) with different functionals (with and without dispersion corrections) compared with experimental data [a]

Complex	PBE	PBE0	PBE0-D3	B3LYP	B3LYP-D3	Expt.
1	2.67	2.66	2.63	2.70	2.65	2.63 [S1]
2	2.66	2.66	2.61	2.70	2.62	–
3	2.50	2.50	2.48	2.52	2.49	2.50 [S2]
3[c]	–	–	2.48	–	–	–
4	2.49[b]	2.48[b]	2.48[b]	2.51[b]	2.49[b]	2.49[b],[S3]
4[c]	–	–	2.56	–	–	–
5	2.36	2.30	2.30	2.34	2.34	2.35 [S4]
6	2.35	2.27	2.28	2.32	2.32	2.28 [S5]
7	2.36	2.33	2.32	2.37	2.35	–
SD[d]	0.04	0.03	0.02	0.04	0.02	
8	–	–	2.64	–	2.65	2.65 [S6]
8'	–	–	2.72	–	–	–
9	–	–	2.62	–	2.62	2.62 [S7]
10	–	–	2.29	–	2.31	2.34 [S4]
11	–	–	2.36	–	2.37	2.43 [S6]
12	–	–	2.14	–	2.17	2.18 [S8]
13	2.32[e]	2.26[e]	2.22[e]	2.27[e]	2.24[e]	2.45 [S9]
14	–	–	2.37	–	2.38	2.40 [S10]
SD[d]	–	–	0.10	–	0.09	

[a] def2-TZVP basis set with small-core ECP for uranium, see Computational Details in main text. [b] Averaged data for two non-equivalent alkyl carbon atoms. [c] Only anionic part of the complex without Li^+ counter-ion(s) was considered. [d] Standard deviation. [e] Note that while the structure optimization was done for a U(VI) singlet ground-state, the X-ray structure of **13** feature all U–L bond-lengths characteristic for a U(IV) complex, in accordance with DFT calculations for a triplet structure (see Discussion in main text).

Table S3. Optimized U=O and U–N bond lengths (in Ångstroms) with different DFT functionals (with and without dispersion corrections), compared with experimental values [a]

	PBE0		PBE0-D3		B3LYP		B3LYP-D3		Expt. [b]	
	d(U=O)	d(U–N)	d(U=O)	d(U–N)	d(U=O)	d(U–N)	d(U=O)	d(U–N)	d(U=O)	d(U–N)
1	1.78	2.31	1.79	2.30	1.81	2.34	1.81	2.32	1.80	2.28
3	1.77	2.49	1.78	2.46	1.79	2.52	1.78	2.48	1.78	2.46
4	1.86	–	1.85	–	1.88	–	1.88	–	1.89	–
5	1.78	2.22	1.78	2.21	1.80	2.26	1.80	2.23	1.80	2.22
6	1.78	2.21	1.78	2.21	1.80	2.24	1.80	2.22	1.80	2.22
SD	0.02	0.02	0.02	0.01	0.01	0.05	0.01	0.02		
8	–	–	1.75	–	–	–	1.77	–	1.76	–
9	–	–	1.75	–	–	–	1.77	–	1.74	–
10	–	–	1.78	2.19	–	–	1.80	2.21	1.81	2.20
11	–	–	1.77	–	–	–	1.79	–	1.76	–
12	–	–	1.76	2.32	–	–	1.78	2.34	1.84	2.31
13	–	2.27[c]	–	2.26[c]	–	2.30[c]	–	2.29[c]	–	2.36
14	–	–	1.79	1.89	–	–	1.82	1.92	1.81	1.92
SD			0.04	0.02			0.03	0.02		

[a] def2-TZVP basis with small-core ECP for uranium, see Computational Details in main text. [b] See Table S2 for references to experimental data. [c] Note that while the structure optimization was done for a U(VI) singlet ground-state, the X-ray structure of **13** feature all U–L bond-lengths characteristic for a U(IV) complex, in accordance with DFT calculations for a triplet structure (see Discussion in main text).

Table S4. Solvent effects on optimized U–C bond lengths (in Ångstroms) using COSMO [a]

Complex	gas phase	benzene (ε=2.3)	THF (ε=7.6)
1	2.633	2.634	2.634
2	2.613	2.612	2.613
3	2.482	2.485	2.488
4[b]	2.478	2.480	2.482
5	2.304	2.302	2.300
6	2.277	2.274	2.271
7	2.323	2.324	2.326

[a] PBE0-D3/def2-TZVP/ECP results, see Computational Details in main text. [b] Averaged data for two non-equivalent alkyl carbon atoms.

Table S5. Optimized U–H and U–C bond lengths (in Ångstroms) with (SO) and without (SR) consideration of spin-orbit effects [a]

Complex	d(U–C/H) SR	d(U–C/H) SO	Δd^{SR-SO} [Å]
$U(CH_3)_6$ (**7'**)	2.353	2.349	0.004
HUF_5 (**15**)	1.906	1.901	0.004
H_2UO_2 (C_{2v}, **18**)	1.957	1.962	–0.006
H_2UO_2 (D_{2h}, **18**)	1.999	1.987	0.012

[a] 2c-ZORA/TZ2P/PBE0 results.

Table S6. Comparison between calculated ^{13}C NMR shielding components (in ppm) of U(VI)-bound carbon atoms at PBE level with (XC) and without consideration of the exchange-correlation kernel [a]

Complex	σ_{2c}^{dia}	σ_{2c}^{para}	σ_{2c}^{SO}	$\sigma_{2c}^{xc,dia}$	$\sigma_{2c}^{xc,para}$	$\sigma_{2c}^{xc,SO}$
1	240.2	–254.4	–65.3	240.3	–254.4	–88.2
2	242.9	–281.1	–58.2	242.9	–281.1	–75.2
3	245.5	–279.6	–139.0	245.5	–280.3	–196.1
4-C1[b]	233.2	–117.0	–89.4	233.3	–119.3	–142.5
4-C2[b]	234.0	–136.0	–99.2	234.1	–139.3	–159.4
5	219.3	–145.9	–70.6	219.4	–148.2	–115.9
6	234.0	–201.9	–52.4	234.1	–205.8	–88.3
7	237.6	–203.2	–96.4	237.7	–212.3	–162.1
8	253.5	–93.5	–12.0	253.6	–93.8	–25.4
9	–	–	–	237.9	–249.3	–99.8
10	–	–	–	259.3	–277.9	–162.7
11	–	–	–	273.4	–247.6	–95.3
12	–	–	–	286.3	–323.7	–72.3
13	–	–	–	290.1	–369.7	–162.2
14	–	–	–	271.9	–287.1	–75.8

[a] 2c-ZORA-SO/TZ2P results at PBE0-D3/def2-TZVP/ECP optimized structures, see Computational Details in main text. [b] Data for two non-equivalent alkyl carbon atoms in **4**.

Table S7. Comparison between calculated ^{13}C NMR shielding components (in ppm) of U(VI)-bound carbon atoms at PBE0 level with (XC) and without consideration of exchange-correlation kernel [a]

Complex	σ_{2c}^{dia}	σ_{2c}^{para}	σ_{2c}^{SO}	$\sigma_{2c}^{xc,dia}$	$\sigma_{2c}^{xc,para}$	$\sigma_{2c}^{xc,SO}$
1	252.0	–269.6	–61.6	252.1	–269.6	–77.7
2	255.6	–301.5	–51.3	255.7	–301.5	–62.2
3	252.0	–269.6	–61.6	250.8	–277.5	–169.0
4-C1[b]	231.8	–105.1	–124.7	231.9	–108.1	–195.0
4-C2[b]	230.9	–126.1	–142.8	231.0	–130.8	–229.0
5	231.7	–165.3	–106.7	231.7	–168.2	–171.9
6	235.0	–215.5	–81.8	235.1	–220.8	–136.5
7	232.0	–200.8	–180.3	232.1	–214.6	–362.7
8	246.2	–70.6	–6.4	246.3	–70.7	–12.6
9	–	–	–	252.9	–265.9	–72.1
10	–	–	–	266.7	–278.8	–222.3
11	–	–	–	263.7	–191.4	–71.4
12	–	–	–	260.5	–342.4	–99.1
13	–	–	–	256.6	–377.5	–389.7
14	–	–	–	259.2	–229.9	–58.2

[a] 2c-ZORA-SO/TZ2P results at PBE0-D3/def2-TZVP/ECP optimized structures, see Computational Details in main text. [b] Data for two non-equivalent alkyl carbon atoms in **4**.

Table S8. Isotropic ^{13}C NMR shifts (in ppm vs. TMS) of U(VI)-bound carbon atoms calculated at different levels of theory for B3LYP-D3/def2-TZVP/ECP optimized structures. Spin-orbit-induced shifts are given in parentheses [a]

Complex	$\delta_{2c}(PBE)$	$\delta_{2c}^{xc}(PBE)$	$\delta_{2c}(PBE0)$	$\delta_{2c}^{xc}(PBE0)$	δ_{exp}
1	270.1 (67.1)	295.8 (92.6)	275.7 (64.6)	294.4 (83.2)	262.8 [S1]
2	285.7 (60.4)	304.3 (79.0)	291.1 (53.7)	303.4 (65.9)	283.6 [S11]
3	365.7 (142.0)	426.6 (202.0)	351.0 (131.3)	392.0 (171.8)	329.4 [S2]
4[b]	178.0 (95.4)	244.7 (158.7)	222.8 (143.2)	324.0 (240.4)	242.9 [S3]
5	186.1 (71.0)	240.8 (123.2)	240.2 (112.7)	323.8 (192.7)	301.0 [S4]
6	207.5 (50.3)	253.0 (91.4)	259.7 (83.4)	333.6 (150.9)	317.4 [S5]
7	255.6 (99.8)	342.9 (176.1)	362.1 (196.7)	690.7 (444.8)	434.3 [S3]

[a] 2c-ZORA-SO/TZ2P results, see Computational Details in main text. [b] Averaged data for two non-equivalent alkyl carbon atoms.

Table S9. Calculated ^{13}C NMR shifts (in ppm vs. TMS) of U(VI)-bound carbon atoms with solvent effects using COSMO both for the structure optimization and NMR shift calculation [a]

Complex	$\delta_{2c}^{xc}(PBE0)$ gas-phase	$\delta_{2c}^{xc}(PBE0)$ benzene (ε=2.3)	$\delta_{2c}^{xc}(PBE0)$ THF (ε=7.6)	δ_{exp}
1	286.8	288.6	–	262.8 [S1],[b]
2	299.5	–	302.3	283.6 [S11],[c]
3	387.3	383.9	–	329.4 [S2],[b]
4[e]	291.5	–	298.3	242.9 [S3],[d]
5	299.9	302.4	–	301.0 [S4],[b]
6	313.7	–	320.2	317.4 [S5],[d]
7	536.8	537.3	537.2	434.3 [S3],[d]
8	28.5	–	34.8	21.2 [S6],[d]

[a] 2c-ZORA-SO/TZ2P results; see Computational Details in main text. [b] Experimental value measured in benzene-d_6. [c] Experimental value measured in pyridine-d_5. [d] Experimental value measured in THF-d_8. [e] Averaged data for two non-equivalent alkyl carbon atoms.

Table S10. Dependence of ^{13}C NMR shifts (in ppm vs. TMS) of U(VI)-bound carbon atoms on EXX admixture. Data for B3LYP-D3/def2-TZVP/ECP optimized structures [a]

Complex	$\delta_{2c}^{xc}(PBE)$	$\delta_{2c}^{xc}(PBE-10HF)$	$\delta_{2c}^{xc}(PBE-15HF)$	$\delta_{2c}^{xc}(PBE0)$	$\delta_{2c}(PBE-40HF)$	δ_{exp}
1	295.8	297.4	297.0	294.4	275.4	262.8[S1]
2	304.3	304.7	304.4	303.4	293.2	283.6[S11]
3	426.6	417.3	410.2	392.0	335.8	329.4[S2]
4[b]	244.7	273.3	291.0	324.0	254.3	242.9[S3]
5	240.8	271.1	285.8	323.8	295.9	301.0[S4]
6	253.0	281.6	296.9	333.6	311.8	317.4[S5]
7	342.8	409.7	461.3	690.7	555.5	434.3[S3]
SD	54.9	38.1	36.3	93.4	41.5	

[a] 2c-ZORA-SO/TZ2P results. [b] Averaged data for two non-equivalent alkyl carbon atoms.

Table S11. Compositions of the U–C bonding NLMOs along with the calculated SO (σ^{SO}) and paramagnetic (σ^{para}) contributions to the isotropic ^{13}C shielding at the PBE level [a]

	U–C	%U	%U(s)	%U(d)	%U(f)	%C	%C(s)	%C(p)	σ^{para}	σ^{SO}
1	σ	17.2	19	47	34	78.6	44	56	–254	–88
2	σ	15.7	19	44	37	79.2	40	60	–281	–75
3	σ	23.8	16	39	45	73.1	39	61	–280	–196
4-C1[b]	σ	23.0	12	31	57	73.2	21	79	–119	–143
4-C2[b]	σ	23.9	11	30	59	72.5	22	78	–139	–159
5	σ	33.0	3	20	78	65.2	22	78	–148	–116
6	σ	31.8	3	20	77	64.3	18	82	–206	–88
7	σ	29.3	7	23	71	68.1	20	80	–212	–162
8	σ	15.9	8	42	50	73.7	7	93	–94	–25
9	σ	17.7	20	43	37	78.8	44	56	–249	–100
10	σ	29.2	6	34	61	67.8	50	50	–278	–163
11	σ	19.8	9	44	47	70.1	19	81	–248	–95
	π	13.9	0	20	80	70.1	0	100		
12	σ	29.9	2	20	77	62.7	19	81	–324	–72
	π	24.3	0	35	65	65.5	0	100		
13	σ	26.8	2	26	71	68.0	32	68	–370	–162
	π	25.0	0	26	74	64.2	0	100		
14	σ	20.7	6	41	53	68.4	16	84	–287	–76
	π	15.0	0	23	76	70.0	2	98		

[a] 2c-ZORA-SO/TZ2P results at PBE0-D3/def2-TZVP/ECP optimized structures; see Computational Details in main text. [b] Data for two non-equivalent alkyl carbon atoms.

Table S12. Compositions of the U–C bonding NLMOs along with the calculated SO (σ^{SO}) and paramagnetic (σ^{para}) contributions to the isotropic ^{13}C shielding at the PBE0 level [a]

	U–C	%U	%U(s)	%U(d)	%U(f)	%C	%C(s)	%C(p)	σ^{para}	σ^{SO}
1	σ	16.4	19	49	32	79.9	44	56	–270	–78
2	σ	14.9	19	47	33	80.7	40	60	–302	–62
3	σ	22.2	17	43	40	75.0	40	60	–278	–169
4-C1[b]	σ	21.7	13	35	52	74.9	22	78	–108	–195
4-C2[b]	σ	22.5	12	34	54	74.2	23	77	–131	–229
5	σ	28.5	3	24	73	66.0	25	75	–168	–172
6	σ	27.7	3	25	72	64.7	20	80	–221	–137
7	σ	28.7	7	25	68	69.2	22	78	–215	–363
8	σ	15.3	7	49	43	75.4	8	92	–71	–13
9	σ	16.3	21	47	32	80.6	44	56	–266	–72
10	σ	28.9	5	34	60	68.2	49	51	–279	–222
11	σ	21.5	5	52	42	70.2	20	80	–191	–71
	π	11.2	0	27	73	73.4	0	100		
12	σ	30.8	2	21	77	62.7	18	82	–342	–99
	π	23.4	0	37	63	67.3	1	99		
13	σ	28.2	5	26	68	67.7	31	69	–378	–390
	π	24.7	0	28	72	65.5	0	100		
14	σ	20.9	5	47	49	69.7	18	82	–230	–58
	π	12.9	0	29	70	72.8	2	98		

[a] 2c-ZORA-SO/TZ2P results at PBE0-D3/def2-TZVP/ECP optimized structures; see Computational Details in main text. [b] Data for two non-equivalent alkyl carbon atoms.

Table S13. Mulliken atomic spin densities at uranium induced by a finite Fermi contact perturbation (perturbation parameter λ=0.01 a.u.) for a U(VI)-bound carbon atom as function of EXX admixture [a]

Complex	PBE	PBE0	PBE-40HF
3	0.1051	0.1046	0.1031
4	0.0471	0.0526	0.0542

[a] TZVP/def2-TZVP basis sets (G09), PBE0-D3 structures.

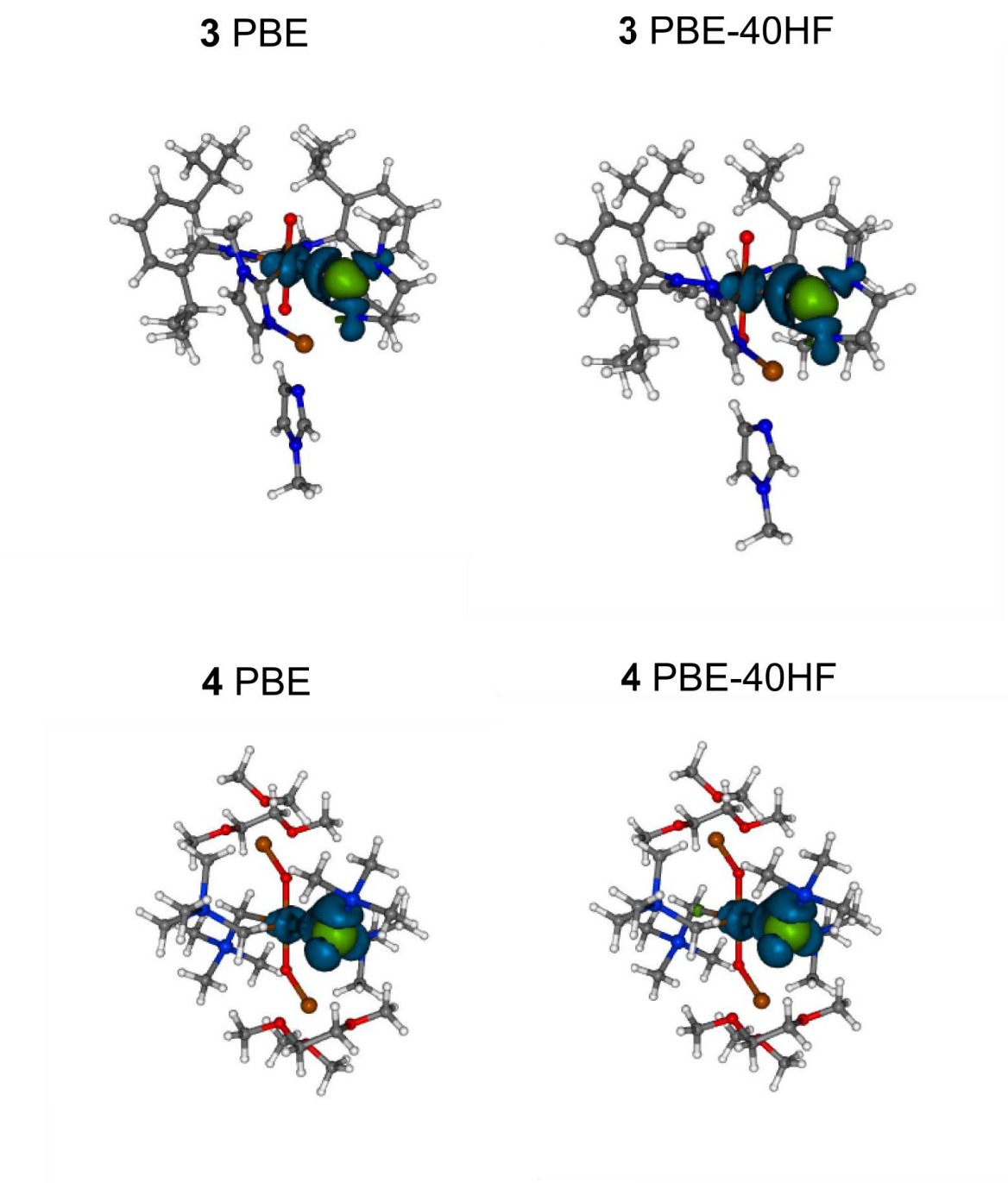

Figure S1. Isosurface plots (±0.0005) of spin densities induced by a finite Fermi contact perturbation (λ=0.01) for a uranium-bound carbon atom in **3** and **4** with PBE and PBE-40HF functionals, respectively.

Table S14. Comparison of computed hydride ^{1}H NMR shifts (in ppm vs. TMS) in uranium(VI) hydride complexes with (xc) and without consideration of the exchange-correlation kernel [a]

Complex	$\delta_{2c}(PBE)$	$\delta_{2c}^{xc}(PBE)$	$\delta_{2c}(PBE0)$	$\delta_{2c}^{xc}(PBE0)$	$\delta_{4c}(PBE)$	$\delta_{4c}^{xc}(PBE)$
15	140.8	265.5	254.3	603.7	137.1	251.8
16	98.2	171.0	168.0	336.6	96.8	163.8
17	100.2	178.4	176.7	348.8	99.2	174.0
18	81.3	132.2	64.5	87.3	85.0	136.9

[a] 2c-ZORA-SO results with TZ2P basis; 4c-mDKS results with Dyall-TZ/IGLO-III basis, see Computational Details in main text**.**

Table S15. Comparison of computed hydride ^{1}H NMR shifts (in ppm vs. TMS) in uranium(VI) hydride complexes for different optimized structures [a]

Complex	$\delta_{2c}^{xc}(PBE)$ PBE0-D3	$\delta_{2c}^{xc}(PBE)$ B3LYP-D3	$\delta_{2c}^{xc}(PBE0)$ PBE0-D3	$\delta_{2c}^{xc}(PBE0)$ B3LYP-D3
15	265.5	295.0	603.7	759.5
16	171.0	190.5	336.6	411.7
17	178.4	195.8	348.8	413.4
18	132.2	153.2	87.3	101.3
19	212.1	240.7	163.4	205.6
20	93.9	90.6	83.2	74.9
21	124.8	100.4	84.1	64.5
22	55.6	59.4	49.8	53.7
23	117.6	125.5	170.5	188.2

[a] 2c-ZORA-SO/TZ2P results, see Computational Details in main text**.**

Table S16. Principal ^{13}C NMR shift tensor components (δ in ppm vs. TMS), the anisotropy (Δδ)[a] and the asymmetry (η)[b] parameters as computed at the PBE0 level with consideration of the exchange-correlation kernel [c]

Complex	δ_{xx}	δ_{yy}	δ_{zz}	Δδ	η
1	236.5	236.5	467.6	231.2	0.00
2	162.1	247.0	490.8	286.2	0.44
3	228.2	262.7	672.3	426.8	0.12
4	36.2	239.8	600.0	462.0	0.66
5	414.2	412.3	74.4	-338.9	0.01
6	528.5	353.2	60.7	-380.2	0.69
7	764.6	708.8	138.3	-598.4	0.14
8	52.5	31.1	3.1	-38.7	0.83
9	129.4	214.5	487.5	315.6	0.40
10	622.3	615.1	41.7	-577.0	0.02
11	20.5	182.6	370.2	268.6	0.90
12	29.2	352.6	737.2	546.3	0.89
13	1073.6	820.2	213.9	-733.0	0.52
14	41.7	182.6	438.3	326.2	0.65

[a] $\Delta\delta = \delta_{zz} - (\delta_{xx} + \delta_{yy})/2$, where $|\delta_{zz} - \delta_{iso}| \geq |\delta_{xx} - \delta_{iso}| \geq |\delta_{yy} - \delta_{iso}|$. [b] $\eta = (\delta_{yy} - \delta_{xx})/(\delta_{zz} - \delta_{iso})$. [c] 2c-ZORA-SO/TZ2P results at PBE0-D3/def2-TZVP/ECP optimized structures, see Computational Details in main text.

Table S17. Principal ^{1}H NMR shift tensor components (δ in ppm vs. TMS), the anisotropy (Δδ)[a] and the asymmetry (η)[b] parameters as computed at the PBE0 level with consideration of the exchange-correlation kernel [c]

Complex	δ_{xx}	δ_{yy}	δ_{zz}	Δδ	η
15	860.0	859.8	91.2	-768.7	0.00
16	424.0	416.6	169.3	-251.0	0.04
17	489.9	479.7	76.8	-408.0	0.04
18	23.7	71.9	166.2	118.3	0.61
19	73.4	116.5	316.9	221.9	0.29
20	27.3	62.9	159.6	114.5	0.47
21	56.0	79.1	114.3	46.8	0.74
22	69.9	51.9	27.5	-33.4	0.81
23	220.8	219.2	71.6	-148.4	0.02

[a] $\Delta\delta = \delta_{zz} - (\delta_{xx} + \delta_{yy})/2$, where $|\delta_{zz} - \delta_{iso}| \geq |\delta_{xx} - \delta_{iso}| \geq |\delta_{yy} - \delta_{iso}|$. [b] $\eta = (\delta_{yy} - \delta_{xx})/(\delta_{zz} - \delta_{iso})$. [c] 2c-ZORA-SO/TZ2P results at PBE0-D3/def2-TZVP/ECP optimized structures, see Computational Details in main text.

Table S18. Optimized Cartesian coordinates of U(VI) complexes **1-23** (PBE0/def2-TZVP/ECP results)

Complex **1**

U	0.0497	0.0416	1.7879
N	-2.2973	0.0373	-0.0589
N	-1.7190	2.8325	-0.7869
N	-0.5783	3.6383	0.8232
C	-3.2401	-0.4152	0.9810
C	-2.5684	-1.4143	1.9202
H	-2.1091	-2.2297	1.3533
H	-3.3149	-1.8482	2.5901
H	-1.7969	-0.9440	2.5246
C	-4.4389	-1.1491	0.3605
H	-5.0574	-0.5045	-0.2655
H	-5.0789	-1.5471	1.1516
H	-4.0933	-1.9870	-0.2505
C	-3.7350	0.7654	1.8229
H	-2.8850	1.2420	2.3161
H	-4.4423	0.4353	2.5893
H	-4.2398	1.5191	1.2128
C	-2.9821	0.7244	-1.1310
H	-3.9337	1.1358	-0.7707
H	-3.2428	0.0547	-1.9684
C	-2.2334	1.8985	-1.7674
H	-1.3998	1.5472	-2.3690
H	-2.9210	2.4428	-2.4179
C	-0.6873	2.5418	0.0345
C	-2.2652	4.0575	-0.5082
H	-3.0969	4.4652	-1.0574
C	-1.5438	4.5709	0.5108
H	-1.6360	5.5186	1.0081
C	0.3656	3.7799	1.9567
C	-0.2088	3.0409	3.1603
H	-1.1932	3.4387	3.4193
H	0.4504	3.1692	4.0218
H	-0.2989	1.9759	2.9472
C	1.7169	3.2083	1.5605
H	1.6677	2.1455	1.3227
H	2.4131	3.3346	2.3923
H	2.1182	3.7372	0.6932
C	0.5374	5.2570	2.2908
H	0.8441	5.8342	1.4154
H	1.3174	5.3503	3.0474
H	-0.3704	5.6973	2.7080
O	-0.0495	-0.0413	-1.7879
N	2.2976	-0.0377	0.0591
N	1.7184	-2.8327	0.7869
N	0.5777	-3.6382	-0.8234

C	3.2406	0.4148	-0.9806
C	2.5691	1.4139	-1.9200
H	2.1096	2.2293	-1.3533
H	3.3158	1.8477	-2.5897
H	1.7977	0.9434	-2.5245
C	4.4391	1.1489	-0.3597
H	5.0574	0.5043	0.2667
H	5.0795	1.5470	-1.1505
H	4.0933	1.9868	0.2513
C	3.7359	-0.7656	-1.8224
H	2.8861	-1.2424	-2.3157
H	4.4433	-0.4352	-2.5887
H	4.2409	-1.5192	-1.2123
C	2.9822	-0.7251	1.1311
H	3.9336	-1.1369	0.7708
H	3.2432	-0.0556	1.9685
C	2.2330	-1.8989	1.7675
H	1.3993	-1.5472	2.3690
H	2.9202	-2.4435	2.4182
C	0.6869	-2.5417	-0.0346
C	2.2645	-4.0578	0.5081
H	3.0963	-4.4654	1.0570
C	1.5429	-4.5710	-0.5109
H	1.6347	-5.5189	-1.0079
C	-0.3659	-3.7794	-1.9572
C	0.2086	-3.0395	-3.1602
H	1.1931	-3.4371	-3.4193
H	-0.4505	-3.1676	-4.0219
H	0.2985	-1.9747	-2.9465
C	-1.7174	-3.2083	-1.5609
H	-1.6684	-2.1458	-1.3221
H	-2.4134	-3.3340	-2.3930
H	-2.1188	-3.7381	-0.6941
C	-0.5372	-5.2563	-2.2922
H	-0.8441	-5.8341	-1.4172
H	-1.3171	-5.3493	-3.0490
H	0.3708	-5.6962	-2.7094

Complex **2**

U	0.0000	0.0000	0.0002
O	0.6210	-0.3130	1.6451
O	-0.6212	0.3129	-1.6447
O	0.4551	-2.0457	-0.5537
O	-0.4546	2.0459	0.5540
C	-2.0402	-1.5094	0.6237
C	2.0402	1.5093	-0.6235
N	-1.7957	-2.7459	1.0374
N	-3.3512	-1.3899	0.4110
N	1.7957	2.7458	-1.0374

N	3.3512	1.3898	-0.4106
C	-2.9833	-3.5986	1.0357
H	-3.0903	-4.1211	1.9886
H	-2.9093	-4.3498	0.2424
C	-4.1030	-2.5913	0.7822
H	-4.7777	-2.8924	-0.0206
H	-4.7040	-2.3938	1.6761
C	2.9834	3.5985	-1.0356
H	3.0904	4.1209	-1.9886
H	2.9093	4.3497	-0.2424
C	4.1031	2.5912	-0.7820
H	4.7778	2.8924	0.0207
H	4.7039	2.3935	-1.6760
C	-0.4681	-3.2667	1.2829
H	-0.5748	-4.2692	1.7034
H	0.0227	-2.6327	2.0237
C	0.4223	-3.3064	0.0239
C	-0.1390	-4.2911	-0.9984
H	-1.1267	-3.9628	-1.3304
H	-0.2142	-5.3040	-0.5920
H	0.5114	-4.3150	-1.8750
C	1.8214	-3.7190	0.4619
H	2.4814	-3.7501	-0.4067
H	1.8254	-4.7047	0.9361
H	2.2231	-2.9849	1.1638
C	-4.0113	-0.1712	0.0945
C	-4.2515	0.7612	1.1108
C	-4.9283	1.9284	0.7764
H	-5.1217	2.6679	1.5453
C	-5.3512	2.1620	-0.5191
H	-5.8742	3.0804	-0.7607
C	-5.0990	1.2295	-1.5088
H	-5.4242	1.4235	-2.5248
C	-4.4258	0.0478	-1.2236
C	-3.8219	0.5288	2.5406
H	-3.2410	-0.3951	2.5707
C	-2.9164	1.6453	3.0511
H	-2.0463	1.7812	2.4063
H	-2.5656	1.4108	4.0593
H	-3.4543	2.5964	3.1042
C	-5.0365	0.3510	3.4486
H	-5.6454	1.2588	3.4677
H	-4.7198	0.1397	4.4732
H	-5.6777	-0.4680	3.1126
C	-4.1695	-0.9595	-2.3189
H	-3.5447	-1.7500	-1.8962
C	-3.3939	-0.3491	-3.4818
H	-3.9650	0.4482	-3.9655
H	-3.1916	-1.1133	-4.2368

H	-2.4418	0.0579	-3.1401
C	-5.4776	-1.5850	-2.7988
H	-6.0358	-2.0419	-1.9775
H	-5.2805	-2.3545	-3.5493
H	-6.1256	-0.8315	-3.2553
C	0.4682	3.2666	-1.2832
H	0.5749	4.2691	-1.7036
H	-0.0225	2.6326	-2.0241
C	-0.4225	3.3063	-0.0244
C	0.1378	4.2918	0.9976
H	1.1257	3.9644	1.3300
H	0.2125	5.3046	0.5907
H	-0.5128	4.3158	1.8740
C	-1.8218	3.7177	-0.4629
H	-2.4820	3.7490	0.4055
H	-1.8264	4.7031	-0.9378
H	-2.2229	2.9829	-1.1644
C	4.0113	0.1712	-0.0942
C	4.2519	-0.7610	-1.1106
C	4.9289	-1.9281	-0.7762
H	5.1227	-2.6673	-1.5453
C	5.3519	-2.1617	0.5192
H	5.8751	-3.0800	0.7607
C	5.0994	-1.2293	1.5090
H	5.4245	-1.4235	2.5250
C	4.4258	-0.0479	1.2239
C	3.8224	-0.5284	-2.5404
H	3.2417	0.3955	-2.5704
C	2.9167	-1.6447	-3.0510
H	2.0465	-1.7805	-2.4061
H	2.5659	-1.4102	-4.0592
H	3.4544	-2.5960	-3.1040
C	5.0370	-0.3508	-3.4484
H	5.6458	-1.2587	-3.4676
H	4.7203	-0.1394	-4.4729
H	5.6783	0.4681	-3.1123
C	4.1691	0.9592	2.3193
H	3.5438	1.7494	1.8968
C	3.3942	0.3483	3.4823
H	3.9658	-0.4487	3.9659
H	3.1916	1.1123	4.2375
H	2.4422	-0.0592	3.1408
C	5.4769	1.5854	2.7990
H	6.0347	2.0427	1.9777
H	5.2795	2.3547	3.5496
H	6.1255	0.8322	3.2553

Complex **3**

U	-0.0531	-0.6315	0.0019

O	1.3850	-1.6727	0.0008
O	-1.5518	0.3488	0.0030
C	-1.2488	-2.0549	-1.6431
C	-1.2471	-2.0555	1.6478
N	-0.8690	-2.9896	2.5679
C	-1.9805	-3.5749	3.1050
C	-3.0436	-2.9864	2.4817
N	-2.5902	-2.0556	1.5979
N	-2.5918	-2.0550	-1.5913
C	-3.0464	-2.9855	-2.4748
C	-1.9842	-3.5735	-3.1000
N	-0.8719	-2.9884	-2.5643
N	1.0473	0.9714	-1.5068
C	1.3309	2.2362	-1.2655
C	1.8098	3.1453	-2.3700
N	1.0494	0.9710	1.5093
C	1.2814	0.4342	2.8038
C	2.5480	-0.0876	3.1185
C	2.7699	-0.5768	4.4005
C	1.7668	-0.5736	5.3507
C	0.5095	-0.1028	5.0159
C	0.2359	0.3989	3.7483
C	0.4861	-3.2811	-2.9474
C	0.4896	-3.2826	2.9489
C	3.6750	-0.1223	2.1122
C	4.8189	0.8035	2.5163
C	-1.1522	0.9139	3.4303
C	-2.2469	0.1458	4.1593
C	1.2780	0.4351	-2.8017
C	2.5446	-0.0856	-3.1184
C	2.7655	-0.5729	-4.4012
C	1.7612	-0.5701	-5.3500
C	0.5038	-0.1009	-5.0132
C	0.2314	0.3999	-3.7450
C	3.6724	-0.1218	-2.1130
C	4.8157	0.8051	-2.5161
C	-1.1563	0.9146	-3.4251
C	-1.3025	2.4075	-3.7154
C	1.3326	2.2359	1.2681
C	1.8126	3.1448	2.3722
C	1.3149	2.8323	0.0014
C	4.1937	-1.5415	1.9058
C	-2.2521	0.1468	-4.1528
C	4.1918	-1.5413	-1.9098
C	-1.2979	2.4066	3.7220
Li	-3.2511	-1.0260	0.0039
N	-4.7397	0.3537	0.0008
C	-6.0503	0.3046	-0.0032
N	-6.5935	1.5396	-0.0112

C	-5.5541	2.4336	-0.0123
C	-4.4147	1.6840	-0.0048
C	-7.9989	1.8572	-0.0174
H	3.4029	-2.1991	-1.5439
H	4.9997	-1.5451	-1.1745
H	4.5902	-1.9571	-2.8387
H	1.5391	3.8917	0.0013
H	3.2750	0.2266	1.1585
H	0.6008	-4.3521	-3.1215
H	1.1459	-2.9831	-2.1352
H	0.7688	-2.7352	-3.8501
H	3.7490	-0.9670	4.6564
H	-1.9268	-4.3394	-3.8566
H	3.7448	-0.9615	-4.6588
H	2.8914	3.2727	-2.2860
H	1.3615	4.1331	-2.2576
H	1.5923	2.7601	-3.3635
H	1.5966	2.7593	3.3658
H	1.3637	4.1325	2.2607
H	2.8941	3.2729	2.2868
H	-4.0981	-3.1849	-2.6190
H	-0.2809	-0.1296	5.7557
H	-1.3220	0.7779	-2.3551
H	3.2729	0.2250	-1.1583
H	4.5928	-1.9594	2.8335
H	5.0011	-1.5442	1.1698
H	3.4043	-2.1984	1.5392
H	-0.2875	-0.1279	-5.7520
H	1.9514	-0.9492	-6.3479
H	1.9581	-0.9534	6.3480
H	-4.0951	-3.1857	2.6275
H	-6.6526	-0.5915	-0.0007
H	-1.9220	-4.3412	3.8610
H	1.1483	-2.9845	2.1357
H	0.6044	-4.3537	3.1223
H	0.7738	-2.7371	3.8514
H	-3.3847	2.0037	-0.0032
H	-1.3193	0.7779	2.3604
H	-2.2778	0.3921	-5.2186
H	-3.2240	0.4154	-3.7331
H	-2.1342	-0.9319	-4.0464
H	5.2697	0.4812	-3.4568
H	5.5960	0.8020	-1.7502
H	4.4776	1.8336	-2.6500
H	4.4814	1.8319	2.6520
H	5.5988	0.8012	1.7500
H	5.2732	0.4778	3.4563
H	-0.6480	3.0143	-3.0913
H	-2.3317	2.7219	-3.5226

H	-1.0732	2.6248	-4.7631
H	-2.3274	2.7211	3.5309
H	-0.6443	3.0140	3.0976
H	-1.0672	2.6230	4.7696
H	-8.2611	2.4274	-0.9102
H	-8.2670	2.4362	0.8680
H	-8.5704	0.9304	-0.0147
H	-5.7182	3.4983	-0.0181
H	-2.1289	-0.9329	4.0526
H	-3.2192	0.4143	3.7408
H	-2.2713	0.3910	5.2251

Complex **4**

U	-0.0004	-0.0024	0.0004
O	1.6803	0.6882	-0.3623
O	-1.6817	-0.6918	0.3631
C	-1.1621	1.8313	-1.2283
C	0.0580	-1.2500	-2.1204
C	1.1619	-1.8375	1.2262
C	-0.0591	1.2426	2.1230
Si	-1.3963	2.2742	2.8387
C	-3.1055	1.5528	2.4946
Si	0.1832	-3.0823	2.1596
C	1.2521	-4.3630	3.0585
Si	-0.1826	3.0706	-2.1682
C	0.8753	2.2406	-3.4869
Si	1.4002	-2.2729	-2.8396
C	1.3751	-4.0236	-2.1452
C	3.1072	-1.5507	-2.4863
C	1.2902	-2.4188	-4.7205
C	-1.2512	4.3474	-3.0730
C	0.9459	4.0431	-1.0158
C	-1.2806	2.4336	4.7182
C	-1.3694	4.0208	2.1338
C	-0.9449	-4.0496	1.0024
C	-0.8750	-2.2590	3.4822
Li	-3.3493	-0.1866	-0.2707
Li	3.3486	0.1894	0.2739
O	4.5917	-1.2347	1.2151
C	4.5781	-2.6391	1.0380
C	4.6778	-0.8790	2.5791
C	4.7723	0.6173	2.6690
O	3.6583	1.1492	2.0003
C	3.5950	2.5563	2.0285
O	-4.5924	1.2439	-1.2049
C	-4.6836	0.8908	-2.5693
C	-4.7819	-0.6051	-2.6620
O	-3.6666	-1.1409	-1.9984
C	-3.6072	-2.5482	-2.0290

C	-4.5738	2.6480	-1.0259
O	4.7353	1.0421	-0.8811
C	4.3005	2.0454	-1.7751
C	5.9564	0.4642	-1.2748
O	-4.7350	-1.0409	0.8851
C	-4.2995	-2.0481	1.7743
C	-5.9536	-0.4617	1.2844
H	-3.7068	3.0892	-1.5260
H	-4.5073	2.8425	0.0431
H	-5.4964	3.0903	-1.4184
H	0.0355	0.3243	2.7258
H	0.8980	1.7702	2.2006
H	1.7352	-2.3163	0.4209
H	1.8693	-1.3209	1.8891
H	3.3341	-1.6256	-1.4204
H	3.1409	-0.4938	-2.7587
H	3.8896	-2.0787	-3.0395
H	-1.9276	3.8596	-3.7822
H	-0.6433	5.0634	-3.6351
H	-1.8631	4.9176	-2.3668
H	-1.8725	1.3147	-1.8879
H	-1.7321	2.3144	-0.4233
H	6.2144	-0.2903	-0.5335
H	6.7481	1.2223	-1.3185
H	-0.8953	-1.7851	-2.1931
H	-0.0465	-0.3331	-2.7235
H	0.3690	4.6870	-0.3476
H	1.6420	4.6754	-1.5742
H	1.5191	3.3492	-0.3969
H	-1.5177	-3.3530	0.3861
H	-1.6415	-4.6840	1.5579
H	-0.3680	-4.6910	0.3318
H	1.5378	1.5007	-3.0335
H	1.4845	2.9732	-4.0250
H	0.2551	1.7218	-4.2235
H	-1.5372	-1.5165	3.0324
H	-0.2546	-1.7445	4.2216
H	-1.4847	-2.9941	4.0163
H	-1.3364	1.4480	5.1899
H	-2.0865	3.0505	5.1286
H	-0.3288	2.8848	5.0131
H	2.0993	-3.0297	-5.1334
H	1.3441	-1.4292	-5.1840
H	0.3407	-2.8708	-5.0217
H	-0.4048	4.5012	2.3221
H	-2.1455	4.6449	2.5863
H	-1.5247	4.0147	1.0522
H	1.5261	-4.0228	-1.0629
H	2.1550	-4.6430	-2.5975

H	0.4127	-4.5055	-2.3401
H	-5.7093	-0.9626	-2.1916
H	-4.7896	-0.9081	-3.7172
H	3.4917	2.9167	3.0575
H	2.7161	2.8482	1.4567
H	4.4909	2.9969	1.5749
H	3.7879	-1.2393	3.1114
H	5.5652	-1.3358	3.0363
H	-4.5033	-2.9870	-1.5740
H	-2.7277	-2.8433	-1.4597
H	-3.5072	-2.9072	-3.0589
H	5.7007	0.9759	2.2012
H	4.7755	0.9226	3.7236
H	-3.7945	1.2501	-3.1037
H	-5.5714	1.3505	-3.0229
H	5.5008	-3.0779	1.4341
H	4.5157	-2.8353	-0.0309
H	3.7109	-3.0824	1.5360
H	0.6441	-5.0822	3.6166
H	1.9277	-3.8784	3.7708
H	1.8649	-4.9293	2.3499
H	-3.3358	1.6218	1.4290
H	-3.8854	2.0850	3.0471
H	-3.1401	0.4974	2.7730
H	3.3128	2.3658	-1.4510
H	4.9969	2.8923	-1.7680
H	4.2267	1.6526	-2.7952
H	5.8614	-0.0100	-2.2583
H	-6.7470	-1.2180	1.3275
H	-5.8548	0.0086	2.2696
H	-6.2118	0.2963	0.5468
H	-4.2212	-1.6586	2.7954
H	-4.9979	-2.8934	1.7671
H	-3.3136	-2.3696	1.4459

Complex **5**

U	0.0086	-0.0028	0.0164
O	-0.6703	-0.0707	-1.6260
N	-0.5266	2.1375	0.1506
N	-1.4351	-1.5444	0.6680
N	1.9835	-0.5925	-0.7815
Si	-1.8355	-2.8453	-0.4389
Si	-2.3533	-1.3851	2.1423
Si	2.4950	0.0391	-2.3357
Si	2.9436	-1.8345	-0.0225
Si	0.5952	3.3299	0.7520
Si	-2.0330	2.6804	-0.5651
C	-3.2273	-2.3595	-1.5902
H	-3.4786	-3.1985	-2.2452

H	-4.1307	-2.0748	-1.0474
H	-2.9266	-1.5194	-2.2199
C	-0.3454	-3.3254	-1.4701
H	0.8716	-2.7067	1.1997
H	-0.6734	-4.0498	-2.2218
H	0.1153	-2.4927	-2.0024
C	-2.2998	-4.4243	0.4692
H	-3.1795	-4.3373	1.1078
H	-2.5091	-5.1985	-0.2753
H	-1.4672	-4.7767	1.0833
C	-3.3578	1.3643	-0.4070
H	-3.0665	0.3921	-0.8056
H	-3.6678	1.2367	0.6316
H	-4.2347	1.6972	-0.9709
C	-1.8152	3.0922	-2.3765
H	-1.5257	2.2002	-2.9369
H	-2.7571	3.4603	-2.7928
H	-1.0543	3.8586	-2.5360
C	-2.7452	4.1683	0.3363
H	-3.6941	4.4346	-0.1395
H	-2.9597	3.9215	1.3793
H	-2.1102	5.0545	0.3207
C	0.0795	3.9769	2.4348
H	-0.8488	4.5482	2.3864
H	-0.0666	3.1675	3.1550
H	0.8582	4.6356	2.8311
C	2.3314	2.6121	0.9451
H	2.5446	2.3650	1.9863
H	2.5437	1.7238	0.3438
H	3.0489	3.3776	0.6356
C	0.7648	4.7826	-0.4236
H	1.4640	5.5073	0.0044
H	1.1675	4.4581	-1.3858
H	-0.1751	5.3026	-0.6128
C	4.4595	-1.1208	0.8190
H	4.1990	-0.3304	1.5279
H	4.9759	-1.9080	1.3765
H	5.1651	-0.7015	0.1001
C	1.9591	-2.7554	1.3005
H	0.4174	-3.8131	-0.8604
H	2.2305	-3.8135	1.2458
H	2.2148	-2.4026	2.3008
C	3.4993	-3.1371	-1.2536
H	4.0997	-3.8877	-0.7304
H	2.6392	-3.6462	-1.6942
H	4.1057	-2.7386	-2.0677
C	4.3647	0.1929	-2.4496
H	4.7420	0.8797	-1.6878
H	4.9040	-0.7498	-2.3541

H	4.6143	0.6170	-3.4271
C	1.8675	1.7876	-2.5826
H	2.1065	2.0922	-3.6062
H	0.7897	1.8935	-2.4561
H	2.3674	2.4861	-1.9092
C	1.8671	-1.0222	-3.7421
H	2.2039	-2.0574	-3.6597
H	0.7750	-1.0178	-3.7627
H	2.2238	-0.6271	-4.6974
C	-4.1903	-1.6334	1.8491
H	-4.5808	-0.8726	1.1695
H	-4.4381	-2.6112	1.4346
H	-4.7189	-1.5342	2.8019
C	-1.7820	-2.6053	3.4463
H	-1.9882	-3.6372	3.1582
H	-0.7088	-2.5217	3.6378
H	-2.3017	-2.4100	4.3892
C	-2.1739	0.3406	2.8882
H	-3.1439	0.6302	3.3020
H	-1.4539	0.3442	3.7084
H	-1.8842	1.1286	2.1883
C	0.8838	0.0850	2.1460
H	0.5198	-0.7779	2.7040
H	1.9710	0.0605	2.0767
H	0.5534	1.0089	2.6199

Complex **6**

U	0.0003	0.0589	-0.1538
O	-0.0800	0.0092	-1.9304
C	0.5568	0.0102	2.0533
H	0.2889	0.9605	2.5200
H	0.1210	-0.8241	2.5990
Si	2.3807	-0.1778	1.6082
C	2.9057	-1.9419	1.9392
C	3.5166	0.9829	2.5318
H	2.1672	-2.6414	1.5397
H	2.9909	-2.1188	3.0149
H	3.8716	-2.1703	1.4826
H	3.4626	0.7750	3.6038
H	4.5518	0.8272	2.2159
H	3.2648	2.0312	2.3696
N	2.1963	0.1818	-0.0877
Si	3.4749	0.5585	-1.2054
C	2.8652	0.6195	-2.9702
C	4.1966	2.2479	-0.8173
C	4.8478	-0.7126	-1.0675
H	2.5032	-0.3457	-3.3268
H	2.0518	1.3381	-3.0906
H	3.6899	0.9303	-3.6186

H	3.4524	3.0380	-0.9476
H	5.0241	2.4619	-1.5002
H	4.5814	2.3140	0.2025
H	5.6441	-0.4881	-1.7826
H	5.2959	-0.7210	-0.0698
H	4.4775	-1.7180	-1.2819
N	-0.6993	-2.0246	0.0434
Si	-0.2179	-3.2518	-1.1061
Si	-1.9237	-2.3665	1.2308
C	1.5302	-2.9437	-1.7013
C	-1.3581	-3.2543	-2.5899
C	-0.1987	-4.9630	-0.3295
C	-2.5858	-0.7640	1.9904
C	-3.3952	-3.2539	0.4788
C	-1.2648	-3.4073	2.6449
H	1.6209	-2.0003	-2.2403
H	1.8172	-3.7470	-2.3863
H	2.2448	-2.9367	-0.8755
H	-1.0483	-4.0186	-3.3081
H	-1.3223	-2.2855	-3.0942
H	-2.3942	-3.4559	-2.3101
H	0.1243	-5.6851	-1.0853
H	-1.1716	-5.2890	0.0412
H	0.5137	-5.0123	0.4982
H	-2.4099	0.1632	1.4350
H	-2.1800	-0.6140	2.9926
H	-3.6719	-0.8573	2.0845
H	-3.8628	-2.6461	-0.2990
H	-4.1430	-3.4411	1.2551
H	-3.1285	-4.2160	0.0381
H	-2.0244	-3.4917	3.4279
H	-1.0084	-4.4163	2.3184
H	-0.3713	-2.9685	3.0964
N	-1.2611	1.8931	-0.0825
Si	-2.6413	1.8969	-1.1600
Si	-0.8568	3.3540	0.7704
C	-3.2910	0.1471	-1.3853
C	-2.1891	2.5860	-2.8382
C	-4.0919	2.8510	-0.4409
C	0.9453	3.3525	1.3109
C	-1.9025	3.5524	2.3125
C	-1.0394	4.8708	-0.3211
H	-2.5431	-0.5908	-1.6831
H	-3.7949	-0.2107	-0.4859
H	-4.0357	0.1741	-2.1873
H	-1.3669	2.0087	-3.2674
H	-3.0417	2.5233	-3.5202
H	-1.8809	3.6315	-2.7810
H	-4.9323	2.7937	-1.1395

H	-3.8835	3.9071	-0.2638
H	-4.4166	2.4069	0.5035
H	1.6165	2.8642	0.5999
H	1.0939	2.8901	2.2874
H	1.2727	4.3927	1.3968
H	-1.7984	2.6779	2.9610
H	-1.5871	4.4314	2.8822
H	-2.9622	3.6669	2.0773
H	-0.7979	5.7643	0.2624
H	-0.3422	4.8238	-1.1619
H	-2.0432	5.0026	-0.7265

Complex **7**

U	0.0000	0.0001	0.0000
C	0.9350	1.6784	-1.3106
H	1.6073	1.0372	-1.9020
H	1.5453	2.1015	-0.4959
C	-0.9817	1.6524	1.3047
H	-0.0866	1.9273	1.8839
H	-1.0576	2.3816	0.4815
C	-1.9155	-0.0213	-1.3116
H	-1.6879	0.8828	-1.8975
H	-2.5859	0.2971	-0.4968
C	0.9816	-1.6523	-1.3046
H	1.0575	-2.3815	-0.4815
H	0.0865	-1.9272	-1.8839
C	1.9155	0.0214	1.3116
H	2.5858	-0.2970	0.4967
H	1.6879	-0.8828	1.8974
C	-0.9350	-1.6783	1.3107
H	-1.5454	-2.1012	0.4960
H	-1.6072	-1.0370	1.9022
Si	0.2947	3.0605	-2.3849
C	1.6841	4.2776	-2.7302
C	-1.1050	4.0031	-1.5608
C	-0.3230	2.3840	-4.0222
H	2.5111	3.7911	-3.2544
H	2.0799	4.6931	-1.7994
H	1.3374	5.1099	-3.3494
H	0.4581	1.8259	-4.5442
H	-1.1788	1.7171	-3.8952
H	-0.6383	3.2036	-4.6735
H	-1.9836	3.3737	-1.3956
H	-1.4129	4.8371	-2.1977
H	-0.8022	4.4208	-0.5968
Si	-2.4921	1.7872	2.3881
C	-2.8498	3.5990	2.7334
C	-4.0107	1.0471	1.5674
C	-2.2082	0.9148	4.0243

H	-2.0123	4.0731	3.2522
H	-3.0167	4.1475	1.8023
H	-3.7406	3.7168	3.3569
H	-4.2332	1.5300	0.6119
H	-4.8820	1.1837	2.2140
H	-3.8992	-0.0255	1.3872
H	-3.0751	1.0491	4.6768
H	-2.0539	-0.1589	3.8972
H	-1.3347	1.3158	4.5443
Si	-2.8058	-1.2544	-2.3886
C	-1.8868	-1.5110	-4.0039
C	-4.5241	-0.6032	-2.7817
C	-2.9977	-2.9140	-1.5324
H	-0.9067	-1.9694	-3.8548
H	-1.7341	-0.5654	-4.5300
H	-2.4613	-2.1691	-4.6615
H	-4.4698	0.3481	-3.3179
H	-5.0955	-0.4354	-1.8646
H	-5.0851	-1.3073	-3.4029
H	-2.0321	-3.3914	-1.3435
H	-3.5217	-2.8204	-0.5772
H	-3.5818	-3.5913	-2.1616
Si	2.4920	-1.7872	-2.3880
C	2.8496	-3.5991	-2.7333
C	4.0106	-1.0472	-1.5674
C	2.2082	-0.9149	-4.0242
H	2.0121	-4.0731	-3.2521
H	3.0165	-4.1475	-1.8021
H	3.7405	-3.7169	-3.3568
H	3.0751	-1.0491	-4.6767
H	2.0537	0.1588	-3.8972
H	1.3347	-1.3160	-4.5444
H	4.8819	-1.1838	-2.2139
H	4.2331	-1.5300	-0.6118
H	3.8992	0.0255	-1.3872
Si	2.8058	1.2544	2.3887
C	2.9977	2.9141	1.5325
C	4.5241	0.6031	2.7817
C	1.8868	1.5109	4.0040
H	2.0322	3.3915	1.3437
H	3.5819	3.5913	2.1618
H	3.5218	2.8204	0.5773
H	5.0851	1.3071	3.4030
H	5.0955	0.4354	1.8646
H	4.4697	-0.3483	3.3178
H	1.7341	0.5652	4.5299
H	0.9067	1.9692	3.8549
H	2.4613	2.1688	4.6616
Si	-0.2946	-3.0604	2.3848

C	0.3233	-2.3840	4.0221
C	1.1050	-4.0031	1.5604
C	-1.6841	-4.2775	2.7302
H	-0.4577	-1.8258	4.5441
H	1.1792	-1.7172	3.8950
H	0.6386	-3.2037	4.6733
H	1.9836	-3.3737	1.3952
H	1.4129	-4.8371	2.1973
H	0.8021	-4.4207	0.5965
H	-1.3373	-5.1098	3.3493
H	-2.0799	-4.6929	1.7994
H	-2.5110	-3.7910	3.2545

Complex **8**

U	-0.8793	-0.1255	-0.3866
S	-0.7878	-3.0099	-0.2390
S	-3.1642	1.6560	-0.5094
S	2.1733	-0.5422	1.2272
P	-2.6856	-2.8092	0.3278
P	-4.2254	0.0064	-0.1095
O	-1.0622	-0.0268	1.3535
O	-0.7415	-0.2148	-2.1279
O	1.3679	-0.5575	-0.0389
O	2.4097	0.7931	1.6940
O	1.7593	-1.5395	2.1636
O	0.1330	2.1725	-0.2863
F	4.6843	-1.1715	1.5435
F	3.6773	-2.3223	0.0222
F	4.2378	-0.2759	-0.3679
C	-3.2106	-1.3500	-0.4721
H	-3.1328	-1.4995	-1.5518
C	3.7920	-1.1165	0.5628
C	-0.0871	2.9329	0.9169
H	0.8706	3.0217	1.4366
H	-0.7428	2.3270	1.5389
C	1.3353	2.5918	-0.9579
H	1.3216	3.6836	-1.0031
C	1.4234	2.0200	-2.3446
C	-0.7220	4.2717	0.6326
H	2.1798	2.2775	-0.3379
C	-2.8287	-2.7782	2.1293
C	-3.6976	-4.2192	-0.1846
C	-4.8300	-0.0223	1.5889
C	-5.7160	0.0047	-1.1338
C	-5.0682	-4.0596	-0.3649
C	-5.8536	-5.1427	-0.7249
C	-5.2702	-6.3878	-0.9099
C	-3.9029	-6.5477	-0.7362
C	-3.1152	-5.4668	-0.3743

H	-5.5208	-3.0834	-0.2311
H	-6.9200	-5.0123	-0.8687
H	-5.8818	-7.2349	-1.1982
H	-3.4459	-7.5183	-0.8885
H	-2.0440	-5.5810	-0.2508
C	-4.0409	-3.0606	2.7549
C	-4.1178	-3.0819	4.1356
C	-2.9859	-2.8326	4.8988
C	-1.7747	-2.5688	4.2787
C	-1.6904	-2.5454	2.8958
H	-4.9237	-3.2779	2.1678
H	-5.0645	-3.2979	4.6159
H	-3.0479	-2.8554	5.9809
H	-0.8826	-2.3865	4.8657
H	-0.7387	-2.3567	2.4150
C	-5.9644	-1.0065	-2.0525
C	-7.1119	-0.9700	-2.8326
C	-8.0090	0.0766	-2.6963
C	-7.7574	1.0956	-1.7853
C	-6.6132	1.0641	-1.0095
H	-5.2641	-1.8256	-2.1604
H	-7.3000	-1.7607	-3.5493
H	-8.9052	0.1052	-3.3049
H	-8.4547	1.9190	-1.6848
H	-6.4088	1.8625	-0.3047
C	-6.0939	-0.5322	1.8751
C	-6.5606	-0.5332	3.1790
C	-5.7633	-0.0397	4.2002
C	-4.4987	0.4557	3.9187
C	-4.0338	0.4762	2.6153
H	-6.7219	-0.9113	1.0777
H	-7.5503	-0.9180	3.3961
H	-6.1278	-0.0430	5.2209
H	-3.8708	0.8325	4.7170
H	-3.0539	0.8745	2.3870
H	-0.9008	4.7886	1.5785
H	-0.0872	4.9155	0.0214
H	-1.6813	4.1438	0.1286
H	2.2906	2.4588	-2.8427
H	1.5573	0.9391	-2.3339
H	0.5335	2.2575	-2.9299

Complex **9**

U	0.0090	-0.0110	0.0014
Cl	3.3932	2.7255	4.5630
Cl	0.6797	1.1802	6.1598
Cl	-1.6024	2.0724	-0.0950
N	1.9861	1.5762	2.5608
N	0.3254	0.6404	3.5333

O	1.2624	0.8976	-0.8144
C	0.8788	0.8392	2.3147
C	2.8832	2.0586	1.5541
C	3.9853	1.2807	1.2134
C	4.8097	1.7505	0.2030
H	5.6697	1.1548	-0.0865
C	4.5586	2.9532	-0.4466
C	3.4592	3.7035	-0.0571
H	3.2531	4.6470	-0.5522
C	2.5996	3.2745	0.9454
C	4.2498	-0.0283	1.8837
H	4.1947	0.0543	2.9718
H	5.2416	-0.3965	1.6219
H	3.5173	-0.7771	1.5677
C	5.4575	3.4186	-1.5496
H	5.1826	4.4167	-1.8924
H	5.4009	2.7415	-2.4066
H	6.5010	3.4451	-1.2266
C	1.3925	4.0702	1.3231
H	1.4209	5.0531	0.8533
H	1.3216	4.2123	2.4046
H	0.4776	3.5676	0.9937
C	2.1249	1.8335	3.9077
C	1.0737	1.2391	4.5241
C	-0.9052	-0.0535	3.7698
C	-2.0797	0.6906	3.8127
C	-3.2676	-0.0009	4.0044
H	-4.1978	0.5573	4.0287
C	-3.2933	-1.3811	4.1558
C	-2.0937	-2.0793	4.1141
H	-2.0996	-3.1593	4.2220
C	-0.8797	-1.4357	3.9203
C	-2.0675	2.1738	3.6268
H	-3.0664	2.5842	3.7730
H	-1.7424	2.4335	2.6158
H	-1.3938	2.6642	4.3346
C	-4.5864	-2.0987	4.3897
H	-5.4313	-1.5383	3.9861
H	-4.7652	-2.2388	5.4601
H	-4.5786	-3.0885	3.9307
C	0.3965	-2.2077	3.8276
H	1.2021	-1.7335	4.3929
H	0.7273	-2.2860	2.7870
H	0.2594	-3.2182	4.2127
Cl	-2.9343	-3.2544	-4.5402
Cl	-1.0503	-0.7851	-6.1672
Cl	1.6229	-2.0926	0.1114
N	-1.7067	-1.9049	-2.5429
N	-0.5674	-0.3902	-3.5355

O	-1.2430	-0.9217	0.8181
C	-0.8676	-0.8706	-2.3074
C	-2.2558	-2.7564	-1.5311
C	-3.4042	-2.3501	-0.8615
C	-3.8938	-3.1861	0.1318
H	-4.7831	-2.8842	0.6760
C	-3.2657	-4.3805	0.4568
C	-2.1209	-4.7438	-0.2397
H	-1.6141	-5.6705	0.0094
C	-1.5965	-3.9479	-1.2474
C	-4.0594	-1.0409	-1.1591
H	-4.1341	-0.8555	-2.2330
H	-5.0641	-1.0121	-0.7373
H	-3.4882	-0.2159	-0.7223
C	-3.8283	-5.2767	1.5157
H	-3.0485	-5.8829	1.9798
H	-4.3301	-4.7031	2.2965
H	-4.5680	-5.9624	1.0909
C	-0.3587	-4.3450	-1.9845
H	-0.0092	-5.3187	-1.6427
H	-0.5340	-4.4077	-3.0620
H	0.4422	-3.6216	-1.8117
C	-1.9296	-2.0683	-3.8935
C	-1.2059	-1.1099	-4.5226
C	0.2979	0.7232	-3.7847
C	1.6654	0.4942	-3.8735
C	2.4854	1.5953	-4.0829
H	3.5575	1.4410	-4.1511
C	1.9711	2.8794	-4.1894
C	0.5949	3.0564	-4.1043
H	0.1772	4.0544	-4.1908
C	-0.2678	1.9892	-3.9065
C	2.2377	-0.8752	-3.7009
H	3.2940	-0.8845	-3.9695
H	2.1540	-1.2018	-2.6598
H	1.7220	-1.6132	-4.3202
C	2.8737	4.0591	-4.3783
H	3.9001	3.7484	-4.5772
H	2.5402	4.6857	-5.2087
H	2.8810	4.6856	-3.4817
C	-1.7449	2.1935	-3.8003
H	-2.2962	1.5151	-4.4560
H	-2.0824	2.0210	-2.7745
H	-2.0086	3.2152	-4.0728

Complex **10**

U	-0.3223	0.0158	-0.7821
O	-1.0049	-0.0856	-2.4264
N	-0.7685	2.1507	-0.6477

N	-1.7314	-1.4676	-0.0280
N	1.6463	-0.6801	-1.4514
Si	-2.1574	-2.8449	-1.0300
Si	-2.5088	-1.2665	1.5316
Si	2.2848	-0.0573	-2.9627
Si	2.5702	-1.8785	-0.5685
Si	0.3945	3.2787	0.0176
Si	-2.2806	2.7458	-1.3107
C	-3.7754	-2.5604	-1.9251
H	-3.9998	-3.4234	-2.5589
H	-4.6187	-2.4065	-1.2515
H	-3.6917	-1.6862	-2.5752
C	-0.8778	-3.1626	-2.3668
H	0.7753	-2.3850	1.1545
H	-1.0163	-4.1869	-2.7266
H	-1.0168	-2.4870	-3.2106
C	-2.2587	-4.4148	-0.0047
H	-3.0092	-4.3736	0.7862
H	-2.5170	-5.2491	-0.6634
H	-1.2955	-4.6419	0.4586
C	-3.6104	1.4253	-1.2379
H	-3.3502	0.5131	-1.7752
H	-3.8726	1.1624	-0.2117
H	-4.5092	1.8348	-1.7091
C	-2.0584	3.2558	-3.0958
H	-1.7781	2.3908	-3.7016
H	-2.9952	3.6548	-3.4947
H	-1.2874	4.0192	-3.2137
C	-2.9669	4.1763	-0.3064
H	-3.9182	4.4843	-0.7508
H	-3.1703	3.8615	0.7203
H	-2.3194	5.0527	-0.2719
C	-0.1079	3.7931	1.7459
H	-1.0269	4.3806	1.7570
H	-0.2635	2.9022	2.3584
H	0.6840	4.3908	2.2068
C	2.1282	2.5416	0.1098
H	2.4180	2.4002	1.1521
H	2.2594	1.5751	-0.3805
H	2.8341	3.2372	-0.3537
C	0.5467	4.8019	-1.0701
H	1.2703	5.4878	-0.6189
H	0.9204	4.5319	-2.0612
H	-0.3889	5.3470	-1.2012
C	3.8915	-1.0631	0.4766
H	3.4469	-0.3510	1.1749
H	4.4337	-1.8166	1.0557
H	4.6185	-0.5276	-0.1365
C	1.4807	-2.9382	0.5359

H	0.1579	-3.0724	-2.0369
H	0.9251	-3.6747	-0.0470
H	2.1430	-3.4931	1.2087
C	3.3713	-3.1229	-1.7269
H	3.9167	-3.8561	-1.1245
H	2.6120	-3.6661	-2.2957
H	4.0767	-2.6897	-2.4367
C	4.1368	0.2359	-2.8588
H	4.3636	0.9705	-2.0820
H	4.7247	-0.6603	-2.6589
H	4.4776	0.6489	-3.8130
C	1.5613	1.6277	-3.3571
H	1.9512	1.9259	-4.3354
H	0.4738	1.6400	-3.4248
H	1.8755	2.3861	-2.6386
C	1.8792	-1.2069	-4.3794
H	2.3154	-2.1983	-4.2465
H	0.7965	-1.3209	-4.4681
H	2.2545	-0.7947	-5.3201
C	-4.3237	-1.7455	1.4516
H	-4.8651	-1.1048	0.7514
H	-4.5002	-2.7836	1.1669
H	-4.7609	-1.5967	2.4442
C	-1.6868	-2.3083	2.8512
H	-1.6910	-3.3699	2.5990
H	-0.6532	-1.9974	3.0125
H	-2.2227	-2.1850	3.7974
C	-2.4978	0.5343	2.0961
H	-3.5276	0.8746	2.2364
H	-1.9784	0.6111	3.0535
H	-2.0111	1.2410	1.4215
C	0.5312	0.1557	1.3346
C	0.9752	0.1580	2.4721
C	1.4991	0.1109	3.7872
C	1.2375	1.1344	4.7039
C	1.7513	1.0645	5.9858
C	2.5279	-0.0200	6.3701
C	2.7914	-1.0399	5.4658
C	2.2825	-0.9795	4.1819
H	0.6313	1.9781	4.3977
H	1.5442	1.8609	6.6908
H	2.9277	-0.0710	7.3761
H	3.3968	-1.8876	5.7645
H	2.4805	-1.7700	3.4684

Complex **11**

U	-0.4755	-0.0008	0.0006
S	-1.5774	2.6643	0.0152
S	-1.5789	-2.6652	-0.0116

P	-3.2884	1.5939	0.1069
P	-3.2895	-1.5940	-0.1007
O	-0.2821	0.0044	-1.7619
O	-0.2813	-0.0061	1.7630
N	1.5646	1.6331	0.0249
N	1.5639	-1.6356	-0.0247
C	-2.8387	0.0000	0.0012
C	1.9023	2.2540	1.1559
H	1.3203	1.9895	2.0314
C	2.9213	3.1875	1.2137
H	3.1570	3.6696	2.1536
C	3.6140	3.4896	0.0530
H	4.4158	4.2189	0.0635
C	3.2596	2.8495	-1.1233
H	3.7670	3.0607	-2.0557
C	2.2267	1.9303	-1.0933
H	1.8985	1.4137	-1.9882
C	2.2253	-1.9342	1.0935
H	1.8965	-1.4188	1.9888
C	3.2582	-2.8535	1.1231
H	3.7649	-3.0660	2.0556
C	3.6134	-3.4921	-0.0537
H	4.4153	-4.2214	-0.0646
C	2.9215	-3.1884	-1.2146
H	3.1580	-3.6693	-2.1549
C	1.9025	-2.2550	-1.1563
H	1.3212	-1.9894	-2.0318
C	-4.1953	-1.9971	-1.6190
C	-4.4284	-2.1055	1.2199
C	-4.4299	2.1075	-1.2108
C	-4.1904	1.9958	1.6278
C	-5.7639	-1.7161	1.1466
C	-6.6213	-1.9646	2.2042
C	-6.1497	-2.6031	3.3435
C	-4.8214	-2.9948	3.4189
C	-3.9609	-2.7481	2.3588
H	-6.1296	-1.2178	0.2551
H	-7.6592	-1.6578	2.1424
H	-6.8209	-2.7968	4.1726
H	-4.4530	-3.4976	4.3061
H	-2.9188	-3.0461	2.4010
C	-4.1325	-1.1098	-2.6860
C	-4.8047	-1.3936	-3.8644
C	-5.5355	-2.5663	-3.9805
C	-5.5911	-3.4601	-2.9187
C	-4.9224	-3.1775	-1.7398
H	-3.5558	-0.1984	-2.5776
H	-4.7618	-0.6917	-4.6895
H	-6.0655	-2.7869	-4.9002

H	-6.1606	-4.3781	-3.0109
H	-4.9680	-3.8711	-0.9071
C	-4.1217	1.1092	2.6951
C	-4.7903	1.3923	3.8758
C	-5.5231	2.5636	3.9939
C	-5.5846	3.4565	2.9318
C	-4.9197	3.1746	1.7505
H	-3.5435	0.1991	2.5852
H	-4.7428	0.6910	4.7011
H	-6.0503	2.7836	4.9154
H	-6.1558	4.3733	3.0255
H	-4.9698	3.8676	0.9177
C	-5.7650	1.7169	-1.1360
C	-6.6243	1.9668	-2.1917
C	-6.1551	2.6077	-3.3307
C	-4.8271	3.0004	-3.4075
C	-3.9647	2.7524	-2.3493
H	-6.1288	1.2166	-0.2449
H	-7.6619	1.6591	-2.1288
H	-6.8278	2.8024	-4.1583
H	-4.4606	3.5050	-4.2945
H	-2.9229	3.0510	-2.3928

Complex **12**

U	-0.0900	2.2500	0.4870
O	-0.1043	3.9490	0.9616
Cl	0.0414	1.5928	2.9938
Cl	-0.2730	3.0129	-1.9984
C	-0.0109	0.2201	-0.1944
P	-1.6405	-0.1900	0.0053
C	-2.4216	-0.7517	-1.5156
C	-3.5482	-1.5704	-1.5005
H	-3.9239	-1.9608	-0.5621
C	-4.1859	-1.8910	-2.6881
H	-5.0618	-2.5290	-2.6742
C	-3.7035	-1.3951	-3.8908
H	-4.2042	-1.6472	-4.8186
C	-2.5845	-0.5744	-3.9075
H	-2.2116	-0.1788	-4.8448
C	-1.9444	-0.2503	-2.7236
H	-1.0883	0.4136	-2.7217
C	-1.8737	-1.4972	1.2153
C	-2.0769	-1.1589	2.5492
H	-2.1548	-0.1158	2.8278
C	-2.1384	-2.1552	3.5098
H	-2.2901	-1.8888	4.5489
C	-1.9951	-3.4853	3.1442
H	-2.0450	-4.2622	3.8986
C	-1.7831	-3.8243	1.8150

H	-1.6643	-4.8629	1.5297
C	-1.7184	-2.8332	0.8510
H	-1.5489	-3.0959	-0.1874
N	-2.1892	1.2506	0.4862
Si	-3.7885	1.9378	0.5969
C	-4.9780	0.7120	1.3630
H	-5.0851	-0.1835	0.7456
H	-5.9688	1.1654	1.4581
H	-4.6532	0.4000	2.3578
C	-4.3760	2.4080	-1.1111
H	-3.6477	3.0635	-1.5959
H	-5.3336	2.9337	-1.0641
H	-4.5043	1.5256	-1.7432
C	-3.6296	3.4450	1.6825
H	-3.2181	3.1788	2.6598
H	-4.6049	3.9137	1.8384
H	-2.9677	4.1935	1.2382
P	1.6645	-0.0133	-0.1114
C	2.1011	-1.2521	1.1134
C	2.5079	-0.8434	2.3783
H	2.6153	0.2134	2.5869
C	2.7316	-1.7866	3.3684
H	3.0432	-1.4647	4.3548
C	2.5411	-3.1337	3.1014
H	2.7136	-3.8694	3.8786
C	2.1184	-3.5429	1.8440
H	1.9550	-4.5944	1.6393
C	1.8947	-2.6051	0.8517
H	1.5523	-2.9230	-0.1271
C	2.3832	-0.5230	-1.6824
C	3.4210	-1.4451	-1.7760
H	3.7995	-1.9313	-0.8849
C	3.9747	-1.7394	-3.0130
H	4.7809	-2.4602	-3.0833
C	3.5004	-1.1110	-4.1543
H	3.9353	-1.3430	-5.1198
C	2.4755	-0.1786	-4.0609
H	2.1118	0.3248	-4.9489
C	1.9174	0.1174	-2.8302
H	1.1366	0.8665	-2.7459
N	2.0932	1.4873	0.3006
Si	3.6218	2.3313	0.3075
C	5.0374	1.1237	0.5133
H	4.9460	0.5371	1.4305
H	5.9849	1.6682	0.5572
H	5.0947	0.4313	-0.3306
C	3.8062	3.2475	-1.3076
H	3.8703	2.5489	-2.1462
H	4.7086	3.8647	-1.3098

H	2.9455	3.8979	-1.4847
C	3.5630	3.5212	1.7414
H	2.7407	4.2328	1.6269
H	4.4932	4.0908	1.8160
H	3.4080	2.9918	2.6850

Complex **13**

C	0.8927	-0.6268	-5.3163
C	0.1287	1.7183	-4.9397
C	2.5743	1.2073	-5.1561
C	-2.6174	-1.9829	-4.8220
C	1.2260	0.7041	-4.6691
C	-2.9965	-0.6590	-4.6739
C	-1.9423	-2.6236	-3.7925
C	-2.7067	0.0218	-3.4993
C	5.2901	-1.3803	-3.2174
C	1.6186	4.0887	-2.5133
C	5.9280	0.9467	-2.5748
C	-1.6637	-1.9466	-2.6200
C	-5.0002	-2.6016	-2.0690
C	-2.0386	-0.6151	-2.4567
C	3.9212	3.8295	-1.6825
C	5.3043	-0.3534	-2.1012
C	2.4582	3.5792	-1.3522
C	-4.0676	3.4462	-1.3792
C	-3.6326	2.1376	-1.2478
C	-3.1584	4.4939	-1.3215
C	-4.3883	-2.5802	-0.6746
C	6.0378	-0.9029	-0.8895
C	-1.8102	4.2280	-1.1381
C	-2.2736	1.8635	-1.0781
C	-1.3723	2.9170	-1.0244
C	2.0685	4.2864	-0.0627
C	-4.7038	-3.8785	0.0633
C	-0.0346	0.0681	-0.4945
C	-4.8346	-1.3894	0.1372
C	-6.1863	-1.2526	0.4270
C	3.9048	-4.1493	0.5327
C	-3.9101	-0.4553	0.6564
C	-0.3294	-3.0462	0.6678
C	-6.6579	-0.2451	1.2476
C	-1.0327	-4.1987	0.9566
C	4.9399	2.0773	1.2817
C	2.8407	-3.4128	1.3400
C	-4.3861	0.5230	1.5629
C	-5.7447	0.6147	1.8299
C	-0.2867	-1.9944	1.5783
C	3.1294	-0.8796	1.7260
C	3.4309	-2.2195	2.0490

C	3.6869	1.6232	2.0239
C	-1.7118	-4.3157	2.1603
C	2.1587	-4.3732	2.3071
C	3.8185	0.1618	2.3842
C	-3.4248	1.3925	2.3314
C	-0.0840	1.9798	2.2258
C	-3.7963	2.8671	2.3581
C	0.3550	0.6808	2.4466
C	4.3593	-2.4793	3.0505
C	-0.9873	-2.1080	2.7741
C	-1.6925	-3.2649	3.0628
C	3.4767	2.5231	3.2347
C	4.7357	-0.1585	3.3785
C	5.0026	-1.4657	3.7292
C	-0.1937	2.8708	3.2810
C	-3.2777	0.8501	3.7513
C	0.7150	0.2896	3.7376
C	0.1141	2.4625	4.5692
C	0.5745	1.1730	4.7953
H	0.7784	-0.4900	-6.3943
H	0.0403	1.8887	-6.0149
H	2.5439	1.3751	-6.2345
H	-2.8428	-2.5149	-5.7393
H	-3.5186	-0.1474	-5.4744
H	-0.8237	1.3428	-4.5689
H	1.6816	-1.3567	-5.1331
H	-0.0377	-1.0245	-4.9127
H	0.3426	2.6700	-4.4551
H	2.8458	2.1466	-4.6712
H	3.3498	0.4694	-4.9457
H	-1.6244	-3.6536	-3.9036
H	4.7233	-1.0187	-4.0766
H	1.9710	3.6577	-3.4492
H	5.3786	1.3436	-3.4305
H	6.3148	-1.5794	-3.5388
H	-3.0029	1.0582	-3.4004
H	1.7153	5.1743	-2.5871
H	4.1939	3.3104	-2.6022
H	6.9612	0.7698	-2.8805
H	-4.6369	-3.4623	-2.6362
H	-4.7501	-1.7005	-2.6309
H	4.8355	-2.3120	-2.8824
H	4.0894	4.8983	-1.8310
H	0.5655	3.8439	-2.3970
H	-6.0901	-2.6747	-2.0171
H	5.9262	1.6935	-1.7807
H	-1.1440	-2.4551	-1.8196
H	4.5735	3.4853	-0.8839
H	-5.1243	3.6478	-1.5116

H	-4.3514	1.3267	-1.2717
H	-3.5026	5.5174	-1.4143
H	7.0642	-1.1533	-1.1656
H	-3.3047	-2.5089	-0.7685
H	2.2282	5.3625	-0.1579
H	-4.2877	-4.7356	-0.4748
H	-1.0964	5.0434	-1.0936
H	-6.8864	-1.9669	0.0053
H	5.5489	-1.8053	-0.5240
H	-0.3202	2.6887	-0.8998
H	4.3453	-3.5014	-0.2256
H	6.0672	-0.1774	-0.0770
H	1.0168	4.1157	0.1714
H	-5.7831	-4.0315	0.1515
H	0.1936	-2.9599	-0.2768
H	3.4546	-4.9974	0.0119
H	-1.0556	-5.0051	0.2327
H	5.0198	1.5996	0.3060
H	2.6655	3.9212	0.7722
H	-4.2829	-3.8685	1.0700
H	2.1017	-3.0502	0.6294
H	4.9306	3.1602	1.1391
H	-7.7176	-0.1507	1.4549
H	4.7051	-4.5251	1.1760
H	2.8295	1.7391	1.3598
H	5.8354	1.8315	1.8582
H	-0.3550	2.2865	1.2241
H	-3.8683	3.2788	1.3503
H	1.6921	-5.1908	1.7542
H	-2.4579	1.2959	1.8405
H	-2.2704	-5.2168	2.3855
H	-6.0940	1.3758	2.5199
H	2.8749	-4.8140	3.0056
H	3.2568	3.5430	2.9093
H	1.3803	-3.8754	2.8881
H	4.5850	-3.5111	3.2932
H	-3.0397	3.4349	2.9066
H	-4.7516	3.0365	2.8618
H	-0.5379	3.8811	3.0952
H	5.2599	0.6447	3.8829
H	4.3744	2.5734	3.8559
H	-1.0243	-1.2828	3.4687
H	-3.0137	-0.2091	3.7347
H	2.6517	2.1817	3.8544
H	-2.2441	-3.3326	3.9931
H	5.7174	-1.6920	4.5118
H	1.1045	-0.7048	3.9180
H	-4.2193	0.9452	4.2997
H	-2.5043	1.3932	4.3004

H	0.0097	3.1533	5.3981
H	0.8412	0.8560	5.7964
I	1.8988	-2.7188	-2.3527
N	-2.5543	-0.5296	0.3536
N	2.1571	-0.5772	0.7260
O	1.3033	0.5077	-3.2531
O	3.9490	-0.0797	-1.7039
O	2.2452	2.1843	-1.1717
P	-1.7609	0.1421	-0.8202
P	0.5178	-0.4618	1.0548
U	1.9902	0.1621	-1.4029

Complex **14**

U	-0.3674	0.0407	0.4976
P	2.2615	1.6066	0.1852
P	2.1990	-1.5799	0.0440
Si	0.4313	3.8130	1.1778
Si	0.5013	-3.6554	1.4004
O	-0.3267	0.0693	2.2902
N	0.8352	2.2700	0.5417
N	0.7917	-2.2123	0.5108
N	-0.8328	0.0012	-1.3332
N	-2.5161	1.5012	0.7323
N	-2.5018	-1.4264	0.8405
N	-5.9390	3.8635	1.0818
N	-5.8297	-3.8891	1.3642
C	1.9062	0.0322	-0.1641
C	-0.5446	-0.0376	-2.6885
C	-0.4455	-1.2700	-3.3636
C	-0.0913	-1.2800	-4.7040
H	0.0108	-2.2405	-5.2023
C	0.1460	-0.1131	-5.4199
C	-0.0052	1.0920	-4.7495
H	0.1618	2.0234	-5.2839
C	-0.3468	1.1567	-3.4050
C	-0.7350	-2.5571	-2.6615
H	-0.3392	-2.5616	-1.6459
H	-0.3018	-3.3955	-3.2085
H	-1.8136	-2.7341	-2.5942
C	0.5730	-0.1595	-6.8555
H	1.6097	-0.4995	-6.9483
H	0.5059	0.8262	-7.3198
H	-0.0445	-0.8495	-7.4364
C	-0.4894	2.4820	-2.7320
H	-1.5371	2.7031	-2.5041
H	-0.1133	3.2831	-3.3705
H	0.0479	2.5101	-1.7831
C	3.0845	2.4044	-1.2308
C	2.8431	1.8602	-2.4893

H	2.2074	0.9851	-2.5661
C	3.4049	2.4274	-3.6211
H	3.1983	1.9942	-4.5935
C	4.2280	3.5386	-3.5045
H	4.6761	3.9803	-4.3878
C	4.4834	4.0802	-2.2521
H	5.1320	4.9438	-2.1550
C	3.9125	3.5178	-1.1208
H	4.1224	3.9416	-0.1465
C	3.4458	1.7755	1.5510
C	4.8126	1.6016	1.3498
H	5.1929	1.4507	0.3456
C	5.6862	1.6173	2.4248
H	6.7480	1.4767	2.2578
C	5.2030	1.8045	3.7120
H	5.8883	1.8177	4.5519
C	3.8404	1.9586	3.9220
H	3.4541	2.0891	4.9268
C	2.9661	1.9330	2.8474
H	1.8980	2.0162	3.0058
C	2.8038	-2.3262	-1.4998
C	2.3790	-3.5729	-1.9394
H	1.6679	-4.1322	-1.3446
C	2.8306	-4.0836	-3.1474
H	2.4837	-5.0531	-3.4871
C	3.7152	-3.3507	-3.9237
H	4.0649	-3.7474	-4.8704
C	4.1426	-2.1020	-3.4925
H	4.8214	-1.5172	-4.1030
C	3.6859	-1.5926	-2.2888
H	3.9901	-0.6051	-1.9608
C	3.5143	-1.8992	1.2520
C	4.7465	-2.4516	0.9255
H	4.9418	-2.7646	-0.0934
C	5.7203	-2.6115	1.9014
H	6.6781	-3.0476	1.6398
C	5.4689	-2.2174	3.2058
H	6.2316	-2.3390	3.9669
C	4.2404	-1.6582	3.5354
H	4.0436	-1.3336	4.5505
C	3.2691	-1.4979	2.5644
H	2.3111	-1.0533	2.8117
C	-0.9532	4.6134	0.1963
H	-0.6636	4.7341	-0.8501
H	-1.1609	5.6070	0.6058
H	-1.8806	4.0397	0.2238
C	1.8475	5.0484	1.1505
H	2.7213	4.6837	1.6963
H	1.5142	5.9707	1.6370

H	2.1540	5.2994	0.1330
C	-0.1185	3.6763	2.9796
H	-0.4428	2.6616	3.2187
H	-0.9400	4.3643	3.1981
H	0.7073	3.9244	3.6512
C	1.9440	-4.8638	1.4581
H	2.2989	-5.1872	0.4776
H	1.6095	-5.7565	1.9971
H	2.7952	-4.4481	2.0003
C	-0.9311	-4.6002	0.6343
H	-1.8485	-4.0119	0.5821
H	-1.1400	-5.5009	1.2194
H	-0.6823	-4.9134	-0.3838
C	0.1215	-3.2665	3.1999
H	1.0581	-3.2077	3.7607
H	-0.4969	-4.0415	3.6618
H	-0.3777	-2.3033	3.3087
C	-3.2578	-1.8128	-0.1916
H	-2.9330	-1.4597	-1.1619
C	-4.3706	-2.6106	-0.0727
H	-4.9108	-2.8845	-0.9672
C	-4.7662	-3.0682	1.1970
C	-3.9910	-2.6226	2.2826
H	-4.2247	-2.9049	3.2987
C	-2.8967	-1.8232	2.0532
H	-2.2897	-1.4801	2.8814
C	-6.5715	-4.3488	0.2174
H	-7.0267	-3.5162	-0.3293
H	-7.3695	-5.0083	0.5506
H	-5.9362	-4.9077	-0.4786
C	-6.1673	-4.3710	2.6797
H	-5.3355	-4.9206	3.1340
H	-7.0169	-5.0457	2.6044
H	-6.4435	-3.5524	3.3529
C	-3.2682	1.8081	-0.3295
H	-2.9170	1.4144	-1.2751
C	-4.4082	2.5731	-0.2670
H	-4.9430	2.7832	-1.1817
C	-4.8392	3.0806	0.9718
C	-4.0602	2.7277	2.0881
H	-4.3127	3.0631	3.0834
C	-2.9388	1.9513	1.9163
H	-2.3322	1.6745	2.7696
C	-6.6474	4.2770	-0.1036
H	-6.0116	4.8633	-0.7772
H	-7.4954	4.8935	0.1859
H	-7.0322	3.4167	-0.6598
C	-6.2876	4.4372	2.3573
H	-6.4708	3.6616	3.1070

H	-7.2009	5.0177	2.2486
H	-5.5020	5.1013	2.7367

Complex **15**

U	0.0000	0.0000	-0.0880
H	0.0000	0.0000	1.8228
F	1.9851	0.0001	0.0842
F	-1.9852	0.0001	0.0842
F	0.0001	1.9851	0.0842
F	0.0001	-1.9852	0.0842
F	0.0000	0.0000	-2.0715

Complex **16**

U	0.0000	0.0005	0.0970
H	0.0000	0.0629	2.0923
C	-0.0001	-0.0998	-2.2318
C	1.6615	-1.6051	0.2093
C	-1.6615	-1.6051	0.2093
C	-1.6241	1.6459	0.1358
C	1.6241	1.6458	0.1358
H	-0.8944	0.3931	-2.6291
H	0.8941	0.3935	-2.6292
H	0.0002	-1.1527	-2.5370
H	2.5169	-1.3726	-0.4308
H	1.9573	-1.5278	1.2668
H	1.2983	-2.6154	0.0044
H	-2.5169	-1.3726	-0.4309
H	-1.2982	-2.6154	0.0044
H	-1.9573	-1.5277	1.2668
H	-1.6616	1.8564	1.2161
H	-2.6016	1.2936	-0.2030
H	-1.3358	2.5508	-0.4054
H	1.3359	2.5508	-0.4054
H	1.6616	1.8564	1.2161
H	2.6017	1.2935	-0.2029

Complex **17**

U	0.0786	-0.0070	0.1642
H	-0.0212	0.0693	2.1160
O	0.1580	-0.0904	-1.8736
O	-1.9155	0.4226	0.2302
O	2.0499	-0.4107	0.4950
O	0.4741	1.9856	0.3573
O	-0.3616	-1.9798	0.4379
C	-0.3797	-0.0255	-3.1580
H	0.0151	-0.8421	-3.7715
H	-1.4718	-0.1082	-3.1308
H	-0.1146	0.9249	-3.6335
C	-1.3211	-2.9921	0.3934

H	-1.2090	-3.6447	1.2649
H	-2.3308	-2.5676	0.4003
H	-1.1960	-3.5948	-0.5124
C	-2.8852	1.4268	0.2918
H	-3.4903	1.4227	-0.6209
H	-3.5439	1.2530	1.1480
H	-2.4157	2.4099	0.4020
C	1.4440	2.9833	0.4741
H	1.4766	3.5874	-0.4387
H	1.2015	3.6368	1.3179
H	2.4322	2.5429	0.6433
C	3.0506	-1.3844	0.4892
H	3.7534	-1.1927	1.3060
H	2.6194	-2.3821	0.6237
H	3.5995	-1.3601	-0.4581

Complex **18**

U	0.0000	0.0000	0.4695
H	0.0000	1.5251	-0.7674
H	0.0000	-1.5251	-0.7674
O	1.7428	0.0000	0.5327
O	-1.7428	0.0000	0.5327

Complex **19**

U	-0.4043	-0.2318	0.0356
O	-0.3251	-0.3680	-1.7308
O	-0.5004	-0.0859	1.8019
H	-0.6053	-2.2750	0.2451
H	-1.0396	1.7295	-0.1952
O	1.8637	-1.4233	-0.0134
O	-2.8373	-0.3682	-0.0679
O	1.5474	1.4070	0.2015
C	2.1027	-2.3974	-1.0486
H	1.1355	-2.8089	-1.3427
H	2.5496	-1.8821	-1.9005
C	3.0021	-3.4466	-0.4225
H	4.0562	-3.1810	-0.5438
H	2.8468	-4.4310	-0.8651
C	2.6002	-3.3751	1.0453
H	3.3495	-3.7865	1.7226
H	1.6526	-3.8941	1.2053
C	2.4014	-1.8881	1.2339
H	1.6949	-1.6327	2.0234
H	3.3504	-1.3704	1.4172
C	-3.5686	0.0002	-1.2571
H	-3.3886	-0.7648	-2.0126
H	-3.1628	0.9525	-1.6046
C	-5.0170	0.1119	-0.8190
H	-5.5632	0.8497	-1.4070

H	-5.5270	-0.8497	-0.9196
C	-4.8853	0.4894	0.6518
H	-5.7805	0.2742	1.2359
H	-4.6481	1.5511	0.7552
C	-3.7032	-0.3497	1.0801
H	-3.1348	0.0551	1.9160
H	-3.9928	-1.3806	1.3069
C	2.1978	1.8092	-1.0177
H	1.4788	1.6993	-1.8326
H	3.0391	1.1355	-1.1926
C	2.6081	3.2579	-0.8130
H	3.6219	3.3209	-0.4085
H	2.5792	3.8236	-1.7446
C	1.5947	3.7383	0.2186
H	1.9200	4.6236	0.7662
H	0.6314	3.9437	-0.2545
C	1.4629	2.5209	1.1029
H	0.5106	2.4493	1.6246
H	2.2864	2.4482	1.8237

Complex **20**

U	0.0283	0.3618	0.0015
O	0.4706	0.3100	-1.7201
O	-0.3560	0.7819	1.6835
H	0.2113	2.4006	-0.2292
C	-0.6879	-2.2214	-0.8415
C	-1.4509	-1.9851	0.3337
C	-0.5720	-2.0011	1.4395
C	0.7400	-2.1649	0.9439
C	0.6630	-2.3288	-0.4658
C	-1.2084	-2.3438	-2.2319
H	-1.2365	-3.3890	-2.5589
H	-0.5836	-1.7934	-2.9397
H	-2.2265	-1.9576	-2.3158
C	-2.9368	-1.8633	0.4108
H	-3.3586	-1.4518	-0.5081
H	-3.2439	-1.2123	1.2329
H	-3.4102	-2.8371	0.5788
C	-0.9604	-1.8685	2.8695
H	-1.8630	-1.2660	2.9850
H	-0.1782	-1.3818	3.4548
H	-1.1551	-2.8464	3.3241
C	1.9766	-2.2629	1.7740
H	1.8937	-1.6682	2.6866
H	2.8585	-1.9148	1.2324
H	2.1716	-3.2963	2.0818
C	1.8011	-2.5796	-1.3940
H	1.8887	-3.6429	-1.6436
H	2.7540	-2.2759	-0.9549

H	1.6772	-2.0305	-2.3304
O	-2.2061	1.1352	-0.6964
C	-2.9968	1.9696	0.1721
H	-3.8740	1.3968	0.4922
H	-2.3851	2.2160	1.0381
C	-3.3791	3.1537	-0.6834
H	-2.5492	3.8633	-0.7200
H	-4.2667	3.6667	-0.3121
C	-3.5834	2.4977	-2.0433
H	-3.5140	3.1980	-2.8759
H	-4.5609	2.0105	-2.0876
C	-2.4670	1.4714	-2.0781
H	-2.7277	0.5527	-2.6058
H	-1.5438	1.8737	-2.4965
O	2.4061	0.7700	0.5040
C	3.3972	0.9691	-0.5207
H	4.0741	0.1073	-0.5179
H	2.8771	1.0183	-1.4753
C	4.1093	2.2387	-0.1182
H	3.5192	3.1062	-0.4231
H	5.1034	2.3169	-0.5593
C	4.1293	2.1103	1.4002
H	4.2696	3.0623	1.9124
H	4.9289	1.4338	1.7136
C	2.7680	1.5085	1.6948
H	2.7640	0.8143	2.5358
H	2.0011	2.2680	1.8514

Complex **21**

U	-0.0501	0.0085	-0.0391
N	-0.0659	-0.0929	-1.8845
N	-0.0145	0.1319	1.8077
H	-0.5161	-2.0315	0.1049
H	-0.7932	1.9641	-0.1590
O	2.1910	-1.2984	-0.1048
O	-2.5576	-0.1811	0.0045
O	1.9576	1.5645	-0.0728
C	2.1838	-2.5548	-0.7921
H	1.3084	-2.5575	-1.4366
H	3.0958	-2.6189	-1.3974
C	2.1419	-3.6345	0.2921
H	2.9221	-4.3800	0.1282
H	1.1753	-4.1365	0.2958
C	2.3573	-2.8586	1.5995
H	3.0402	-3.3554	2.2902
H	1.3989	-2.7032	2.0972
C	2.8838	-1.5213	1.1201
H	2.6648	-0.6841	1.7796
H	3.9633	-1.5587	0.9181

C	-3.4573	0.9093	-0.2539
H	-3.0647	1.4824	-1.0925
H	-3.4636	1.5609	0.6244
C	-4.8066	0.2636	-0.5011
H	-5.6330	0.9260	-0.2414
H	-4.9100	-0.0156	-1.5534
C	-4.7258	-0.9837	0.3689
H	-5.4307	-1.7640	0.0801
H	-4.9061	-0.7304	1.4178
C	-3.2861	-1.4087	0.1673
H	-2.8457	-1.9514	1.0013
H	-3.1555	-2.0104	-0.7364
C	2.7523	1.7827	-1.2438
H	2.0806	1.9403	-2.0923
H	3.3394	0.8806	-1.4210
C	3.5749	3.0187	-0.9427
H	4.4791	2.7548	-0.3870
H	3.8731	3.5462	-1.8496
C	2.6194	3.8146	-0.0624
H	3.1156	4.5684	0.5495
H	1.8626	4.3101	-0.6759
C	1.9746	2.7266	0.7713
H	0.9442	2.9401	1.0543
H	2.5639	2.4895	1.6646
C	-0.3717	-0.1592	-3.2986
C	-1.6618	-0.9532	-3.4920
C	0.7763	-0.8529	-4.0281
H	1.7136	-0.3190	-3.8569
H	0.8949	-1.8776	-3.6709
H	0.5873	-0.8839	-5.1048
H	-1.5539	-1.9528	-3.0667
H	-1.9094	-1.0430	-4.5535
H	-2.4905	-0.4538	-2.9849
C	-0.3650	0.2507	3.2095
C	0.8638	-0.0635	4.0588
C	-1.4827	-0.7383	3.5310
H	-2.3718	-0.5006	2.9428
H	-1.1711	-1.7544	3.2819
H	-1.7472	-0.6963	4.5914
H	1.2101	-1.0820	3.8714
H	0.6332	0.0299	5.1237
H	1.6760	0.6285	3.8225
C	-0.5479	1.2571	-3.8409
H	0.3754	1.8286	-3.7262
H	-0.8117	1.2360	-4.9024
H	-1.3310	1.7777	-3.2875
C	-0.8370	1.6740	3.4954
H	-1.6885	1.9240	2.8603
H	-1.1300	1.7814	4.5440

H	-0.0409	2.3901	3.2829

Complex **22**

U	-0.0067	1.8443	0.0110
O	-0.0060	1.6544	-1.7351
O	-0.0098	1.6657	1.7575
U	-0.0005	-1.8443	0.0110
O	-0.0019	-1.6543	-1.7351
O	0.0011	-1.6657	1.7575
H	1.1804	0.0021	0.0165
H	-1.1879	-0.0022	0.0161
C	0.7037	4.3355	-0.9819
C	1.1373	4.3045	0.3753
C	-0.0028	4.3603	1.2074
C	-1.1396	4.3108	0.3705
C	-0.7003	4.3395	-0.9848
C	1.5823	4.3449	-2.1842
H	1.8047	5.3684	-2.5042
H	1.1145	3.8277	-3.0231
H	2.5413	3.8570	-1.9933
C	2.5555	4.2994	0.8413
H	3.2222	3.8237	0.1181
H	2.6655	3.7760	1.7937
H	2.9293	5.3182	0.9903
C	-0.0056	4.4458	2.6919
H	0.8691	3.9589	3.1254
H	-0.8857	3.9653	3.1217
H	-0.0025	5.4896	3.0238
C	-2.5598	4.3135	0.8307
H	-2.6765	3.7904	1.7825
H	-3.2261	3.8415	0.1047
H	-2.9286	5.3342	0.9784
C	-1.5738	4.3540	-2.1908
H	-1.7855	5.3788	-2.5142
H	-2.5380	3.8754	-2.0026
H	-1.1074	3.8305	-3.0266
C	-1.1362	-4.3085	0.3753
C	0.0040	-4.3603	1.2074
C	1.1407	-4.3067	0.3705
C	0.7015	-4.3370	-0.9848
C	-0.7025	-4.3379	-0.9819
C	-2.5545	-4.3084	0.8414
H	-2.9246	-5.3284	0.9907
H	-3.2228	-3.8352	0.1179
H	-2.6663	-3.7850	1.7935
C	0.0071	-4.4459	2.6919
H	-0.8699	-3.9631	3.1254
H	0.8849	-3.9612	3.1219
H	0.0090	-5.4896	3.0238

C	2.5609	-4.3045	0.8308
H	2.6758	-3.7813	1.7827
H	3.2255	-3.8301	0.1049
H	2.9333	-5.3240	0.9783
C	1.5751	-4.3485	-2.1907
H	2.5374	-3.8660	-2.0027
H	1.1066	-3.8271	-3.0267
H	1.7908	-5.3725	-2.5138
C	-1.5811	-4.3504	-2.1842
H	-1.7988	-5.3746	-2.5050
H	-1.1156	-3.8304	-3.0228
H	-2.5422	-3.8669	-1.9930

Complex **23**

U	-0.0709	-0.0038	-0.1867
H	0.6388	0.0603	1.5741
O	-0.7502	-0.0655	-1.8360
N	-0.5361	2.1142	0.1261
N	-1.4313	-1.5129	0.6308
N	1.9502	-0.5934	-0.7997
Si	-1.8747	-2.8668	-0.3917
Si	-2.1693	-1.3275	2.2053
Si	2.5589	-0.0031	-2.3345
Si	2.8865	-1.7396	0.1307
Si	0.6046	3.1903	0.8989
Si	-2.0239	2.7505	-0.5504
C	-3.3483	-2.4365	-1.4588
H	-3.6440	-3.2988	-2.0631
H	-4.2096	-2.1345	-0.8590
H	-3.1011	-1.6181	-2.1385
C	-0.4325	-3.3259	-1.4994
H	0.8671	-2.8436	1.1972
H	-0.7595	-4.1236	-2.1733
H	-0.0726	-2.5068	-2.1236
C	-2.2527	-4.4197	0.5932
H	-3.0859	-4.3099	1.2887
H	-2.5126	-5.2169	-0.1100
H	-1.3787	-4.7519	1.1587
C	-3.3648	1.4405	-0.4895
H	-3.1066	0.5195	-1.0146
H	-3.6337	1.1882	0.5385
H	-4.2608	1.8449	-0.9700
C	-1.7713	3.2758	-2.3272
H	-1.4979	2.4157	-2.9430
H	-2.6941	3.7001	-2.7326
H	-0.9849	4.0277	-2.4216
C	-2.7013	4.1967	0.4371
H	-3.6304	4.5292	-0.0358
H	-2.9417	3.8979	1.4602

H	-2.0292	5.0545	0.4823
C	0.0198	3.7381	2.5906
H	-0.8845	4.3464	2.5486
H	-0.1829	2.8753	3.2290
H	0.8022	4.3340	3.0703
C	2.2641	2.3506	1.1663
H	2.2370	1.6709	2.0201
H	2.6365	1.7901	0.3067
H	2.9977	3.1327	1.3865
C	0.9197	4.7030	-0.1673
H	1.6366	5.3610	0.3323
H	1.3410	4.4215	-1.1354
H	0.0152	5.2841	-0.3560
C	4.3505	-0.9297	0.9700
H	4.0261	-0.0979	1.5997
H	4.8515	-1.6603	1.6121
H	5.0860	-0.5490	0.2603
C	1.8597	-2.5085	1.5027
H	0.4073	-3.7150	-0.9203
H	2.4020	-3.3858	1.8697
H	1.7346	-1.8210	2.3411
C	3.4948	-3.1443	-0.9562
H	4.0725	-3.8501	-0.3523
H	2.6590	-3.6898	-1.4001
H	4.1378	-2.8036	-1.7697
C	4.4295	0.1565	-2.3545
H	4.7733	0.8769	-1.6086
H	4.9548	-0.7845	-2.1858
H	4.7310	0.5299	-3.3379
C	1.9094	1.7280	-2.6483
H	2.2425	2.0475	-3.6403
H	0.8205	1.7998	-2.6376
H	2.3102	2.4420	-1.9253
C	2.0207	-1.1170	-3.7368
H	2.3562	-2.1460	-3.5908
H	0.9320	-1.1215	-3.8248
H	2.4334	-0.7589	-4.6842
C	-4.0316	-1.5421	2.0991
H	-4.4779	-0.7893	1.4450
H	-4.3255	-2.5238	1.7236
H	-4.4708	-1.4242	3.0941
C	-1.4766	-2.5443	3.4476
H	-1.6955	-3.5814	3.1904
H	-0.3925	-2.4381	3.5311
H	-1.9094	-2.3458	4.4328
C	-1.8539	0.3812	2.9180
H	-2.5317	0.5127	3.7678
H	-0.8322	0.4784	3.2891
H	-2.0357	1.2040	2.2249

References

[S1] P. L. Arnold, I. J. Casely, Z. R. Turner and C. D. Carmichael, *Chem. Eur. J.*, 2008, **14**, 10415–10422.

[S2] M. F. Schettini, G. Wu and T. W. Hayton, *Chem. Commun.*, 2012, **48**, 1484–1486.

[S3] L. A. Seaman, P. Hrobárik, M. F. Schettini, S. Fortier, M. Kaupp and T. W. Hayton, *Angew. Chem. Int. Ed. Engl.*, 2013, **52**, 3259–3263.

[S4] A. J. Lewis, P. J. Carroll and E. J. Schelter, *J. Am. Chem. Soc.*, 2013, **135**, 13185–13192.

[S5] S. Fortier, N. Kaltsoyannis, G. Wu and T. W. Hayton, *J. Am. Chem. Soc.*, 2011, **133**, 14224–14227.

[S6] J.-C. Tourneux, J.-C. Berthet, T. Cantat, P. Thuéry, N. Mézailles and M. Ephritikhine, *J. Am. Chem. Soc.*, 2011, **133**, 6162–6165.

[S7] W. J. Oldham Jr., S. M. Oldham, W. H. Smith, D. A. Costa, B. L. Scott and K. D. Abney, *Chem. Commun.*, 2001, 1348–1349.

[S8] D. P. Mills, O. J. Cooper, F. Tuna, E. J. L. McInnes, E. S. Davies, J. McMaster, F. Moro, W. Lewis, A. J. Blake and S. T. Liddle, *J. Am. Chem. Soc.*, 2012, **134**, 10047–10054.

[S9] O. J. Cooper, D. P. Mills, J. McMaster, F. Tuna, E. J. L. McInnes, W. Lewis, A. J. Blake and S. T. Liddle, *Chem. - Eur. J.*, 2013, **19**, 7071–7083.

[S10] E. Lu, O. J. Cooper, J. McMaster, F. Tuna, E. J. L. McInnes, W. Lewis, A. J. Blake and S. T. Liddle, *Angew. Chem. Int. Ed.*, 2014, **53**, 6696–6700.

[S11] S. A. Mungur, S. T. Liddle, C. Wilson, M. J. Sarsfield and P. L. Arnold, *Chem. Commun.*, 2004, 2738–2739.